ENDOCANNABINOID MODULATION AND METABOLIC MATURATION IN THE SUPERIOR OLIVARY COMPLEX

Graduate School of
Systemic Neurosciences
LMU Munich

Dissertation of the Graduate School of Systemic Neurosciences

Ludwig-Maximilians-University Munich

Submitted by Barbara Trattner

Supervisor: PD Dr. Lars Kunz

2nd reviewer: Prof. Dr. Benedikt Grothe

Date of the oral defense: November 27th, 2013

Table of contents

Initial Summary

In my thesis I described and characterised the endocannabinoid system in the medial and the lateral superior olive (MSO and LSO, respectively) of the Mongolian gerbil (*Meriones unguiculatus*). These two nuclei of the auditory brainstem deal with the extraction of interaural time or interaural level difference from sound sources and thereby enable a meaningful orientation in an acoustic environment. The endocannabinoid system has a neuromodulatory function that could allow adaptation of neuronal firing to the stimulus environment. In my studies I could show the presence of endocannabinoid components both anatomically as well as functionally by using histochemical and electrophysiological approaches. In addition, I characterised the endocannabinoid system during the development of the auditory system and observed an unexpected change during the time period around functional hearing onset: Before hearing onset, the cannabinoid receptors are primarily expressed presynaptically at excitatory glutamatergic as well as inhibitory glycinergic synaptic terminals. Endocannabinoids are produced postsynaptically, giving rise to depolarisation-induced suppression of transmitter release, which is a well-described negative feedback mechanism. After hearing onset, cannabinoid receptor expression is observed mostly postsynaptically and therefore the endocannabinoid system does not lead anymore to a retrograde regulation of synaptic inputs but rather influences cellular physiological properties directly. My research indicates that by endocannabinoid signalling, neurones in the MSO adapt their membrane potential through a CB1-dependent mechanism. Additionally, endocannabinoids directly modulate glycinergic receptors in a CB1-independent way. Both mechanisms constitute a possible autocrine feedback, since endocannabinoids can be produced by the neurones themselves during times of high cellular activity.

Moreover, I investigated the role of the endocannabinoid system in shaping the morphology of MSO principal neurones. For this approach, pregnant and lactating Mongolian gerbils were administered cannabinoid receptor antagonists and agonists during the developmental time period of MSO development in their offspring. The offspring was then sacrificed and MSO neurones were visualised by Golgi staining or electroporation and subsequently three-dimensionally reconstructed. The

resulting morphological changes represented the basis for the simulation of MSO neurones, which I have programmed in NEURON. By this approach I have observed that the morphological alterations inflicted by over-stimulation or blockage of the endocannabinoid system cause large effects on the biophysical and computational properties of these neurones and could greatly impact the precision of sound localisation.

Furthermore, I studied the development of the MSO and LSO as well as of the medial nucleus of the trapezoid body (MNTB), which has glycinergic projections to the other two nuclei, with respect to maturation of neuronal metabolism. I carried out immunohistochemical and histological stainings of metabolic marker proteins and quantified their expression patterns and abundance throughout the development of the auditory system. Specifically, the amounts and activity of mitochondria, the density of glucose transporter 3 as well as Na^+/K^+ ATPase were investigated. I additionally carried out stainings for lactate dehydrogenase and monocarboxylate transporter 1, which were however only present in very low amounts, indicating that glucose is the major metabolic fuel in the auditory brainstem. Interestingly, mitochondria, GLUT3 and Na^+/K^+ ATPase are up-regulated during the time of hearing onset and saturate during the phase of refinement of auditory circuits. However we found that in the MNTB the time before hearing onset is most crucial, whereas in the MSO and LSO the major part of metabolic maturation occurs in the period after hearing onset. Our findings indicate that neurones do not require a lot of energy to process behaviourally-irrelevant spontaneous activity generated in the cochlea before hearing onset. Only at the time of hearing onset, when signals become behaviourally meaningful, is the metabolic machinery up-regulated – until the system has fully matured and refined. A computational model calculating the theoretical ATP consumption by these neurones at various developmental time points reached similar conclusions.

Introduction

Structure and function of the superior olivary complex

The superior olivary complex (SOC) is part of the mammalian auditory brainstem (Harrison & Feldman 1970) and its neurones are the first cells receiving binaural inputs (Brugge & Geisler 1978, Thompson & Schofield 2000). Functionally, the SOC is of great importance for the computation of sound source localisation in our surround, thus enabling accurate orientation and navigation in acoustic space (Grothe *et al.* 2010).

Anatomically the SOC consists of three primary nuclei, namely the medial nucleus of the trapezoid body (MNTB), the lateral superior olive (LSO) and the medial superior olive (MSO), as well as of a number of periolivary nuclei. All three primary nuclei receive direct innervation from the cochlear nucleus (CN), which is the first relay station of the auditory nerve in the brain (Thompson & Schofield 2000). For an overview of the SOC of the Mongolian gerbil, which is the experimental animal of choice when investigating SOC properties (see at the end of this chapter), please refer to Figure 1.

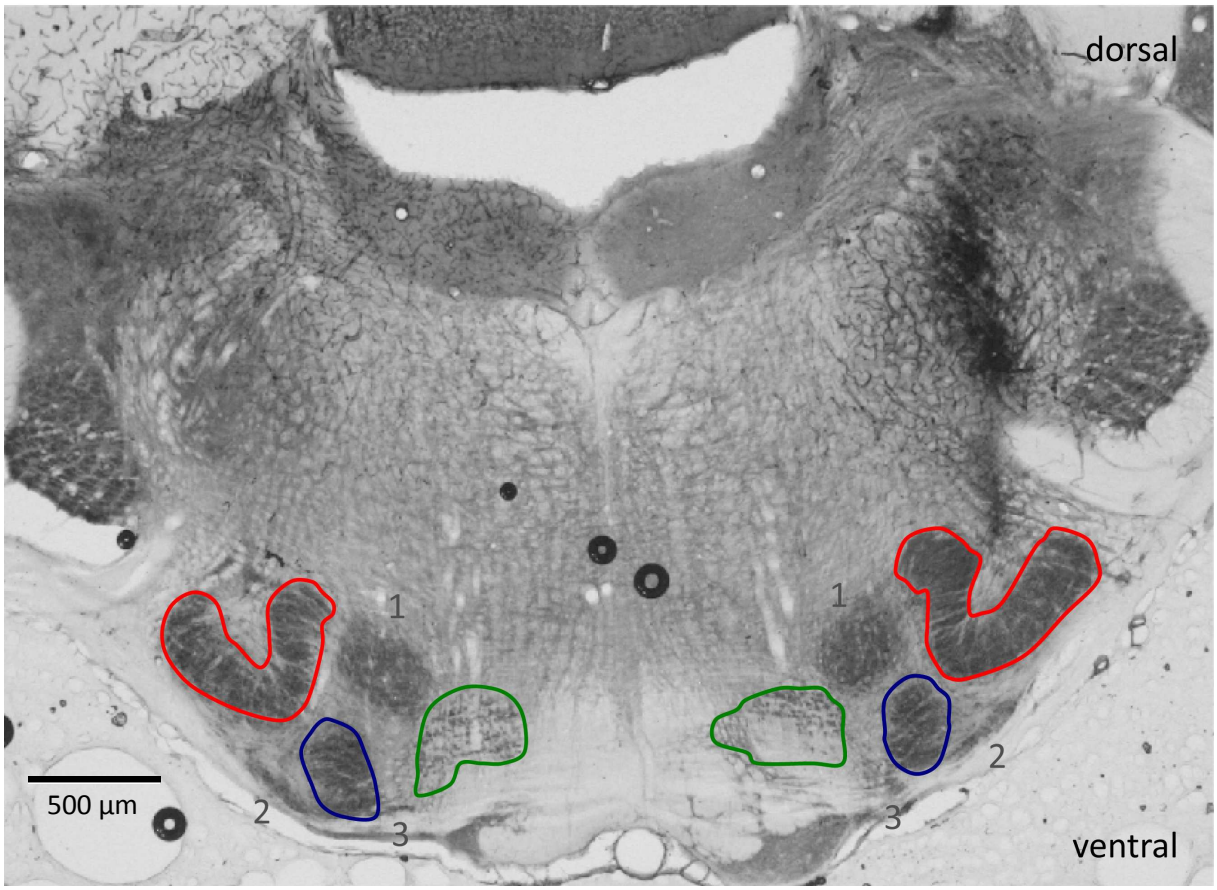

Figure 1. Appearance of the gerbil superior olivary complex

The auditory brainstem of an adult Mongolian gerbil (*Meriones unguiculatus*) at the age of postnatal day (P) 100 was sectioned and histologically stained for cytochrome *c* oxidase, which provides dark labelling of SOC nuclei. This particular section provides a good overview of the principal SOC nuclei. The LSO is circled in red, the MSO is circled in blue and the MNTB is circled in green. The nucleus dorsal to the MSO, which is clearly visible in the cytochrome *c* staining (1) is the superior periolivary nucleus (SPN). Ventrolateral to the MSO the lateral nucleus of the trapezoid body (LNTB) is visible on both sides (2). Ventromedial to the MSO the ventral nucleus of the trapezoid body (VNTB) is starting to appear in this sectioning plane (3).

The localisation of a sound source in the vertical plane, i.e. its elevation, is extracted from monaural cues arising from an interaction of the sound wave with the head and the ears. This interaction leads

to a direction-specific attenuation of particular frequencies that allows the determination of the vertical position of a sound source (Grothe et al. 2010).

Information about the horizontal localisation of a sound source is computed by the LSO and MSO, mainly by evaluating interaural level difference (ILD) and interaural time difference (ITD), respectively. Due to the fact that the sound at that ear, which is closer to the sound source, is louder (stronger in amplitude) and arrives earlier than at the other ear, the azimuthal localisation of the sound source in space can be calculated (Rayleigh & Strutt 1907, Thompson 1882). To achieve this task, both LSO as well as MSO neurones receive and compare inputs from both ears, as depicted in Figure 2.

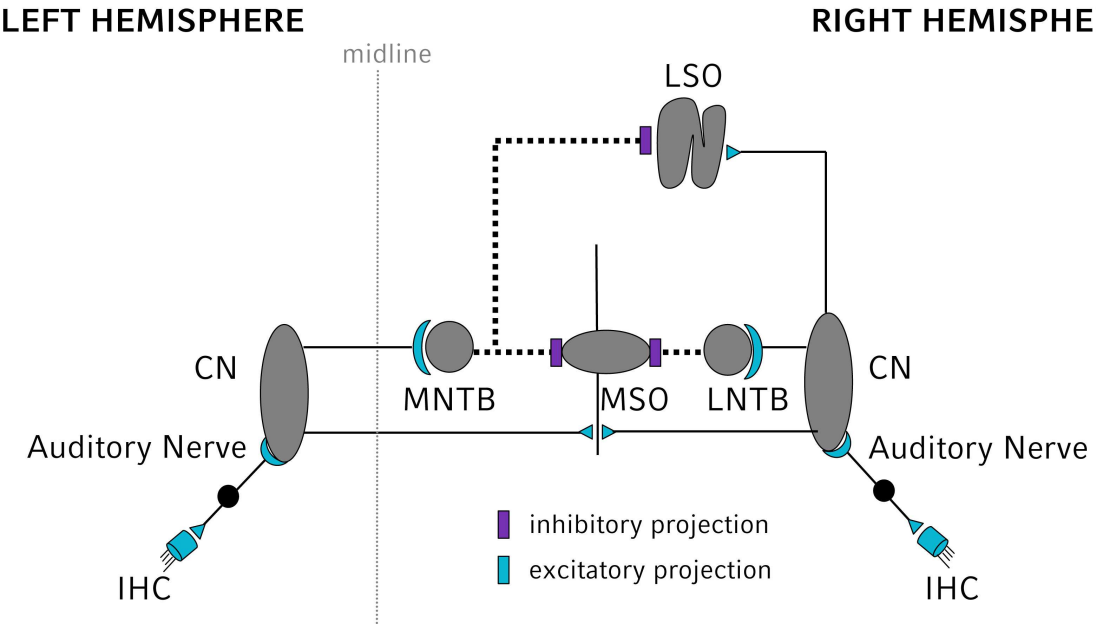

Figure 2. Overview of the auditory brainstem circuitry

Auditory signals are transduced into neuronal activity by the inner hair cells (IHC), which transmit the information via the auditory nerve to the first station of the auditory brainstem, the cochlear nucleus (CN). The CN sends excitatory projections to the ipsilateral lateral superior olive (LSO), to the ipsilateral lateral nucleus of the trapezoid body (LNTB), to both medial superior olives (MSO) as well as to the contralateral medial nucleus of the trapezoid body (MNTB). MNTB and LNTB provide inhibitory glycinergic projections to the ipsilateral MSO and LSO (MNTB) and to the ipsilateral MSO (LNTB). For a review on how sound localisation is achieved by this circuitry please refer to (Grothe et al. 2010). This figure is taken from (Trattner *et al.* 2013a).

The LSO mainly compares the loudness or amplitude the sound source produces at the two ears. The LSO is important in the localisation of high-frequent sound sources, which produce an amplitude difference at the two ears. This ILD is generated by the shadowing effect of the head that occurs at the short wavelengths of high-frequent sounds. LSO neurones are tonotopically organised (Guinan *et al.* 1972, Caird & Klinke 1983), with low-frequency neurones being present mainly in the lateral limb and high-frequency sensitive neurones being located mainly in the medial limb. LSO neurones receive an excitatory glutamatergic connection from spherical bushy cells (SBCs) of the ipsilateral

CN and an inhibitory glycinergic projection from the ipsilateral MNTB, which in turn receives input from globular bushy cells (GBCs) of the contralateral CN. GBCs possess high temporal precision (Joris *et al.* 1994b, Joris *et al.* 1994a) and very thick axons (Morest 1968a, Morest 1968b), which allow high-speed signal transmission. They synapse on the MNTB, forming the large calyx of Held synapse (Morest 1968b), which reliably enables temporally accurate and fast synaptic transmission (Mc Laughlin *et al.* 2008, Hermann *et al.* 2007). Glycinergic MNTB neurones in turn project to the ipsilateral LSO. By a simple subtraction of excitatory and inhibitory inputs the ILD is computed (Moore & Caspary 1983, Boudreau & Tsuchitani 1968, Caird & Klinke 1983, Park *et al.* 1996, Sanes 1990).

The MSO computes the difference in arrival time of the sound at the two ears and is important in low frequency sound source localisation, which is not achievable by comparing interaural level difference, due to the large wavelength of the sound wave compared to the head size. Neurones in the MSO are organised in a frequency-specific manner with high-frequency neurones lying at the ventral end of the nucleus and low-frequency neurones lying at the dorsal end (Goldberg & Brown 1969). MSO principal cells are bipolar neurones with two principal dendrites extending along the medio-lateral axis of the nucleus (Kapfer *et al.* 2002, Rautenberg *et al.* 2009, Chirila *et al.* 2007, Stotler 1953). These neurones receive excitatory glutamatergic inputs from SBCs of both CNs on their dendrites and also bilateral inhibitory inputs that are confined mainly to their somata (Werthat *et al.* 2008, Kapfer et al. 2002). The inhibitory inputs are glycinergic in nature and originate from the ipsilateral lateral nucleus of the trapezoid body (LNTB) and the MNTB, which are in turn driven by GBCs in the ipsilateral and contralateral CN, respectively. MSO neurones, which show the highest spiking rate for the same frequency, generally also respond to the same ITD (Brand *et al.* 2002). The neurones are tuned in a way that the maximal slope of the ITD function (i.e. spike number per ITD) is close to 0 ITD, i.e. represents the middle of the physiological range of ITDs. This ensures that the neurones are most sensitive to changes in this area (Brand et al. 2002). MSO neurones compute their output through a complex interaction of binaural excitatory and inhibitory inputs. The ITD functions of opposite MSO nuclei are adjusted like a mirror image (Grothe et al. 2010). The similar

distribution of best ITDs throughout the population of MSO neurones suggests that information about the sound source localisation is extracted from the population activity of all MSO cells rather than from the firing of a few cells (McAlpine *et al.* 2001). The activity of the MSOs in both brain hemispheres is compared and thereby the ITD can be determined in the sense of a relative rate code (Grothe 2003, Grothe et al. 2010). The inhibitory inputs are necessary for adjusting the maximal slope to the physiological range and thereby they enable the sensitive detection of behaviourally relevant ITD cues (Brand et al. 2002, Pecka *et al.* 2008).

The Mongolian gerbil (*Meriones unguiculatus*) is very suited as experimental animal to investigate both physiological as well as anatomical properties of its SOC, as this rodent possess an audible spectrum and an organisation of the auditory brainstem similar to that of humans (Heffner & Heffner 1988, Muller 1990). Unlike many other rodents, their audible spectrum extends to low frequencies, which requires an MSO to localise low frequency sound sources. Thus, especially for investigating the MSO or mechanisms of low frequency sound localisation, the Mongolian gerbil is the animal of choice. At birth, Mongolian gerbils are deaf. The onset of hearing occurs between postnatal day (P)12 and 13 in these animals (Woolf & Ryan 1984).

Development of morphological and physiological properties of SOC neurones

Before hearing onset the machinery and circuitry to transduce sound is already present in the auditory brainstem. At that time the system is driven by spontaneous activity, which does not convey any behaviourally meaningful information. These spontaneous firing periods are caused by spontaneous ATP (adenosine-5'-triphosphate) release of supporting cells in the cochlea and are only present as long as the auditory system is insensitive to sound stimulation (Tritsch *et al.* 2007, Tritsch & Bergles 2010). After the onset of hearing all SOC neurones undergo a developmental maturation - generally referred to as "refinement" - in both morphological as well as physiological terms, during which the connections are being fine-tuned to the auditory environment the animals are exposed to (Rautenberg et al. 2009, Chirila et al. 2007, Magnusson *et al.* 2005, Walcher *et al.* 2011, Sanes *et al.* 1992). These developmental changes were shown in many instances to depend on the ability of the animals to perceive sound (Ford *et al.* 2009, Seidl & Grothe 2005, Kapfer et al. 2002, Werthat et al. 2008) and thus it can be stated that auditory perception marked by hearing onset is the necessary trigger for the observed physiological and morphological changes. Since other groups have, however, only reported a mere coincidence between hearing onset and changes in physiological properties (Magnusson et al. 2005, Hassfurth *et al.* 2010, Walcher et al. 2011), a causal relationship between the sound-evoked activity and "refinement" can not be established for all parameters changing after hearing onset. In addition to sound as a trigger, of course developmentally regulated genetic programmes could be responsible for changing the physiological properties of neurones, e.g. by changing receptor or transmitter expression (Kaiser *et al.* 2011, Vannucci 1994, Blaesse *et al.* 2005).

Considering the maturation of physiological properties, MSO neurones of P8 gerbils have been shown to exhibit for instance a lower resting membrane potential and action potential threshold when compared to adult animals. Moreover, MSO neurone action potential amplitude decreases drastically after hearing onset. Many basic physiological properties such as the input resistance and time constant of the membrane are also subject to change during the first week after hearing onset (Scott *et al.* 2005). Concerning the synaptic inputs that the cells receive, the onset of hearing in MSO neurones is accompanied by an activity-dependent reorganisation of the glycinergic inputs to MSO

somata (Kapfer et al. 2002). Physiologically, the kinetics of these inhibitory inputs accelerate after hearing onset and are matured only by P17 (Magnusson et al. 2005). In addition, the kinetics of excitatory postsynaptic potentials increase during this period, which is likely due to an alteration in K^+ currents (Chirila et al. 2007). Interestingly the inhibitory axons projecting to the MSO themselves also undergo a morphological and physiological change that is activity-dependent (Werthat et al. 2008). Furthermore, the inhibitory transmitter GABA differentially controls MSO neuronal inputs before and after hearing onset (Hassfurth et al. 2010). In gerbils, which have not yet reached hearing onset, GABA released from MNTB terminals directly activates $GABA_A$ receptors on MSO neurones (Smith *et al.* 2000) and additionally acts via presynaptically located metabotropic $GABA_B$ receptors to retrogradely depress excitatory and inhibitory transmitter release (Hassfurth et al. 2010). In animals after hearing onset, $GABA_A$ signalling is no longer present and GABA release mainly controls the strength of inhibitory inputs via retrograde $GABA_B$ signalling. A reduction in inhibitory postsynaptic current amplitude caused by $GABA_B$ - dependent retrograde suppression of inhibition would allow to dynamically adjust ITD computation within the range of one second by shifting the peak of the ITD function closer to the midline (Hassfurth et al. 2010). During high-frequency stimulation $GABA_B$ receptors could also act to enhance synaptic efficacy by enabling sustained transmitter release and thereby extending the dynamic range (Brenowitz *et al.* 1998). Maturation of morphological characteristics of MSO neurones is not reached before approximately two weeks after hearing onset. Especially the complexity of dendrites and the average dendritic length are decreased, whereas the cellular volume is increased during this period of time (Chirila et al. 2007, Rautenberg et al. 2009, Rogowski & Feng 1981, Kiss & Majorossy 1983). Since ITDs extracted by MSO neurones are in the range of microseconds, the accurate and precise computation thereof is of vital behavioural importance. The exact computation of output signals relies critically on the neuronal morphology (Rall *et al.* 1992, London & Hausser 2005, Meseke *et al.* 2009, Duch & Levine 2000, Womack & Khodakhah 2002) and thus the strict regulation of this morphological maturation is of extreme importance for the functional output of these neurones.

In LSO neurones many electrophysiological properties reach adult-like levels already during embryogenesis, however input resistance, time constant and spike duration decrease significantly

during postnatal development, to name but a few changes (Kandler & Friauf 1995a). Tonotopic precision of the MNTB-LSO synapse is functionally already present and refined before hearing onset (Kim & Kandler 2003, Kim & Kandler 2010) and only structurally refined after hearing onset (Sanes & Friauf 2000, Kandler *et al.* 2009). Interestingly, glycinergic postsynaptic potentials originating from the MNTB are depolarising in the embryonic LSO and gain their adult-like hyperpolarising character already well before hearing onset (Kandler & Friauf 1995b, Kakazu *et al.* 1999). In these early developmental stages the glycinergic synapses originating from the MNTB co-release glutamate and GABA (Kotak *et al.* 1998, Gillespie *et al.* 2005, Kandler & Friauf 1995b), however, at the time of hearing onset these synapses already reached the adult-like configuration and are purely glycinergic. Like in MSO neurones, also LSO neurones exhibit a great acceleration of postsynaptic potentials after hearing onset (Walcher et al. 2011). Retrograde GABAergic signalling via presynaptically located $GABA_B$ receptors exerts a very important role in the adult LSO to balance excitatory and inhibitory inputs and allow accurate sound localisation (Magnusson *et al.* 2008, Grothe & Koch 2011). *In vivo* recordings of LSO neurones demonstrated that $GABA_B$ receptors retrogradely regulate the sensitivity that these neurones exhibit to interaural level differences. GABA is released by LSO neurones themselves during spiking activity and acts to decrease mainly excitatory postsynaptic currents via presynaptic $GABA_B$ signalling. This mechanism might provide a means of adjusting sound localisation sensitivity to the sound environment (Magnusson et al. 2008). A role of the endocannabinoid system during the development of LSO circuits has also been suggested previously by means of immunohistochemistry in rats throughout development (Chi & Kandler 2012). Morphologically, dendritic arborisations of LSO neurones become spatially more confined to a smaller area during postnatal development. In addition, these neurones undergo a decrease in total dendritic length and also the number of dendritic branching points per neurone is reduced during postnatal development (Sanes et al. 1992, Rietzel & Friauf 1998).

The MNTB is targeted by developing axons from the CN that form the characteristic calyx of Held synapse on MNTB somata. These synapses adopt their characteristic morphology and physiology well before hearing onset, i.e. between P2 (Hoffpauir *et al.* 2006) and P5 (Kil *et al.* 1995). From birth

onwards, evoked postsynaptic currents in the MNTB increase markedly up to P4 with very prominent AMPA and NMDA receptor components (Hoffpauir et al. 2006). The adult-like fenestration of the calyces occurs in a frequency-dependent manner and is dependent on the ability of the animals to perceive sound (Ford et al. 2009). Calyces in the MNTB do not seem to be subject to pruning. However there is a large increase in non-neuronal cell death in the MNTB that occurs at the time of hearing onset (Rodriguez-Contreras *et al.* 2006).

To summarise these findings it can be stated that all nuclei of the SOC undergo maturation during postnatal development. The extent, to which these changes affect the fundamental computational properties of the neurones, however varies greatly between the different regions. As described above, a connection between hearing onset and physiological changes is established for many characteristics. I investigated the role of endocannabinoid modulation throughout the developmental period ranging from before hearing onset until the end of the refinement phase. Additionally, I investigated the role of endocannabinoid signalling on the morphological development of MSO neurones, which will be outlined in the following chapter. Since many neuronal transmitter systems undergo adaptation during this period it is conceivable that also endocannabinoid modulation is adjusted during this time.

Neuronal modulation by the endocannabinoid system

The endocannabinoid system consists of several endocannabinoid compounds, their respective transporters, enzymes and their endogenous receptors CB1 and CB2. Both receptors are G-protein coupled transmembrane receptors, with CB1 being well known for its abundant roles in neuronal physiology. CB2 seems to be more involved in processes of immunology as well as bone and fat metabolism, even though it might also play an important role in the brain (Atwood & Mackie 2010, Ashton *et al.* 2006, Baek *et al.* 2008).

The neuronal endocannabinoid system is generally described as a retrograde modulatory system in many brain areas (Katona & Freund 2012, Herkenham *et al.* 1990), which suppresses presynaptic transmitter release in a negative feed-back process that is governed by postsynaptic activity (Figure 3).

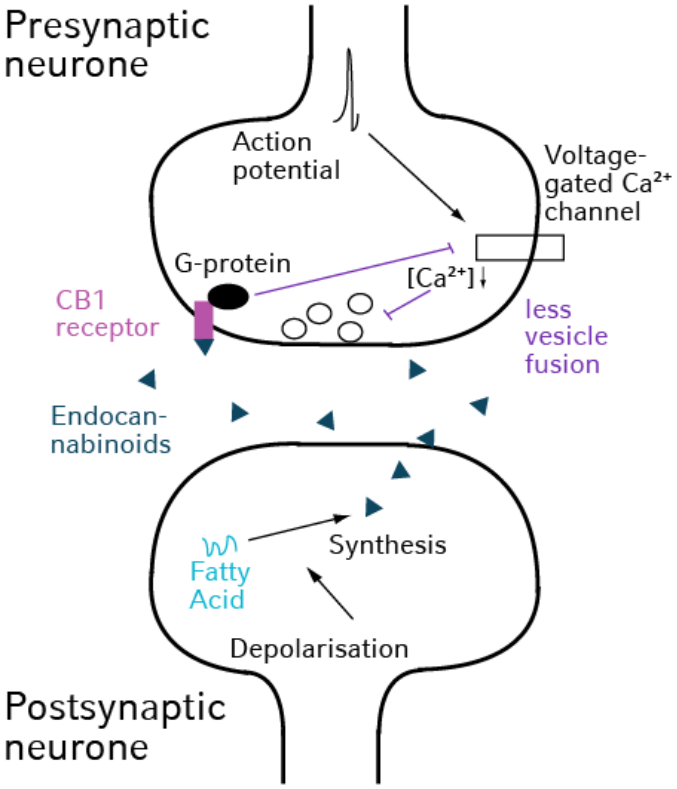

Figure 3. Depolarisation-induced suppression of transmitter release

Endocannabinoid synthesis from membrane fatty acids is activated by neuronal activity in the postsynaptic cell. Endocannabinoids bridge the synaptic cleft and bind to presynaptically located CB1 receptors, which – upon activation – inhibit voltage-gated Ca^{2+} channels in a G-protein coupled manner. Thereby neurotransmitter release from the presynapse is reduced owing to less Ca^{2+} influx, which is required for vesicle fusion with the cell membrane. This negative feedback mechanism results in less stimulation of the postsynaptic neurone by presynaptic inputs. This figure was modified from (Trattner et al. 2013a).

Endocannabinoid synthesis is initiated in the postsynaptic cell by elevated Ca^{2+} levels, which activate enzymes that produce various endocannabinoid types such as anandamide (AEA) or 2-arachidonylglycerole (2-AG) from membrane fatty acids (Ueda *et al.* 2011, Liu *et al.* 2006, Di Marzo 2011, Alger & Kim 2011). In addition, endocannabinoid synthesis can also be driven by metabotropic glutamate receptor (mGluR) activity, both as a result of increased Ca^{2+} levels (Kushmerick *et al.*

2004) or independent of Ca^{2+} rise (Maejima *et al.* 2001), possibly by the direct activation of phospholipase Cβ (Hashimotodani *et al.* 2005, Maejima et al. 2001). The synthesised endocannabinoids cross the postsynaptic membrane and the synaptic cleft (Chicca *et al.* 2012, Marsicano & Chaouloff 2012) and bind to presynaptically located CB1 (Domenici *et al.* 2006, Kawamura *et al.* 2006). Via their associated G-protein, activated CB1 receptors lead to the inhibition of both P/Q- as well as N-type voltage-gated Ca^{2+} channels (Guo & Ikeda 2004, Mackie & Hille 1992, Mackie *et al.* 1995, Twitchell *et al.* 1997, Lozovaya *et al.* 2009) and thus attenuate presynaptic transmitter release by reducing vesicle fusion (Chevaleyre *et al.* 2006, Castillo *et al.* 2012, Katona & Freund 2012, Ohno-Shosaku *et al.* 2012). Depending on whether the presynaptic transmitter exerts an inhibitory or an excitatory action on the postsynaptic neurone, this mechanism is called depolarisation-induced suppression of inhibition (DSI) (Wilson & Nicoll 2001, Ohno-Shosaku *et al.* 2001, Pitler & Alger 1992, Pitler & Alger 1994) or depolarisation-induced suppression of excitation (DSE) (Kreitzer & Regehr 2001). DSI has generally been described for GABAergic synapses, however recently also the possibility of a retrograde modulation of glycinergic synapses by endocannabinoids has been documented in rat and mouse hypoglossal neurones (Mukhtarov *et al.* 2005) and suggested for the rat LSO (Chi & Kandler 2012).

In addition to inhibiting voltage-gated Ca^{2+} channels (Mackie & Hille 1992, Mackie et al. 1995, Twitchell et al. 1997) in a G-protein coupled manner, CB1 receptors can also interact through their associated G-protein with G-protein-coupled inward rectifying K^+ (GIRK) channels (Henry & Chavkin 1995, Guo & Ikeda 2004, Bacci *et al.* 2004) and thereby alter the K^+ conductance of the neurone. By this mechanism, endocannabinoid signalling can decrease a neurone's resting membrane potential (Bacci et al. 2004) and thus alter its firing properties and computational output. Moreover, an endocannabinoid-dependent modulation of other types of K^+ channels has also been observed (Childers *et al.* 1993, Deadwyler *et al.* 1993, Deadwyler *et al.* 1995).

In addition to their action via the classical CB1 receptor, some endocannabinoids can also modulate other neurotransmitter receptors in various ways: AEA has been described to directly bind to

Transient Receptor Potential Vanilloid 1 (TRPV1) receptors in the brain, acting as an agonist there (Ross 2003, Puente *et al.* 2011, Chavez *et al.* 2010).

The endogenous cannabinoids AEA and 2-AG can also – in contrast to some synthetic CB1 agonists such as WIN 55,212-2 – directly bind to glycine receptors and modulate the current that they pass. Depending on the endocannabinoid type, its concentration, the glycine receptor composition and possibly also on the exact brain area, endocannabinoids can either decrease (Lozovaya *et al.* 2005, Lozovaya *et al.* 2011) or increase (Hejazi *et al.* 2006) glycine receptor mediated currents via this pathway.

The endocannabinoid system has been shown to interact directly and indirectly with a variety of other neurotransmitter systems, mainly by activation of metabotropic pathways. Often, activation of metabotropic receptors leads to an elevation in intracellular Ca^{2+} concentration, thus driving endocannabinoid synthesis. Thereby metabotropic receptors provide additional means to the conventional postsynaptic depolarisation to initiate endocannabinoid signalling (Kushmerick et al. 2004, Puente et al. 2011, Zhao *et al.* 2011, Gyombolai *et al.* 2012, Best & Regehr 2008, Hashimotodani et al. 2005).

In the auditory brainstem, endocannabinoid signalling has been extensively studied in the dorsal CN, where especially excitatory inputs by parallel fibres are modulated by endocannabinoids (Zhao et al. 2011, Zhao *et al.* 2009, Sedlacek *et al.* 2011) and long-term synaptic plasticity is adjusted by an interplay between the cholinergic and endocannabinoid system (Zhao & Tzounopoulos 2011). In the MNTB it has been reported that excitatory glutamateric neurotransmission from the calyx of Held is subject to CB1-dependent DSE, which can be elicited by activation of metabotropic glutamate receptors (Kushmerick et al. 2004). In the LSO immunohistochemical stainings have been published recently, which show CB1 localisation on the glycinergic terminals targeting the LSO (Chi & Kandler 2012).

In addition to modulating neuronal physiology, the endocannabinoid system has been shown to have an important impact on the development of neuronal morphology in various regions of the brain: Cerebellar Purkinje cells acquire longer and less branched dendrites when they are maintained in cell culture in the presence of a CB1 antagonist, compared to control conditions without a CB1 antagonist. Here GABAergic signalling shapes the morphology of developing dendrites in an endocannabinoid-dependent way (Kawaguchi *et al.* 2010). CB1 knock-out mice on the other hand show neurones in the motor cortex, which display a decreased dendritic field and a reduction in synapse number compared to wild-type littermates (Ballesteros-Yanez *et al.* 2007). Very recently it has been reported, that neural growth factor (NGF) can directly regulate endocannabinoid availability in the brain and thereby impact morphological development of the neurones (Keimpema *et al.* 2013).

Taken together – The endocannabinoid system can shape both neuronal physiology as well as morphology through a variety of different pathways and mechanisms, of which probably many more are yet to be discovered.

Metabolic maturation in neurones

In order to perform their task of computing and relaying information accurately, neurones require a lot of energy in the form of ATP. Glucose is the main metabolic substrate used for ATP generation in the mammalian brain. Other substrates such as lactate or ketone bodies can also be oxidised to yield energy (Castro *et al.* 2009, Dienel & Hertz 2001), however their use becomes more important during hypoglycaemia (Vannucci *et al.* 1981, Erecinska *et al.* 2004) and metabolic cooperation between neurones and astroglia (Allaman *et al.* 2011, Belanger *et al.* 2011). Glucose is transported into the brain by a process of facilitated diffusion through glucose transporters (GLUTs). Neurones of the central nervous system predominantly express the GLUT3 subtype (Vannucci *et al.* 1997). It has been demonstrated that GLUT3 expression generally rises in the third postnatal week, depending however on the exact brain region (Vannucci 1994). The up-regulation of GLUT3 appears to be rather tightly correlated to functional activity and neurotransmission, as it has also been predominantly localised to pre- and postsynaptic endings (Leino *et al.* 1997, Mantych *et al.* 1992, Ferreira *et al.* 2011). Lactate is taken up by monocarboxylate transporters (MCT) and can be converted to pyruvate via lactate dehydrogenase (LDH) or further to glucose via the Cori cycle.

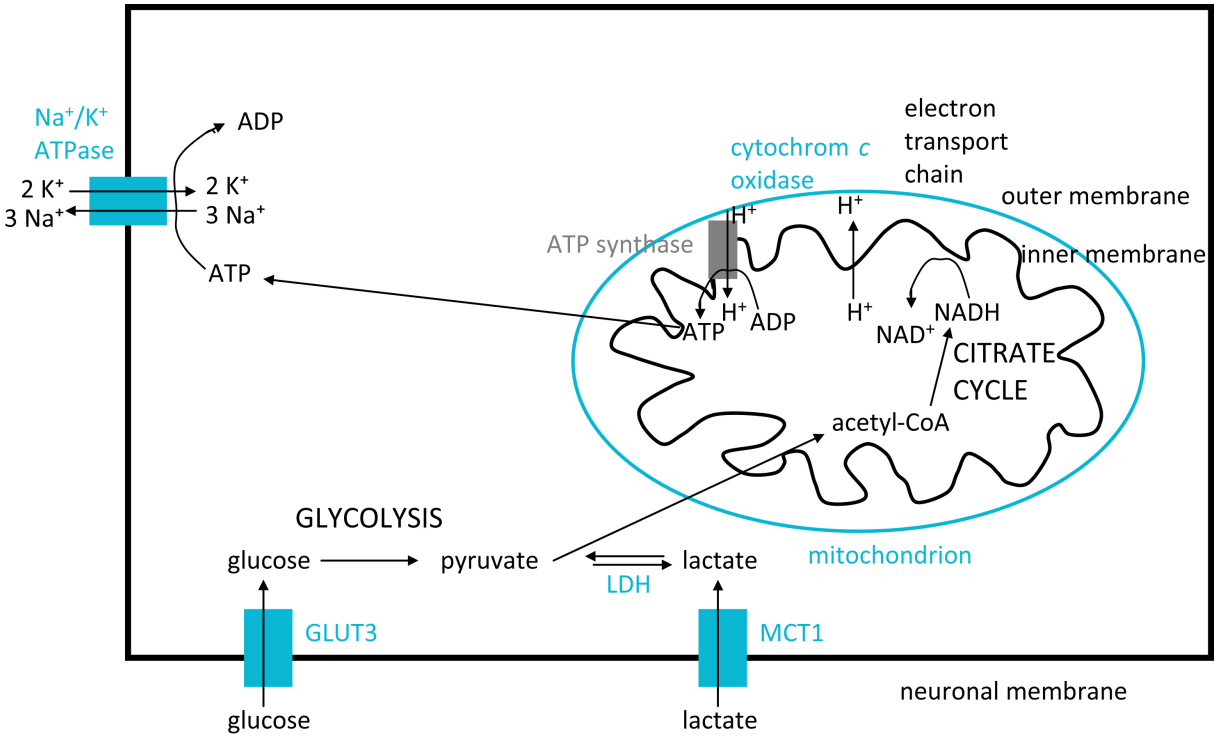

Figure 4. Overview of cellular ATP production and use

Neurones mainly use glucose as a substrate for ATP generation, which is taken up mostly via GLUT3 transporters into the cytoplasm, where glucose is metabolised to pyruvate in a process called glycolysis. Alternatively during hypoglycaemia or metabolic interaction with astrocytes, neurones can take up lactate through monocarboxylate transporter 1 (MCT1). Lactate can be converted to pyruvate by the lactate dehydrogenase (LDH) enzyme. Pyruvate is taken up into the mitochondria, where it is metabolised in the citric cycle and further via oxidative phosphorylation and the electron transport chain, which drive ATP synthesis. The cytochrome *c* oxidase catalyses an important step in this metabolic pathway. In neurones, most of the generated ATP is used by the Na^+/K^+ ATPase, an enzyme that sets the resting membrane potential through the establishment of Na^+ and K^+ gradients across the neuronal membrane.

The cellular energy equivalent ATP is produced in the mitochondrial oxidative phosphorylation (see Figure 4), where nutrients such as pyruvate are oxidised to generate an electron gradient across the mitochondrial membrane that is used to regenerate ATP from ADP. The cytochrome *c* oxidase (COX) is a mitochondrial enzyme crucially involved in this chain reaction of successive oxidations. Its activity can thus be used as a direct read-out of mitochondrial efficiency (Wong-Riley 1989, Kann

et al. 2003). In several nuclei of the central auditory system, such as the inferior colliculus and the cochlear nucleus, the activity and density of mitochondria have been shown to coincide with the functional onset of hearing in animals (Pysh 1970, Ryugo *et al.* 2006, Wong-Riley *et al.* 1978). Also in other brain areas neuronal and COX activity have been shown to highly correlate (Wong-Riley & Carroll 1984, Wong-Riley 1972).

The ATP produced in the mitochondria is used for cellular homeostasis processes, growth and mainly for generating neuronal activity. The Na^+/K^+ ATPase plays an important role in enabling neuronal excitation and firing as it maintains an asymmetric distribution of Na^+ and K^+ across the cell membrane at the expense of ATP hydrolysis (Skou 1957, Skou 1965). Thereby the cellular resting membrane potential, which is the basis for neuronal activity, can be set and restored. During high neuronal activity more than 50% of the cellular ATP is expended on ionic movements (Attwell & Laughlin 2001). The tight coupling between mitochondrial ATP production and ATP consumption by Na^+/K^+ ATPase activity in consequence of neuronal spiking ensures that the energy is not generated until it is actually spent (Erecinska et al. 2004). In line with this observation several studies have demonstrated that Na^+/K^+ ATPase activity increases during postnatal development with the fastest change during the period of active synaptogenesis (Fukuda & Prince 1992, Haglund *et al.* 1985). The pattern of activity rise coincides with that for development of mitochondria and augmentation of oxidative metabolism (Erecinska et al. 2004). If the functional sensory input is blocked, energy production goes down (Wong-Riley & Carroll 1984, Wong-Riley *et al.* 1989a, Wong-Riley *et al.* 1989b, Wong-Riley et al. 1978). This suggests that neuronal activity controls energy expenditure and not the other way around (Wong-Riley 1989). On the other hand, other scientists have suggested that the high metabolic demands of the brain limit neuronal activity and thereby favoured an evolution of energy efficient processes (Attwell & Laughlin 2001, Aiello & Wheeler 1995, Sarpeshkar 1998).

To calculate neuronal energy expenditure in a mathematical model, it is possible to relate neuronal metabolic processes to the energy required by the Na^+/K^+ ATPase for regeneration of the Na^+

gradient due to firing (Nawroth *et al.* 2007, Howarth *et al.* 2010, Howarth *et al.* 2012), since most of the cellular ATP is used for Na^+/K^+ ATPase activity (Attwell & Laughlin 2001). Several energetic components such as the maintenance of the resting membrane potential, the generation of action potentials and postsynaptic excitatory currents can be considered in this model. Since Na^+/K^+ ATPase activity is tightly linked to mitochondrial ATP production (Jorgensen *et al.* 2003, Erecinska et al. 2004) and glucose is the main substrate for ATP production in the mammalian brain, results of this model can be well compared to expression levels of metabolic markers described above and studied in my thesis (Trattner *et al.* 2013b).

References

Aiello, L. C. and Wheeler, P. (1995) The Expensive-Tissue Hypothesis: The Brain and the Digestive System in Human and Primate Evolution. *Current Anthropology*, 36, 199-221.

Alger, B. E. and Kim, J. (2011) Supply and demand for endocannabinoids. *Trends in neurosciences*, 34, 304-315.

Allaman, I., Belanger, M. and Magistretti, P. J. (2011) Astrocyte-neuron metabolic relationships: for better and for worse. *Trends Neurosci*, 34, 76-87.

Ashton, J. C., Friberg, D., Darlington, C. L. and Smith, P. F. (2006) Expression of the cannabinoid CB2 receptor in the rat cerebellum: an immunohistochemical study. *Neurosci Lett*, 396, 113-116.

Attwell, D. and Laughlin, S. B. (2001) An energy budget for signaling in the grey matter of the brain. *J Cereb Blood Flow Metab*, 21, 1133-1145.

Atwood, B. K. and Mackie, K. (2010) CB2: a cannabinoid receptor with an identity crisis. *Br J Pharmacol*, 160, 467-479.

Bacci, A., Huguenard, J. R. and Prince, D. A. (2004) Long-lasting self-inhibition of neocortical interneurons mediated by endocannabinoids. *Nature*, 431, 312-316.

Baek, J. H., Zheng, Y., Darlington, C. L. and Smith, P. F. (2008) Cannabinoid CB2 receptor expression in the rat brainstem cochlear and vestibular nuclei. *Acta Otolaryngol*, 128, 961-967.

Ballesteros-Yanez, I., Valverde, O., Ledent, C., Maldonado, R. and DeFelipe, J. (2007) Chronic cocaine treatment alters dendritic arborization in the adult motor cortex through a CB1 cannabinoid receptor-dependent mechanism. *Neuroscience*, 146, 1536-1545.

Belanger, M., Allaman, I. and Magistretti, P. J. (2011) Brain energy metabolism: focus on astrocyte-neuron metabolic cooperation. *Cell Metab*, 14, 724-738.

Best, A. R. and Regehr, W. G. (2008) Serotonin evokes endocannabinoid release and retrogradely suppresses excitatory synapses. *J Neurosci*, 28, 6508-6515.

Blaesse, P., Ehrhardt, S., Friauf, E. and Nothwang, H. G. (2005) Developmental pattern of three vesicular glutamate transporters in the rat superior olivary complex. *Cell Tissue Res*, 320, 33-50.

Boudreau, J. C. and Tsuchitani, C. (1968) Binaural interaction in the cat superior olive S segment. *J Neurophysiol*, 31, 442-454.

Brand, A., Behrend, O., Marquardt, T., McAlpine, D. and Grothe, B. (2002) Precise inhibition is essential for microsecond interaural time difference coding. *Nature*, 417, 543-547.

Brenowitz, S., David, J. and Trussell, L. (1998) Enhancement of synaptic efficacy by presynaptic GABA(B) receptors. *Neuron*, 20, 135-141.

Brugge, J. F. and Geisler, C. D. (1978) Auditory mechanisms of the lower brainstem. *Annu Rev Neurosci*, 1, 363-394.

Caird, D. and Klinke, R. (1983) Processing of binaural stimuli by cat superior olivary complex neurons. *Exp Brain Res*, 52, 385-399.

Castillo, P. E., Younts, T. J., Chavez, A. E. and Hashimotodani, Y. (2012) Endocannabinoid signaling and synaptic function. *Neuron*, 76, 70-81.

Castro, M. A., Beltran, F. A., Brauchi, S. and Concha, II (2009) A metabolic switch in brain: glucose and lactate metabolism modulation by ascorbic acid. *J Neurochem*, 110, 423-440.

Chavez, A. E., Chiu, C. Q. and Castillo, P. E. (2010) TRPV1 activation by endogenous anandamide triggers postsynaptic long-term depression in dentate gyrus. *Nat Neurosci*, 13, 1511-1518.

Chevaleyre, V., Takahashi, K. A. and Castillo, P. E. (2006) Endocannabinoid-mediated synaptic plasticity in the CNS. *Annu Rev Neurosci*, 29, 37-76.

Chi, D. H. and Kandler, K. (2012) Cannabinoid receptor expression at the MNTB-LSO synapse in developing rats. *Neurosci Lett*, 509, 96-100.

Chicca, A., Marazzi, J., Nicolussi, S. and Gertsch, J. (2012) Evidence for bidirectional endocannabinoid transport across cell membranes. *J Biol Chem*, 287, 34660-34682.

Childers, S. R., Pacheco, M. A., Bennett, B. A., Edwards, T. A., Hampson, R. E., Mu, J. and Deadwyler, S. A. (1993) Cannabinoid receptors: G-protein-mediated signal transduction mechanisms. *Biochem Soc Symp*, 59, 27-50.

Chirila, F. V., Rowland, K. C., Thompson, J. M. and Spirou, G. A. (2007) Development of gerbil medial superior olive: integration of temporally delayed excitation and inhibition at physiological temperature. *J Physiol*, 584, 167-190.

Deadwyler, S. A., Hampson, R. E., Bennett, B. A., Edwards, T. A., Mu, J., Pacheco, M. A., Ward, S. J. and Childers, S. R. (1993) Cannabinoids modulate potassium current in cultured hippocampal neurons. *Receptors Channels*, 1, 121-134.

Deadwyler, S. A., Hampson, R. E., Mu, J., Whyte, A. and Childers, S. (1995) Cannabinoids modulate voltage sensitive potassium A-current in hippocampal neurons via a cAMP-dependent process. *J Pharmacol Exp Ther*, 273, 734-743.

Di Marzo, V. (2011) Endocannabinoid signaling in the brain: biosynthetic mechanisms in the limelight. *Nature neuroscience*, 14, 9-15.

Dienel, G. A. and Hertz, L. (2001) Glucose and lactate metabolism during brain activation. *J Neurosci Res*, 66, 824-838.

Domenici, M. R., Azad, S. C., Marsicano, G., Schierloh, A., Wotjak, C. T., Dodt, H. U., Zieglgansberger, W., Lutz, B. and Rammes, G. (2006) Cannabinoid receptor type 1 located on presynaptic terminals of principal neurons in the forebrain controls glutamatergic synaptic transmission. *J Neurosci*, 26, 5794-5799.

Duch, C. and Levine, R. B. (2000) Remodeling of membrane properties and dendritic architecture accompanies the postembryonic conversion of a slow into a fast motoneuron. *J Neurosci*, 20, 6950-6961.

Erecinska, M., Cherian, S. and Silver, I. A. (2004) Energy metabolism in mammalian brain during development. *Prog Neurobiol*, 73, 397-445.

Ferreira, J. M., Burnett, A. L. and Rameau, G. A. (2011) Activity-dependent regulation of surface glucose transporter-3. *J Neurosci*, 31, 1991-1999.

Ford, M. C., Grothe, B. and Klug, A. (2009) Fenestration of the calyx of Held occurs sequentially along the tonotopic axis, is influenced by afferent activity, and facilitates glutamate clearance. *J Comp Neurol*, 514, 92-106.

Fukuda, A. and Prince, D. A. (1992) Postnatal development of electrogenic sodium pump activity in rat hippocampal pyramidal neurons. *Brain Res Dev Brain Res*, 65, 101-114.

Gillespie, D. C., Kim, G. and Kandler, K. (2005) Inhibitory synapses in the developing auditory system are glutamatergic. *Nat Neurosci*, 8, 332-338.

Goldberg, J. M. and Brown, P. B. (1969) Response of binaural neurons of dog superior olivary complex to dichotic tonal stimuli: some physiological mechanisms of sound localization. *J Neurophysiol*, 32, 613-636.

Grothe, B. (2003) New roles for synaptic inhibition in sound localization. *Nat Rev Neurosci*, 4, 540-550.

Grothe, B. and Koch, U. (2011) Dynamics of binaural processing in the mammalian sound localization pathway - The role of GABA(B) receptors. *Hear Res.*

Grothe, B., Pecka, M. and McAlpine, D. (2010) Mechanisms of sound localization in mammals. *Physiol Rev*, 90, 983-1012.

Guinan, J. J., Norris, B. E. and Guinan, S. S. (1972) Single Auditory Units in the Superior Olivary Complex: II: Locations of Unit Categories and Tonotopic Organization. *International Journal of Neuroscience*, 4, 147-166.

Guo, J. and Ikeda, S. R. (2004) Endocannabinoids modulate N-type calcium channels and G-protein-coupled inwardly rectifying potassium channels via CB1 cannabinoid receptors heterologously expressed in mammalian neurons. *Mol Pharmacol*, 65, 665-674.

Gyombolai, P., Pap, D., Turu, G., Catt, K. J., Bagdy, G. and Hunyady, L. (2012) Regulation of endocannabinoid release by G proteins: a paracrine mechanism of G protein-coupled receptor action. *Mol Cell Endocrinol*, 353, 29-36.

Haglund, M. M., Stahl, W. L., Kunkel, D. D. and Schwartzkroin, P. A. (1985) Developmental and regional differences in the localization of Na,K-ATPase activity in the rabbit hippocampus. *Brain Res*, 343, 198-203.

Harrison, J. M. and Feldman, M. L. (1970) Anatomical aspects of the cochlear nucleus and superior olivary complex. *Contrib Sens Physiol*, 4, 95-142.

Hashimotodani, Y., Ohno-Shosaku, T., Tsubokawa, H., Ogata, H., Emoto, K., Maejima, T., Araishi, K., Shin, H. S. and Kano, M. (2005) Phospholipase Cbeta serves as a coincidence detector

through its Ca2+ dependency for triggering retrograde endocannabinoid signal. *Neuron*, 45, 257-268.

Hassfurth, B., Grothe, B. and Koch, U. (2010) The mammalian interaural time difference detection circuit is differentially controlled by GABAB receptors during development. *J Neurosci*, 30, 9715-9727.

Heffner, R. S. and Heffner, H. E. (1988) Sound localization and use of binaural cues by the gerbil (Meriones unguiculatus). *Behav Neurosci*, 102, 422-428.

Hejazi, N., Zhou, C., Oz, M., Sun, H., Ye, J. H. and Zhang, L. (2006) Delta9-tetrahydrocannabinol and endogenous cannabinoid anandamide directly potentiate the function of glycine receptors. *Mol Pharmacol*, 69, 991-997.

Henry, D. J. and Chavkin, C. (1995) Activation of inwardly rectifying potassium channels (GIRK1) by co-expressed rat brain cannabinoid receptors in Xenopus oocytes. *Neurosci Lett*, 186, 91-94.

Herkenham, M., Lynn, A. B., Little, M. D., Johnson, M. R., Melvin, L. S., de Costa, B. R. and Rice, K. C. (1990) Cannabinoid receptor localization in brain. *Proc Natl Acad Sci U S A*, 87, 1932-1936.

Hermann, J., Pecka, M., von Gersdorff, H., Grothe, B. and Klug, A. (2007) Synaptic transmission at the calyx of Held under in vivo like activity levels. *J Neurophysiol*, 98, 807-820.

Hoffpauir, B. K., Grimes, J. L., Mathers, P. H. and Spirou, G. A. (2006) Synaptogenesis of the calyx of Held: rapid onset of function and one-to-one morphological innervation. *J Neurosci*, 26, 5511-5523.

Howarth, C., Gleeson, P. and Attwell, D. (2012) Updated energy budgets for neural computation in the neocortex and cerebellum. *J Cereb Blood Flow Metab*.

Howarth, C., Peppiatt-Wildman, C. M. and Attwell, D. (2010) The energy use associated with neural computation in the cerebellum. *J Cereb Blood Flow Metab*, 30, 403-414.

Jorgensen, P. L., Hakansson, K. O. and Karlish, S. J. (2003) Structure and mechanism of Na,K-ATPase: functional sites and their interactions. *Annu Rev Physiol*, 65, 817-849.

Joris, P. X., Carney, L. H., Smith, P. H. and Yin, T. C. (1994a) Enhancement of neural synchronization in the anteroventral cochlear nucleus. I. Responses to tones at the characteristic frequency. *J Neurophysiol*, 71, 1022-1036.

Joris, P. X., Smith, P. H. and Yin, T. C. (1994b) Enhancement of neural synchronization in the anteroventral cochlear nucleus. II. Responses in the tuning curve tail. *J Neurophysiol*, 71, 1037-1051.

Kaiser, A., Alexandrova, O. and Grothe, B. (2011) Urocortin-expressing olivocochlear neurons exhibit tonotopic and developmental changes in the auditory brainstem and in the innervation of the cochlea. *J Comp Neurol*, 519, 2758-2778.

Kakazu, Y., Akaike, N., Komiyama, S. and Nabekura, J. (1999) Regulation of intracellular chloride by cotransporters in developing lateral superior olive neurons. *J Neurosci*, 19, 2843-2851.

Kandler, K., Clause, A. and Noh, J. (2009) Tonotopic reorganization of developing auditory brainstem circuits. *Nat Neurosci*, 12, 711-717.

Kandler, K. and Friauf, E. (1995a) Development of electrical membrane properties and discharge characteristics of superior olivary complex neurons in fetal and postnatal rats. *Eur J Neurosci*, 7, 1773-1790.

Kandler, K. and Friauf, E. (1995b) Development of glycinergic and glutamatergic synaptic transmission in the auditory brainstem of perinatal rats. *J Neurosci*, 15, 6890-6904.

Kann, O., Schuchmann, S., Buchheim, K. and Heinemann, U. (2003) Coupling of neuronal activity and mitochondrial metabolism as revealed by NAD(P)H fluorescence signals in organotypic hippocampal slice cultures of the rat. *Neuroscience*, 119, 87-100.

Kapfer, C., Seidl, A. H., Schweizer, H. and Grothe, B. (2002) Experience-dependent refinement of inhibitory inputs to auditory coincidence-detector neurons. *Nat Neurosci*, 5, 247-253.

Katona, I. and Freund, T. F. (2012) Multiple functions of endocannabinoid signaling in the brain. *Annu Rev Neurosci*, 35, 529-558.

Kawaguchi, K., Habara, T., Terashima, T. and Kikkawa, S. (2010) GABA modulates development of cerebellar Purkinje cell dendrites under control of endocannabinoid signaling. *J Neurochem*, 114, 627-638.

Kawamura, Y., Fukaya, M., Maejima, T., Yoshida, T., Miura, E., Watanabe, M., Ohno-Shosaku, T. and Kano, M. (2006) The CB1 cannabinoid receptor is the major cannabinoid receptor at excitatory presynaptic sites in the hippocampus and cerebellum. *J Neurosci*, 26, 2991-3001.

Keimpema, E., Tortoriello, G., Alpar, A. et al. (2013) Nerve growth factor scales endocannabinoid signaling by regulating monoacylglycerol lipase turnover in developing cholinergic neurons. *Proc Natl Acad Sci U S A*, 110, 1935-1940.

Kil, J., Kageyama, G. H., Semple, M. N. and Kitzes, L. M. (1995) Development of ventral cochlear nucleus projections to the superior olivary complex in gerbil. *J Comp Neurol*, 353, 317-340.

Kim, G. and Kandler, K. (2003) Elimination and strengthening of glycinergic/GABAergic connections during tonotopic map formation. *Nat Neurosci*, 6, 282-290.

Kim, G. and Kandler, K. (2010) Synaptic changes underlying the strengthening of GABA/glycinergic connections in the developing lateral superior olive. *Neuroscience*, 171, 924-933.

Kiss, A. and Majorossy, K. (1983) Neuron morphology and synaptic architecture in the medial superior olivary nucleus. Light- and electron microscope studies in the cat. *Exp Brain Res*, 52, 315-327.

Kotak, V. C., Korada, S., Schwartz, I. R. and Sanes, D. H. (1998) A developmental shift from GABAergic to glycinergic transmission in the central auditory system. *J Neurosci*, 18, 4646-4655.

Kreitzer, A. C. and Regehr, W. G. (2001) Retrograde inhibition of presynaptic calcium influx by endogenous cannabinoids at excitatory synapses onto Purkinje cells. *Neuron*, 29, 717-727.

Kushmerick, C., Price, G. D., Taschenberger, H., Puente, N., Renden, R., Wadiche, J. I., Duvoisin, R. M., Grandes, P. and von Gersdorff, H. (2004) Retroinhibition of presynaptic Ca2+ currents by endocannabinoids released via postsynaptic mGluR activation at a calyx synapse. *J Neurosci*, 24, 5955-5965.

Leino, R. L., Gerhart, D. Z., van Bueren, A. M., McCall, A. L. and Drewes, L. R. (1997) Ultrastructural localization of GLUT 1 and GLUT 3 glucose transporters in rat brain. *J Neurosci Res*, 49, 617-626.

Liu, J., Wang, L., Harvey-White, J. et al. (2006) A biosynthetic pathway for anandamide. *Proc Natl Acad Sci U S A*, 103, 13345-13350.

London, M. and Hausser, M. (2005) Dendritic computation. *Annu Rev Neurosci*, 28, 503-532.

Lozovaya, N., Min, R., Tsintsadze, V. and Burnashev, N. (2009) Dual modulation of CNS voltage-gated calcium channels by cannabinoids: Focus on CB1 receptor-independent effects. *Cell Calcium*, 46, 154–162.

Lozovaya, N., Mukhtarov, M., Tsintsadze, T., Ledent, C., Burnashev, N. and Bregestovski, P. (2011) Frequency-Dependent Cannabinoid Receptor-Independent Modulation of Glycine Receptors by Endocannabinoid 2-AG. *Front Mol Neurosci*, 4, 13.

Lozovaya, N., Yatsenko, N., Beketov, A., Tsintsadze, T. and Burnashev, N. (2005) Glycine receptors in CNS neurons as a target for nonretrograde action of cannabinoids. *J Neurosci*, 25, 7499-7506.

Mackie, K. and Hille, B. (1992) Cannabinoids inhibit N-type calcium channels in neuroblastoma-glioma cells. *Proc Natl Acad Sci U S A*, 89, 3825-3829.

Mackie, K., Lai, Y., Westenbroek, R. and Mitchell, R. (1995) Cannabinoids activate an inwardly rectifying potassium conductance and inhibit Q-type calcium currents in AtT20 cells transfected with rat brain cannabinoid receptor. *J Neurosci*, 15, 6552-6561.

Maejima, T., Hashimoto, K., Yoshida, T., Aiba, A. and Kano, M. (2001) Presynaptic inhibition caused by retrograde signal from metabotropic glutamate to cannabinoid receptors. *Neuron*, 31, 463-475.

Magnusson, A. K., Kapfer, C., Grothe, B. and Koch, U. (2005) Maturation of glycinergic inhibition in the gerbil medial superior olive after hearing onset. *J Physiol*, 568, 497-512.

Magnusson, A. K., Park, T. J., Pecka, M., Grothe, B. and Koch, U. (2008) Retrograde GABA signaling adjusts sound localization by balancing excitation and inhibition in the brainstem. *Neuron*, 59, 125-137.

Mantych, G. J., James, D. E., Chung, H. D. and Devaskar, S. U. (1992) Cellular localization and characterization of Glut 3 glucose transporter isoform in human brain. *Endocrinology*, 131, 1270-1278.

Marsicano, G. and Chaouloff, F. (2012) Moving bliss: a new anandamide transporter. *Nat Neurosci*, 15, 5-6.

Mc Laughlin, M., van der Heijden, M. and Joris, P. X. (2008) How secure is in vivo synaptic transmission at the calyx of Held? *J Neurosci*, 28, 10206-10219.

McAlpine, D., Jiang, D. and Palmer, A. R. (2001) A neural code for low-frequency sound localization in mammals. *Nat Neurosci*, 4, 396-401.

Meseke, M., Evers, J. F. and Duch, C. (2009) Developmental changes in dendritic shape and synapse location tune single-neuron computations to changing behavioral functions. *J Neurophysiol*, 102, 41-58.

Moore, M. J. and Caspary, D. M. (1983) Strychnine blocks binaural inhibition in lateral superior olivary neurons. *J Neurosci*, 3, 237-242.

Morest, D. K. (1968a) The collateral system of the medial nucleus of the trapezoid body of the cat, its neuronal architecture and relation to the olivo-cochlear bundle. *Brain Res*, 9, 288-311.

Morest, D. K. (1968b) The growth of synaptic endings in the mammalian brain: a study of the calyces of the trapezoid body. *Z Anat Entwicklungsgesch*, 127, 201-220.

Mukhtarov, M., Ragozzino, D. and Bregestovski, P. (2005) Dual Ca2+ modulation of glycinergic synaptic currents in rodent hypoglossal motoneurones. *J Physiol*, 569, 817-831.

Muller, M. (1990) Quantitative comparison of frequency representation in the auditory brainstem nuclei of the gerbil, Pachyuromys duprasi. *Exp Brain Res*, 81, 140-149.

Nawroth, J. C., Greer, C. A., Chen, W. R., Laughlin, S. B. and Shepherd, G. M. (2007) An energy budget for the olfactory glomerulus. *J Neurosci*, 27, 9790-9800.

Ohno-Shosaku, T., Maejima, T. and Kano, M. (2001) Endogenous cannabinoids mediate retrograde signals from depolarized postsynaptic neurons to presynaptic terminals. *Neuron*, 29, 729-738.

Ohno-Shosaku, T., Tanimura, A., Hashimotodani, Y. and Kano, M. (2012) Endocannabinoids and retrograde modulation of synaptic transmission. *Neuroscientist*, 18, 119-132.

Park, T. J., Grothe, B., Pollak, G. D., Schuller, G. and Koch, U. (1996) Neural delays shape selectivity to interaural intensity differences in the lateral superior olive. *J Neurosci*, 16, 6554-6566.

Pecka, M., Brand, A., Behrend, O. and Grothe, B. (2008) Interaural time difference processing in the mammalian medial superior olive: the role of glycinergic inhibition. *J Neurosci*, 28, 6914-6925.

Pitler, T. A. and Alger, B. E. (1992) Postsynaptic spike firing reduces synaptic GABAA responses in hippocampal pyramidal cells. *J Neurosci*, 12, 4122-4132.

Pitler, T. A. and Alger, B. E. (1994) Depolarization-induced suppression of GABAergic inhibition in rat hippocampal pyramidal cells: G protein involvement in a presynaptic mechanism. *Neuron*, 13, 1447-1455.

Puente, N., Cui, Y., Lassalle, O., Lafourcade, M., Georges, F., Venance, L., Grandes, P. and Manzoni, O. J. (2011) Polymodal activation of the endocannabinoid system in the extended amygdala. *Nat Neurosci*, 14, 1542-1547.

Pysh, J. J. (1970) Mitochondrial changes in rat inferior colliculus during postnatal development: an electron microscopic study. *Brain Res*, 18, 325-342.

Rall, W., Burke, R. E., Holmes, W. R., Jack, J. J., Redman, S. J. and Segev, I. (1992) Matching dendritic neuron models to experimental data. *Physiol Rev*, 72, S159-186.

Rautenberg, P. L., Grothe, B. and Felmy, F. (2009) Quantification of the three-dimensional morphology of coincidence detector neurons in the medial superior olive of gerbils during late postnatal development. *J Comp Neurol*, 517, 385-396.

Rayleigh, L. and Strutt, J. (1907) XII. On our perception of sound direction. *Philosophical Magazine Series 6*, 13, 214-232.

Rietzel, H. J. and Friauf, E. (1998) Neuron types in the rat lateral superior olive and developmental changes in the complexity of their dendritic arbors. *J Comp Neurol*, 390, 20-40.

Rodriguez-Contreras, A., de Lange, R. P., Lucassen, P. J. and Borst, J. G. (2006) Branching of calyceal afferents during postnatal development in the rat auditory brainstem. *J Comp Neurol*, 496, 214-228.

Rogowski, B. A. and Feng, A. S. (1981) Normal postnatal development of medial superior olivary neurons in the albino rat: a Golgi and Nissl study. *J Comp Neurol*, 196, 85-97.

Ross, R. A. (2003) Anandamide and vanilloid TRPV1 receptors. *Br J Pharmacol*, 140, 790-801.

Ryugo, D. K., Montey, K. L., Wright, A. L., Bennett, M. L. and Pongstaporn, T. (2006) Postnatal development of a large auditory nerve terminal: the endbulb of Held in cats. *Hear Res*, 216-217, 100-115.

Sanes, D. H. (1990) An in vitro analysis of sound localization mechanisms in the gerbil lateral superior olive. *J Neurosci*, 10, 3494-3506.

Sanes, D. H. and Friauf, E. (2000) Development and influence of inhibition in the lateral superior olivary nucleus. *Hear Res*, 147, 46-58.

Sanes, D. H., Song, J. and Tyson, J. (1992) Refinement of dendritic arbors along the tonotopic axis of the gerbil lateral superior olive. *Brain Res Dev Brain Res*, 67, 47-55.

Sarpeshkar, R. (1998) Analog versus digital: extrapolating from electronics to neurobiology. *Neural Comput*, 10, 1601-1638.

Scott, L. L., Mathews, P. J. and Golding, N. L. (2005) Posthearing developmental refinement of temporal processing in principal neurons of the medial superior olive. *J Neurosci*, 25, 7887-7895.

Sedlacek, M., Tipton, P. W. and Brenowitz, S. D. (2011) Sustained firing of cartwheel cells in the dorsal cochlear nucleus evokes endocannabinoid release and retrograde suppression of parallel fiber synapses. *J Neurosci*, 31, 15807-15817.

Seidl, A. H. and Grothe, B. (2005) Development of sound localization mechanisms in the mongolian gerbil is shaped by early acoustic experience. *J Neurophysiol*, 94, 1028-1036.

Skou, J. C. (1957) The influence of some cations on an adenosine triphosphatase from peripheral nerves. *Biochim Biophys Acta*, 23, 394-401.

Skou, J. C. (1965) Enzymatic Basis for Active Transport of Na+ and K+ across Cell Membrane. *Physiol Rev*, 45, 596-617.

Smith, A. J., Owens, S. and Forsythe, I. D. (2000) Characterisation of inhibitory and excitatory postsynaptic currents of the rat medial superior olive. *J Physiol*, 529 Pt 3, 681-698.

Stotler, W. A. (1953) An experimental study of the cells and connections of the superior olivary complex of the cat. *J Comp Neurol*, 98, 401-431.

Thompson, A. M. and Schofield, B. R. (2000) Afferent projections of the superior olivary complex. *Microsc Res Tech*, 51, 330-354.

Thompson, S. P. (1882) LI. On the function of the two ears in the perception of space. *Philosophical Magazine Series 5*, 13, 406-416.

Trattner, B., Berner, S., Grothe, B. and Kunz, L. (2013a) Depolarisation-induced suppression of a glycinergic synapse in the superior olivary complex by endocannabinoids. *J Neurochem.*

Trattner, B., Gravot, C. M., Grothe, B. and Kunz, L. (2013b) Metabolic Maturation of Auditory Neurones in the Superior Olivary Complex. *PLoS One*, 8, e67351.

Tritsch, N. X. and Bergles, D. E. (2010) Developmental regulation of spontaneous activity in the Mammalian cochlea. *J Neurosci*, 30, 1539-1550.

Tritsch, N. X., Yi, E., Gale, J. E., Glowatzki, E. and Bergles, D. E. (2007) The origin of spontaneous activity in the developing auditory system. *Nature*, 450, 50-55.

Twitchell, W., Brown, S. and Mackie, K. (1997) Cannabinoids inhibit N- and P/Q-type calcium channels in cultured rat hippocampal neurons. *J Neurophysiol*, 78, 43-50.

Ueda, N., Tsuboi, K., Uyama, T. and Ohnishi, T. (2011) Biosynthesis and degradation of the endocannabinoid 2-arachidonoylglycerol. *Biofactors*, 37, 1-7.

Vannucci, R. C., Nardis, E. E., Vannucci, S. J. and Campbell, P. A. (1981) Cerebral carbohydrate and energy metabolism during hypoglycemia in newborn dogs. *Am J Physiol*, 240, R192-199.

Vannucci, S. J. (1994) Developmental expression of GLUT1 and GLUT3 glucose transporters in rat brain. *J Neurochem*, 62, 240-246.

Vannucci, S. J., Maher, F. and Simpson, I. A. (1997) Glucose transporter proteins in brain: delivery of glucose to neurons and glia. *Glia*, 21, 2-21.

Walcher, J., Hassfurth, B., Grothe, B. and Koch, U. (2011) Comparative post-hearing development of inhibitory inputs to the lateral superior olive in gerbils and mice. *J Neurophysiol.*

Werthat, F., Alexandrova, O., Grothe, B. and Koch, U. (2008) Experience-dependent refinement of the inhibitory axons projecting to the medial superior olive. *Dev Neurobiol*, 68, 1454-1462.

Wilson, R. I. and Nicoll, R. A. (2001) Endogenous cannabinoids mediate retrograde signalling at hippocampal synapses. *Nature*, 410, 588-592.

Womack, M. and Khodakhah, K. (2002) Active contribution of dendrites to the tonic and trimodal patterns of activity in cerebellar Purkinje neurons. *J Neurosci*, 22, 10603-10612.

Wong-Riley, M. and Carroll, E. W. (1984) Effect of impulse blockage on cytochrome oxidase activity in monkey visual system. *Nature*, 307, 262-264.

Wong-Riley, M. T. (1972) Changes in the dorsal lateral geniculate nucleus of the squirrel monkey after unilateral ablation of the visual cortex. *J Comp Neurol*, 146, 519-548.

Wong-Riley, M. T. (1989) Cytochrome oxidase: an endogenous metabolic marker for neuronal activity. *Trends Neurosci*, 12, 94-101.

Wong-Riley, M. T., Merzenich, M. M. and Leake, P. A. (1978) Changes in endogenous enzymatic reactivity to DAB induced by neuronal inactivity. *Brain Res*, 141, 185-192.

Wong-Riley, M. T., Tripathi, S. C., Trusk, T. C. and Hoppe, D. A. (1989a) Effect of retinal impulse blockage on cytochrome oxidase-rich zones in the macaque striate cortex: I. Quantitative electron-microscopic (EM) analysis of neurons. *Vis Neurosci*, 2, 483-497.

Wong-Riley, M. T., Trusk, T. C., Tripathi, S. C. and Hoppe, D. A. (1989b) Effect of retinal impulse blockage on cytochrome oxidase-rich zones in the macaque striate cortex: II. Quantitative electron-microscopic (EM) analysis of neuropil. *Vis Neurosci*, 2, 499-514.

Woolf, N. K. and Ryan, A. F. (1984) The development of auditory function in the cochlea of the mongolian gerbil. *Hear Res*, 13, 277-283.

Zhao, Y., Rubio, M. and Tzounopoulos, T. (2011) Mechanisms underlying input-specific expression of endocannabinoid-mediated synaptic plasticity in the dorsal cochlear nucleus. *Hear Res*.

Zhao, Y., Rubio, M. E. and Tzounopoulos, T. (2009) Distinct functional and anatomical architecture of the endocannabinoid system in the auditory brainstem. *J Neurophysiol*, 101, 2434-2446.

Zhao, Y. and Tzounopoulos, T. (2011) Physiological Activation of Cholinergic Inputs Controls Associative Synaptic Plasticity via Modulation of Endocannabinoid Signaling. *J Neurosci*, 31, 3158-3168.

Aim of this thesis

During my PhD thesis, I investigated several functional and developmental aspects of the auditory brainstem. The aims of my thesis were:

(1) To describe the physiological development and the functional consequences of endocannabinoid signalling in the medial and lateral superior olive (MSO and LSO, respectively) in the auditory brainstem of the Mongolian gerbil (*Meriones unguiculatus*). To this extent I sought to answer the following questions: Is a functional endocannabinoid system present in these nuclei and if so, what are the physiological consequences of its activity? I investigated the expression of cannabinoid receptors and enzymes by means of immunohistochemistry and characterised the underlying physiology with patch-clamp recordings throughout a developmental window from before hearing onset until auditory maturity of the experimental animal. Additionally I studied the influence of the endocannabinoid system on the morphological development of MSO neurones, which is crucial for correctly performing the task of sound localisation, and whether endocannabinoid action on morphological development could affect neuronal signal processing.

(2) To describe the metabolic maturation of several important nuclei in the auditory brainstem, namely the MSO, LSO and the medial nucleus of the trapezoid body (MNTB). These specialised neurones are supposed to have a high energy demand to exert their function based on their neuronal specialisations and I was interested in whether their metabolic requirements were affected by the onset of hearing. In this context I carried out immunohistochemical and histological stainings of metabolic markers in these nuclei and quantified their abundance and expression patterns throughout postnatal development.

List of publications

- Barbara Trattner, Céline Marie Gravot, Benedikt Grothe and Lars Kunz; Metabolic Maturation of Auditory Neurones in the Superior Olivary Complex; in: PLOS ONE 8 (6), 2013, e67351
- Barbara Trattner, Sarah Berner, Benedikt Grothe and Lars Kunz; Depolarisation-induced suppression of a glycinergic synapse in the superior olivary complex by endocannabinoids; in: Journal of Neurochemistry; accepted July 2013

Abstracts

Metabolic Maturation of Auditory Neurones in the Superior Olivary Complex

Barbara Trattner, Céline Marie Gravot, Benedikt Grothe & Lars Kunz

PLOS ONE 8 (6), 2013, e67351

Neuronal activity is energetically costly, but despite its importance, energy production and consumption has been studied in only a few neurone types. Neuroenergetics is of special importance in auditory brainstem nuclei, where neurones exhibit various biophysical adaptations for extraordinary temporal precision, and show particularly high firing rates. We have studied the development of energy metabolism in three principal nuclei of the superior olivary complex (SOC) involved in precise binaural processing in the Mongolian gerbil (*Meriones unguiculatus*). We used immunohistochemistry to quantify metabolic markers for energy consumption (Na^+/K^+-ATPase) and production (mitochondria, cytochrome c oxidase activity and glucose transporter 3 (GLUT3)). In addition, we calculated neuronal ATP consumption for different postnatal ages (P0-90) based upon published electrophysiological and morphological data. Our calculations relate neuronal processes to the regeneration of Na^+ gradients perturbed by neuronal firing, and thus to ATP consumption by Na^+/K^+-ATPase. The developmental changes of calculated energy consumption closely resemble those of metabolic markers. Both increase before and after hearing onset occuring at P12-13 and reach a plateau thereafter. The increase in Na^+/K^+-ATPase and mitochondria precedes the rise in GLUT3 levels and is already substantial before hearing onset, whilst GLUT3 levels are scarcely detectable at this age. Based on

these findings we assume that auditory inputs crucially contribute to metabolic maturation. In one nucleus, the medial nucleus of the trapezoid body (MNTB), the initial rise in marker levels and calculated ATP consumption occurs distinctly earlier than in the other nuclei investigated, and is almost completed by hearing onset. Our study shows that the mathematical model used is applicable to brainstem neurones. Energy consumption varies markedly between SOC nuclei with their different neuronal properties. Especially for the medial superior olive (MSO), we propose that temporally precise input integration is energetically more costly than the high firing frequencies typical for all SOC nuclei.

Depolarization-induced suppression of a glycinergic synapse in the superior olivary complex by endocannabinoids

Barbara Trattner, Sarah Berner, Benedikt Grothe & Lars Kunz

Journal of Neurochemistry; accepted July 2013

The neuronal endocannabinoid system is known to depress synaptic inputs retrogradely in an activity-dependent manner. This mechanism was generally described for excitatory glutamatergic and inhibitory GABAergic synapses. Here we report that neurones in the auditory brainstem of the Mongolian gerbil (*Meriones unguiculatus*) retrogradely regulate the strength of their inputs via the endocannabinoid system. By means of whole-cell patch-clamp recordings we found that retrograde endocannabinoid signalling attenuates both glycinergic and glutamatergic postsynaptic currents in the same types of neurones. In accordance, we detected the cannabinoid receptor 1 (CB1) at excitatory and inhibitory pre-synapses as well as the endocannabinoid-synthesising enzymes (diacylglycerol lipase α/β, DAGLα/β) postsynaptically by immunohistochemical stainings. Our study was performed with animals aged 10-15 days, i.e. during the time window around the onset of hearing. Therefore, we suggest that retrograde endocannabinoid signalling has a part in adapting inputs during the functionally important switch from spontaneously generated to sound-related signals.

The role of the endocannabinoid system in morphological development of neurones in the medial superior olive

Barbara Trattner, Alexandra Klein, Lara Jansen, Michael Stransky, Philipp Rautenberg, Benedikt Grothe & Lars Kunz

Unpublished manuscript

The medial superior olive (MSO) is an auditory brainstem nucleus, which is responsible for the precise extraction of interaural time differences (ITDs) to enable sound source localization in low-frequency hearing mammals. To perform this functionally highly relevant task, these neurons rely on their exactly shaped morphology. Recently, we demonstrated the anatomical presence and physiological functionality of the endocannabinoid system in MSO neurons of the Mongolian gerbil (*Meriones unguiculatus*) (Trattner *et al.*, 2013). This rodent possesses a similar frequency coverage and anatomical organization of the auditory system as humans. Now we investigated how endocannabinoids are involved in shaping the morphology of MSO neurons during development. By administration of a cannabinoid receptor 1 (CB1) agonist and antagonist to pregnant and lactating females, respectively, the fetuses and pups received the substances for one week via the placenta and for another two weeks via the mothers' milk. By subsequent dye-electroporation or Golgi-staining of MSO neurons, we visualized morphological differences resulting from an over-stimulation or a blockage of the endocannabinoid system. We could show that neurons from animals treated with CB1 antagonists possessed on average a higher surface area, bigger volume, bigger mean cross section area, as well as changes in the soma proportions and dendritic arborisation. A conductance-based computational model showed that these morphological differences could lead to changes in the biophysical

computation of the neurons. We found that already the passive membrane properties such as input resistance and action potential threshold are to a great extent altered by the induced morphological changes.

Postsynaptic endocannabinoid signalling modulates responses of adult MSO neurones

Barbara Trattner, Benedikt Grothe & Lars Kunz

Unpublished manuscript

The neuronal endocannabinoid system (ECS) is generally known for retrograde depression of synaptic inputs via presynaptic cannabinoid receptor 1 (CB1). In this study, however, we report that in the medial superior olive (MSO) of the Mongolian Gerbil (*Meriones unguiculatus*), a brainstem nucleus involved in computing sound localisation, a shift in the expression and functionality of the ECS occurs during auditory development. We previously observed that during the time of hearing onset retrograde endocannabinoid signalling coincides with presynaptic CB1 localisation. After hearing onset the auditory system undergoes a so-called refinement period, during which connections are fine-tuned to the auditory environment. We discovered that after refinement CB1 is localised postsynaptically, whereas endocannabinoid-synthesising enzymes are still expressed in postsynaptic somata and dendrites. Using patch-clamp electrophysiological recordings we found that endocannabinoids on one hand directly act on glycine receptors, depressing their currents, and on the other hand lead to neuronal hyperpolarisation in a CB1-dependent way. Our results suggest that this hyperpolarisation could be mediated by a GIRK conductance, activated by the G-protein coupled to CB1. We could elicit hyperpolarisation by CB1 agonist administration, high neuronal stimulation and/or mGluR1 agonism, which indicates that various mechanisms can trigger endocannabinoid synthesis. Functionally these modulations exerted by the ECS could have a huge impact on the computational properties of MSO neurones, since these neurones rely on precise glycinergic inhibition to allow the

integration of physiologically relevant auditory stimuli. In this way the ECS could have a function in adapting the auditory system to changing acoustic environments.

OPEN ACCESS Freely available online

PLOS ONE

Metabolic Maturation of Auditory Neurones in the Superior Olivary Complex

Barbara Trattner[1,2]*, Céline Marie Gravot[1,2], Benedikt Grothe[1], Lars Kunz[1]*

1 Department of Biology II, Division of Neurobiology, Ludwig Maximilians University Munich, Martinsried, Germany, **2** Graduate School of Systemic Neurosciences, Ludwig Maximilians University Munich, Martinsried, Germany

Abstract

Neuronal activity is energetically costly, but despite its importance, energy production and consumption have been studied in only a few neurone types. Neuroenergetics is of special importance in auditory brainstem nuclei, where neurones exhibit various biophysical adaptations for extraordinary temporal precision and show particularly high firing rates. We have studied the development of energy metabolism in three principal nuclei of the superior olivary complex (SOC) involved in precise binaural processing in the Mongolian gerbil (*Meriones unguiculatus*). We used immunohistochemistry to quantify metabolic markers for energy consumption (Na^+/K^+-ATPase) and production (mitochondria, cytochrome c oxidase activity and glucose transporter 3 (GLUT3)). In addition, we calculated neuronal ATP consumption for different postnatal ages (P0–90) based upon published electrophysiological and morphological data. Our calculations relate neuronal processes to the regeneration of Na^+ gradients perturbed by neuronal firing, and thus to ATP consumption by Na^+/K^+-ATPase. The developmental changes of calculated energy consumption closely resemble those of metabolic markers. Both increase before and after hearing onset occurring at P12–13 and reach a plateau thereafter. The increase in Na^+/K^+-ATPase and mitochondria precedes the rise in GLUT3 levels and is already substantial before hearing onset, whilst GLUT3 levels are scarcely detectable at this age. Based on these findings we assume that auditory inputs crucially contribute to metabolic maturation. In one nucleus, the medial nucleus of the trapezoid body (MNTB), the initial rise in marker levels and calculated ATP consumption occurs distinctly earlier than in the other nuclei investigated, and is almost completed by hearing onset. Our study shows that the mathematical model used is applicable to brainstem neurones. Energy consumption varies markedly between SOC nuclei with their different neuronal properties. Especially for the medial superior olive (MSO), we propose that temporally precise input integration is energetically more costly than the high firing frequencies typical for all SOC nuclei.

Citation: Trattner B, Gravot CM, Grothe B, Kunz L (2013) Metabolic Maturation of Auditory Neurones in the Superior Olivary Complex. PLoS ONE 8(6): e67351. doi:10.1371/journal.pone.0067351

Editor: Maurice J. Chacron, McGill University, Canada

Received January 16, 2013; **Accepted** May 16, 2013; **Published** June 27, 2013

Funding: The authors thank the Graduate School of Systemic Neurosciences (GSN-LMU; http://www.gsn.uni-muenchen.de/index.html) and the Graduate School 1373 (DFG; http://www.dfg.de/en/index.jsp) for providing a grant to BT. This work was largely funded by the DFG (CRC870/TPB13; http://www.dfg.de/en/index.jsp). The funders had no role in study design, data collection and analysis, decision to publish, or preparation of the manuscript.

Competing Interests: The authors have declared that no competing interests exist.

* E-mail: trattner@bio.lmu.de (BT); lars.kunz@bio.lmu.de (LK)

Introduction

In spite of the importance of energetics for neuronal function, very few studies have addressed the relationship between neuronal energy supply and metabolic demands [1,2,3]. Quantitative studies, which have been published so far, focussed mainly on the cerebellum, the cerebral cortex and the olfactory glomerulus [4,5,6,7], but neurones in brainstem nuclei have not yet been investigated in this context. The neurones of the superior olivary complex (SOC) in the mammalian auditory brainstem, which are responsible for localising sounds in space, exhibit various biophysical adaptations (e.g. a very low input resistance) that facilitate fast and temporally accurate auditory processing and display some of the highest firing rates in the brain. These neurones are, therefore, of special interest from the standpoint of neuroenergetics, as also measurements by Sokoloff and colleagues revealed high rates of glucose utilisation in auditory nuclei (for a review see [8]).

We have monitored developmental changes in the SOC of the Mongolian gerbil (*Meriones unguiculatus*), a model organism whose auditory system shows broad similarity to that of humans with respect to its frequency-response profile and the organisation of its brainstem [9,10,11]. More specifically, we have investigated the three SOC nuclei involved in precise binaural processing, i.e. the medial superior olive (MSO), the lateral superior olive (LSO) and the medial nucleus of the trapezoid body (MNTB). Notably, the calyx of Held synapse in the MNTB allows for extremely fast, efficient and reliable synaptic information transfer, resulting in firing rates of up to several hundred hertz, during phase-locking to the fine-structure or the envelope of acoustic stimuli for instance [12,13]. These properties are pivotal prerequisites for the function of the MNTB in computing the location of sound sources in space, thereby enabling orientation and navigation using auditory cues [14,15,16,17,18,19,20]. Amplitude differences between the sounds reaching the two ears – so-called interaural level differences – are encoded in the LSO [21,22,23], while differences in arrival times – so-called interaural time differences – are extracted by the MSO [14,18,24].

Developmental changes in energy consumption have only rarely been at the focus of neuroenergetics studies [25]. Our aim here

was to investigate how the metabolic activity of SOC neurones changes during early postnatal stages, a period during which these neurones show the profound functional alterations that underpin the evolving ability to hear. In gerbils this ability first appears on postnatal day 12–13, as the rodents gradually become sensitive to auditory stimuli [26]. The developmental regulation of energy availability in the auditory brainstem is interesting, because neuronal circuits are already fully formed prior to hearing onset, but are driven only by spontaneous activity from the cochlea [27,28,29,30,31,32,33]. Furthermore, it is known that this "precocious" and often synchronous burst firing helps to refine the tonotopic organisation of the SOC nuclei [34,35]. After hearing onset, SOC neurones undergo an additional physiological maturation (for review on the LSO see [36]) during which biophysical properties [37,38,39,40,41,42], cell morphology [31,43,44,45], neuronal connectivity [31,46,47] and response patterns [48,49] are fine-tuned in accordance with the auditory demands. In order to achieve the precision and speed required for accurate auditory perception, these neurones obviously have to develop the metabolic capacity to sustain this capability.

To address the issue of neuroenergetics and the development of its constituent processes in the auditory brainstem, we employed two complementary approaches using a mathematical model to calculate energy consumption during neuronal activity and immunohistochemical methods to quantify levels of selected metabolic markers in MSO, LSO and MNTB. We calculated the energy consumption of these neurones during development based on electrophysiological and morphological parameters for animals of different ages taken from the literature. In many nuclei of the auditory system, development before and after hearing onset coincides with changes in the electrophysiological and morphological properties (for references see above). Our mathematical modelling is based on the approach used by Attwell and others, which relates all neuronal processes to the regeneration of the perturbed Na^+ gradient and consequently to the energy required to power the membrane Na^+/K^+-ATPase [50,51,52,53]. The energy-consuming processes we considered were the maintenance of resting membrane potential, the generation of action potentials and postsynaptic excitatory currents, since these have been shown to be the most prominent energy users in other neurones and are closely related to the location of the metabolic markers we have quantified.

We analysed and compared expression levels of several metabolic markers in the three SOC nuclei. As cytochrome c oxidase (COX) catalyses a crucial step in mitochondrial adenosine-5′-triphosphate (ATP) production, its activity can thus serve as a direct read-out of mitochondrial efficiency and neuronal activity [51,52]. In both the inferior colliculus and in the endbulb of Held synapse in the cochlear nucleus, a developmentally regulated increase in mitochondrial density has already been shown to coincide with hearing onset [53,54]. The Na^+/K^+-ATPase plays a fundamental part in neural excitation and firing since it maintains an asymmetric ion distribution across the cell membrane and restores ionic gradients during neuronal activity [55]. Thus, Na^+/K^+-ATPase activity initiated by neuronal activity is tightly coupled to mitochondrial ATP production [55,56]. Glucose, as the main metabolic substrate for ATP production in the mammalian brain is transported into neurones by glucose transporters (GLUTs), with GLUT3 being the predominant subtype [57,58,59,60]. Indeed, the up-regulation of GLUT3 appears to be tightly correlated with functional activity and neurotransmission [58,60,61,62].

Materials and Methods

Ethics Statement

The experiments described in the following were in compliance with institutional guidelines, and with State (Bavarian) and German Federal laws, and were carried out in accordance with the European Communities Council Directive of 24 November 1986 (86/609/EEC). The local government of Upper Bavaria (Regierung von Oberbayern) approved the study (Ref. No. 55.2-1-54-2531-105-10).

Animals

We used 21 animals altogether, of both sexes, for this study: 12 for immunohistochemical stainings (2 in each age group), and 9 for COX activity stainings (3 animals at P7; 2 at P10, P14, and P30, respectively). Animals in the same age group were from different litters. For both types of experiments, animals were anaesthetised using 100 mg/kg body weight metamizol (Novalgin®, sanofi aventis) p.o., followed by 200 mg/kg body weight pentobarbital (Narcoren®, Merial GmbH, Halbergmoos, Germany) i.p. After the animals had reached a state of deep anaesthetic stage, marked by a complete loss of the flexor reflex at all limbs, they were perfused with Ringer solution supplemented with 0.1% heparin (Meditech Vertriebs GmbH, Parchim, Germany) at a flow rate of 4 ml/min for 10 min followed by 4% paraformaldehyde (PFA) solution for 20 min. Brains were then post-fixed overnight in 4% PFA at 4°C.

Immunohistochemistry

Using a Leica VT1200S vibratome, 50 µm sections of the auditory brainstem were collected. The sections were washed 4 times in 0.1 M PBS for 5 min each. Non-specific binding sites were saturated with a blocking solution containing 1% BSA and additionally 0.3% Triton X-100 and 0.1% saponin to allow better penetration of the antibodies into the tissue. The sections were incubated in this blocking solution for 1 hour at room temperature on a shaker. The sections were then incubated in the primary antibody mix (diluted in blocking solution) overnight at 4°C on a shaker. The specificity of all primary antibodies used has been previously published and the relevant publications are indicated for the respective antibodies. The primary antibodies used were: chicken anti-Map2 (1:1000, Neuromics, CH22103 [45,63]), mouse anti-ATPase (1:1000, DSHB, a5 [64,65]), rabbit anti-synapsin (1:100, SySy, 106 002 [66]), rabbit anti-GLUT3 (1:100, abcam, ab41525 [62,67]) and mouse anti-mitochondria (1:500, abcam, ab3298 [68]). The anti-mitochondria antibody was raised against a non-glycosylated protein component of the mitochondrial membrane obtained from a partially purified mitochondrial preparation. The anti-GLUT3 antibody is directed against the intracellular C-terminal of GLUT3. Therefore intracellular as well as membrane-bound GLUT3 is labelled [62], and the intracellular GLUT3 fraction is detectable as a consequence of the relatively fast turnover rate of the protein [69]. Every staining always contained an anti-Map2 co-staining to enable the determination of the cell size, which was important during our subsequent analysis. In addition, stainings for Na^+/K^+-ATPase were always carried out together with anti-synapsin staining. Next day, sections were washed 4 times in 0.1 M PBS for 5 min each, and then incubated with the appropriate secondary antibodies for 2–3 hours at room temperature on a shaker. Secondary antibodies used were: donkey anti-chick Cy3 (1:300, Dianova, 703-166-155), goat anti-rabbit Alexa488 (1:400, Molecular Probes, A-11034) and goat anti-mouse DyLight 649 (1:300, Dianova, 115-495-205). Finally, the tissue slices were mounted with Vectashield supplemented with

DAPI (H-1200, Vector). We have standardised our immunohistochemical stainings by using the protocol described above to ensure equal conditions for all sections. In addition, we ensured that no staining gradient (e.g. due to overlaying sections or adhering of the section to the staining tank) was present in those sections used for analysis.

COX Activity

For analysis of COX activity [51,70], animals were perfused and brains were treated as described above, except that post-fixation in 4% PFA was terminated after only 4 hours to avoid denaturation of the enzyme. Sections of the auditory brainstem were prepared as outlined above, washed 4 times in 0.1 M PBS and subsequently incubated in staining solution (containing 60 mg 3,3′-diaminobenzidine (Sigma Aldrich, D5637) and 20 mg cytochrome *c* (Sigma Aldrich, 30398)/90 ml 0.1 M PBS) in the dark at 37°C until the colour reaction developed. We made sure to incubate all the slices that needed to be directly compared in the same staining solution for the same time. Hence, the sections from the different age groups in each experiment were always incubated together in the same solution for the same period of time. This ensured that no intensity differences due to variations in the reactivity of the enzyme appeared between age groups. Note that, however, the intensity of COX staining might be varying between different sets of experiments. Sections were washed 3 times in 0.1 M PBS, mounted on gelatine-coated slides, subsequently dehydrated and embedded in malinol.

Image Acquisition

To visualise immunohistochemical stainings, confocal optical sections were acquired with a Leica 6000CS SP5 confocal laser-scanning microscope (Leica Microsystems, Mannheim) equipped with a Plan 63×/NA1.32 oil immersion objective. Fluorochromes were visualised by using an argon laser with an excitation wavelength of 488 nm (emission 494–555 nm for Alexa488), a DPSS laser with a laser line at 561 nm (emission 565–606 nm for Cy3) and a helium-neon laser with an excitation wavelength of 633 nm (emission 640–740 nm for DyLight649). For each optical section the images were collected sequentially for the different fluorochromes. Stacks were obtained with axial distances of 300 nm – the image size was 512×512 pixels. The voxel size was either 60.18 nm×60.18 nm×300 nm (zoom 8×) or 160 nm×160 nm×300 nm (zoom 3×). To improve the signal-to-noise ratio, each section image was averaged from six successive line scans. The cells analysed in this study were selected at random and originated from different sections. Acquisition and analysis of images was performed by observers, who were unaware of the age of the animal.

Image Editing and Quantification

After stack acquisition, we corrected Z chromatic shift between colour channels. RGB stacks, montages of RGB optical sections and maximum-intensity projections were generated by using *ImageJ* (1.39q Wayan Rasband, National Institutes of Health, USA, http://rsb.info.nih.gov/ij/, Java 1.5.0_06) and *Adobe Photoshop* (8.0.1) software. Quantification of the stainings was performed by a custom-written thresholding procedure in *ImageJ*. We obtained the cross-sectional area of the neurone by drawing the contour within a single optic plane using the Map2 staining pattern as an indicator, as the expression level of this marker remains constant during the different developmental stages in the soma of the cells. The threshold square was positioned in an area where no specific staining of the respective antigen was observed (nucleus). The site and area of the nucleus was identified by DAPI staining. For the determination of the threshold a scaling factor of 5 was employed, as this factor showed the best magnification level for the images. The program then computed the number of pixels within the cell area that lie above the threshold, which was determined beforehand. The percentage of the pixels above the threshold gave us the percentage of the soma, which was positive for the antigen of interest (mitochondria, Na^+/K^+-ATPase or GLUT3) and represents the marker level (in % per area). To avoid a bias of the plane of the confocal image within the cell, we averaged across several optical sections within a single cell. To rule out any bias in the data due to a non-uniform distribution of staining across the cell, we checked the distribution of the respective antigen in some sample cells across all optical sections (n = 5 cells) and verified that the percentage of positive pixels was highly uniform (data not shown).

Statistical analysis of the immunohistochemical quantifications for the different age groups was performed using the software *Prism5* (5.00 for Windows, GraphPad Software, San Diego California USA, www.graphpad.com). Statistical dependence between metabolic marker levels and age was analysed by means of the nonparametric Spearman correlation test. The parameters obtained (Spearman correlation coefficients; P values) are given in the figure legend.

Energy Calculations

All calculations of energy consumption by different processes are based on the assumption that regeneration of resting Na^+ and K^+ gradients by the Na^+/K^+-ATPase consumes one ATP molecule for pumping two K^+ ions in and three Na^+ ions out [71,72,73,74]. Therefore, all energy values are expressed as number of ATP molecules consumed per second and per cell. The relevant energy-utilising processes considered were (1) maintenance of resting membrane potential, (2) generation of action potentials in soma and dendrites and (3) postsynaptic AMPA currents. E_{Vr}, the energy required for maintenance of resting membrane potential (V_r) is assumed to be determined by the Na^+ current (I_{Na}) driven by the Na^+/K^+-ATPase, which maintains the Na^+ (and K^+) gradient across the plasma membrane. Thus, E_{Vr} depends on V_r, input resistance (R_{in}) and the reversal potentials for Na^+ (V_{Na}) and K^+ (V_K). To determine E_{AP}, the energy necessary for generation of action potentials (AP), we calculated the charge (Q) needed to recharge the plasma membrane during an AP. Assuming Q is carried solely by Na^+ [75,76,77,78], we calculated the amount of ATP expended by the Na^+/K^+-ATPase in pumping this amount of Na^+ back out. Therefore, E_{AP} depends upon AP amplitude (ΔV), specific membrane capacitance (C_s), surface area of soma (A_{soma}) and dendrites ($A_{dendrite}$), and the firing frequency (f). In calculating the energy (E_{post}) utilised for postsynaptic excitatory AMPA currents we considered this dependence on f and the flow of charge through glutamate receptors necessary for generating an AP. This charge was estimated from the current threshold for AP generation ($I_{AP\text{-}thr}$) and decay time (τ_{decay}) of excitatory postsynaptic currents (EPSCs). A detailed description including formulae is given in Text S1. The rationale for disregarding contributions from other neuronal processes is given in the Discussion. All parameters necessary for the calculations were taken from the literature (see Text S1, Fig. S1) and originate from the Mongolian gerbil (unless otherwise noted), the mouse or the rat. Depending on the temperature at which the relevant study was performed, all values were corrected for T = 37°C. All data available for a given parameter were fitted as described in Text S1, and parameters for postnatal ages ranging from 0 to 90 days were calculated utilising the appropriate mathematical function. As the influence of f on calculated energy values is crucial, we give a

detailed explanation of our choice of values for f in the Discussion. The values used represent mean firing rates over longer periods of time (>1 s) and we therefore selected as upper limits for f: 100 Hz (before hearing onset), 200 Hz (APs after hearing onset) and 400 Hz (inputs after hearing onset) [18,48,75,77,79,80,81,82,83,84].

Results

Developmental Changes in Levels of Metabolic Markers

To determine whether metabolic maturation correlates with developmental alterations in the functional activity of SOC neurones, we investigated the density and distribution of several metabolic markers in the nuclei MNTB, MSO and LSO prior to hearing onset (P7 and P10), immediately after hearing onset (P14, "refinement phase"), and at intervals up to the adult stage (P25, P30 and P90) (Figs. 1, 2, 3, 4). The levels of Na^+/K^+-ATPase and synapsin as well as mitochondrial density begin to increase before hearing onset in all nuclei investigated (Fig. 4). Na^+/K^+-ATPase expression rises early during development with the most prominent up-regulation appearing already between P7 and P10 in the MSO and LSO (Figs. 4A, E and F) and between P7 and P14 in MNTB (Figs. 4A and G). In the MSO, mitochondria and synapsin expression show a more gradual increase over a longer period, between P7 and P25 (Figs. 4C, D and E), whereas their expression patterns in the LSO and MNTB resemble more to that of the Na^+/K^+-ATPase. The levels of all studied markers continue to increase until P25, after which their expression levels remain unchanged until P90 (Figs. 4).

The increase in COX activity correlates well with the up-regulation of mitochondria (Figs. 4C and 5). COX activity starts to increase in all investigated nuclei prior to hearing onset, and rises continuously until P30. In order to confirm the specificity of COX activity staining, brain sections were incubated in the normal staining solution containing cytochrome c or in staining solution devoid of cytochrome c, to quantify the background reaction caused by other oxidative enzymes (Fig. 6A). Comparison of the two conditions confirms that the specific COX staining yields a much higher reactivity than the control assay. This is also apparent in the quantification (Fig. 6B): When the average intensity of the non-specific staining is subtracted from the specific COX staining, all pixels lie above the threshold. Only in the area around the nuclei does the intensity appear to be more or less equal under both conditions. In line with this observation, COX activity levels off at P30 (Fig. 5). The intracellular distribution of COX also changes during development. At the early developmental stages investigated, COX is highly abundant in cellular somata, whereas in the adult animals COX activity in the fibres is comparatively increased. This gives rise to a presumably diffuse COX staining at P30, because owing to the similar intensity of staining in somata and surrounding fibres, the different cellular compartments are difficult to discriminate. We compared the results obtained from the auditory brainstem nuclei to the staining of cerebellar Purkinje cells (Fig. 6C) to exclude a general developmental effect, which should be independent of hearing onset. Since the animals begin to move around before the onset of hearing − a task for which the cerebellum is crucial − cerebellar neurones already display a high and behaviourally relevant level of activity at this early stage. No increase of COX activity was observed in cerebellar Purkinje cells during the developmental stages examined, indicating that the changes observed in the auditory brainstem indeed reflect the altered metabolic states of SOC neurones.

Of all the metabolic markers investigated, GLUT3 is the latest to appear. Its levels rise only after the onset of hearing, i.e. between P14 and P25, in all nuclei investigated (Figs. 4B and E–G). In the MSO and LSO, GLUT3 expression is almost undetectable before P14, whereas expression begins earlier in the MNTB, where the transporter is already detectable by P10 (Figs. 1, 2, 3). The anti-GLUT3 antibody is directed against the intracellular C-terminal and the protein exhibits a relatively fast turnover, which accounts for the substantial cytoplasmic staining observed [62,69].

Among the SOC nuclei investigated, the MNTB stands out. Expression levels of all metabolic markers tested are higher than in the MSO or LSO at all developmental stages examined. The effect is most prominent for GLUT3 expression and mitochondria (Figs. 4B and C). Overall, the time courses of marker expression are similar (Figs. 1, 2, 3, 4). However, COX activity shows its most prominent increase already before hearing onset, i.e. between P7 and P10, and increases only slightly thereafter in the MNTB. In MSO and LSO the increase in COX activity takes place much more gradually between P7 and P30 (Fig. 5).

Mathematical Modelling of Developmental Changes in Energy Consumption

A comparison between calculated energy consumption, partitioned between different neuronal processes, in the three SOC nuclei during development is depicted in Fig. 7. A firing frequency of 100 Hz was chosen for all processes, since this value represents the upper limit of spontaneous activity before hearing onset and a reasonable mean activity thereafter (see Discussion). MSO and LSO neurones exhibit similar time courses for E_{total} and for each of the individual components of energy consumption, whereas the profiles for the MNTB show some special features. In both MSO and LSO the E_{total} profile is characterised by a rather shallow rise before hearing onset, which becomes markedly steeper during post-hearing onset refinement phase and levels off around P25 (MSO) and P30 (LSO), respectively. In the LSO a slow decrease over time is observed thereafter. The rise in E_{total} is essentially attributable to an increase in E_{Vr}, whilst E_{AP} and E_{post} decrease. This developmental pattern is very pronounced in the MSO, where E_{total} is dominated by E_{Vr} and the two become virtually synonymous after P20. In the MNTB in contrast, E_{total} increases considerably prior to hearing onset and levels off immediately thereafter. Absolute values of E_{total} at saturation are much higher in the MSO than in the other SOC nuclei (2× and 10× higher than in LSO and MNTB, respectively) due to differing relative contributions and absolute values of individual components of energy use.

We also compared the developmental trajectory of calculated total ATP consumption (E_{total}) with the observed pattern of metabolic marker expression (Fig. 8). As mean firing frequency over longer periods of time are not known, we accounted for this uncertainty by calculating the energy components for a lower (10 Hz) and an upper estimate (100; 200/400 Hz) of mean firing frequency in addition to 100 Hz. Furthermore, Fig. 8 shows the developmental changes in the value of $1/R_{in}$ which is an important electrophysiological characteristic, especially for leaky adult MSO and LSO neurones, and determines E_{Vr}. A detailed description and comparison of the developmental changes depicted in Fig. 8 and their physiological implications follows in the Discussion section.

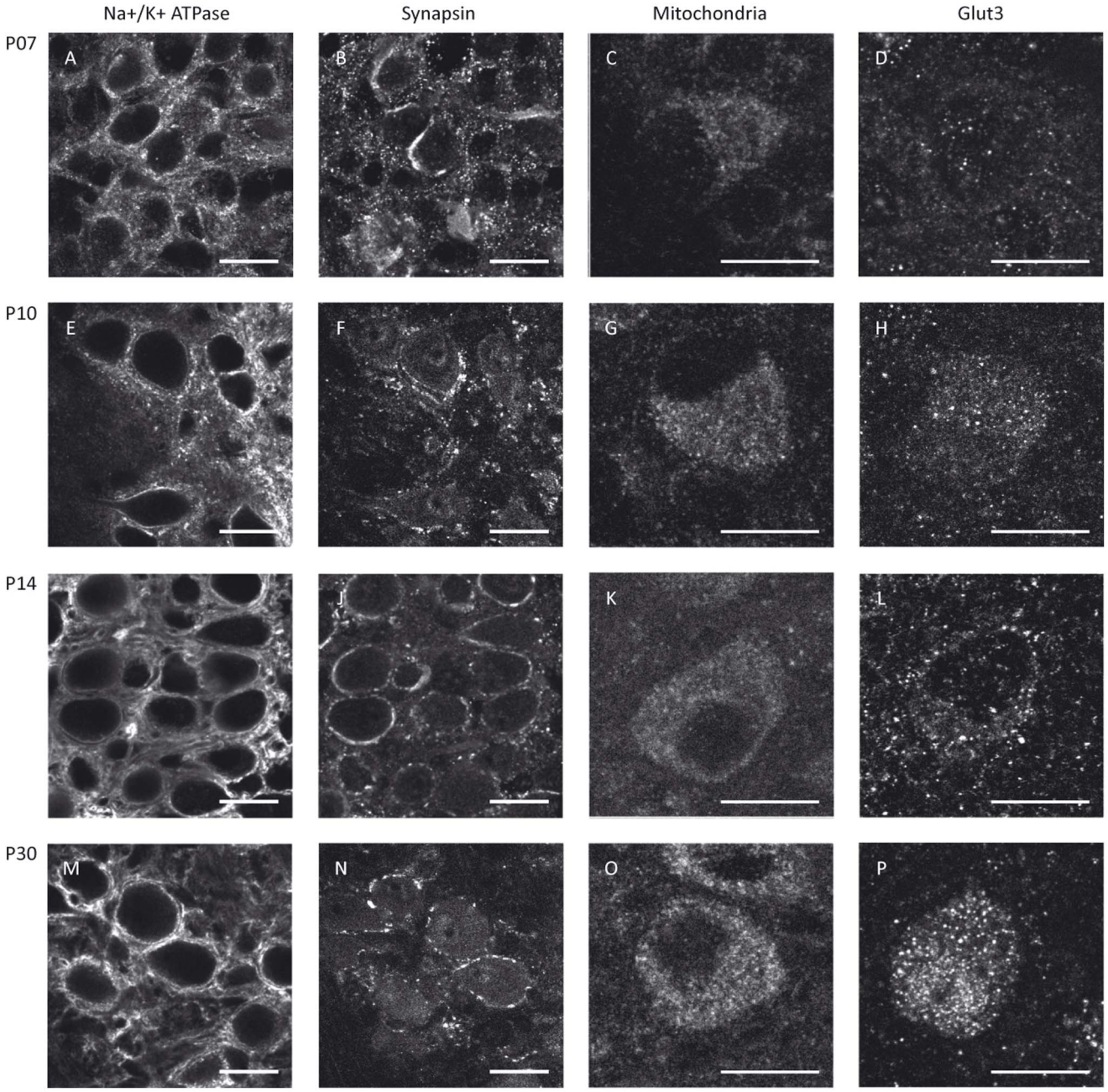

Figure 1. Metabolic maturation in the MNTB. MNTB neurones of Mongolian gerbils at P7 (A–D), P10 (E–H), P14 (I–L) or P30 (M–P) were immunohistochemically stained for Na^+/K^+-ATPase (A, E, I, M), synapsin (B, F, J, N), mitochondria (C, G, K, O) or GLUT3 (D, H, L, P). The sample stainings depicted for Na^+/K^+-ATPase and synapsin were taken from a double-staining of both markers in the same sections. Scale bar = 20 μm.
doi:10.1371/journal.pone.0067351.g001

Discussion

Developmental Alterations of Neuronal Energetics

We have studied the maturation of neuronal energy metabolism in brainstem nuclei for the first time by calculating energy consumption using a mathematical model and quantifying metabolic marker levels in three superior olivary complex (SOC) nuclei of the Mongolian gerbil over the first three months of postnatal life (P0–90). In general, the developmental changes in metabolic marker levels parallel the time course of calculated energy consumption in each nucleus. The overall pattern of energy use, and the relative contributions of different neuronal processes to total ATP consumption, varied between the nuclei. Most notably, relative to MSO and LSO, the MNTB exhibits a distinctly earlier and faster maturation of all parameters, which is almost completed by the time of hearing onset. Otherwise, the basic sequence of events is the same in all three nuclei. After the up-regulation of the Na^+/K^+-ATPase, the number of mitochondria rises, and this is followed by an increased expression of GLUT3 after the onset of hearing. Na^+/K^+-ATPase expression has already reached 85% of its mature level at hearing onset, whereas GLUT3 expression is scarcely detectable prior to that point.

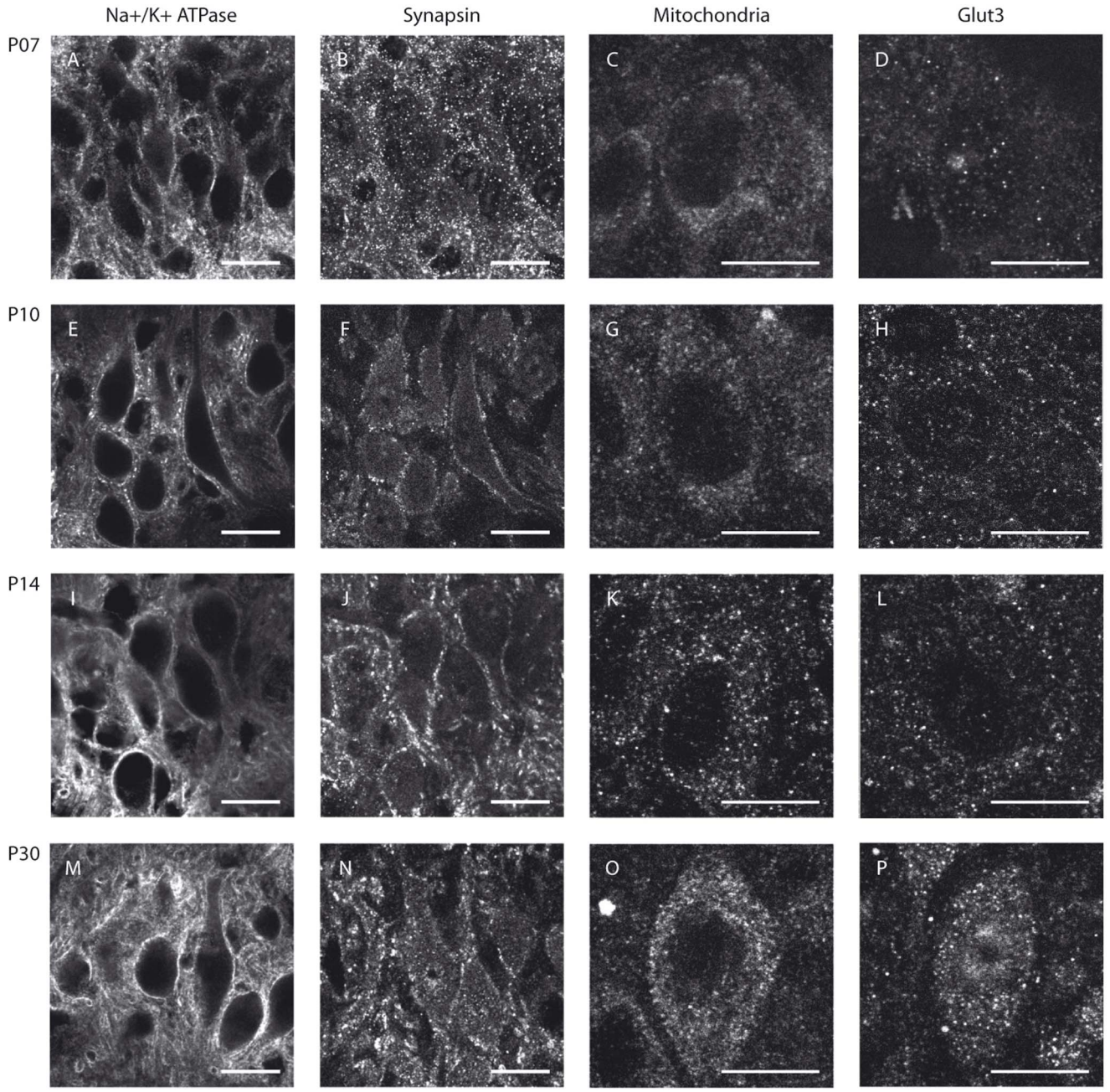

Figure 2. Metabolic maturation in the MSO. MSO neurones of Mongolian gerbils at P7 (A–D), P10 (E–H), P14 (I–L) or P30 (M–P) were immunohistochemically stained for Na^+/K^+-ATPase (A, E, I, M), synapsin (B, F, J, N), mitochondria (C, G, K, O) or GLUT3 (D, H, L, P). The sample stainings depicted for Na^+/K^+-ATPase and synapsin were taken from a double-staining of both markers in the same sections. Scale bar = 20 μm.
doi:10.1371/journal.pone.0067351.g002

The increase in expression of metabolic markers around the time of hearing onset (P12–13 in gerbils) relates to a process of progressive functional changes in the SOC nuclei, and does not represent a general developmental effect, which coincidentally parallels the maturation of the auditory senses. This finding is supported by a Western blotting study of the rat brainstem, which showed no change in levels of GLUT3 and Na^+/K^+-ATPase during the time period P10–14 [78].

One might argue that before hearing onset, neurones could make use of carbon sources other than glucose, such as ketone bodies or lactate [79,81,82,85]. However, glucose is the overwhelmingly predominant fuel for the CNS, whilst other carbon sources are more important during hypoglycaemia [56], and for metabolic cooperation between astrocytes and neurones [79], respectively. Another possibility is that, prior to hearing onset, glucose uptake occurs via a transporter other than GLUT3. However, GLUT3 up-regulation is generally associated with a higher energy demand in neurones [62]. In addition, we found high expression levels already at P10 in MNTB neurones, which is compatible with their generally earlier maturation.

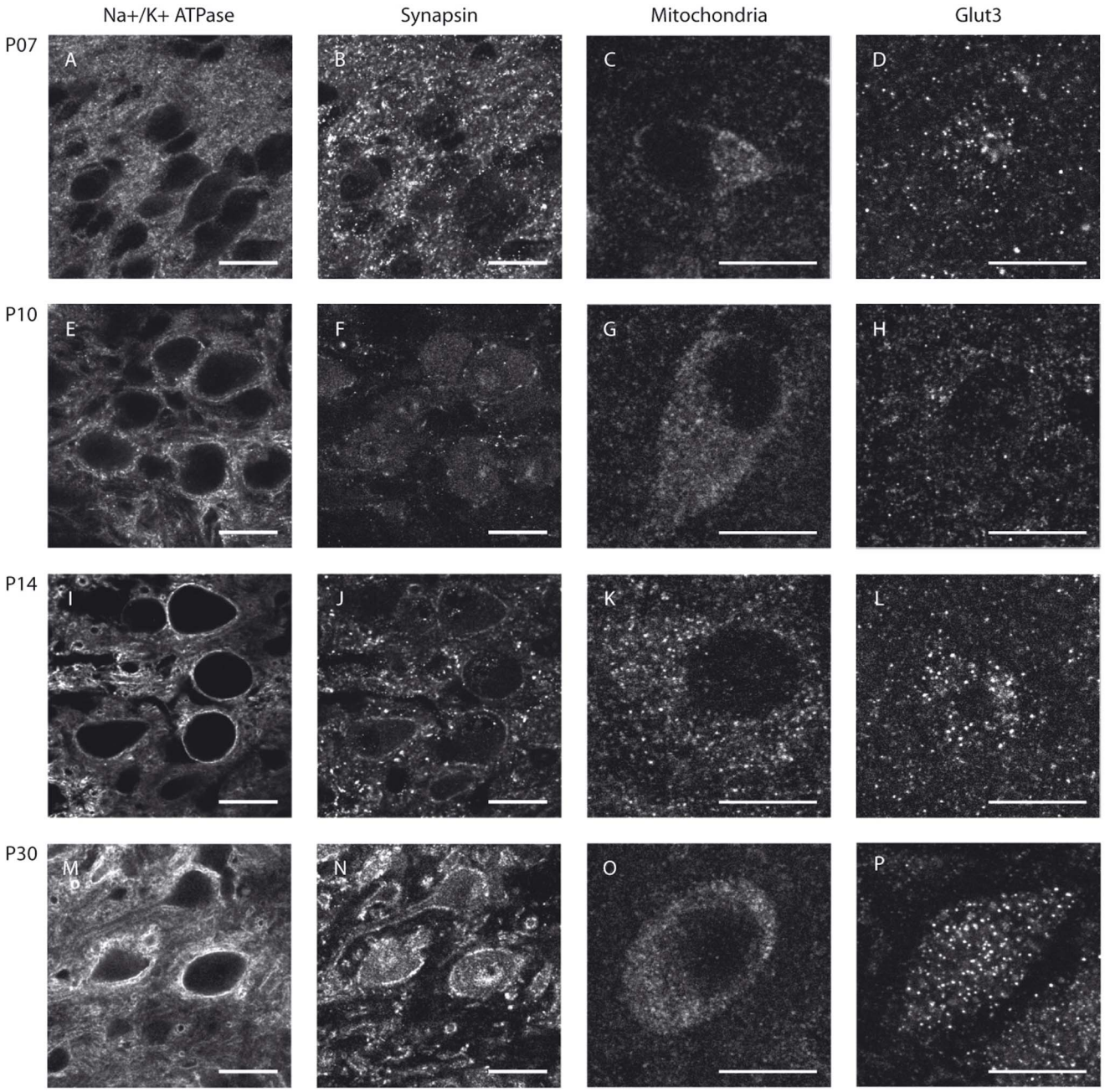

Figure 3. Metabolic maturation in the LSO. LSO neurones of Mongolian gerbils at P7 (A–D), P10 (E–H), P14 (I–L) or P30 (M–P) were immunohistochemically stained for Na^+/K^+-ATPase (A, E, I, M), synapsin (B, F, J, N), mitochondria (C, G, K, O) or GLUT3 (D, H, L, P). The sample stainings depicted for Na^+/K^+-ATPase and synapsin were taken from a double-staining of both markers in the same sections. Scale bar = 20 μm.
doi:10.1371/journal.pone.0067351.g003

Physiological Relevance

The expression of the Na^+/K^+-ATPase is up-regulated conjointly with mitochondrial density, indicating that metabolic maturation is coupled to the developing capability of these neurones to respond to auditory inputs. This development continues after hearing onset, when relevant auditory inputs arrive in the SOC nuclei and might thus contribute to further maturation, at least in MSO and LSO. The comparatively late up-regulation of GLUT3 relative to the other markers suggests that energy availability is ultimately regulated at the level of glucose uptake into the cell. This makes sense as un-metabolised glucose will affect the composition of the cytoplasm, especially by changing its osmolarity. In addition, high glucose oxidation rates would enhance production of reactive oxygen species and perhaps cause neurotoxicity [83].

Our findings indicate that processing of behaviourally irrelevant spontaneous activity, which occurs before hearing onset and with a rather low firing frequency, is not highly energy consuming. The periods of spontaneous firing are caused by the spontaneous release of ATP by supporting cells in the cochlea [26] and might serve as an important priming cue for the correct development of neuronal circuits and physiological properties of SOC neurones

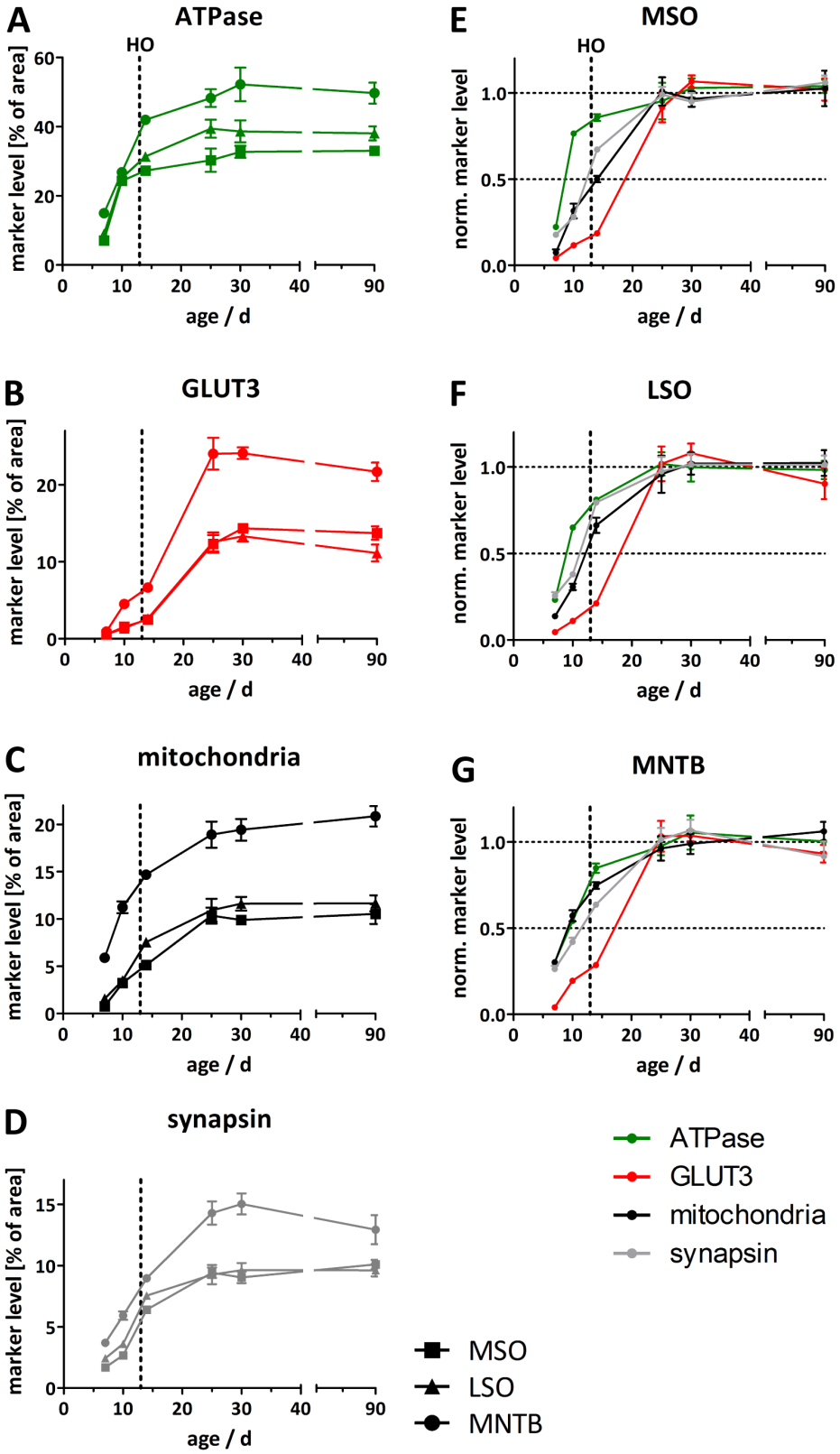

Figure 4. Quantification of relative levels of metabolic markers in the MSO, LSO and MNTB. The marker levels (in % of cross-sectional area) for Na^+/K^+-ATPase (A), GLUT3 (B), mitochondria (C) or synapsin (D) are plotted for different ages during the developmental period tested. Circles represent data points obtained from analysing MNTB neurones, squares those from MSO and triangles those from LSO neurones. A comparison of development of metabolic marker levels (Na^+/K^+-ATPase, green; GLUT3, red; mitochondria, black; synapsin, grey) in SOC nuclei normalised to mean values of saturation (P25, P30 and P90) is shown for the MSO (E), LSO (F) and MNTB (G). The vertical line represents the time of hearing onset (HO) in the Mongolian gerbil. Data are represented as means ± SEM (n = 5 neurones/data point). Statistical dependence between metabolic marker levels

and age was analysed by means of the nonparametric Spearman correlation test. The parameters obtained (Spearman correlation coefficients r; P values) are for the MNTB: ATPase (r = 0.9429; P = 0.0167), GLUT3 (0.8286; 0.0583), mitochondria (1.000; 0.0028), synapsin (0.8286; 0.0583), for the MSO: ATPase (1.000; 0.0028), GLUT3 (0.9429; 0.0167), mitochondria (0.9429; 0.0167), synapsin (0.9429; 0.0167), and for the LSO: ATPase (0.7714; 0.1028), GLUT3 (0.8286; 0.0583), mitochondria (1.000; 0.0028), synapsin (0.9429; 0.0167).
doi:10.1371/journal.pone.0067351.g004

[38,84,85]; for review see: [86]. The firing rates range from 0.1 to 110 Hz [13,87,88] and we used values of 10 to 100 Hz for our calculations.

The assumed mean firing frequencies are of special importance for the mathematical model, since they affect both E_{AP} and E_{post}. In adult animals, when sound-related information from the cochlea arrives in the SOC, maximal mean firing frequencies of 250 Hz for MSO [18,89] and up to 350 Hz for LSO [48,77] and MNTB [75,77,90,91,92] have been measured. In the refinement phase, an age-related rise in maximal frequency was observed as well [18,48,93,94]. Utilising the mathematical model we calculated mean energy consumption over long periods of time (>1s). As maximal firing frequencies given in the literature are normally maintained for only several 100 ms, they most probably overestimate the true physiological values. We have therefore worked with f values ranging from 10 Hz to 200 Hz postsynaptic AP generation, and 400 Hz for presynaptic inputs. This range, together with that for pre-hearing onset neurones, gives a reasonable estimate of the range of ATP consumption rates in the neurones studied.

Glucose uptake as well as ATP production and consumption are assumed to proceed at rather low level under resting conditions, but the neurone must be capable of responding to high energy demands during periods of high neuronal activity. Hence, the necessary numbers of mitochondria, enzymes and transporters must be available and potentially functional. And indeed, that is what our immunohistochemical studies revealed. Therefore, it seems most appropriate to compare the marker levels with calculated energy values for the highest frequencies used. For low-frequency firing (10 Hz), the total ATP consumption (E_{total}) is

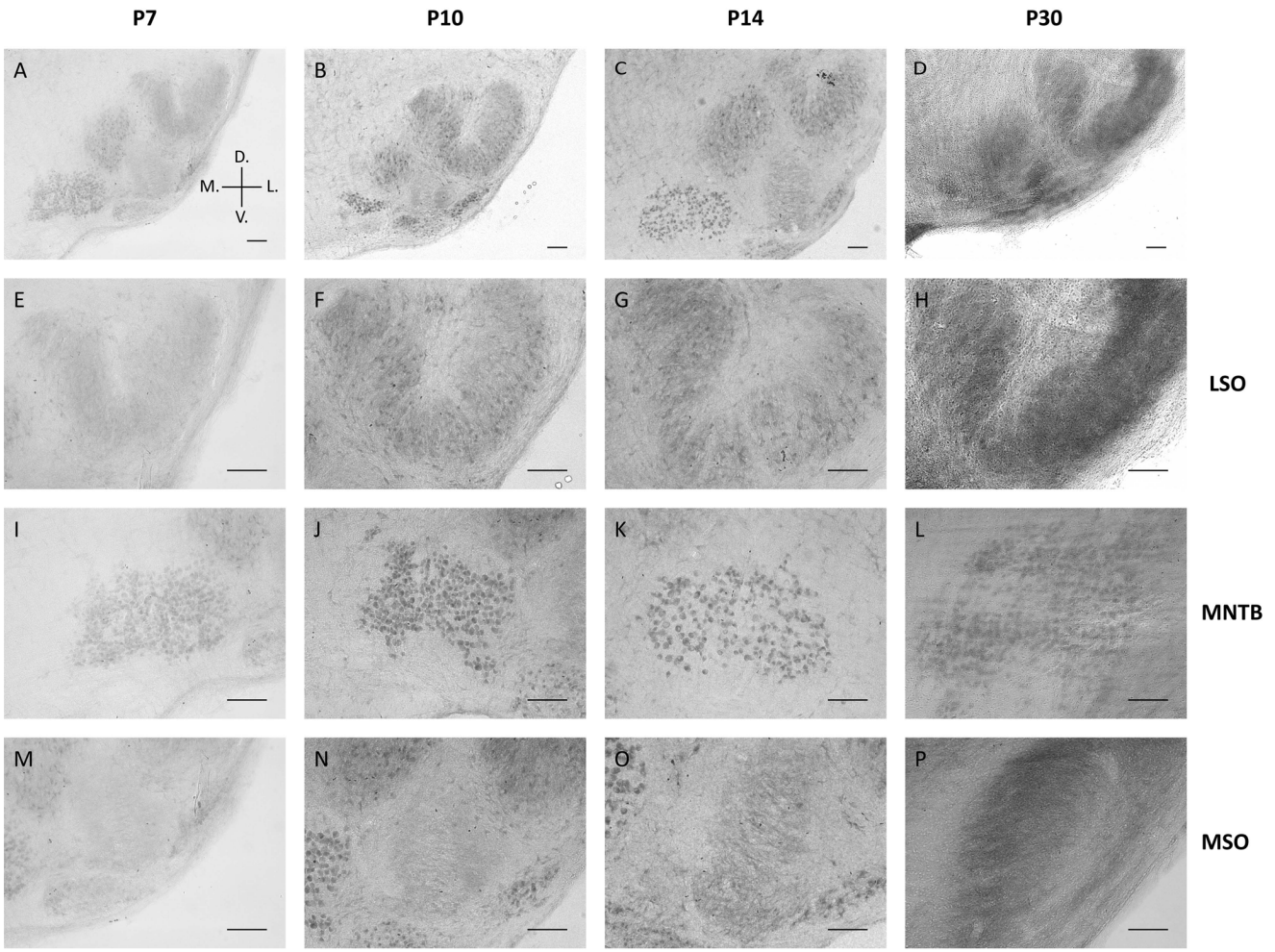

Figure 5. COX activity during development in the auditory brainstem. Representative images of COX activity stainings at different developmental stages of Mongolian gerbils. Images A–D show an overview of the auditory brainstem, E–H show the lateral superior olive (LSO), I–L show the medial nucleus of the trapezoid body (MNTB) and M–P show the medial superior olive (MSO). Images were taken at P7 (A, E, I & M), P10 (B, F, J & N), P14 (C, G, K & O), and P30 (D, H, L & P). Orientation in the brainstem is given in A: D., dorsal; V., ventral; M., medial; L., lateral. Scale bar = 100 μm.
doi:10.1371/journal.pone.0067351.g005

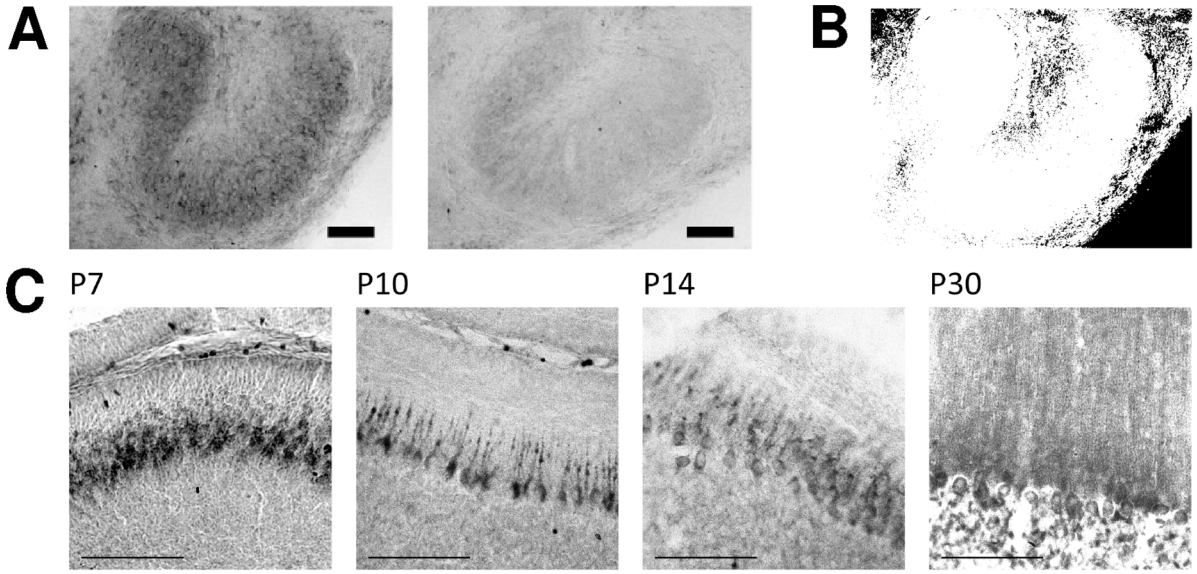

Figure 6. Control experiments for COX activity detection. (A) The majority of the colour reaction is caused by the specific COX activity. The figure depicts one example (LSO, P7) of a control experiment to test for a reaction of unspecific oxidative enzymes. To this, we incubated brain sections in staining solution for COX reaction containing either cytochrome c (left) or no cytochrome c (right). Scale bar = 100 μm. In B the mean average intensity of the unspecific reaction of 3′3-diaminobenzidine was subtracted from the intensity of the specific COX staining. White pixels represent a value above threshold. (C) COX activity in cerebellar Purkinje cells of gerbils aged P7-P30. Scale bars = 100 μm.
doi:10.1371/journal.pone.0067351.g006

mainly dominated by energy used to maintain the resting membrane potential. As E_{Vr} values are in turn mainly determined by R_{in}, the time course of E_{total} parallels that of $1/R_{in}$. The provision of a wide dynamic range of firing frequencies between 0 and almost 1000 Hz seems to depend on a dynamic metabolic range. Particularly in the MNTB, the difference in total ATP consumption associated with different firing frequencies is enormous.

MSO & LSO

Whilst the temporal profile of metabolic marker levels and calculated energy values are very consistent for all three nuclei, the absolute values differ considerably. MNTB marker levels are clearly higher than for MSO/LSO, whereas E_{total} declines in the order MSO>LSO>MNTB. How can the high calculated values in the MSO be explained? Quite obviously, E_{total} is determined by E_{Vr}, and thus, by R_{in} irrespective of firing frequency. Low R_{in} values due to a high membrane conductance in MSO neurones are a prerequisite for their main function, i.e. highly precise coincidence detection in the μs range. Therefore, we conclude that in case of the MSO, temporally accurate input integration needs more energy than the attainment of high activity levels. This implies that metabolic demands rise with the development of the ability to localise sources of sound.

MNTB

The metabolic maturation of the MNTB deviates from that of the MSO and LSO in a number of respects, and this is reflected in the results of both mathematical modelling and the immunohistochemical study of metabolic markers. Essentially in the MNTB, changes begin earlier and proceed at a faster pace. For example, mitochondrial density in the MNTB has reached half-saturation values by P10− a level not attained in MSO/LSO before hearing onset. GLUT3 expression becomes evident by P10, whereas in the other nuclei GLUT3 is almost un-detectable before hearing onset, in agreement with a previous report [60]. Since GLUT3 is responsible for most glucose uptake, this observation supports the argument that MNTB neurones mature early. Our results are in agreement with data from other groups, who have reported early structural and functional maturation of the MNTB by P2–P5 compared to other SOC nuclei [27,84,87] and shown that electrophysiological features of principal MNTB neurones remain constant after P14 [40]. Accordingly, the large calyces of Held are already clearly visible by P7 in sections stained for synapsin. Absolute levels of all markers are clearly higher in MNTB than in MSO and LSO, and by P10, they have almost reached values that are seen in MSO and LSO neurones only at saturation, which has been reported for mitochondrial density, COX activity and GLUT3 levels in adult animals [15,16,88].

Why are the absolute levels of metabolic markers at their highest in the MNTB, while the calculated values for ATP consumption are the lowest? One explanation would be that spontaneous activity occurs in the MNTB after hearing onset [13] and exhibits an even higher firing frequency than before [73]. Another reason could be the high frequency firing bursts (up to 800 Hz) of very short duration (a few ms) observed in the developing MNTB [89]. Both would make higher frequency firing more likely for the MNTB than for the other nuclei. This was not considered in our calculation, but it would increase E_{AP} and E_{post} and hence E_{total} for the MNTB and could raise energy values to levels close to those of MSO and LSO. The MNTB with its calyx of Held synapse could also be energetically costly for other reasons. We assumed equal efficiency factors (EF) for AP generation in all nuclei, but the EF in the MNTB might well be higher than in other nuclei and, as a consequence, ATP consumption in the MNTB could be higher than calculated. Finally, there are the energy-consuming processes, which were not considered in our mathematical model, but would be reflected in metabolic marker levels. Due to the specialisation of the large MNTB synapse, larger numbers of ion channels and transporters might be expressed in the postsynaptic membrane. Expression and turnover of these proteins, as well as postsynaptic neurotransmitter

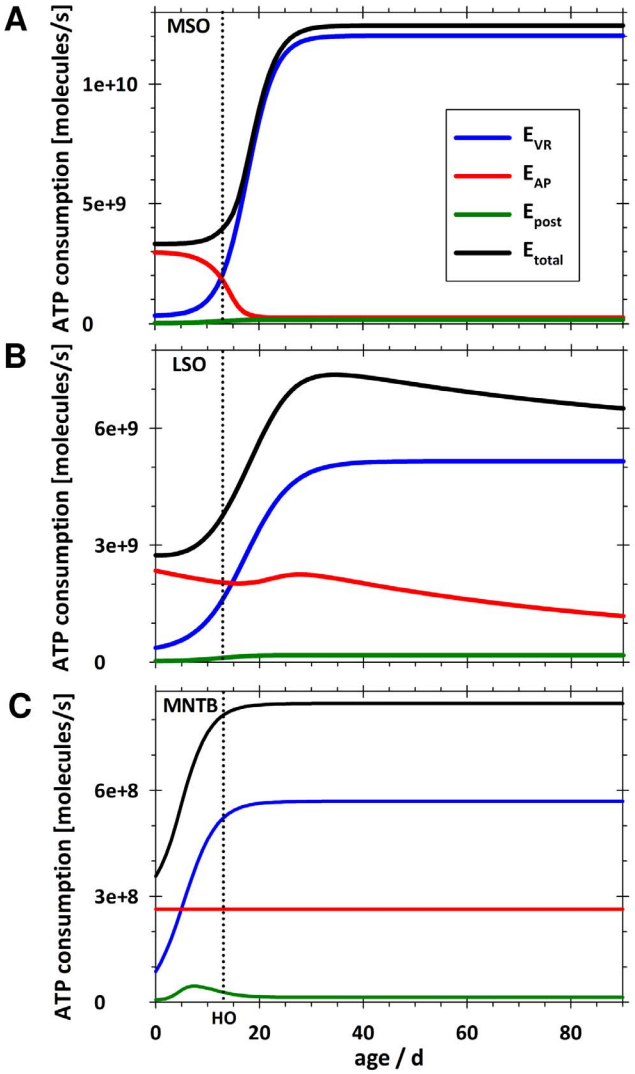

Figure 7. Energy consumption in SOC nuclei (at 100 Hz) increases during maturation. The calculated values for total ATP consumption (E_{total}) per cell as well as the individual components E_{Vr} (energy for maintenance of resting membrane potential), E_{AP} (energy for generation of somatic and dendritic APs, and E_{post} (energy for postsynaptic excitatory currents) rise during development for MSO (A), LSO (B), and MNTB (C). The firing frequency for both inputs and postsynaptic AP generation was 100 Hz. Note the difference in total energy for the three nuclei. HO, hearing onset.
doi:10.1371/journal.pone.0067351.g007

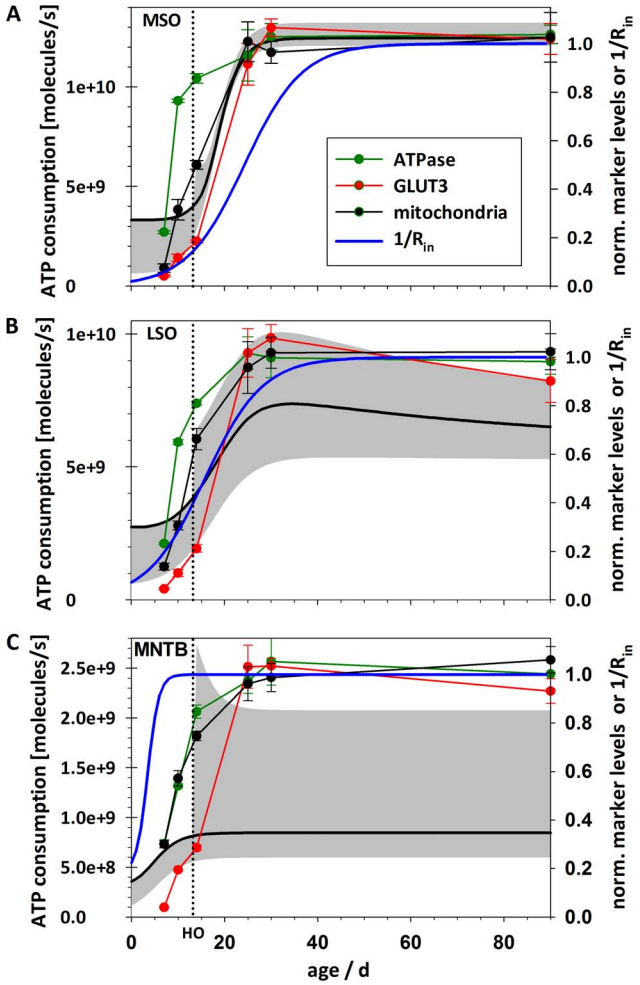

Figure 8. Comparison of time course of total energy consumption (E_{total}) and development of metabolic markers. The grey area depicts E_{total} per cell between low (lower margin of area) and high mean firing rates (upper margin of area) for MSO (A), LSO (B), and MNTB (C). For the low rate we used 10 Hz before and after hearing onset (both inputs and postsynaptic AP generation). As an upper estimation we used 100 Hz for all components before hearing onset and after hearing onset 200 Hz (postsynaptic AP generation) and 400 Hz (inputs), respectively. The black line represents the values for 100 Hz before and after hearing onset (both inputs and postsynaptic AP generation) depicted in Fig. 7. HO, hearing onset.
doi:10.1371/journal.pone.0067351.g008

uptake and metabolism consume energy and, therefore, housekeeping processes might require more energy in the MNTB than in other nuclei. All these factors - individually or in combination - could result in the true energy consumption being higher than calculated by our model.

Mathematical Model

Our use of the mathematical model developed by Attwell and others [4,5,6,50] to illuminate the neuroenergetics of the SOC nuclei proves that it can be successfully adapted to specialised auditory neurones on the one hand and developmental issues on the other. A comparison with results on cerebral cortex, cerebellum and olfactory glomerulus shows a similar range of absolute energy consumption, and of variability in the fractional contribution of different neuronal processes [4,5,6,50]. Like every other model, it is based on several assumptions, which have been debated in the literature [5,6,50] and are discussed in detail below.

The energy-consuming tasks we considered are: maintenance of resting membrane potential, generation of action potentials and postsynaptic excitatory currents, as these have been shown to be the most prominent sources of energy expenditure in other neurones, and are closely related to the postsynaptic localisation of the metabolic markers we have quantified. With regard to AP generation we included somatic and dendritic components, but excluded axonal excitability. As the axonal constituent is sufficiently provided for by local ATP production [90], it is not related to the metabolic marker localisation we analysed. Postsynaptic inhibitory currents were disregarded because the metabolic demand for inhibitory neurotransmission is assumed to be much lower than for the excitatory signalling [91,92,93]. It is

estimated that regeneration of the Cl^- gradient requires less than 1% of the energy needed to implement an equivalent change in the Na^+ gradient [5,6,50], since Cl^- has to be transported against a shallower electrochemical gradient. Therefore developmental changes in intracellular Cl^- concentrations [94,95,96,97] are irrelevant (see below). Postsynaptic metabotropic processes are assumed to be energetically less demanding [5,6,50]. NMDA currents in the MNTB are treated as AMPA currents in the estimates outlined in Text S1. Neurotransmitter recycling was not included in our calculations, since various cell types (e.g. glial cells) are involved and the contribution of the postsynaptic neurone has been calculated to be rather small [5,6,50]. The same holds for Ca^{2+}-dependent, presynaptic processes involved in neurotransmitter release [5,6,50], which are, moreover, not related to the postsynaptic localisation of our metabolic markers. The amount of energy a neurone expends on "housekeeping" functions unrelated to neuronal excitability is not known, although some authors assume it to be in the range of 25% of the cellular energy consumption. In light of this uncertainty, we have not considered this parameter, but will discuss its implications below.

Estimation of Model Parameters

The electrophysiological and morphological parameters plugged into the mathematical model were extracted from the literature. Wherever possible, the values derive from studies on the gerbil, but they were also taken from mouse and rat, whose developmental programmes and time point of hearing onset are comparable to the gerbil's [26,74,84,98,99,100]. An exception must be made for the MSO, which is related to low-frequency hearing, and among rodents, is only substantially present in the gerbil. Since the datasets available for different parameters differ in size, their accuracy varies. In addition, the age range of published data determines the accuracy of the parameters extrapolated to a range P0–90. In cases, where data for a certain parameter were only available for one age group, uniformity was assumed or, if physiologically reasonable, an age dependency similar to that in one of the other SOC nuclei was employed. The latter approach was also used if no data at all were available for a particular parameter in a given nucleus. A detailed description of parameter estimation, including references, can be found in Text S1. In all nuclei, R_{in}, $I_{AP\text{-}thr}$ and τ_{decay} change with maturation, with R_{in} having the largest published dataset. In some of the nuclei, the following parameters also undergo maturation: ΔV_{soma} (MSO), $\Delta V_{dendrite}$ (MSO), $A_{dendrite}$ (MSO, LSO), whilst V_r, and A_{soma} are constant in all of them. We chose an AP efficiency factor of 2, which represents the upper limit of the latest published data (for discussion see [2]) and is close to the value of 4, which was used for similar calculations and is based on results of Hodgkin [101]. Concentrations for Na^+ and K^+, and hence the corresponding reversal potentials, were chosen to be constant due to lack of data. However, as developmental alteration of intracellular Cl^- concentrations has been reported in the SOC [94,95,96,97], a dependence of Na^+ and K^+ concentrations on age cannot be excluded. A possible contribution to V_r and R_{in} from a potential Cl^- conductance was neglected due to missing data as well.

Conclusions

Using a combination of quantitative immunohistochemistry and mathematical modelling of energy consumption, we were able to describe generalised developmental schemes as well as nucleus-specific variations for the major components of the SOC in the gerbil. We found that the period preceding hearing onset is most crucial for the MNTB, whilst in MSO/LSO the refinement phase after hearing onset represents a pivotal developmental phase. Neuronal input resistance (R_{in}), which represents an important electrophysiological parameter and can be most reliably obtained from the literature for a wide age range, dominates energy consumption, especially in leaky MSO neurones and at low firing frequencies. For the MSO, we propose that coincidence detection with its requirement for temporal precision and high-frequency phase-locking represents a metabolically more costly process than high-frequency firing itself. For the MNTB, we suggest that cellular processes related to its specialised type of synapse contribute to ATP consumption and account for the observed discrepancies between immunohistochemical quantification and mathematical modelling. Further detailed experimental and modelling efforts are necessary, if we are to understand neuroenergetics in the SOC. A comparative analysis of further auditory neurones, as well as functional studies (e.g. NAD(P)H and flavoprotein imaging) in acute brain slices in combination with electrophysiological recordings could deepen our understanding of neuroenergetics. It has long been known that neurones produce only as much energy as they require [51] and our data support this assumption. For other sensory systems such as the visual system of the macaque, it has been demonstrated that inactivation of the sensory pathway decreases the activity of COX [102,103]. A reduction of COX activity in auditory brainstem nuclei has been reported either caused by conductive hearing loss in Mongolian gerbils [104] or following unilateral deafening of cats [105]. It would, thus, be intriguing to investigate whether deafening of gerbils before the onset of hearing interferes with the observed maturation of metabolic markers in auditory brainstem nuclei.

Supporting Information

Figure S1 Dependence of electrophysiological parameters on age. Absolute (top) and relative values (bottom) for all three SOC nuclei.
(TIF)

Text S1 Description of the mathematical model.
(DOC)

Acknowledgments

We thank Dr. Olga Alexandrova for help with the analysis of immunohistochemical images, Dr. Susanne Radtke-Schuller for neuroanatomical and histological expertise, Sarah Berner for practical help with the COX activity stainings and Dr. Felix Felmy for intense discussions and helpful ideas regarding model parameters.

Author Contributions

Conceived and designed the experiments: BT LK. Performed the experiments: BT CMG. Analyzed the data: BT CMG LK. Wrote the paper: BT CMG BG LK. Mathematical modelling: LK.

References

1. Hertz L, Dienel GA (2002) Energy metabolism in the brain. Int Rev Neurobiol 51: 1–102.
2. Dienel GA, Hertz L (2001) Glucose and lactate metabolism during brain activation. J Neurosci Res 66: 824–838.
3. Korf J, Gramsbergen JB (2007) Timing of potential and metabolic brain energy. J Neurochem 103: 1697–1708.
4. Nawroth JC, Greer CA, Chen WR, Laughlin SB, Shepherd GM (2007) An energy budget for the olfactory glomerulus. J Neurosci 27: 9790–9800.

5. Howarth C, Gleeson P, Attwell D (2012) Updated energy budgets for neural computation in the neocortex and cerebellum. J Cereb Blood Flow Metab.
6. Howarth C, Peppiatt-Wildman CM, Attwell D (2010) The energy use associated with neural computation in the cerebellum. J Cereb Blood Flow Metab 30: 403–414.
7. Shetty PK, Galeffi F, Turner DA (2012) Cellular Links between Neuronal Activity and Energy Homeostasis. Front Pharmacol 3: 43.
8. Sokoloff L (1981) Localization of functional activity in the central nervous system by measurement of glucose utilization with radioactive deoxyglucose. J Cereb Blood Flow Metab 1: 7–36.
9. Heffner RS, Heffner HE (1988) Sound localization and use of binaural cues by the gerbil (Meriones unguiculatus). Behav Neurosci 102: 422–428.
10. Muller M (1990) Quantitative comparison of frequency representation in the auditory brainstem nuclei of the gerbil, Pachyuromys duprasi. Exp Brain Res 81: 140–149.
11. Lesica NA, Lingner A, Grothe B (2010) Population coding of interaural time differences in gerbils and barn owls. J Neurosci 30: 11696–11702.
12. Grothe B, Park TJ (1998) Sensitivity to interaural time differences in the medial superior olive of a small mammal, the Mexican free-tailed bat. J Neurosci 18: 6608–6622.
13. Hermann J, Pecka M, von Gersdorff H, Grothe B, Klug A (2007) Synaptic transmission at the calyx of Held under in vivo like activity levels. J Neurophysiol 98: 807–820.
14. Goldberg JM, Brown PB (1969) Response of binaural neurons of dog superior olivary complex to dichotic tonal stimuli: some physiological mechanisms of sound localization. J Neurophysiol 32: 613–636.
15. Forsythe ID, Barnes-Davies M (1993) The binaural auditory pathway: excitatory amino acid receptors mediate dual timecourse excitatory postsynaptic currents in the rat medial nucleus of the trapezoid body. Proc Biol Sci 251: 151–157.
16. Smith PH, Joris PX, Yin TC (1998) Anatomy and physiology of principal cells of the medial nucleus of the trapezoid body (MNTB) of the cat. J Neurophysiol 79: 3127–3142.
17. Oertel D (1999) The role of timing in the brain stem auditory nuclei of vertebrates. Annu Rev Physiol 61: 497–519.
18. Brand A, Behrend O, Marquardt T, McAlpine D, Grothe B (2002) Precise inhibition is essential for microsecond interaural time difference coding. Nature 417: 543–547.
19. Taschenberger H, Leao RM, Rowland KC, Spirou GA, von Gersdorff H (2002) Optimizing synaptic architecture and efficiency for high-frequency transmission. Neuron 36: 1127–1143.
20. Grothe B, Pecka M, McAlpine D (2010) Mechanisms of sound localization in mammals. Physiol Rev 90: 983–1012.
21. Tollin DJ, Koka K, Tsai JJ (2008) Interaural level difference discrimination thresholds for single neurons in the lateral superior olive. J Neurosci 28: 4848–4860.
22. Tollin DJ, Yin TC (2002) The coding of spatial location by single units in the lateral superior olive of the cat. II. The determinants of spatial receptive fields in azimuth. J Neurosci 22: 1468–1479.
23. Boudreau JC, Tsuchitani C (1968) Binaural interaction in the cat superior olive S segment. J Neurophysiol 31: 442–454.
24. Grothe B, Sanes DH (1994) Synaptic inhibition influences the temporal coding properties of medial superior olivary neurons: an in vitro study. J Neurosci 14: 1701–1709.
25. Schuchmann S, Buchheim K, Heinemann U, Hosten N, Buttgereit F (2005) Oxygen consumption and mitochondrial membrane potential indicate developmental adaptation in energy metabolism of rat cortical neurons. Eur J Neurosci 21: 2721–2732.
26. Tritsch NX, Yi E, Gale JE, Glowatzki E, Bergles DE (2007) The origin of spontaneous activity in the developing auditory system. Nature 450: 50–55.
27. Kil J, Kageyama GH, Semple MN, Kitzes LM (1995) Development of ventral cochlear nucleus projections to the superior olivary complex in gerbil. J Comp Neurol 353: 317–340.
28. Kandler K, Friauf E (1993) Pre- and postnatal development of efferent connections of the cochlear nucleus in the rat. J Comp Neurol 328: 161–184.
29. Rubel EW, Fritzsch B (2002) Auditory system development: primary auditory neurons and their targets. Annu Rev Neurosci 25: 51–101.
30. Friauf E, Kandler K (1990) Auditory projections to the inferior colliculus of the rat are present by birth. Neurosci Lett 120: 58–61.
31. Youssoufian M, Couchman K, Shivdasani MN, Paolini AG, Walmsley B (2008) Maturation of auditory brainstem projections and calyces in the congenitally deaf (dn/dn) mouse. J Comp Neurol 506: 442–451.
32. Tritsch NX, Bergles DE (2010) Developmental regulation of spontaneous activity in the Mammalian cochlea. J Neurosci 30: 1539–1550.
33. Tritsch NX, Rodriguez-Contreras A, Crins TT, Wang HC, Borst JG, et al. (2010) Calcium action potentials in hair cells pattern auditory neuron activity before hearing onset. Nat Neurosci 13: 1050–1052.
34. Kim G, Kandler K (2003) Elimination and strengthening of glycinergic/GABAergic connections during tonotopic map formation. Nat Neurosci 6: 282–290.
35. Kandler K (2004) Activity-dependent organization of inhibitory circuits: lessons from the auditory system. Curr Opin Neurobiol 14: 96–104.
36. Sanes DH, Friauf E (2000) Development and influence of inhibition in the lateral superior olivary nucleus. Hear Res 147: 46–58.
37. Kandler K, Friauf E (1995) Development of glycinergic and glutamatergic synaptic transmission in the auditory brainstem of perinatal rats. J Neurosci 15: 6890–6904.
38. Kandler K, Friauf E (1995) Development of electrical membrane properties and discharge characteristics of superior olivary complex neurons in fetal and postnatal rats. Eur J Neurosci 7: 1773–1790.
39. Magnusson AK, Kapfer C, Grothe B, Koch U (2005) Maturation of glycinergic inhibition in the gerbil medial superior olive after hearing onset. J Physiol 568: 497–512.
40. Scott LL, Mathews PJ, Golding NL (2005) Posthearing developmental refinement of temporal processing in principal neurons of the medial superior olive. J Neurosci 25: 7887–7895.
41. Chirila FV, Rowland KC, Thompson JM, Spirou GA (2007) Development of gerbil medial superior olive: integration of temporally delayed excitation and inhibition at physiological temperature. J Physiol 584: 167–190.
42. Walcher J, Hassfurth B, Grothe B, Koch U (2011) Comparative post-hearing development of inhibitory inputs to the lateral superior olive in gerbils and mice. J Neurophysiol.
43. Sanes DH, Song J, Tyson J (1992) Refinement of dendritic arbors along the tonotopic axis of the gerbil lateral superior olive. Brain Res Dev Brain Res 67: 47–55.
44. Ford MC, Grothe B, Klug A (2009) Fenestration of the calyx of Held occurs sequentially along the tonotopic axis, is influenced by afferent activity, and facilitates glutamate clearance. J Comp Neurol 514: 92–106.
45. Rautenberg PL, Grothe B, Felmy F (2009) Quantification of the three-dimensional morphology of coincidence detector neurons in the medial superior olive of gerbils during late postnatal development. J Comp Neurol 517: 385–396.
46. Kapfer C, Seidl AH, Schweizer H, Grothe B (2002) Experience-dependent refinement of inhibitory inputs to auditory coincidence-detector neurons. Nat Neurosci 5: 247–253.
47. Werthat F, Alexandrova O, Grothe B, Koch U (2008) Experience-dependent refinement of the inhibitory axons projecting to the medial superior olive. Dev Neurobiol 68: 1454–1462.
48. Sanes DH, Rubel EW (1988) The ontogeny of inhibition and excitation in the gerbil lateral superior olive. J Neurosci 8: 682–700.
49. Seidl AH, Grothe B (2005) Development of sound localization mechanisms in the mongolian gerbil is shaped by early acoustic experience. J Neurophysiol 94: 1028–1036.
50. Attwell D, Laughlin SB (2001) An energy budget for signaling in the grey matter of the brain. J Cereb Blood Flow Metab 21: 1133–1145.
51. Wong-Riley MT (1989) Cytochrome oxidase: an endogenous metabolic marker for neuronal activity. Trends Neurosci 12: 94–101.
52. Kann O, Schuchmann S, Buchheim K, Heinemann U (2003) Coupling of neuronal activity and mitochondrial metabolism as revealed by NAD(P)H fluorescence signals in organotypic hippocampal slice cultures of the rat. Neuroscience 119: 87–100.
53. Pysh JJ (1970) Mitochondrial changes in rat inferior colliculus during postnatal development: an electron microscopic study. Brain Res 18: 325–342.
54. Ryugo DK, Montey KL, Wright AL, Bennett ML, Pongstaporn T (2006) Postnatal development of a large auditory nerve terminal: the endbulb of Held in cats. Hear Res 216–217: 100–115.
55. Jorgensen PL, Hakansson KO, Karlish SJ (2003) Structure and mechanism of Na,K-ATPase: functional sites and their interactions. Annu Rev Physiol 65: 817–849.
56. Erecinska M, Cherian S, Silver IA (2004) Energy metabolism in mammalian brain during development. Prog Neurobiol 73: 397–445.
57. Vannucci SJ, Maher F, Simpson IA (1997) Glucose transporter proteins in brain: delivery of glucose to neurons and glia. Glia 21: 2–21.
58. Leino RL, Gerhart DZ, van Bueren AM, McCall AL, Drewes LR (1997) Ultrastructural localization of GLUT 1 and GLUT 3 glucose transporters in rat brain. J Neurosci Res 49: 617–626.
59. Castro MA, Beltran FA, Brauchi S, Concha II (2009) A metabolic switch in brain: glucose and lactate metabolism modulation by ascorbic acid. J Neurochem 110: 423–440.
60. Nehlig A (1997) Cerebral energy metabolism, glucose transport and blood flow: changes with maturation and adaptation to hypoglycaemia. Diabetes Metab 23: 18–29.
61. Mantych GJ, James DE, Chung HD, Devaskar SU (1992) Cellular localization and characterization of Glut 3 glucose transporter isoform in human brain. Endocrinology 131: 1270–1278.
62. Ferreira JM, Burnett AL, Rameau GA (2011) Activity-dependent regulation of surface glucose transporter-3. J Neurosci 31: 1991–1999.
63. Kaiser A, Alexandrova O, Grothe B (2011) Urocortin-expressing olivocochlear neurons exhibit tonotopic and developmental changes in the auditory brainstem and in the innervation of the cochlea. J Comp Neurol 519: 2758–2778.
64. Lebovitz RM, Takeyasu K, Fambrough DM (1989) Molecular characterization and expression of the (Na++K+)-ATPase alpha-subunit in Drosophila melanogaster. EMBO J 8: 193–202.
65. Curtis LM, ten Cate WJ, Rarey KE (1993) Dynamics of Na,K-ATPase sites in lateral cochlear wall tissues of the rat. Eur Arch Otorhinolaryngol 250: 265–270.

66. Lazarevic V, Schone C, Heine M, Gundelfinger ED, Fejtova A (2011) Extensive remodeling of the presynaptic cytomatrix upon homeostatic adaptation to network activity silencing. J Neurosci 31: 10189–10200.
67. Gomez O, Ballester-Lurbe B, Poch E, Mesonero JE, Terrado J (2010) Developmental regulation of glucose transporters GLUT3, GLUT4 and GLUT8 in the mouse cerebellar cortex. J Anat 217: 616–623.
68. Zhu J, Qiu Z, Wiese C, Ishii Y, Friedrichsen J, et al. (2005) Nuclear and mitochondrial localization signals overlap within bovine herpesvirus 1 tegument protein VP22. J Biol Chem 280: 16038–16044.
69. Khayat ZA, McCall AL, Klip A (1998) Unique mechanism of GLUT3 glucose transporter regulation by prolonged energy demand: increased protein half-life. Biochem J 333 (Pt 3): 713–718.
70. Seligman AM, Karnovsky MJ, Wasserkrug HL, Hanker JS (1968) Nondroplet ultrastructural demonstration of cytochrome oxidase activity with a polymerizing osmiophilic reagent, diaminobenzidine (DAB). J Cell Biol 38: 1–14.
71. Pecka M, Brand A, Behrend O, Grothe B (2008) Interaural time difference processing in the mammalian medial superior olive: the role of glycinergic inhibition. J Neurosci 28: 6914–6925.
72. Joshi I, Shokralla S, Titis P, Wang LY (2004) The role of AMPA receptor gating in the development of high-fidelity neurotransmission at the calyx of Held synapse. J Neurosci 24: 183–196.
73. Sonntag M, Englitz B, Kopp-Scheinpflug C, Rubsamen R (2009) Early postnatal development of spontaneous and acoustically evoked discharge activity of principal cells of the medial nucleus of the trapezoid body: an in vivo study in mice. J Neurosci 29: 9510–9520.
74. Crins TT, Rusu SI, Rodriguez-Contreras A, Borst JG (2011) Developmental changes in short-term plasticity at the rat calyx of Held synapse. J Neurosci 31: 11706–11717.
75. Kopp-Scheinpflug C, Tolnai S, Malmierca MS, Rubsamen R (2008) The medial nucleus of the trapezoid body: comparative physiology. Neuroscience 154: 160–170.
76. Hermann J, Grothe B, Klug A (2009) Modeling short-term synaptic plasticity at the calyx of held using in vivo-like stimulation patterns. J Neurophysiol 101: 20–30.
77. Wu SH, Kelly JB (1993) Response of neurons in the lateral superior olive and medial nucleus of the trapezoid body to repetitive stimulation: intracellular and extracellular recordings from mouse brain slice. Hear Res 68: 189–201.
78. Vannucci SJ, Clark RR, Koehler-Stec E, Li K, Smith CB, et al. (1998) Glucose transporter expression in brain: relationship to cerebral glucose utilization. Dev Neurosci 20: 369–379.
79. Allaman I, Belanger M, Magistretti PJ (2011) Astrocyte-neuron metabolic relationships: for better and for worse. Trends Neurosci 34: 76–87.
80. Vannucci RC, Nardis EE, Vannucci SJ, Campbell PA (1981) Cerebral carbohydrate and energy metabolism during hypoglycemia in newborn dogs. Am J Physiol 240: R192–199.
81. Belanger M, Allaman I, Magistretti PJ (2011) Brain energy metabolism: focus on astrocyte-neuron metabolic cooperation. Cell Metab 14: 724–738.
82. Pellerin L, Magistretti PJ (1994) Glutamate uptake into astrocytes stimulates aerobic glycolysis: a mechanism coupling neuronal activity to glucose utilization. Proc Natl Acad Sci U S A 91: 10625–10629.
83. Horvath TL, Andrews ZB, Diano S (2009) Fuel utilization by hypothalamic neurons: roles for ROS. Trends Endocrinol Metab 20: 78–87.
84. Hoffpauir BK, Grimes JL, Mathers PH, Spirou GA (2006) Synaptogenesis of the calyx of Held: rapid onset of function and one-to-one morphological innervation. J Neurosci 26: 5511–5523.
85. Kim G, Kandler K (2010) Synaptic changes underlying the strengthening of GABA/glycinergic connections in the developing lateral superior olive. Neuroscience 171: 924–933.
86. Kandler K, Clause A, Noh J (2009) Tonotopic reorganization of developing auditory brainstem circuits. Nat Neurosci 12: 711–717.
87. Nakamura PA, Cramer KS (2011) Formation and maturation of the calyx of Held. Hear Res 276: 70–78.
88. Gonzalez-Lima F, Jones D (1994) Quantitative mapping of cytochrome oxidase activity in the central auditory system of the gerbil: a study with calibrated activity standards and metal-intensified histochemistry. Brain Res 660: 34–49.
89. Taschenberger H, von Gersdorff H (2000) Fine-tuning an auditory synapse for speed and fidelity: developmental changes in presynaptic waveform, EPSC kinetics, and synaptic plasticity. J Neurosci 20: 9162–9173.
90. Harris JJ, Attwell D (2012) The energetics of CNS white matter. J Neurosci 32: 356–371.
91. Waldvogel D, van Gelderen P, Muellbacher W, Ziemann U, Immisch I, et al. (2000) The relative metabolic demand of inhibition and excitation. Nature 406: 995–998.
92. Attwell D, Gibb A (2005) Neuroenergetics and the kinetic design of excitatory synapses. Nat Rev Neurosci 6: 841–849.
93. Hasenstaub A, Otte S, Callaway E, Sejnowski TJ (2010) Metabolic cost as a unifying principle governing neuronal biophysics. Proc Natl Acad Sci U S A 107: 12329–12334.
94. Balakrishnan V, Becker M, Lohrke S, Nothwang HG, Guresir E, et al. (2003) Expression and function of chloride transporters during development of inhibitory neurotransmission in the auditory brainstem. J Neurosci 23: 4134–4145.
95. Kakazu Y, Akaike N, Komiyama S, Nabekura J (1999) Regulation of intracellular chloride by cotransporters in developing lateral superior olive neurons. J Neurosci 19: 2843–2851.
96. Ehrlich I, Lohrke S, Friauf E (1999) Shift from depolarizing to hyperpolarizing glycine action in rat auditory neurones is due to age-dependent Cl- regulation. J Physiol 520 Pt 1: 121–137.
97. Lohrke S, Srinivasan G, Oberhofer M, Doncheva E, Friauf E (2005) Shift from depolarizing to hyperpolarizing glycine action occurs at different perinatal ages in superior olivary complex nuclei. Eur J Neurosci 22: 2708–2722.
98. Finck A, Schneck CD, Hartman AF (1972) Development of cochlear function in the neonate Mongolian gerbil (Meriones unguiculatus). J Comp Physiol Psychol 78: 375–380.
99. Woolf NK, Ryan AF (1984) The development of auditory function in the cochlea of the mongolian gerbil. Hear Res 13: 277–283.
100. Woolf NK, Ryan AF (1985) Ontogeny of neural discharge patterns in the ventral cochlear nucleus of the mongolian gerbil. Brain Res 349: 131–147.
101. Hodgkin A (1975) The optimum density of sodium channels in an unmyelinated nerve. Philos Trans R Soc Lond B Biol Sci 270: 297–300.
102. Wong-Riley MT, Tripathi SC, Trusk TC, Hoppe DA (1989) Effect of retinal impulse blockage on cytochrome oxidase-rich zones in the macaque striate cortex: I. Quantitative electron-microscopic (EM) analysis of neurons. Vis Neurosci 2: 483–497.
103. Wong-Riley M, Carroll EW (1984) Effect of impulse blockage on cytochrome oxidase activity in monkey visual system. Nature 307: 262–264.
104. Tucci D, Cant NB, Durham D (2002) Conductive hearing loss results in changes in cytochrome oxidase activity in gerbil central auditory system. J Assoc Res Otolaryngol 3: 89–106.
105. Wong-Riley MT, Merzenich MM, Leake PA (1978) Changes in endogenous enzymatic reactivity to DAB induced by neuronal inactivity. Brain Res 141: 185–192.

Journal of Neurochemistry

JOURNAL OF NEUROCHEMISTRY | 2013

doi: 10.1111/jnc.12369

ORIGINAL ARTICLE

Depolarization-induced suppression of a glycinergic synapse in the superior olivary complex by endocannabinoids

Barbara Trattner,*,† Sarah Berner,*,† Benedikt Grothe* and Lars Kunz*

*Department of Biology II, Division of Neurobiology, Ludwig Maximilians University Munich, Martinsried, Germany

†Graduate School of Systemic Neurosciences, Ludwig Maximilians University Munich, Martinsried, Germany

Abstract

The neuronal endocannabinoid system is known to depress synaptic inputs retrogradely in an activity-dependent manner. This mechanism has been generally described for excitatory glutamatergic and inhibitory GABAergic synapses. Here, we report that neurones in the auditory brainstem of the Mongolian gerbil (*Meriones unguiculatus*) retrogradely regulate the strength of their inputs via the endocannabinoid system. By means of whole-cell patch-clamp recordings, we found that retrograde endocannabinoid signalling attenuates both glycinergic and glutamatergic post-synaptic currents in the same types of neurones. Accordingly, we detected the cannabinoid receptor 1 in excitatory and inhibitory pre-synapses as well as the endocannabinoid-synthesising enzymes (diacylglycerol lipase α/β, DAGLα/β) post-synaptically through immunohistochemical stainings. Our study was performed with animals aged 10–15 days, that is, in the time window around the onset of hearing. Therefore, we suggest that retrograde endocannabinoid signalling has a role in adapting inputs during the functionally important switch from spontaneously generated to sound-related signals.

Keywords: CB1, DSE, DSI, LSO, MSO, retrograde.

Endocannabinoids are lipid-derived molecules produced on demand, which activate cannabinoid receptors. The endocannabinoid system operates as a retrograde negative feedback system in many brain areas (Herkenham *et al.* 1990; Katona and Freund 2012). Upon stimulation of a post-synaptic cell, endocannabinoid synthesis is initiated via a Ca^{2+}- dependent activation of endocannabinoid synthesising enzymes, which leads to the activation of pre-synaptic cannabinoid receptor 1 (CB1) (Liu *et al.* 2006; Alger and Kim 2011; Di Marzo 2011; Ueda *et al.* 2011; Castillo *et al.* 2012). CB1 receptors are G-protein coupled and – upon activation – attenuate Ca^{2+} influx into the pre-synaptic terminal and thus transmitter release by blocking vesicle fusion (Guo and Ikeda 2004). This feedback mechanism is called depolarization-induced suppression of inhibition (DSI) (Pitler and Alger 1992, 1994; Ohno-Shosaku *et al.* 2001; Wilson and Nicoll 2001) or depolarization-induced suppression of excitation (DSE) (Kreitzer and Regehr 2001), depending on whether the released neurotransmitter exerts an inhibitory or an excitatory action on the post-synaptic neurone (Ohno-Shosaku *et al.* 2012). DSI and DSE have been observed throughout the brain for GABAergic and glutamatergic synapses to provide a means for a cell to

Received April 27, 2013; revised manuscript received July 9, 2013; accepted July 9, 2013.

Address correspondence and reprint requests to Barbara Trattner and Lars Kunz, Department of Biology II, Division of Neurobiology, Ludwig Maximilians University Munich, D-82152 Martinsried, Germany.
E-mails: trattner@bio.lmu.de; lars.kunz@bio.lmu.de

Abbreviations used: 2-AG, 2-arachidonylglycerol; BAPTA, 1,2-bis (o-aminophenoxy)ethane-N,N,N',N'-tetraacetic acid; CB1, cannabinoid receptor 1; CN, cochlear nucleus; DAGL, diacylglycerollipase; DAPI, 4′,6-diamidino-2-phenylindole; DSE, depolarization-induced suppression of excitation; DSI, depolarization-induced suppression of inhibition; eEPSC, evoked excitatory post-synaptic current; eIPSC, evoked inhibitory post-synaptic current; GlyT2, glycine transporter 2; LNTB, lateral nucleus of the trapezoid body; LSO, lateral superior olive; MAP2, microtubule associated protein 2; MNTB, medial nucleus of the trapezoid body; MSO, medial superior olive; PBS, phosphate buffered saline; PFA, paraformaldehyde; P, postnatal day; PPR, paired pulse response; THL, tetrahydrolipstatin; VGluT1, vesicular glutamate transporter 1.

down-regulate its inputs in an activity-dependent manner. Retrograde glycinergic DSI has so far only been reported once in hypoglossal motor neurones of mice and rats (Mukhtarov *et al.* 2005). Direct modulation of glycinergic currents by binding of endocannabinoids to post-synaptic glycine receptors has been thoroughly investigated, leading to depression (Lozovaya *et al.* 2005) or potentiation of glycine receptor-mediated currents (Hejazi *et al.* 2006).

We studied a potential retrograde modulation of glycinergic neurotransmission by endocannabinoids in two nuclei of the superior olivary complex in the auditory brainstem, namely the medial and the lateral superior olive (MSO and LSO, respectively). These nuclei are involved in localization of sound sources in an acoustic environment and their neurones receive excitatory glutamatergic as well as inhibitory glycinergic projections (Kandler and Friauf 1995; Brand *et al.* 2002; Grothe 2003; Pecka *et al.* 2008; Grothe *et al.* 2010) (Fig. 1). Especially the strength of the glycinergic projections is crucial for allowing the computation of sound related inputs in the physiological range (Brand *et al.* 2002; Grothe 2003). Therefore, the existence of a potential DSI mechanism in these auditory neurones would be important in the context of adaptation to changes in the acoustic environment. In the LSO of young rats, which have not yet developed functional hearing, expression of the CB1 receptor at glycinergic medial nucleus of the trapezoid body (MNTB) terminals has already been shown by immunohistochemistry and a modulatory involvement of the endocannabinoid system in stimulus processing has been suggested (Chi and Kandler 2012). Electrophysiological recordings in other nuclei of the auditory brainstem revealed a strong impact of endocannabinoid signalling on excitatory neurotransmission (DSE) for the MNTB (Kushmerick *et al.* 2004) and the dorsal cochlear nucleus (Zhao *et al.* 2009; Sedlacek *et al.* 2011; Zhao and Tzounopoulos 2011).

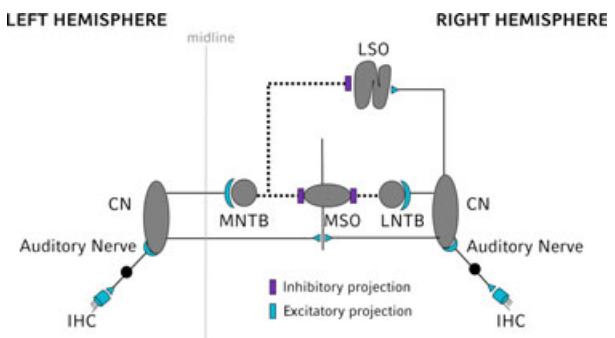

Fig. 1 Overview of the auditory brainstem circuitry. Auditory signals are transduced into neuronal activity by the inner hair cells (IHC), which transmit the information via the auditory nerve to the first station of the auditory brainstem, the cochlear nucleus (CN). The CN sends excitatory projections to the ipsilateral lateral superior olive (LSO), the ipsilateral later nucleus of the trapezoid body (LNTB), the ipsi- and contralateral medial superior olives (MSO) as well as to the contralateral medial nucleus of the trapezoid body (MNTB). MNTB and LNTB provide inhibitory glycinergic projections to the ipsilateral MSO and LSO or the ipsilateral MSO, respectively. For a review on sound localization please refer to (Grothe *et al.* 2010).

To examine a possible influence of endocannabinoid signalling in MSO and LSO neurones, we studied the distribution of CB1 and of endocannabinoid-synthesising enzymes diacylglycerol lipases α/β (DAGLα/β) by immunohistochemical stainings. In addition, we performed electrophysiological recordings to investigate, whether post-synaptic currents are influenced by retrograde endocannabinoid signalling. We conducted our study in the Mongolian gerbil (*Meriones unguiculatus*), which represents a suitable model organism for auditory neurosciences, as it possesses an audible spectrum and an organization of the auditory brainstem similar to humans (Heffner and Heffner 1988; Muller 1990).

Materials and methods

Animals

All experiments complied with institutional guidelines and national and regional laws. Ethical clearance for animal experiments was granted by the 'Regierung von Oberbayern'. Mongolian gerbils (*Meriones unguiculatus;* both sexes) at post-natal day (P) 10 and P13–15 (majority P13) were used. All animals were bred in the animal house of the Department of Biology II, Ludwig Maximilians University Munich.

Immunohistochemistry

Animals were anaesthetized using 100 mg/kg body weight metamizol (Novalgin®; Sanofi-Aventis Deutschland GmbH, Frankfurt, Germany), p.o., followed by 200 mg/kg body weight pentobarbital (Narcoren®; Merial GmbH, Hallbergmoos, Germany), i.p. After the animals had reached a deep anaesthetic stage, they were transcardially perfused at a flow rate of 4 mL/min with Ringer solution supplemented with 0.1% heparin (Meditech Vertriebs GmbH, Parchim, Germany) for 10 min followed by 4% paraformaldehyde (PFA) for 20 min. The brains were post-fixed overnight in 4% PFA at 4°C. Using a Leica VT1200S vibratome (Leica Microsystems GmbH, Wetzlar, Germany), 50 µm sections of the auditory brainstem were collected and washed 4 times in 0.1 M phosphate buffered saline (PBS) for 5 min each. Then, unspecific binding sites were blocked using a blocking solution (0.3% Triton X-100, 0.1% saponine and 1% bovine serum albumin) for 1 hour at 22°C on a shaker. Sections were incubated in the primary antibody mix diluted in blocking solution over night at 4°C on a shaker. Primary antisera used were: chicken anti-microtubule associated protein 2 [MAP2, 1 : 1000; Neuromics (Edina, MN, USA), CH22103], rabbit anti-CB1 [1 : 300; Alomone Labs (Jerusalem, Israel), ACR-001], mouse anti-vesicular glutamate transporter 1 [VGluT1, 1 : 500; EMD Millipore Cooperation (Billerica, MA, USA), MAB5502], guinea pig anti-glycine transporter 2 (GlyT2, 1 : 1000, Millipore, AB1773) as well as rabbit anti-DGLα (1 : 500) and rabbit anti-DGLβ (1 : 500, both gift from Dr. Ken Mackie, Indiana University). Thereafter, sections were washed four times in 0.1 M PBS for 5 min each and incubated with secondary antibodies for 3–4 h at 22°C on

a shaker. Secondary antisera used were: donkey anti-rabbit DyLight 649 [1 : 300; Dianova GmbH (Hamburg, Germany), 711-496-152], donkey anti-rabbit DyLight 488 (1 : 100, Dianova, 711-486-152), goat anti-mouse Cy5 (1 : 100, Dianova, 115-175-166), donkey anti-guinea pig Cy3 (1 : 300, Millipore, AP193C), goat anti-chick Alexa488 [1 : 400; Molecular probes (Life Technologies GmbH, Darmstadt, Germany), A11039] and donkey anti-chick Cy3 (1 : 300, Dianova, 703-166-155). Afterwards, the sections were washed four times in 0.1 M PBS for 10 min each. Finally, the slices were mounted with Vectashield supplemented with 4′,6-diamidino-2-phenylindole (DAPI) (H-1200; Vector Laboratories Inc., Burlingame, CA, USA).

To visualize immunohistochemical stainings, confocal optical sections were acquired with a Leica 6000CS SP5 confocal laser-scanning microscope (Leica Microsystems, Mannheim, Germany) equipped with a Plan 63x/NA1.32 oil immersion objective. Fluorochromes were visualized by using a UV laser with an excitation wavelength of 405 nm (emission 420–475 nm for DAPI), an argon laser with an excitation wavelength of 488 nm (emission 494–555 nm for Alexa 488/DyLight 488), a DPSS laser with a laser line of 561 nm (emission 565–606 nm for Cy3) and a helium-neon laser with an excitation wavelength of 633 nm (emission 640–740 nm for DyLight 649). For each optical section the images were collected sequentially for the different fluorochromes. Stacks were obtained with axial distances of 300 nm – the image size was 512 × 512 pixels. To obtain an improved signal-to-noise ratio each section image was averaged from four successive line scans. The images shown in the figures of this publication are single images from the stacks and thus have an axial distance of 300 nm.

Electrophysiological recordings

Animals were anaesthetized with isoflurane, followed by rapid decapitation. The brains were removed and placed in ice-cold dissecting solution containing (in mM, all from Sigma-Aldrich Chemie GmbH, München, Germany): 50 sucrose, 25 NaCl, 25 $NaHCO_3$, 2.5 KCl, 1.25 NaH_2PO_4, 3 $MgCl_2$, 0.1 $CaCl_2$, 25 glucose, 0.4 ascorbic acid, 3 myo-inositol and 2 Na-pyruvate. The pH amounted to 7.4 when bubbled with 95% O_2 and 5% CO_2. Horizontal brainstem sections of 200 μm thickness were cut using a VT1000S vibratome (Leica). Slices were incubated in extracellular recording solution continuously bubbled with 95% O_2 and 5% CO_2 for 45 min at 36°C and then stored at 22°C until use. The extracellular recording solution contained (in mM, all from Sigma-Aldrich): 125 NaCl, 25 $NaHCO_3$, 2.5 KCl, 1.25 NaH_2PO_4, 2 $CaCl_2$, 1 $MgCl_2$, 25 glucose, 0.4 ascorbic acid, 3 myo-inositol and 2 Na-pyruvate.

For recording, slices were transferred into a chamber mounted on a microscope (Olympus BX51WI, Olympus Europa Holding GmbH, Hamburg, Germany) and continuously perfused with fresh extracellular recording solution at room temperature (≈ 22°C). Voltage-clamp whole-cell recordings were performed with an EPC9 amplifier (HEKA Elektronik Dr. Schulze GmbH, Lambrecht/Pfalz, Germany) on visually identified MSO neurones. Cells were clamped at −60 mV unless stated otherwise. Series resistance was compensated to a residual of 3–4 MΩ. Glass pipettes used for recording had a resistance between 2.0 and 4.5 MΩ. The intracellular solution contained in mM (all from Sigma-Aldrich): 105 Cs-gluconate, 26.7 CsCl, 10 HEPES, 20 TEA-Cl, 3.3 $MgCl_2$, 2 Na_2ATP, 0.2 NaGTP, 3 Na-phosphocreatine and 1 EGTA. The solution was adjusted to pH 7.2 with CsOH. To investigate whether retrograde endocannabinoid signalling is dependent on a rise in post-synaptic Ca^{2+} levels, we carried out some recordings in the presence of 30 mM 1,2-bis(o-aminophenoxy)ethane-N,N,N',N'-tetraacetic acid (BAPTA) (Sigma-Aldrich) in the intracellular recording solution. Glycinergic post-synaptic currents for DSI recordings were pharmacologically isolated by adding 50 μM D-APV (BioTrend Chemikalien GmbH, Köln, Germany), 20 μM DNQX (BioTrend) and 10 μM gabazine (Sigma-Aldrich) to the extracellular recording solution. Excitatory post-synaptic currents for DSE recordings were pharmacologically isolated by supplementing the extracellular solution with 0.5 μM strychnine (Sigma-Aldrich) and 10 μM gabazine. To investigate the effects of the endocannabinoid system on evoked post-synaptic currents the following CB1 agonists and antagonists were used: rimonabant (2 μM, Cayman Chemical Company, Ann Arbor, MI, USA), WIN 55,212-2 mesylate (1 μM, BioTrend) and anandamide (1 μM, Cayman Chemical). Recordings with tetrahydrolipstatin (THL) to test an involvement of 2-arachidonylglycerol (2-AG) in endocannabinoid signalling, were carried out in brain slices that were incubated in 10 μM THL (Cayman Chemicals) in extracellular recording solution for 1.5 h prior to the recording, which was also carried out in the presence of 10 μM THL.

Glycinergic currents were evoked by placing a bipolar tungsten electrode at the fibre bundle originating in the ipsilateral MNTB. Excitatory currents for DSE recordings were evoked by placing the stimulation electrode dorso-lateral to the MSO, to stimulate fibres originating in the ipsilateral cochlear nucleus. Fibres were stimulated with a rate of 0.33 Hz and pulse duration of 0.2 ms. The stimulus strength was set generally to 2–3 V for inhibitory currents and to 3–9 V for excitatory currents. The reason for this difference is that inhibitory fibres originating from the MNTB are easy to target as they run in a thick fibre bundle. Excitatory fibres cannot be located visually under the microscope and thus we sometimes had to apply higher stimulation strengths to recruit fibres that run deeper within the tissue. Before starting a DSI/DSE experiment, we ensured that the baseline current amplitude was stable for at least 21 stimulations (≥ 1 min). For conducting DSI/DSE experiments the cell was depolarized for 5 s to 0 mV, representing the standard protocol for DSI induction (Wilson and Nicoll 2001), after seven stimulations, which were used to calculate the baseline current for normalization. For DSI recordings also other depolarization protocols were tested to evoke endocannabinoid signalling: Either depolarization to 0 mV for 0.5 s or the StimAP stimulus. The StimAP stimulus is a voltage-clamp stimulus given instead of the 5 s constant depolarization to 0 mV that was generally used to elicit DSI. The stimulus consisted of a square wave pulse alternating between −40 and +40 mV at a frequency of 200 Hz for a duration of 5 s. This stimulus mimics the membrane response during a high frequent action potential train. For quantification all currents were normalized to the average baseline current before the depolarization pulse. During pharmacological experiments values for each time point were calculated by averaging the amplitudes of the three evoked post-synaptic currents (ePSCs) preceding depolarization (before depol.), the amplitudes of the first three ePSCs following depolarization (after depol.) or the amplitudes of the 12th to 14th ePSC after depolarization (recovery). For paired-pulse ratio (PPR) recordings, a pulse length of 0.2 ms and an inter-pulse interval of 9.8 ms were used.

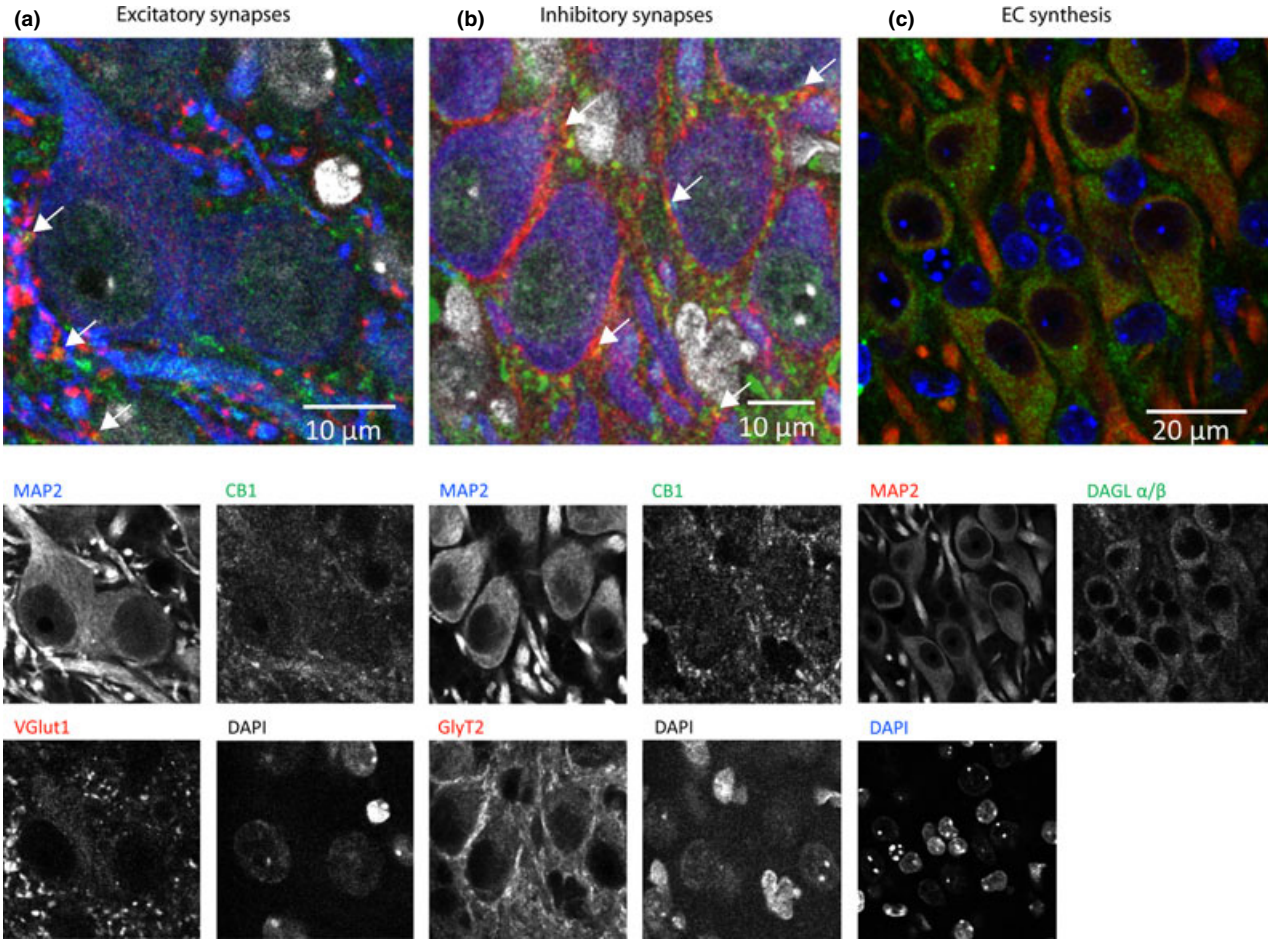

Fig. 2 Cannabinoid receptor 1 (CB1) and diacylglycerol lipase α/β (DAGLα/β) are expressed in medial superior olive (MSO) neurones at P13. (a, b) Neuronal expression of CB1 and partial co-localization (yellow; arrows) with vesicular glutamate transporter 1 (VGluT1) (a) and glycine transporter 2 (GlyT2) (b). (c) The 2-AG synthesising enzymes DAGL α/β are expressed somatically by microtubule associated protein 2 (MAP2)-positive neurones as well as, in lower amounts, by other brain cells. The neuronal somata and dendritic processes are visualized with a MAP2 staining and nuclei were stained by DAPI. The color, in which the respective antigen is depicted in the overlay image, is identical to the color, in which the protein name is written above the corresponding single image.

Statistics

Statistical analyses were performed using Prism 5.0 (Graphpad Software Inc., La Jolla, CA, USA). Average values are given as mean ± SEM. We compared PPR data using a paired *t*-test. All other data were tested for deviation from 1.0 with a one-sample *t*-test, as all data were normalized. We assigned significance for $p < 0.1$. The respective *p*-values are given in the Figure legends.

Results

The endocannabinoid system is expressed in neurones of the MSO and LSO

Using immunohistochemistry, we detected a strong neuronal CB1 expression in the MSO and LSO at both P10 (not shown) and P13 (Figs 2 and 3). CB1 was partially co-localized with VGluT1 (Figs 2a and 3a; arrows mark sites of co-localization), which is a pre-synaptic marker for excitatory glutamatergic synapses, as well as with GlyT2 (Figs 2b and 3b; arrows mark sites of co-localization), a pre-synaptic marker for inhibitory glycinergic synapses. Considering endocannabinoid production, we investigated the expression of DAGLα/β with immunohistochemical labelling. We observed that DAGLα/β were expressed somatically by most neurones at both P10 (not shown) and P13 in the MSO (Fig. 2c) and LSO (Fig. 3c), as indicated by a co-localization with the neuronal marker MAP2. Lower levels of DAGLα/β were also detected in MAP2-negative cells, which are presumably glial cells (Fig. 2c).

Endocannabinoids retrogradely modulate glycinergic neurotransmission

We showed that inhibitory glycinergic currents, evoked by stimulation of axons originating from the MNTB, were reduced in amplitude upon depolarization of the

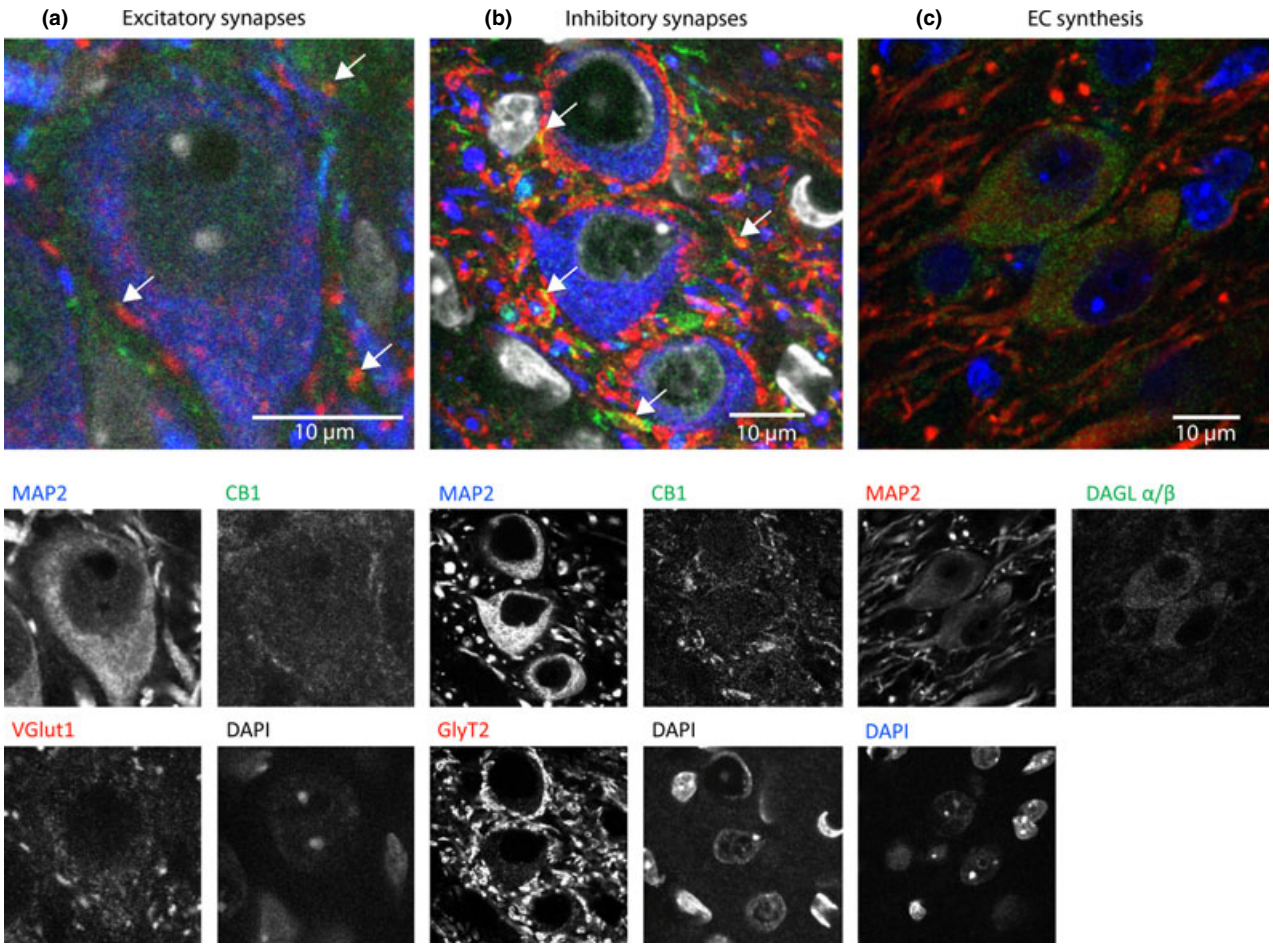

Fig. 3 Immunohistochemical localization of cannabinoid receptor 1 (CB1) and diacylglycerol lipase α/β (DAGLα/β) in lateral superior olive (LSO) neurones at P13. (a, b) Neuronal expression of CB1 and partial co-localization (yellow; arrows) with vesicular glutamate transporter 1 (VGluT1) (a) and glycine transporter 2 (GlyT2) (b). (c) The 2-AG synthesising enzymes DAGL α/β are expressed somatically by neurones as well as, in lower amounts, by other brain cells. The neuronal somata and dendritic processes are visualized with a microtubule associated protein 2 (MAP2) staining and nuclei were stained by DAPI. The color, in which the respective antigen is depicted in the overlay image, is identical to the color, in which the protein name is written above the corresponding single image.

post-synaptic cell, in both MSO (P10, Fig. 4a; P13 Fig. 4b) and LSO (P13, Fig. 8a; P10 not shown) for both age groups. The amplitude and time course of DSI was similar in MSO and LSO for both P10 and P13 (Fig. 4c). Generally, a depolarization of 5 s to 0 mV resulted in about 45% current amplitude reduction and the baseline amplitude was reached again within 20–30 s after depolarization. As the standard protocol with a depolarization pulse of 0 mV for 5 s does not represent a physiological input in these neurones, we tried to elicit DSI using more relevant stimuli in MSO neurones at P13 (Fig. 4d). A constant depolarization to 0 mV for 0.5 s did not result in any alteration of evoked current amplitude. However, a square wave function at 200 Hz with a maximum of +40 mV for 5 s (StimAP), which simulates a 200 Hz action potential train and thus represents a physiologically more relevant stimulus than the constant depolarization generally used in the literature (Wilson and Nicoll 2001), elicited DSI in a similar way. As the CB1 antagonist rimonabant completely blocked DSI of glycinergic currents (Fig. 6a), we conclude that DSI is retrogradely mediated by endocannabinoids. Endocannabinoid-dependent DSI has been previously shown to depend on raised post-synaptic Ca^{2+} levels (Ohno-Shosaku *et al.* 2001). Thus, we performed recordings in MSO neurones at P13 with 30 mM BAPTA in the intracellular solution. When intracellular Ca^{2+} was chelated by BAPTA, glycinergic DSI could not be elicited with 5 s depolarization to 0 mV (Fig. 7a).

To provide further evidence that the observed DSI is caused by endocannabinoid signalling, a series of pharmacological experiments was conducted. First, the paired-pulse ratio was shown to increase upon the wash-in of the synthetic CB1 receptor agonist WIN 55,212-2, which indicates a

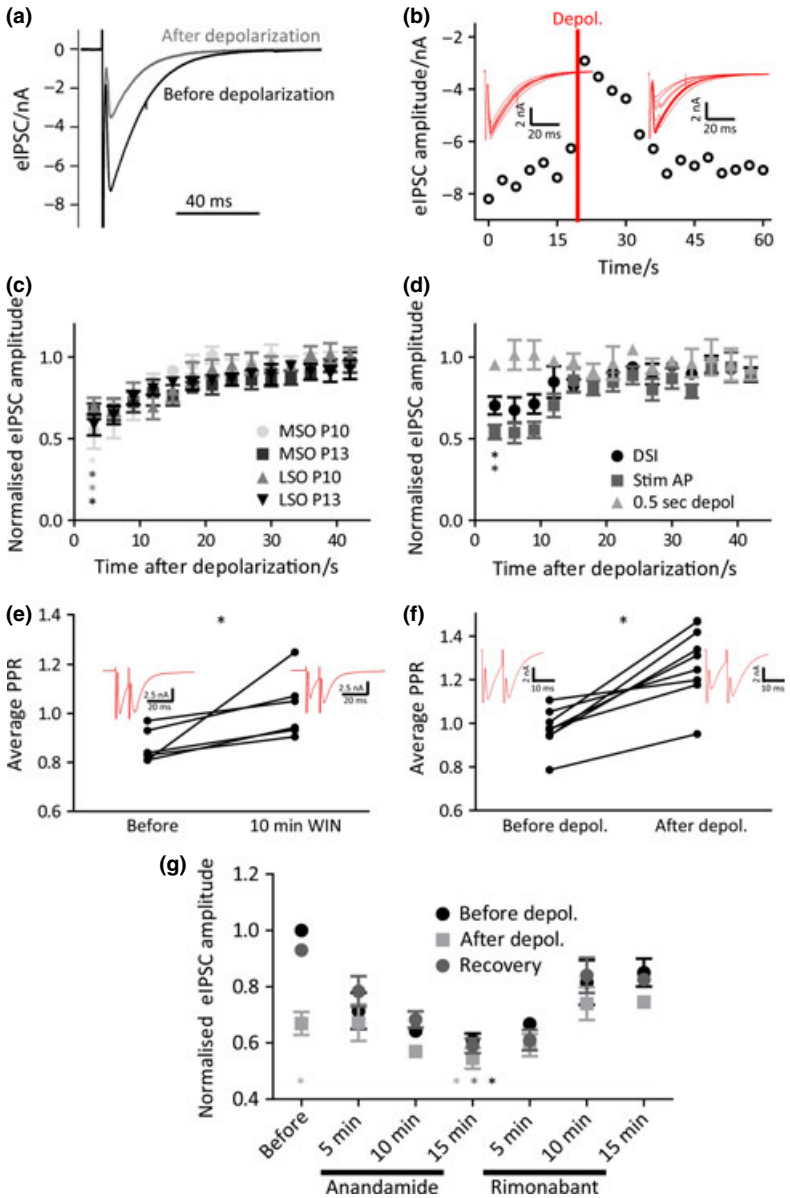

Fig. 4 Endocannabinoid-dependent retrograde modulation of glycinergic synapses. (a) Upon depolarization for 5 s at 0 mV evoked inhibitory post-synaptic current (eIPSC) is reduced (sample trace from medial superior olive (MSO) neurone, P10). (b) The time course of a DSI experiment for an MSO P13 neurone was quantified. The first seven eIPSCs represent values before depolarization (circles) and were used to establish a baseline for DSI quantification. Sample traces for this neurone are given as red current traces for the currents before depolarization and after depolarization. The red line indicates the timepoint of depolarization. The scale bar in the inset is valid for all sample traces of this panel. (c) Amplitude of DSI and time course of its recovery are similar in MSO and lateral superior olive (LSO) at both ages. The first values after induction deviate significantly from 1.0 (MSO P13: $n = 6$ cells, $p = 0.0009$; LSO P13: $n = 7$ cells, $p = 0.0007$; MSO P10: $n = 7$ cells, $p = 0.0063$; LSO P10: $n = 7$ cells, $p = 0.0017$). (d) The StimAP stimulus (200 Hz square wave with an amplitude maximum of 40 mV for 5 s, $n = 5$ cells) produced a similar response as depolarization to 0 mV for 5 s (DSI; $n = 5$ MSO neurones, P13). A constant depolarization to 0 mV for 0.5 s did not cause DSI ($n = 5$ cells). The first values after induction are significantly different from 1.0 for DSI ($p = 0.0055$) and StimAP ($p = 0.0005$), but not for 0.5 s depol. ($p > 0.1$). (e) PPR was increased by WIN 55,212-2 in all MSO cells tested (P13, $n = 6$ cells, $p = 0.0374$). Sample traces of an MSO P13 neurone are shown as a red inset with scale bars. (f) PPR was increased by depolarization for 5 s to 0 mV in all MSO cells tested (P13, $n = 8$ cells, $p = 0.0008$). Sample traces of an MSO P13 neurone are shown as a red inset with scale bars. (g) Wash-in of anandamide or rimonabant affected the eIPSC amplitude in MSO neurones (P13, $n = 5$ cells). The normalized amplitudes after depolarization as well the values at the end of anandamide application differed significantly from 1.0 (depolarization: $p = 0.0173$; anandamide: $p = 0.0006$), whereas the final value for rimonabant did not ($p > 0.1$).

pre-synaptic mechanism in the MSO (Fig. 4e) and LSO (data not shown, $n = 3$, $p = 0.0199$; paired t-test). In addition, we checked whether the paired-pulse ratio was also affected by post-synaptic depolarization. Depolarization to 0 mV for 5 s significantly increased the paired-pulse ratio ($n = 8$, $p = 0.0008$, paired t-test), supporting that our depolarization stimulus indeed is adequate to elicit endocannabinoid signalling (Fig. 4f). Wash-in of the endogenous CB1 receptor agonist anandamide decreased evoked inhibitory post-synaptic current (eIPSC) to about 60%, whereas subsequent wash-in of the CB1 receptor inverse agonist rimonabant rescued eIPSC to about 80% of baseline and eliminated the effect of depolarization on current amplitude (Figs 4g and 8b). Application of the CB1 agonist WIN 55,212-2 instead of anandamide led to a comparable suppression of inhibitory post-synaptic currents, which was, however, less in amplitude (72% of the original value) when compared to anandamide application. As with anandamide, rimonabant was unable to fully recover the baseline current (87% of the original value), but blocked DSI in favor of a CB-mediated endocannabinoid action (Figure S1). Rimonabant application alone completely abolished the effect of depolarization and inhibitory post-synaptic currents were no longer reduced by depolarising the cell for 5 s to 0 mV (Fig. 6a). This block of the effect by rimonabant shows that the effect observed is mediated by retrograde cannabinoid signalling. Furthermore, we were interested, whether 2-AG contributes to endocannabinoid signalling, as we found high levels of DAGLα/β immunohistochemically (Figs 2c and 3c). To this extent we conducted electrophysiological recordings in MSO P13 neurones in the presence of THL, which is an inhibitor of the DAGLα/β enzymes and should thus block DSI, if 2-AG was necessary for DSI induction. Our recordings show that DSI cannot be elicited in the presence of 10 μM THL (Fig. 7c), suggesting that 2-AG is the main endocannabinoid mediating DSI in the MSO at P13.

Endocannabinoids retrogradely modulate glutamatergic neurotransmission

Excitatory glutamatergic currents, evoked by stimulation of axons originating from the ipsilateral cochlear nucleus, were reduced upon a depolarization to 0 mV for 5 s in both MSO (Fig. 5a and b) and LSO neurones (Fig. 8c). The current amplitude at P13 was reduced by around 30% (MSO) and 38% (LSO), respectively. The time course of DSE was similar in neurones of both nuclei (Fig. 5c). DSE could also be evoked – to a lesser extent – by the StimAP stimulus, which caused a reduction in current amplitude to about 78% of the original value in MSO P13 cells (Fig. 5d). DSE is also mediated by retrograde endocannabinoid signalling, as it cannot be evoked in the presence of the CB1 antagonist rimonabant (Fig. 6b). To test, whether DSE is also dependent on intracellular Ca^{2+} increase, we conducted experiments where the intracellular recording solution was supplemented with 30 mM BAPTA. When Ca^{2+} was chelated by BAPTA, DSE could not be elicited (Fig. 7b), which strongly indicates a Ca^{2+} dependency of our effect, as would be expected from retrograde endocannabinoid-mediated DSI.

The paired-pulse ratio of evoked glutamatergic currents was increased upon administration of the CB1 agonist WIN 55,212-2 (Fig. 5e) or by constant depolarization for 5 s to 0 mV (Fig. 5f), which indicates a pre-synaptic mode of action.

To test the dependence of DSE on retrograde endocannabinoid signalling, pharmacological experiments were carried out (Figs 5g and 8d). Wash-in of anandamide depressed evoked excitatory current amplitude by about 40% and subsequent treatment of the neurones with rimonabant recovered the full baseline current amplitude after 15 min. Application of rimonabant alone completely blocked depolarization-induced suppression of glutamatergic currents, strongly indicating that the effect observed is retrogradely mediated by endocannabinoids (Fig. 6b). Furthermore, we investigated, whether 2-AG also mediates DSE, by trying to evoke DSE in the presence of 10 μM of the DAGLα/β inhibitor THL. Our results show that we were unable to elicit DSE, when 2-AG was not produced (Fig. 7d), indicating that 2-AG is necessary for DSE induction.

Discussion

The data presented here show that a retrograde endocannabinoid system is functionally active for both inhibitory glycinergic and excitatory glutamatergic synapses targeting the same neurones in the developing MSO and LSO (P10-15). We found the presence of pre-synaptic CB1 receptors as well as somatic expression of diacylglycerol lipase α/β, enzymes critically involved in the synthesis of one of the most important endocannabinoids (i.e. 2-arachidonylglycerol, 2-AG) (Best and Regehr 2010). The pre-synaptic CB1 receptors were partially co-localized with VGluT1 (Figs 2a and 3a; arrows mark co-localization sites), a marker for excitatory glutamatergic synapses, as well as with GlyT2 (Figs 2b and 3b; arrows mark co-localization sites), a marker for glycinergic terminals indicative of modulation of glycinergic and glutamatergic neurotransmission by retrograde endocannabinoid signalling. In accordance with our findings in the LSO, CB1 expression on glycinergic terminals originating from the MNTB has been reported in developing rats (Chi and Kandler 2012). However, our immunohistochemical experiments suggest an additional extrasynaptic localization of CB1 receptors (Figs 2 and 3) and their involvement in volume transmission by endocannabinoids (Fuxe *et al.* 2012).

To determine, whether the endocannabinoid system components detected by immunohistochemistry also play a functional role in neuronal signalling, we conducted a series

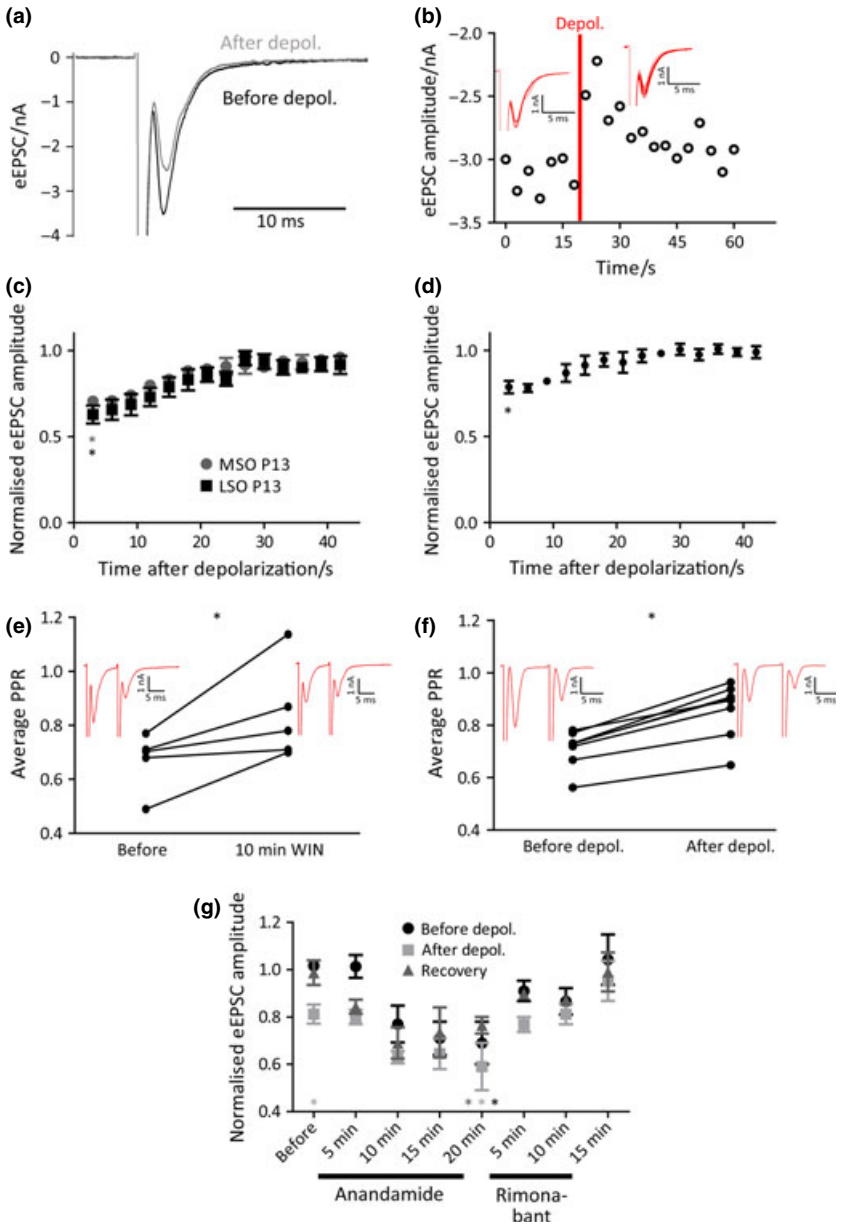

Fig. 5 Endocannabinoid-dependent retrograde modulation of glutamatergic synapses. (a) Depolarization for 5 s to 0 mV results in depression of evoked excitatory post-synaptic currents (eEPSCs) [sample trace from medial superior olive (MSO) neurone, P13]. (b) The time course of one DSE experiment for an MSO P13 neurone was quantified. Sample traces for this neurone are given as red current traces for the currents before and after depolarization. The timepoint at which depolarization occurred is marked by the red vertical line. The scale bar in the inset is valid for all sample traces of this panel. (c) Amplitude of DSE and time course of its recovery are similar in MSO and lateral superior olive (LSO) at P13. The first values after induction deviate significantly from 1.0 (MSO P13: $n = 6$ cells, $p < 0.0001$; LSO P13: $n = 5$ cells, $p = 0.0020$). (d) The StimAP stimulus elicited DSE in a similar way, but with lesser amplitude as the constant depolarization for 5 s to 0 mV. The first values after induction deviate significantly from 1.0 (MSO P13, $n = 7$ cells, $p < 0.001$) (e) PPR was increased by WIN 55,212-2 in all MSO neurones tested (P13, $n = 5$ cells, $p = 0.0328$). Sample traces of an MSO P13 neurone are shown as a red inset with scale bars. (f) PPR was increased by depolarization for 5 sec to 0 mV in all MSO cells tested (P13, $n = 8$ cells, $p < 0.0001$). Sample traces of an MSO P13 neurone are shown as a red inset with scale bars. (g) Wash-in of anandamide or rimonabant affected the eEPSC amplitude in MSO neurones at P13 ($n = 6$ cells). The normalized amplitudes after depolarization as well the values at the end of anandamide application differed significantly from 1.0 (depolarization: $p = 0.0025$; anandamide: $p = 0.0937$), whereas the final value for rimonabant did not ($p > 0.1$).

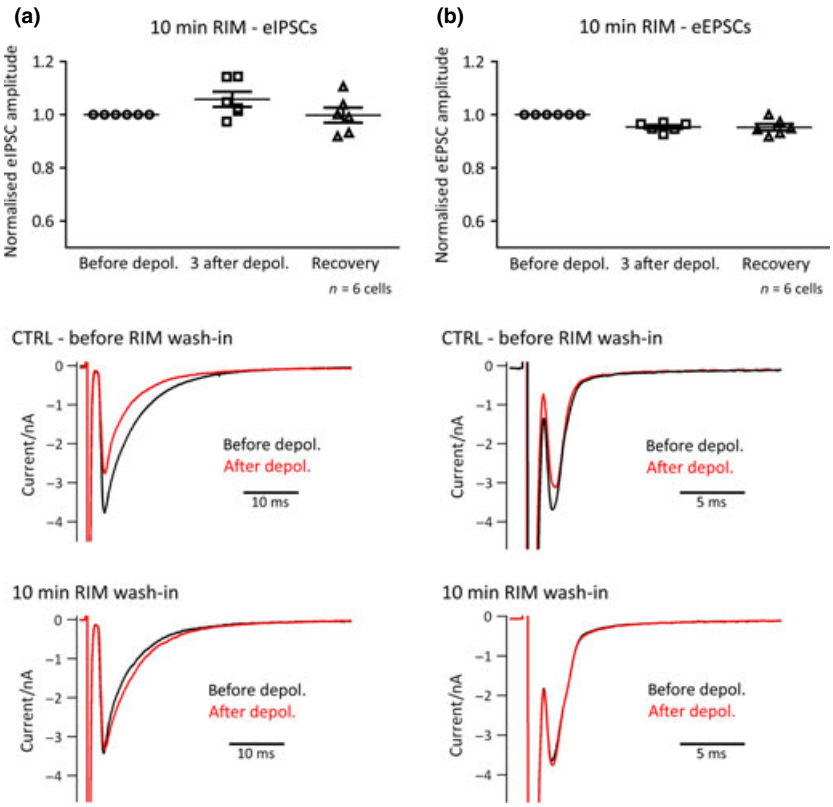

Fig. 6 The cannabinoid receptor 1 (CB1) antagonist rimonabant blocks the induction of depolarization-induced suppression of inhibition (DSI) and depolarization-induced suppression of excitation (DSE). (a) When rimonabant (RIM) has been washed in for 10 min the induction of DSI is blocked [P13 medial superior olive (MSO), $n = 6$ cells]. The sample traces represent DSI recordings before the wash-in of rimonabant (CTRL) and 10 min after RIM wash-in. (b) RIM wash-in for 10 min prevents the induction of DSE as well (P13 MSO, $n = 6$ cells). The sample traces of DSE recordings were recorded before the wash-in of rimonabant (CTRL) and 10 min after RIM wash-in.

of electrophysiological recordings. Firstly, we observed an endocannabinoid-dependent retrograde depression of evoked glycinergic currents in both MSO and LSO at P10 and P13 (Figs 4, 8a and b), which was blocked by the CB1 antagonist rimonabant (Fig. 6a) and required the rise of intracellular Ca^{2+} levels induced by depolarization (Fig. 7a), as it is generally described for DSI (Ohno-Shosaku *et al.* 2001). Until now DSI has mostly been described for GABAergic synapses (Ohno-Shosaku *et al.* 2001; Wilson and Nicoll 2001) with one exception; in rodent hypoglossal motoneurones glycinergic DSI has been reported as well (Mukhtarov *et al.* 2005). Both amplitude and time course of our glycinergic DSI are comparable to those reported for GABAergic DSI (Ohno-Shosaku *et al.* 2001; Wilson and Nicoll 2001). This is plausible as the processes of both DSI and DSE affect neurotransmitter release by interacting with the same players (CB1, G proteins, voltage-dependent Ca^{2+} channels, etc.). Neurotransmitter specific processes (e.g. at the post-synapse) are not affected and, thus, DSI and DSE (i.e. their amplitude, duration and time course) are supposed to be independent of the type of neurotransmitter (Katona and Freund 2012). However, when we compared glycinergic DSI in the MSO to glycinergic DSI previously reported in hypoglossal motor neurones of rat and mouse (Mukhtarov *et al.* 2005), glycinergic DSI in our study was smaller in amplitude and recovered faster from depression (Fig. 4b, c and d). Reasons for these observed discrepancies could be differences in species, animal age or stimulation procedure.

We could show a retrograde action of the endocannabinoid system on the release of glycinergic neurotransmitter vesicles by the complete prevention of DSI in the presence of rimonabant (Fig. 6a). Furthermore, we were interested whether a direct modulation of the glycine receptor by endocannabinoids might also be involved (Lozovaya *et al.* 2005). Unlike in the case of anandamide-evoked depression of evoked excitatory post-synaptic current (eEPSCs) – rimonabant could not fully revert the anandamide-evoked depression of glycinergic currents in the MSO (Figs 4g and 5g). In contrast to anandamide, the synthetic CB1 agonist WIN 55,212-2 does not directly modulate glycine receptors (Lozovaya *et al.* 2005), but has the disadvantage of directly modulating voltage-gated Ca^{2+} currents (Nemeth *et al.* 2008). However, recordings with WIN 55,212-2 yielded similar results as with anandamide in the MSO (Figure S1), that is, subsequent rimonabant wash-in could not fully recover the baseline amplitude of the currents. Therefore, we conclude that the inability of rimonabant to recover the baseline current amplitude after CB1 agonist administration is probably not caused by a CB1-independent endocannabinoid modulation of glycine receptors. On the basis of the complete blockage of DSI and DSE in the presence of rimonabant, we conclude that endocannabinoid signalling operates mainly retrogradely at this synapse.

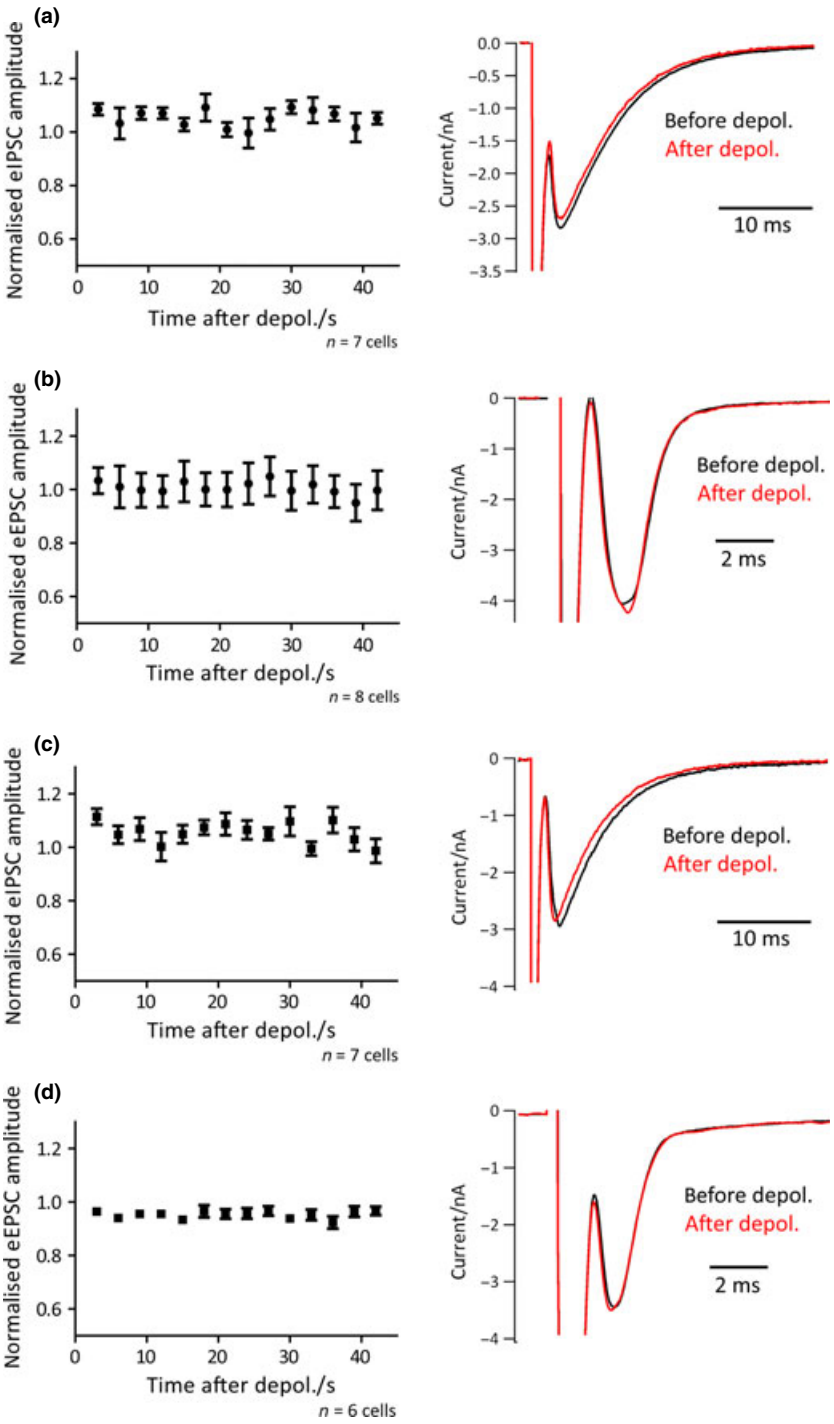

Fig. 7 Retrograde endocannabinoid signalling is mediated by 2-AG and dependent on a post-synaptic rise in Ca^{2+} levels. (a, b) 30 mM BAPTA in the intracellular solution completely abolished DSI [a; medial superior olive (MSO) P13, $n = 7$ cells] and DSE (b; MSO P13, $n = 8$ cells). (c, d) Incubation of the brain slices with THL, a diacylglycerol lipase α/β (DAGLα/β) blocker, prevented induction of DSI (c; MSO P13, $n = 7$ cells) and DSE (d; MSO P13, $n = 6$ cells).

Secondly, we also detected a retrograde modulation of glutamatergic synaptic transmission with a time course of recovery similar to glycinergic DSI found in this study and previously reported data on glutamatergic DSE (Kreitzer and Regehr 2001) (Fig. 5b and c). DSE induction was dependent on a rise in intracellular Ca^{2+} levels (Fig. 7b) and could be blocked by rimonabant (Fig. 6b), which proves that it is mediated by retrograde endocannabinoid signalling via pre-synaptically located CB1 receptors. A depression of glutamatergic currents could further be achieved by wash in of the endogenous CB1 agonist anandamide (Fig. 5g). In addition, we could also show electrophysiologically that the activity of the DAGLα/β enzymes is necessary for the induction of DSI and DSE (Fig. 7c and d), as suggested by our immunohistochemical stainings (Figs 2c and 3c).

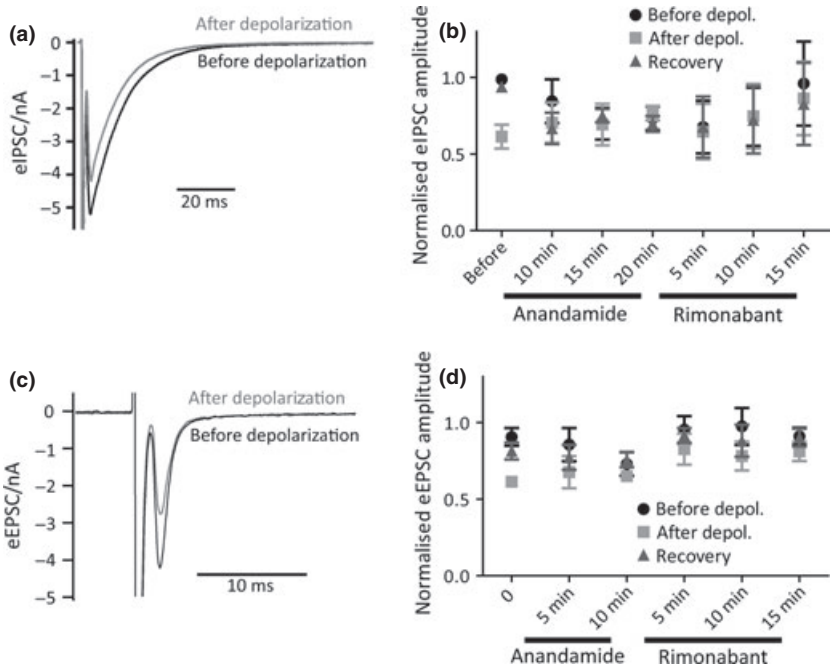

Fig. 8 Retrograde endocannabinoid signalling is present in lateral superior olive (LSO) neurones. (a) Depolarization for 5 s to 0 mV results in DSI (sample trace, P13). (b) Wash-in of anandamide or rimonabant affected the evoked inhibitory post-synaptic current amplitude in LSO neurones (P13, $n = 4$ cells). The normalized amplitudes after depolarization as well the values at the end of anandamide application differed significantly from 1.0 (depolarization: $p = 0.0484$; anandamide: $p = 0.0465$), whereas the final value for rimonabant did not ($p > 0.1$). (c) Depolarization for 5 s to 0 mV results in DSE (sample trace, P13). (d) Wash-in of anandamide or rimonabant affected the evoked excitatory post-synaptic current (eEPSC) amplitude in LSO neurones (P13, $n = 3$ cells). The normalized amplitudes after depolarization as well the values at the end of anandamide application differed significantly from 1.0 (depolarization: $p = 0.0321$; anandamide: $p = 0.0983$), whereas the final value for rimonabant did not ($p > 0.1$).

Hearing onset in Mongolian gerbils occurs at P12-13 (Woolf and Ryan 1984). Before hearing onset, neurones in the auditory brainstem are stimulated by spontaneous activity, which is generated by ATP-signalling in cochlear hair cells (Tritsch *et al.* 2007). This spontaneous activity is required for the correct development of auditory circuits as well as for the fine-tuning of tonotopic maps (Kandler 2004; Leake *et al.* 2006; Leao *et al.* 2006). As retrograde endocannabinoid signalling acts as a negative feedback loop, inhibiting the inputs received by the neuron, it is conceivable that the endocannabinoid system is involved in balancing the spontaneous activity and thereby contributes to the functional development of the auditory system before hearing onset (Chi and Kandler 2012). After hearing onset, the endocannabinoid system could help adjusting the stimulus strength of physiological inputs. The persisting endocannabinoid system might help to attenuate these new stimuli until further mechanisms for adaptation to the acoustic environment have been established and, thereby, protect MSO and LSO neurones from excitotoxicity. As endocannabinoid signalling acts because of the hydrophobicity of the compounds very locally (Brown *et al.* 2003), it is conceivable that a selective modulation of certain inputs enables accurate computation of sound source localization in ambient noise.

Interestingly, we found that endocannabinoids modulate glycinergic and glutamatergic neurotransmission to a similar extent. As the balance between these two inputs is crucial for the physiological function of sound source localization achieved by MSO and LSO neurones, retrograde endocannabinoid signalling might exert its adjusting function without affecting the balance between excitatory and inhibitory inputs. Like in other neuronal systems, depolarization by glutamatergic stimulation might – via Ca^{2+} influx through post-synaptic voltage-sensitive Ca^{2+} channels – stimulate endocannabinoid synthesis (Ueda *et al.* 2011) (Fig. 7a and b). In addition, stimulation of post-synaptic metabotropic receptors might also enhance endocannabinoid synthesis (Katona and Freund 2012). With both mechanisms, excitatory synaptic activity would be a necessary prerequisite not only for glutamatergic DSE but also for glycinergic DSI in these neurones. This represents a reasonable assumption, as both excitatory and inhibitory inputs have to be activated in parallel in order that MSO and LSO neurones can exert their main function in the context of localization of sound sources (Grothe *et al.* 2010). On the basis of the time

window during which the endocannabinoid actions have been observed, we suggest a role in development of functional hearing.

Acknowledgements

We express our sincere thanks to Ken Mackie, Indiana University, who gave us DAGLα and DAGLβ antibodies as a present. We are grateful for inspiring discussions with Felix Felmy. The authors thank the Graduate School of Systemic Neurosciences (GSN-LMU) and the Graduate School 1373 (TU Munich, DFG) for providing a grant to BT. This work was largely funded by the DFG (Collaborative Research Center 870).

Conflict of interest

The authors declare no competing financial interests.

Supporting information

Additional supporting information may be found in the online version of this article at the publisher's web-site:

Figure S1. The CB1 agonist WIN 55,212-2 depresses glycinergic post-synaptic currents retrogradely.

References

Alger B. E. and Kim J. (2011) Supply and demand for endocannabinoids. *Trends Neurosci.* **34**, 304–315.

Best A. R. and Regehr W. G. (2010) Identification of the synthetic pathway producing the endocannabinoid that mediates the bulk of retrograde signaling in the brain. *Neuron* **65**, 291–292.

Brand A., Behrend O., Marquardt T., McAlpine D. and Grothe B. (2002) Precise inhibition is essential for microsecond interaural time difference coding. *Nature* **417**, 543–547.

Brown S. P., Brenowitz S. D. and Regehr W. G. (2003) Brief presynaptic bursts evoke synapse-specific retrograde inhibition mediated by endogenous cannabinoids. *Nat. Neurosci.* **6**, 1048–1057.

Castillo P. E., Younts T. J., Chavez A. E. and Hashimotodani Y. (2012) Endocannabinoid signaling and synaptic function. *Neuron* **76**, 70–81.

Chi D. H. and Kandler K. (2012) Cannabinoid receptor expression at the MNTB-LSO synapse in developing rats. *Neurosci. Lett.* **509**, 96–100.

Di Marzo V. (2011) Endocannabinoid signaling in the brain: biosynthetic mechanisms in the limelight. *Nat. Neurosci.* **14**, 9–15.

Fuxe K., Borroto-Escuela D. O., Romero-Fernandez W. *et al.* (2012) Extrasynaptic neurotransmission in the modulation of brain function. Focus on the striatal neuronal-glial networks. *Front. Physiol.* **3**, 136.

Grothe B. (2003) New roles for synaptic inhibition in sound localization. *Nat. Rev. Neurosci.* **4**, 540–550.

Grothe B., Pecka M. and McAlpine D. (2010) Mechanisms of sound localization in mammals. *Physiol. Rev.* **90**, 983–1012.

Guo J. and Ikeda S. R. (2004) Endocannabinoids modulate N-type calcium channels and G-protein-coupled inwardly rectifying potassium channels via CB1 cannabinoid receptors heterologously expressed in mammalian neurons. *Mol. Pharmacol.* **65**, 665–674.

Heffner R. S. and Heffner H. E. (1988) Sound localization and use of binaural cues by the gerbil (Meriones unguiculatus). *Behav. Neurosci.* **102**, 422–428.

Hejazi N., Zhou C., Oz M., Sun H., Ye J. H. and Zhang L. (2006) Delta9-tetrahydrocannabinol and endogenous cannabinoid anandamide directly potentiate the function of glycine receptors. *Mol. Pharmacol.* **69**, 991–997.

Herkenham M., Lynn A. B., Little M. D., Johnson M. R., Melvin L. S., de Costa B. R. and Rice K. C. (1990) Cannabinoid receptor localization in brain. *Proc. Natl Acad. Sci. USA* **87**, 1932–1936.

Kandler K. (2004) Activity-dependent organization of inhibitory circuits: lessons from the auditory system. *Curr. Opin. Neurobiol.* **14**, 96–104.

Kandler K. and Friauf E. (1995) Development of glycinergic and glutamatergic synaptic transmission in the auditory brainstem of perinatal rats. *J. Neurosci.* **15**, 6890–6904.

Katona I. and Freund T. F. (2012) Multiple functions of endocannabinoid signaling in the brain. *Annu. Rev. Neurosci.* **35**, 529–558.

Kreitzer A. C. and Regehr W. G. (2001) Retrograde inhibition of presynaptic calcium influx by endogenous cannabinoids at excitatory synapses onto Purkinje cells. *Neuron* **29**, 717–727.

Kushmerick C., Price G. D., Taschenberger H., Puente N., Renden R., Wadiche J. I., Duvoisin R. M., Grandes P. and von Gersdorff H. (2004) Retroinhibition of presynaptic Ca2+ currents by endocannabinoids released via postsynaptic mGluR activation at a calyx synapse. *J. Neurosci.* **24**, 5955–5965.

Leake P. A., Hradek G. T., Chair L. and Snyder R. L. (2006) Neonatal deafness results in degraded topographic specificity of auditory nerve projections to the cochlear nucleus in cats. *J. Comp. Neurol.* **497**, 13–31.

Leao R. N., Sun H., Svahn K., Berntson A., Youssoufian M., Paolini A. G., Fyffe R. E. and Walmsley B. (2006) Topographic organization in the auditory brainstem of juvenile mice is disrupted in congenital deafness. *J. Physiol.* **571**, 563–578.

Liu J., Wang L., Harvey-White J. *et al.* (2006) A biosynthetic pathway for anandamide. *Proc. Natl Acad. Sci. USA* **103**, 13345–13350.

Lozovaya N., Yatsenko N., Beketov A., Tsintsadze T. and Burnashev N. (2005) Glycine receptors in CNS neurons as a target for nonretrograde action of cannabinoids. *J. Neurosci.* **25**, 7499–7506.

Mukhtarov M., Ragozzino D. and Bregestovski P. (2005) Dual Ca2+ modulation of glycinergic synaptic currents in rodent hypoglossal motoneurones. *J. Physiol.* **569**, 817–831.

Muller M. (1990) Quantitative comparison of frequency representation in the auditory brainstem nuclei of the gerbil, Pachyuromys duprasi. *Exp. Brain Res.* **81**, 140–149.

Nemeth B., Ledent C., Freund T. F. and Hajos N. (2008) CB1 receptor-dependent and -independent inhibition of excitatory postsynaptic currents in the hippocampus by WIN 55,212-2. *Neuropharmacology* **54**, 51–57.

Ohno-Shosaku T., Maejima T. and Kano M. (2001) Endogenous cannabinoids mediate retrograde signals from depolarized postsynaptic neurons to presynaptic terminals. *Neuron* **29**, 729–738.

Ohno-Shosaku T., Tanimura A., Hashimotodani Y. and Kano M. (2012) Endocannabinoids and retrograde modulation of synaptic transmission. *Neuroscientist* **18**, 119–132.

Pecka M., Brand A., Behrend O. and Grothe B. (2008) Interaural time difference processing in the mammalian medial superior olive: the role of glycinergic inhibition. *J. Neurosci.* **28**, 6914–6925.

Pitler T. A. and Alger B. E. (1992) Postsynaptic spike firing reduces synaptic GABAA responses in hippocampal pyramidal cells. *J. Neurosci.* **12**, 4122–4132.

Pitler T. A. and Alger B. E. (1994) Depolarization-induced suppression of GABAergic inhibition in rat hippocampal pyramidal cells: G protein involvement in a presynaptic mechanism. *Neuron* **13**, 1447–1455.

Sedlacek M., Tipton P. W. and Brenowitz S. D. (2011) Sustained firing of cartwheel cells in the dorsal cochlear nucleus evokes endocannabinoid release and retrograde suppression of parallel fiber synapses. *J. Neurosci.* **31**, 15807–15817.

Tritsch N. X., Yi E., Gale J. E., Glowatzki E. and Bergles D. E. (2007) The origin of spontaneous activity in the developing auditory system. *Nature* **450**, 50–55.

Ueda N., Tsuboi K., Uyama T. and Ohnishi T. (2011) Biosynthesis and degradation of the endocannabinoid 2-arachidonoylglycerol. *BioFactors* **37**, 1–7.

Wilson R. I. and Nicoll R. A. (2001) Endogenous cannabinoids mediate retrograde signalling at hippocampal synapses. *Nature* **410**, 588–592.

Woolf N. K. and Ryan A. F. (1984) The development of auditory function in the cochlea of the mongolian gerbil. *Hear. Res.* **13**, 277–283.

Zhao Y. and Tzounopoulos T. (2011) Physiological activation of cholinergic inputs controls associative synaptic plasticity via modulation of endocannabinoid signaling. *J. Neurosci.* **31**, 3158–3168.

Zhao Y., Rubio M. E. and Tzounopoulos T. (2009) Distinct functional and anatomical architecture of the endocannabinoid system in the auditory brainstem. *J. Neurophysiol.* **101**, 2434–2446.

The role of the endocannabinoid system in the morphological development of neurons in the medial superior olive

Running title: Endocannabinoids modulate neuronal morphological development

Barbara Trattner[1,2], Alexandra Klein[1], Lara Jansen[1], Michael Stransky[1], Philipp Rautenberg[1], Benedikt Grothe[1] & Lars Kunz[1]

[1]Ludwig Maximilians University Munich, Department of Biology II, Division of Neurobiology, Martinsried, Germany

[2]Ludwig Maximilians University Munich, Graduate School of Systemic Neurosciences, Martinsried, Germany

Correspondence:

Barbara Trattner & Dr. Lars Kunz

Ludwig Maximilians University Munich

Department of Biology II

Division of Neurobiology

D-82152 Planegg-Martinsried, Germany

trattner@bio.lmu.de; lars.kunz@bio.lmu.de

Number of words: 6.942

Number of figures: 8

ABSTRACT

The medial superior olive (MSO) is an auditory brainstem nucleus, which is responsible for the precise extraction of interaural time differences (ITDs) to enable sound source localization in low-frequency hearing mammals. To perform this functionally highly relevant task, these neurons rely on their exactly shaped morphology. Recently, we demonstrated the anatomical presence and physiological functionality of the endocannabinoid system in MSO neurons of the Mongolian gerbil (*Meriones unguiculatus*) (Trattner *et al.*, 2013). This rodent possesses a similar frequency coverage and anatomical organization of the auditory system as humans. Now we investigated how endocannabinoids are involved in shaping the morphology of MSO neurons during development. By administration of a cannabinoid receptor 1 (CB1) agonist and antagonist to pregnant and lactating females, respectively, the fetuses and pups received the substances for one week via the placenta and for another two weeks via the mothers' milk. By subsequent dye-electroporation or Golgi-staining of MSO neurons, we visualized morphological differences resulting from an over-stimulation or a blockage of the endocannabinoid system. We could show that neurons from animals treated with CB1 antagonists possessed on average a higher surface area, bigger volume, bigger mean cross section area, as well as changes in the soma proportions and dendritic arborisation. A conductance-based computational model showed that these morphological differences could lead to changes in the biophysical computation of the neurons. We found that already the passive membrane properties such as input resistance and action potential threshold are to a great extent altered by the induced morphological changes.

INTRODUCTION

The medial superior olive (MSO) is a nucleus located in the auditory brainstem of low-frequency hearing mammals. Neurons of the MSO process so-called interaural time differences (ITDs) (Goldberg & Brown, 1969; Yin & Chan, 1990) and thereby contribute greatly to the detection of sound sources in our environment and thus acoustic navigation (Grothe *et al.*, 2010). The accurate computation of ITDs by means of a coincidence detection mechanism requires a very high temporal precision in the range of microseconds to guarantee efficient orientation. Therefore, the physiological properties of MSO neurons undergo an extensive development before hearing ability is fully developed (Scott *et al.*, 2005; Chirila *et al.*, 2007) as well as adjustments depending on auditory experience thereafter (Magnusson *et al.*, 2005; Scott *et al.*, 2005; Werthat *et al.*, 2008; Hassfurth *et al.*, 2010). Along with physiological and metabolic (Trattner *et al.*, 2013b) changes, the morphological maturation of MSO neurons is tightly regulated during development (Rogowski & Feng, 1981; Kiss & Majorossy, 1983; Chirila *et al.*, 2007; Rautenberg *et al.*, 2009), because the exact computation of output signals critically relies on the neuronal morphology (Rall *et al.*, 1992; Mainen & Sejnowski, 1996; Duch & Levine, 2000; Womack & Khodakhah, 2002; London & Hausser, 2005; Meseke *et al.*, 2009). Our experimental animal is the Mongolian gerbil (*Meriones unguiculatus*), which has an audible spectrum and an organization of the auditory brainstem similar to humans (Heffner & Heffner, 1988; Muller, 1990) and is thus suited for auditory research on the MSO.

The endocannabinoid system is generally described as a retrograde transmitter system regulating synaptic plasticity (Chevaleyre *et al.*, 2006; Mackie, 2008). In neurons, the most important receptor of the endocannabinoid system is the cannabinoid receptor 1 (CB1), which is expressed presynaptically (Wilson & Nicoll, 2001; Kawamura *et al.*, 2006) or postsynaptically (Bacci *et al.*, 2004) by neurons as well as glial cells (Navarrete & Araque, 2008) and upon activation by agonists regulates the excitability of the neurons. In addition, the presence of the cannabinoid receptor 2 (CB2) has been demonstrated in some neurons and glia (Ashton *et al.*, 2006; Baek *et al.*, 2008), however its role for neuronal physiology is generally considered a less influential one than that of CB1. The most abundant endogenous agonists for the cannabinoid receptors are the endocannabinoids anandamide

(AEA) and 2-arachidonylglycerol (2-AG). In several nuclei of the auditory brainstem, an expression of CB1 as well as electrophysiological consequences of its presence have already been shown (Kushmerick *et al.*, 2004; Zhao *et al.*, 2009; Zhao & Tzounopoulos, 2011; Chi & Kandler, 2012). We could recently show that CB1-dependent 2-AG signaling is involved in retrograde depression of excitatory and inhibitory currents in the MSO (Trattner *et al.*, 2013a). In addition to modulating the physiology of neurons, the endocannabinoid system has recently been shown to exert an important influence on the development of neuronal morphology in various brain areas: In the cerebellum it has been shown that Purkinje cells acquire longer and less branched dendrites when cultured *in vitro* in the presence of a CB1 antagonist, compared to control conditions (Kawaguchi *et al.*, 2010). In the motor cortex, neurons of CB1 knock-out mice display a decreased dendritic field with a reduced number of synapses compared to wild type littermates (Ballesteros-Yanez *et al.*, 2007). Since especially in the MSO retrograde endocannabinoid signaling has been physiologically demonstrated (Trattner *et al.*, 2013a) and it was suggested that endocannabinoids can shape neuronal morphology by regulating transmitter release (Kawaguchi *et al.*, 2010), it would be conceivable that endocannabinoids influence morphological development of MSO neurons via these mechanisms. To investigate such a contribution, we administered either a CB1 agonist (AEA) or a CB1 inverse agonist (rimonabant, RIM) to pregnant and lactating gerbils and studied the morphology of MSO neurons of their pups at postnatal day 14 (P14) by Golgi Staining or single-cell electroporation. In order to test whether the morphological differences observed cause functional changes in neuronal computation, we programmed a NEURON model (Hines & Carnevale, 1997; 2000) of MSO neurons (Zhou *et al.*, 2005).

MATERIALS AND METHODS

Animal experiments

All our animal experiments were carried out in accordance with the European Communities Council Directive of 24 November 1986 (86/609/EEC). The district government of Upper Bavaria (Regierung von Oberbayern) approved the study (55.2-1-54-2532-11-11). Female Mongolian gerbils (*Meriones unguiculatus*) were injected subcutaneously every second day from the last week of pregnancy onwards with 0.02 mg/kg body weight anandamide (AEA), rimonabant (RIM) or the equivalent volume of the solvent alone (1:1 saline:propylene-glycole) (Wenger *et al.*, 1997a; Wenger *et al.*, 1997b). AEA is an endogenous agonist for both CB1 and CB2, whereas RIM exerts the action of an inverse agonist to CB1 receptors. Both AEA as well as RIM are lipophilic substances, which pass the blood brain barrier and are thus also likely to pass the placental barrier and to be enriched in the breast milk. Thereby the pups receive the active compound either through the placental chord or via the milk (Astley & Little, 1990; Liu *et al.*, 2002; Picksak & Stichtenoth, 2008; Taylor *et al.*, 2010). In order to reduce stress levels of the mother, the experimenters handled the animals before the start of the experiment and the animals received Nutrical Vitaminpaste (Albrecht GmbH, Aulendorf, Germany) after the injections as a treat. The pups were decapitated at P14 after having reached a deep isoflurane (Forene®, Abbott AG, Switzerland) anesthesia and the brains were either processed for Golgi staining or electroporation.

Golgi staining

Golgi staining of MSO neurons was performed using the FD Rapid Golgi Stain Kit (FD NeuroTechnologies, Columbia MD, USA) and brains were processed according to the manufacturer's instructions. The auditory brainstem was transversely sliced at 150 µm using a vibratome (VT1200S, Leica, Wetzlar, Germany).

Electroporation

The brainstem was quickly isolated in ice-cold dissecting solution which contained (in mM) 125 NaCl, 25 $NaHCO_3$, 2.5 KCl, 1.25 NaH_2PO_4, 3 $MgCl_2$, 0.1 $CaCl_2$, 25 glucose, 0.4 ascorbic acid, 3 myo-inositol and 2 Na-pyruvate at a pH of 7.35. The solution was bubbled with 95% O_2 and 5% CO_2. The brainstem was quickly sliced to 200 µm transversal slices using a Vibratome (VT1000S, Leica, Wetzlar, Germany) and sections were kept in incubation solution (same composition as dissecting solution except for 2 mM $CaCl_2$ and 1 mM $MgCl_2$) for 45 min at 37°C, while bubbled with 95% O_2 and 5% CO_2. During electroporation the brain sections were continuously perfused with incubation solution at room temperature. MSO neurons were visually identified under the control of an Olympus BX51WI and electroporated with 1 mM Alexa488 (Molecular Probes, Eugene, OR) using glass capillaries of a resistance between 3.0 and 3.5 M□. The dye-loaded pipette was pressed onto a selected cell and a 25 msec long voltage pulse of an intensity of 15 to 20 V was applied. The voltage pulse was triggered with a EPC9 amplifier (HEKA Elektronik) and generated with an ISO-Flex stimulus isolator (A.M.P.I., Jerusalem, Israel). Approximately every 5th cell within the MSO was electroporated to limit the amount of overlapping dendrites. After electroporation, the slices were fixed in PFA at 4°C over night and subsequently mounted with Vectashield (H-1000, Vector, AXXORA, Lörach, Germany).

Microscopy

Golgi-stained neurons were visualized under bright field using a Zeiss Axio Imager M1 (Carl Zeiss AG, Oberkochen, Germany) and z-stacks with an optical slice thickness of 1.675 µm were acquired using the AxioCam software at a 40x magnification. The resulting stacks were merged into a single projection using the FIJI depth of field plug-in (http://fiji.sc/wiki/index.php/Fiji) for ImageJ software (1.39q Wayan Rasband, National Institutes of Health, USA, http://rsb.info.nih.gov/ij/, Java 1.5.0_06).

Electroporated neurons were visualized using a Leica 6000CS SP5 confocal laser-scanning microscope (Leica Microsystems, Mannheim, Germany) equipped with a Plan 63x/NA1.32 oil immersion objective. Alexa488 was excited by using an argon laser (488 nm) and fluorescence was

detected at 494 - 555 nm. Stacks were obtained with axial distances of 210 nm; resulting in a voxel size of 240 nm x 240 nm x 210 nm. The image size was 1024x1024 pixels. To obtain an improved signal-to-noise ratio, each section image was averaged from four successive line scans. In order to comprise every dendrite in its full length, several image stacks from different positions around the soma were collected for each neuron.

AMIRA image processing

Picture stacks from confocal microscopy were processed with the AMIRA 4.1 software (Mercury Computer Systems, TGS Unit, Düsseldorf, Germany) and the additional add-in "Skeleton tree"; a specialized algorithm for morphological reconstructions, which was developed by Dr. Jan Evers (Schmitt *et al.*, 2004; Evers *et al.*, 2005). The concept of "Skeleton tree" is based on fitting cylindrical compartments, each corresponding to a small neural segment, into dendrites and soma of the neuron's 3D image. After importing the different image stacks of single cells into AMIRA 4.1 and merging them to one picture, the user manually labels starting, end and branching points of each dendrite. An algorithm then computes the neuronal structure by evaluating grey values of the image. This initialization approximates the shape of the skeleton tree and a second algorithm smoothens the borders and adjusts the shape with great detail. The resulting data of the skeleton were stored in swc-format, which describes neural morphology as a list of rows, each characterizing a single compartment due to morphological properties. Subsequently, these data were computed by an algorithm developed in the Morphjongleur software by Michael Stransky, LMU München, (https://github.com/G-Node/Morphjongleur). These results elucidate the overall neuronal architecture, including the number of branches, the total length, the surface and the volume of each MSO neuron as well as their mean cross section area (mcsa), given by the quotient of volume and length. Additionally, to examine a neuron's three-dimensional expansions, a principal component analysis (PCA) was conducted in order to calculate the principal axis of a neuron. The PCA was also calculated in the Morphjongleur software using a Python Module (http://mdp-toolkit.sourceforge.net/). To describe the three-dimensional dendritic field the convex hull of the neurons was calculated in Python.

Image analysis

Additional morphological properties were assessed from two-dimensional screenshots of the skeletons using the "measure" tool of the software ImageJ (1.39q Wayan Rasband, National Institutes of Health, USA, http://rsb.info.nih.gov/ij/, Java 1.5.0_06). The neuron's soma diameter and length were manually measured by fitting a straight line between the extreme borders of these structures. Furthermore, the soma area was measured by drawing a free hand line around the circumference of each soma. Soma surface was mathematically calculated out of soma diameter and length with the formula for the surface area of a prolate spheroid ($A = 2\pi b \times \left[b + \frac{a^2}{\sqrt{a^2 - b^2}} - \arcsin\left(\frac{\sqrt{a^2 - b^2}}{a} \right) \right]$, where A represents the surface area, a corresponds to the length of the long half-axis and b corresponds to the length of the short half-axis. The length of the dendritic branches of first, second, third and forth order were assessed by drawing a free hand line along their paths and results of each dendritic order were averaged for every cell. Dendritic field expansions in two-dimensions were analyzed via fitting a convex polygon to a screenshot of the skeleton tree that joins the most distal points of dendritic processes.

Sholl analysis

For an additional assessment of the neuronal branching patterns, a Sholl analysis for the two-dimensional images of the skeletons was performed. The ImageJ plug-in "Advanced Sholl analysis" (http://imagejdocu.tudor.lu/doku.php?id=plugin:analysis:asa:start) uses an algorithm, which is based on the original publication by Sholl and colleagues (Sholl, 1953). The algorithm creates a series of concentric circles around the centre of a neuronal arbor and counts the number of intersections of each dendrite within these circles. Centre point and the size of the initial radius were chosen in a manner that the first circle intersects every first order dendrite and the following radius step size was set to 5 µm. The maximum radius comprised the endpoint of the longest dendrite. The results were either displayed as the number of intersections per circle perimeter plotted against the radius or as number of intersections per area enclosed by the corresponding circle plotted against the radius. Other outputs of this analysis are the Sholl regression coefficient k, which is equivalent to the

slope of the linear regression in a semi-logarithmical plot of the number of intersections per circle area against the radius, the critical value r_c, describing the radius at which there is a maximum number of intersections, and the local maximum N_m, which corresponds to the number of intersections at r_c.

Modelling

To investigate a potential influence of different morphological characteristics on neuronal computation, a bipolar MSO model was programmed in the NEURON environment (Hines & Carnevale, 1997; 2000) based on the multi-compartmental MSO model established by the Colburn and colleagues (Zhou *et al.*, 2005). Our model cell consisted of one soma (1 segment), one active axon (51 segments) connected to the soma, as well as primary (5 segments) and secondary dendrites (5 segments). The geometrical parameters represent our experimental results and differ for the three experimental groups (Table 1). To calculate resting membrane potential, input resistance and action potential current threshold of the neurons, we simulated the morphology of each neuron individually and plotted the data as means ± S.E.M.

	d(SOMA)	L(SOMA)	n 1° DENDRITES	L 1° DENDRITES	n 2° DENDRITES	L 2° DENDRITES	MCSA (µm²)/ d (µm)
CTRL	11.21 µm	33.96 µm	2.3	38.39	4.67	60.90	4.957/2.512
AEA	10.95 µm	31.19 µm	2.1	41.06	3.67	41.58	3.997/2.256
RIM	15.19 µm	31.00 µm	3.0	54.45	4.00	45.65	7.658/3.123

Table 1. Morphological properties applied in the model of MSO neurons of different experimental groups. d = diameter, L = length, n = number, MCSA = mean cross section area

The membrane properties assigned to the different compartments were kept identical for the three experimental groups to ensure that potential differences in neuronal computation are determined purely by morphological variations. Details on ion channels considered in the model are given by

Table 2. The resting membrane potential was maintained at -60 mV and the simulation temperature was set to 38°C. The kinetics of K_{HVA} and HCN channels were based on the recent models of type II cells in the AVCN (Rothman & Manis, 2003). The kinetics of K_{LVA} channels applied in our model are based on the description of the K_v1 channel in the gerbil MSO (Mathews *et al.*, 2010). The configuration of Na^+ channels was set according to the characterization of MSO Na^+ channels (Svirskis *et al.*, 2004).

SOMA	{G_{Na} = 0.1 S/cm², $G_{L(Na)}$ = 0.002 S/cm², E_{Na} = 50 mV}
AXON	{G_{Na} = 0.3 S/cm², G_{LTK} = 0.03 S/cm², G_{HTK} = 0.02 S/cm², G_H = 0.0015 S/cm², $G_{L(Na)}$ = 0.002 S/cm², E_{Na} = 50 mV, E_K = -100 mV, E_H = -35 mV}

Table 2. Ionic conductances and equilibrium potentials in different neuronal compartments. G = conductance, LTK = Low-threshold K^+, HTK = High-threshold K^+, pas = passive K^+ leak, L(Na) = passive Na^+ leak.

Ten excitatory synapses were evenly scattered along the first half of each primary dendrite. Ten inhibitory synapses were located on the soma (Kapfer *et al.*, 2002). The precise configuration of excitatory and inhibitory synapses and their input is indicated in Table 3.

EX. SYNAPSE	{tau1 = 0.1 msec, tau2 = 0.3 msec, E = 0 mV}
INH. SYNAPSE	{tau1 = 0.1 msec, tau2 = 1.5 msec, E = -90 mV}
INPUT	{type = GaussStim, input period = 2 msec, arrival time of input spikes = 0 msec, number = 10000, phase-locking factor = 20}

Table 3. Properties of excitatory and inhibitory synapses and their input.

To test whether MSO function would be affected by the differing morphology in the three groups, we shifted the relative timing between contralateral excitatory and somatic inhibitory inputs and quantified the shift in the resulting EPSP peak. The peak shift was determined by comparing the EPSP peak without and with inhibition (personal communication with Mike Myoga).

Statistics

All statistical analysis was performed using the software Prism 5.02 (GraphPad Software, San Diego California USA, www.graphpad.com). Altogether, 18 neurons were electroporated and reconstructed using AMIRA and 19 Golgi-stained neurons were analyzed, i.e. 6 (AMIRA) or 6-7 (Golgi) neurons per experimental group, respectively. The neurons within one group belong to animals from at least two different breeding pairs. Statistical outliers were defined as data points outside the 95% confidence interval and were removed from the general analysis. All data are displayed as mean ± S.E.M. Data was tested for normal distribution using the Kolmogorov-Smirnov Test. We used a one-way ANOVA with *post hoc* Tukey Test or Student t test in case of only two groups (Figure 7) being compared to each other to test for statistical significance. For Sholl analysis of intersections of dendritic arbors per area we fitted each data set with a double exponential function and analyzed these fits statistically using the extra-sum-of-square test. The significance level for all tests was set to $p \leq 0.05$.

RESULTS

Comparison of electroporation and Golgi staining for reconstruction of neuronal morphology

Figure 1 provides an overview of the neuronal morphology visualized with different methods. Using the Golgi method, it is evident that especially at the end of the dendritic arbor the branches stop in a dead end with thickenings or swellings. Especially thin dendrites were not always seen with this method, but the dendritic tree was rather limited to thick processes in the vicinity of the soma. This impossibility of resolving the fine structure is a clear limitation of the Golgi staining method. Precipitations of the staining substance within the brain slice and the impossibility to control, which neurons were stained further aggravated the isolation of single neurons. Owing to these limitations of Golgi staining, we used mainly neurons from electroporation for reconstruction and subsequent data analysis. From the maximum projection of single neuron confocal stacks, the neuron was reconstructed in three dimensions using the software AMIRA and the skeleton tree add-in. It is obvious, that especially fine dendritic branches are visible much more clearly in the reconstruction than in the maximum projection. Especially the endings of the dendrites are lost in the maximum projection, whereas the reconstruction allows the visualization of the full dendritic tree. For a comparative discussion on the quality of Golgi stain and AMIRA reconstructions please refer also to Figure 7.

The endocannabinoid system modulates the development of cellular morphological parameters

Using the AMIRA reconstructions of single MSO neurons visualized by electroporation, we first analyzed general morphological parameters (Figure 2). We observed an overall reduction in the number of dendritic branches as well as total neuronal length in the AEA and RIM condition when compared to the CTRL condition. AEA neurons displayed 9.6 ± 2.8 branches/cell, equating 20% less dendritic branches than CTRL cells (12.0 ± 1.4) and total neuronal length was reduced from 644 ± 43 µm to 495 ± 54 µm (-24%). Neurons treated with RIM possessed 9.2 ± 2.2 branches on average, which corresponds to a decrease of 23%, and showed a reduction in neuronal length of 15% (547 ± 25

μm) (Figure 2A and 2B). Neuronal surface was reduced by 31% (from 3130 ± 378 μm² to 2174 ± 116 μm² on average) in AEA neurons, whereas it showed a slight increase by 10% (3454 ± 350 μm² on average) in RIM treated neurons. However, the neuronal surface of RIM treated MSO neurons was significantly larger than in AEA treated neurons (Figure 2C). The total neuronal volume, which is influenced by the neuronal length and its surface, showed a slight reduction of 14% (from 2585 ± 360 μm³ to 2213 ± 324 μm³ on average) in MSO neurons of AEA treated animals. In MSO neurons of RIM treated neurons on the other hand the total neuronal volume was significantly increased by 98% to 5136 ± 618 μm³ when compared to the CTRL condition (Figure 2D). Since the neuronal length was slightly decreased in RIM treated animals, we suggest that in addition to the moderate increase in neuronal surface, also the diameters of dendritic branches might have a substantial influence on the neuronal volume in this case. This suggestion is supported by the observation that also the mean cross section area (mcsa), which is defined by the quotient of neuronal volume and length, was significantly enlarged in RIM neurons when compared to AEA neurons. Under AEA conditions the mcsa was reduced by 19% (from 4.96 ± 0.78 μm² to 4.00 ± 0.30 μm² on average), whereas RIM treatment led to mcsa enlargement by 54% (to 7.66 ± 0.93 μm² on average), when compared to the CTRL condition (Figure 2E).

Somatic morphology was examined using the neuronal AMIRA reconstructions as well as the projections from the Golgi stained neurons. Results showed a rather consistent value for soma length of neurons under each condition, which amounted to 32.46 ± 1.41 μm on average (Figure 3A). Soma diameter was also constant between CTRL and AEA neurons and amounted to 11.8 ± 0.9 μm, whereas the diameter of RIM neurons was enlarged to 14.4 ± 1.3 μm, which corresponds to an increase of 29% (Figure 3B). Furthermore RIM neurons showed a similar soma area, when compared to CTRL neurons in both Golgi stain and reconstructed neurons (RIM: 358 ± 39 μm², CTRL: 332 ± 35 μm²), which contrasted to a 21% reduction of soma area of AEA neurons (260 ± 18 μm²) (Figure 3C). Values for the soma surface, which was mathematically calculated, remained relatively consistent between the three experimental groups, with AEA neurons showing a decrease of 10% (from 1014 ± 98 μm² in CTRL to 910 ± 117 μm² in AEA) and RIM neurons showing an increase of 15% (1174 ± 133 μm²) (Figure 3D). As an additional value for soma morphology, we calculated the

ratio between soma length and diameter, which resulted in a significant difference between RIM and both CTRL and AEA neurons. The length/diameter ratio was highly decreased in RIM neurons and amounted to 1.84 ± 0.15, which corresponds to a 36% reduction when compared to an average value of 2.89 ± 0.02 in CTRL and AEA neurons (Figure 3E). Neurons from animals treated with RIM possessed a slightly shorter but thicker soma, which generally appeared more roundish. However, it is noticeable that the soma surface remained unchanged despite the observed differences in somatic shape.

The endocannabinoid system modulates the development of the dendritic field

The dendritic fields as well as dendritic branching patterns were analyzed using the AMIRA reconstructed neurons, due to limitations in the fine resolution of dendritic arbors in the Golgi staining. The Golgi staining would induce a bias towards thick primary and secondary processes and not cover the full spectrum of dendritic branches. Analysis of both two-dimensional as well as three-dimensional dendritic field showed a reduction of field size for MSO neurons of AEA and RIM treated animals with the AEA condition showing a prominent decrease of 27% (from 21075 ± 2692 μm^2 to 15429 ± 870 μm^2) in two dimensions and 13% (from 32931 ± 4031 μm^3 to 28727 ± 1431 μm^3) in three dimensions. Dendritic field size of MSO neurons of RIM treated pups decreased by 11% (to 18862 ± 687 μm^2) in two dimensions and remained almost unchanged in three dimensions (32758 ± 1342 μm^3) (Figure 4A). The number of primary dendrites remained unchanged in the AEA condition (2.166 ± 0.167 compared to 2.333 ± 0.211). However, MSO neurons from RIM treated animals exhibited on average 3.167 ± 0.477 primary dendrites. The number of secondary dendrites (CTRL: 4.67 ± 0.33, AEA: 3.67 ± 0.33, 4.00 ± 0.73) as well as the number of tertiary dendrites (CTRL: 4.833 ± 1.046, AEA: 5.000 ± 1.000, RIM: 3.833 ± 0.980) remained almost unchanged between the three experimental groups. Furthermore, the dendritic branch lengths per dendritic order were analyzed (Figure 4B). Primary dendrites showed a 42% increased value for RIM neurons (from 38.4 ± 2.0 µm to 54.5 ± 7.6 µm); whereas the lengths of AEA first order dendrites remained almost unaffected by the treatment (39.6 ± 7.7 µm). The length of secondary dendrites was reduced in both AEA (-31%, from 60.9 ± 5.6 µm to 41.6 ± 2.5 µm) as well as RIM (-25%, to 45.7 ± 8.5 µm) condition. Tertiary

dendrites slightly increased in AEA neurons (+10%, from 27.8 ± 3.6 µm to 30.7 ± 4.6 µm) and RIM treated neurons showed a reduction in the length of third order dendrites by 29% (to 19.9 ± 1.2 µm). Since only few of the analyzed neurons possessed fourth order dendrites the results are rather imprecise and thus excluded from this paper.

Using a principal component analysis (PCA) we examined the three-dimensional expansions of MSO neurons in the three experimental conditions (Figure 5D). The results showed a consistent expansion in the x-plane (medio – lateral) between the three groups, which amounted to around 2.62 ± 5.88 µm (Figure 5A). In the y-plane (dorso - ventral), the extent of RIM neurons was clearly enlarged by 21% (from 89.7 ± 11.6 µm to 108.5 ± 9.0 µm) when compared to the control condition. Values of AEA neurons only slightly decreased compared to the values of CTRL neurons in the y-plane (-11%, to 79.97 ± 2.6 µm) (Figure 5B). In the z-plane (rostro-caudal) RIM neurons showed an increased extension of 24% on average (from 13.65 ± 1.7 µm to 16.88 ± 1.4 µm), whereas AEA neurons showed a reduction of 16% (to 11.49 ± 0.7 µm) (Figure 5C).

Sholl analysis supports the morphological findings

The comparison of the Sholl analysis of neurons under CTRL condition corroborates our finding that reconstruction of electroporated neurons allowed the visualization of much finer dendritic processes than those seen with Golgi staining (Figure 6A). This especially becomes apparent when comparing the number of intersections per area per radius: Golgi stained neurons showed comparably less intersections starting from a radius r = 75 µm from the soma until the end of dendritic branches (Figure 6B). This is also apparent as the slope of the decline - represented by the regression coefficient k - was lower in the Golgi stained neurons (k = -0.02375 ± 0.0011) when compared to the AMIRA reconstructed neurons (k = -0.01717 ± 0.0198). Furthermore, the critical value (Golgi: 50.0 ± 6.3 µm, AMIRA: 65.8 ± 6.0 µm) as well as the local maximum (Golgi: 4.25 ± 0.25, AMIRA: 5.78 ± 0.25) was significantly increased in AMIRA reconstructed neurons (Figure 6C). For these reasons, we have not used the data obtained from Sholl analysis of our Golgi stained neurons.

Comparison of a Sholl analysis of dendritic branching patterns of the AMIRA reconstructed electroporated neurons (Figure 7A and 7B) revealed a small difference in the number of intersections per area between CTRL, AEA and RIM conditions at radii bigger than 110 µm: In accordance with the results from dendritic field measurements (Figure 4A) MSO neurons from AEA treated animals were the shortest cells and displayed less intersections at distances far from the soma (Figure 7C). MSO neurons from the RIM group behaved more similarly to neurons of the CTRL condition, as was also revealed by dendritic field measurements (Figure 4A), however at distances very far from the soma, RIM neurons also displayed less intersections than the control condition (Figure 7C). Overall the Sholl analysis yielded very similar results between all three groups and also the regression coefficient k revealed almost no differences between the experimental groups (CTRL: -0.0172 ± 0.0004, AEA: -0.0219 ± 0.0016, RIM: -0.0184 ± 0.0003) (Figure 7D). The critical value, which indicates the radius with the maximum number of intersections, was increased by 26% in AEA neurons (from 65.8 ± 2.6 µm to 82.7 ± 3.0 µm) and by 8% in RIM neurons (to 71.3 ± 6.7 µm) (Figure 7D). This indicates a delayed ramification of the neuronal arbor at both experimental conditions when compared to the control condition. The local maximum, however, which indicates the number of intersections at the critical value, remained almost unaffected (CTRL: 5.78 ± 0.20, AEA: 5.44 ± 0.18, RIM: 5.64 ± 0.22) (Figure 7D).

A computational model predicts an impact of morphological differences on neuronal physiology

Using the NEURON environment, we programmed an MSO neuron model and investigated how the morphological differences resulting from interactions with the endocannabinoid system during development change the biophysical properties of the neurons. For quantification of biophysical parameters such as the resting membrane potential, the input resistance and the current threshold for eliciting an action potential, we ran the MSO model for individual neurons and then pooled the results for the respective groups. Interestingly, already passive parameters of the neurons are influenced to a great extent. While the resting membrane potential remained almost unchanged at around – 63 ± 1.3 mV (Figure 8A), the input resistance decreased significantly from 21.3 ± 2.6 M□

in the CTRL group to 15.3 ± 1.6 M□ in RIM neurons and increased significantly to 26.9 ± 1.5 M□ in AEA neurons (Figure 8B). Consequently the IV curve during stimulation at the soma, which was simulated for the averaged morphology of an MSO neuron of each of the experimental groups, was shifted by the morphological changes: The voltage deflection upon current injection was smaller in RIM neurons, when compared to CTRL neurons, and slightly increased in AEA neurons compared to CTRL neurons (Figure 8D). Accordingly also the current threshold required for eliciting an action potential varied between the three groups and was significantly higher in RIM neurons (1.14 ± 0.14 nA) when compared to AEA (0.53 ± 0.44 nA) and CTRL neurons (0.67 ± 0.62 nA) (Figure 8C). These results likely stem from the fact that RIM neurons on average possess more and thicker primary dendrites as well as an increased soma size. This increased neuronal volume acts as a current sink and decreases the resistance of the cell.

To investigate, whether MSO function is changed owing to the morphological changes quantified and included in our computational model, we shifted the inhibitory and excitatory inputs in time relative to each other and measured the shift in the resulting EPSP peak. The shifts in the EPSP peak timing were determined by comparing the peak of the EPSP with inhibition and without inhibition. Interestingly, the peak shift was maximal at inhibition lagging for 0.2 msec behind excitation in all groups as has been experimentally observed in MSO electrophysiological recordings (Mike Myoga, unpublished results), however the magnitude of this peak shift was different in the three experimental groups (CTRL max = -225 μsec; AEA max = -300 μsec; RIM max = -200 μsec) (Figure 8E). Previous modeling of MSO physiology revealed that the magnitude of this peak shift is also altered by the strength of excitatory inputs relative to inhibitory inputs (Mike Myoga and Simon Lehnert, unpublished results). Since the balance of excitation and inhibition is crucial for MSO neurons to accurately perform their task in sound localization, a morphological change that mimics such a disproportion could have detrimental effects on the functional output of the MSO.

DISCUSSION

Reconstruction of electroporated neurones yields more detailed insights into morphology compared to Golgi staining

The comparison of Sholl analysis between Golgi stained and electroporated MSO neurons reveals some of the limitations of Golgi stainings that are also immediately obvious when looking at the sections: Electroporation and subsequent AMIRA reconstruction allowed the visualization of much finer dendritic arborisation than the Golgi staining technique. One problem with the Golgi staining is especially the formation of precipitations in the tissue combined with a higher background, which aggravates the differentiation of dendrites originating from different neurons. In addition, the Golgi stain does not allow to control for which neurons are stained and thus an overlap of neurons of interest is sometimes inevitable.

Our results show that the Golgi stain when compared to electroporation and AMIRA reconstruction is not the method of choice to analyze dendritic arborisation due to the inability to display thinner and more distal processes. In addition, also the soma morphology was not equally reflected by Golgi stain and electroporation. The shape of the soma is best conserved using the electroporation approach.

The morphological quantification of MSO neurons from control animals corresponds well to results from the literature, given that differences in species, animal age, staining technique and quantification methods allow only for limited comparison. The somatic parameters especially the length/diameter ratio, match the findings of colleagues well (Rogowski & Feng, 1981; Rautenberg *et al.*, 2009). Differences become more apparent when comparing dendritic morphology, where our absolute values of dendritic length are located between the results obtained by Chirila and colleagues (Chirila *et al.*, 2007) and Rautenberg and co-workers (Rautenberg *et al.*, 2009). These discrepancies likely result from differences in the reconstruction and quantification procedure. The same holds true for dendritic arborisation, where our results compare well to the data of Rogowski and Feng and Chirila and colleagues (Rogowski & Feng, 1981; Chirila *et al.*, 2007) but contrast the data obtained by

Rautenberg and others (Rautenberg *et al.*, 2009), probably owing to changes in the way the morphology was quantified. Conclusively, the appearance of the MSO neurons of the same developmental stage in the Chirila study (Chirila *et al.*, 2007) compare best to the morphology of our analyzed neurons.

Role of the endocannabinoid system in development of MSO neurone morphology

Considering the effects of the endocannabinoid system on development of neuronal morphology, the reduction of the branching points by 31% induced by attenuating the endocannabinoid system corresponds well to the findings of Kawaguchi and colleagues (2010), who observed that *in vitro* culture of cerebellar Purkinje cells in the presence of the CB1 antagonist AM251 leads to a reduction of branching points by 38%. RIM treatment in our study led to a decrease of the dendritic field size by 14%, which compares to the 20% reduction in dendritic field size that Ballesteros-Yanez *et al.* (2007) documented in motor cortex neurons of CB1 knock-out mice. In contrast, Kawaguchi *et al.* (2010) described elongated dendrites in the presence of CB1 antagonists. This discrepancy might arise simply from differences in the active substance administration, brain area, examination procedures or cell culture vs. brain sections.

The rather large variance of morphological data obtained is in accordance with the literature on both MSO neuron morphology (Rogowski & Feng, 1981; Chirila *et al.*, 2007; Rautenberg *et al.*, 2009) and the impact of the endocannabinoid system on neuronal development (Ballesteros-Yanez et al., 2007, Chirila et al., 2007, Kawaguchi et al., 2010).. However, there are further aspects to be considered, which might explain this variability: we assumed every MSO neuron to be equal in terms of CB1 receptor expression, but the opposite is indicated by our immunohistochemical stainings (Trattner *et al.*, 2013a). Consequently, treatment with CB1 pharmaca might affect each neuron to a varying extent.

Possible functional meaning and implication of endocannabinoid-induced morphological changes in the MSO in the context of auditory processing

The MNTB provides the major inhibitory input to the MSO, which is of great relevance for the precise computation of ITDs (Brand *et al.*, 2002). The MNTB is organized tonotopically and maintains this tonotopic information in its projections to the MSO (Guinan *et al.*, 1972; Werthat *et al.*, 2008), which thus itself possesses a dorso-ventral tonotopic axis (Goldberg & Brown, 1969; Kandler *et al.*, 2009). Since we observed a significant reduction of the dendritic field of AEA treated MSO neurons as well as an increase in the dorso-ventral (y-axis PCA) extension of RIM treated neurons (Figure 5), these alterations could correlate with a decrease or an increase in inputs from different tonotopic MNTB areas. For the lateral superior olive (LSO), which is a neighboring brainstem nucleus to the MSO and is also involved in sound localization, it has been shown that the morphology of the individual neurons depends on their specific tonotopic position (Stotler, 1953; Rietzel & Friauf, 1998). An alteration of the dendritic arborisation of the neurons might thus indeed affect their tonotopic representation. By spanning a decreased (AEA) or an increased (RIM) amount of tonotopic layers, the MSO neurons might be targeted by a decreased (AEA) or an increased (RIM) number of MNTB neurons. This could affect the tonotopy of the connectivity.

MSO neurons from RIM treated animals displayed a decreased soma length/soma diameter ratio and generally had a more roundish somata appearance (Figure 3). The inhibitory and excitatory inputs to MSO neurons are spatially segregated with inhibitory inputs targeting mainly the somata and excitatory inputs targeting mainly the dendrites (Kapfer *et al.*, 2002). The defined arrangement of inhibitory inputs is dependent on auditory experience of the animal and crucial for the correct extraction of ITDs (Brand *et al.*, 2002; Pecka *et al.*, 2008). Changing the shape of the soma might thus affect the computation of these inhibitory inputs and thereby influence the coincidence detection by which the ITD is compiled.

Neurons from RIM treated animals displayed a significant increase in neuronal surface and volume. Since the neuronal volume depends on the neuron's total length and its diameters we suspect that in the RIM condition the neuronal diameters have a substantial impact on the huge increase in neuronal volume. This suggestion is supported by the result that the mean cross section area was

substantially increased in the RIM condition. Changing the diameters of neuronal processes fundamentally impacts the signal computation as the passive electrotonic conduction of potentials along the dendrites is to a great extent determined by the internal resistance of the dendrite, as can be expressed with the neuronal length constant λ (Cole & Hodgkin, 1939; Rall, 1959; Kernell & Zwaagstra, 1989; Vetter *et al.*, 2001). The internal resistance of the dendrite depends on the diameter of the dendrite – a condition which is also fulfilled by our computational MSO model, which shows a highly decreased input resistance in the RIM group (Figure 8B). A decreased internal resistance in the case of broader dendrites (RIM) allows the membrane voltage to travel with less attenuation for a longer time and thus the threshold for action potential initiation is reached earlier. This could have far reaching consequences on the integration of input signals and computation of output signals and thus directly affect the behavioral consequences of ITD detection.

Concerning the functional implications that a changed MSO morphology would lead to, we investigated how EPSP timing resulting from a combination of excitatory and inhibitory inputs is altered in the three experimental groups. We simulated how EPSP timing is influenced by differences in arrival time of excitation relative to inhibition. As previously shown experimentally by electrophysiological recordings in MSO neurons (Mike Myoga, unpublished results), the results of our modeling also demonstrate that the maximal EPSP shift occurs at inhibition lagging 0.2 msec behind excitation in all three groups. However the magnitude of that EPSP shift differs drastically between the groups. As shown by others before (Mike Myoga, unpublished results) an increase in the EPSP shift can be obtained by increasing the excitation to inhibition ratio: If the strength of excitation relative to inhibition is increased, the amplitude of the EPSP peak shift is augmented. The morphological differences quantified for the three experimental groups exert a similar effect, which could have detrimental consequences for the firing timing in response to different ITDs in MSO neurons. Since precisely timed inhibition is vital for correct ITD detection (Brand *et al.*, 2002; Grothe, 2003; Pecka *et al.*, 2008), a morphological alteration, which mimics the effects of a changed excitation/inhibition balance, could seriously impair correct ITD computation.

Possible mechanisms for endocannabinoid modulation of development of MSO neuron morphology

The mechanism through which endocannabinoids shape neuronal morphology remains elusive. It seems that already in early stages of development neural growth factor (NGF) can regulate the availability of endocannabinoids in some brain areas and thereby shapes neuronal morphology (Keimpema *et al.*, 2013). In the cerebellum it was proposed that endocannabinoids affect dendritogenesis by interfering with GABA release from Purkinje cell inputs (Kawaguchi *et al.*, 2010); possibly through a retrograde negative feedback signaling such as depolarization-induced suppression of inhibition (DSI), whereas in cortical areas an involvement of cocaine – which slows dopamine reuptake – signaling via CB1 has been shown to regulate neuronal morphology (Ballesteros-Yanez *et al.*, 2007). Possibly different mechanisms through which the endocannabinoid system can impact morphological development are present in the brain, which have however not been studied in detail. Since we found DSI and depolarization-induced suppression of excitation (DSE) in MSO neurons between P10 and P15 (Trattner *et al.*, 2013a), we could imagine a mechanism similar to that reported of Kawaguchi and colleagues, that a differential regulation of neurotransmitter release could induce morphological changes (Kawaguchi *et al.*, 2010).

CONCLUSION

Taken together, our results support the hypothesis that the endocannabinoid system plays a crucial role in the morphological maturation of MSO neurons. Chronic stimulation as well as blockage of the CB1 receptor lead to altered somatic and dendritic morphology of MSO neurons at the onset of functional hearing and thus may disturb the development of structures required for high precision ITD detection. This assumption is supported by our modeling of biophysical parameters based on the altered morphology observed. It would be interesting to address the question whether MSO neurons compensate for the physiological effects these morphological changes trigger, for instance by changing the expression profile of ion channels. Future *in vivo* recordings of MSO neurons of AEA and RIM treated animals could elucidate whether the observed morphological differences result in functional consequences. It would be especially interesting to assess whether neurons express a broadening/narrowing of the best frequency due to dendritic field adaptations or changes in the excitability or signal integration due to alterations in dendritic diameter.

ACKNOWLEDGEMENTS

We would like to thank Dr. Susanne Radtke-Schuller for valuable discussions on neuroanatomy and Golgi Staining, Céline Marie Gravot and Hilde Wohlfrom for establishing the Golgi Stain in our laboratory, Melanie Sotgia for excellent technical assistance, Simon Lehnert for discussions on MSO modeling and Dr. Olga Alexandrova for assistance with the microscopes. The authors thank the Graduate School of Systemic Neurosciences (GSN-LMU) and the Graduate School 1373 (DFG) for providing a grant to BT. This work was largely funded by the DFG (CRC870/TPB13).

AUTHOR'S CONTRIBUTIONS

BT and LK conceived the experiments. BT carried out the immunohistochemistry, the animal experiments, electroporation, programmed the NEURON model and supervised Golgi staining and data analysis. AK and LJ conducted the Golgi staining and performed data analysis. MS and PL wrote programs for data analysis and provided important inputs in discussions about the theoretical background of the paper. BT, LK, AK and BG wrote the manuscript.

COMPETING INTERESTS

The authors declare no conflict of interests.

ABBREVIATIONS

2-AG	2-Arachidonylglycerol
AEA	Anandamide (CB1/CB2 agonist)
CB1	Cannabinoid Receptor 1
CB2	Cannabinoid Receptor 2
CTRL	Control
DAGL	Diacylglycerollipase
DSE	Depolarization-induced Suppression of Excitation
DSI	Depolarization-induced Suppression of Inhibition
ITD	Interaural Time Difference

LSO	Lateral Superior Olive
MNTB	Medial Nucleus of the Trapezoid Body
MSO	Medial Superior Olive
PBS	Phosphate-buffered saline
PFA	Paraformaldehyde
RIM	Rimonabant (CB1 inverse agonist)

REFERENCES

Ashton, J.C., Friberg, D., Darlington, C.L. & Smith, P.F. (2006) Expression of the cannabinoid CB2 receptor in the rat cerebellum: an immunohistochemical study. *Neurosci Lett*, **396**, 113-116.

Astley, S.J. & Little, R.E. (1990) Maternal marijuana use during lactation and infant development at one year. *Neurotoxicol Teratol*, **12**, 161-168.

Bacci, A., Huguenard, J.R. & Prince, D.A. (2004) Long-lasting self-inhibition of neocortical interneurons mediated by endocannabinoids. *Nature*, **431**, 312-316.

Baek, J.H., Zheng, Y., Darlington, C.L. & Smith, P.F. (2008) Cannabinoid CB2 receptor expression in the rat brainstem cochlear and vestibular nuclei. *Acta Otolaryngol*, **128**, 961-967.

Ballesteros-Yanez, I., Valverde, O., Ledent, C., Maldonado, R. & DeFelipe, J. (2007) Chronic cocaine treatment alters dendritic arborization in the adult motor cortex through a CB1 cannabinoid receptor-dependent mechanism. *Neuroscience*, **146**, 1536-1545.

Brand, A., Behrend, O., Marquardt, T., McAlpine, D. & Grothe, B. (2002) Precise inhibition is essential for microsecond interaural time difference coding. *Nature*, **417**, 543-547.

Chevaleyre, V., Takahashi, K.A. & Castillo, P.E. (2006) Endocannabinoid-mediated synaptic plasticity in the CNS. *Annu Rev Neurosci*, **29**, 37-76.

Chirila, F.V., Rowland, K.C., Thompson, J.M. & Spirou, G.A. (2007) Development of gerbil medial superior olive: integration of temporally delayed excitation and inhibition at physiological temperature. *J Physiol*, **584**, 167-190.

Cole, K.S. & Hodgkin, A.L. (1939) Membrane and Protoplasm Resistance in the Squid Giant Axon. *J Gen Physiol*, **22**, 671-687.

Duch, C. & Levine, R.B. (2000) Remodeling of membrane properties and dendritic architecture accompanies the postembryonic conversion of a slow into a fast motoneuron. *J Neurosci*, **20**, 6950-6961.

Evers, J.F., Schmitt, S., Sibila, M. & Duch, C. (2005) Progress in functional neuroanatomy: precise automatic geometric reconstruction of neuronal morphology from confocal image stacks. *J Neurophysiol*, **93**, 2331-2342.

Goldberg, J.M. & Brown, P.B. (1969) Response of binaural neurons of dog superior olivary complex to dichotic tonal stimuli: some physiological mechanisms of sound localization. *J Neurophysiol*, **32**, 613-636.

Grothe, B. (2003) New roles for synaptic inhibition in sound localization. *Nat Rev Neurosci*, **4**, 540-550.

Grothe, B., Pecka, M. & McAlpine, D. (2010) Mechanisms of sound localization in mammals. *Physiol Rev*, **90**, 983-1012.

Guinan, J.J., Norris, B.E. & Guinan, S.S. (1972) Single Auditory Units in the Superior Olivary Complex: II: Locations of Unit Categories and Tonotopic Organization. *International Journal of Neuroscience*, **4**, 147-166.

Hassfurth, B., Grothe, B. & Koch, U. (2010) The mammalian interaural time difference detection circuit is differentially controlled by GABAB receptors during development. *J Neurosci*, **30**, 9715-9727.

Heffner, R.S. & Heffner, H.E. (1988) Sound localization and use of binaural cues by the gerbil (Meriones unguiculatus). *Behav Neurosci*, **102**, 422-428.

Hines, M.L. & Carnevale, N.T. (1997) The NEURON simulation environment. *Neural Comput*, **9**, 1179-1209.

Hines, M.L. & Carnevale, N.T. (2000) Expanding NEURON's repertoire of mechanisms with NMODL. *Neural Comput*, **12**, 995-1007.

Kandler, K., Clause, A. & Noh, J. (2009) Tonotopic reorganization of developing auditory brainstem circuits. *Nat Neurosci*, **12**, 711-717.

Kapfer, C., Seidl, A.H., Schweizer, H. & Grothe, B. (2002) Experience-dependent refinement of inhibitory inputs to auditory coincidence-detector neurons. *Nat Neurosci*, **5**, 247-253.

Kawaguchi, K., Habara, T., Terashima, T. & Kikkawa, S. (2010) GABA modulates development of cerebellar Purkinje cell dendrites under control of endocannabinoid signaling. *J Neurochem*, **114**, 627-638.

Kawamura, Y., Fukaya, M., Maejima, T., Yoshida, T., Miura, E., Watanabe, M., Ohno-Shosaku, T. & Kano, M. (2006) The CB1 cannabinoid receptor is the major cannabinoid receptor at excitatory presynaptic sites in the hippocampus and cerebellum. *J Neurosci*, **26**, 2991-3001.

Keimpema, E., Tortoriello, G., Alpar, A., Capsoni, S., Arisi, I., Calvigioni, D., Hu, S.S., Cattaneo, A., Doherty, P., Mackie, K. & Harkany, T. (2013) Nerve growth factor scales endocannabinoid signaling by regulating monoacylglycerol lipase turnover in developing cholinergic neurons. *Proc Natl Acad Sci U S A*, **110**, 1935-1940.

Kernell, D. & Zwaagstra, B. (1989) Dendrites of cat's spinal motoneurones: relationship between stem diameter and predicted input conductance. *J Physiol*, **413**, 255-269.

Kiss, A. & Majorossy, K. (1983) Neuron morphology and synaptic architecture in the medial superior olivary nucleus. Light- and electron microscope studies in the cat. *Exp Brain Res*, **52**, 315-327.

Kushmerick, C., Price, G.D., Taschenberger, H., Puente, N., Renden, R., Wadiche, J.I., Duvoisin, R.M., Grandes, P. & von Gersdorff, H. (2004) Retroinhibition of presynaptic Ca2+ currents by endocannabinoids released via postsynaptic mGluR activation at a calyx synapse. *J Neurosci*, **24**, 5955-5965.

Liu, W.M., Duan, E.K. & Cao, Y.J. (2002) Effects of anandamide on embryo implantation in the mouse. *Life Sci*, **71**, 1623-1632.

London, M. & Hausser, M. (2005) Dendritic computation. *Annu Rev Neurosci*, **28**, 503-532.

Mackie, K. (2008) Signaling via CNS cannabinoid receptors. *Mol Cell Endocrinol*, **286**, S60-65.

Magnusson, A.K., Kapfer, C., Grothe, B. & Koch, U. (2005) Maturation of glycinergic inhibition in the gerbil medial superior olive after hearing onset. *J Physiol*, **568**, 497-512.

Mainen, Z.F. & Sejnowski, T.J. (1996) Influence of dendritic structure on firing pattern in model neocortical neurons. *Nature*, **382**, 363-366.

Mathews, P.J., Jercog, P.E., Rinzel, J., Scott, L.L. & Golding, N.L. (2010) Control of submillisecond synaptic timing in binaural coincidence detectors by K(v)1 channels. *Nat Neurosci*, **13**, 601-609.

Meseke, M., Evers, J.F. & Duch, C. (2009) Developmental changes in dendritic shape and synapse location tune single-neuron computations to changing behavioral functions. *J Neurophysiol*, **102**, 41-58.

Muller, M. (1990) Quantitative comparison of frequency representation in the auditory brainstem nuclei of the gerbil, Pachyuromys duprasi. *Exp Brain Res*, **81**, 140-149.

Navarrete, M. & Araque, A. (2008) Endocannabinoids mediate neuron-astrocyte communication. *Neuron*, **57**, 883-893.

Pecka, M., Brand, A., Behrend, O. & Grothe, B. (2008) Interaural time difference processing in the mammalian medial superior olive: the role of glycinergic inhibition. *J Neurosci*, **28**, 6914-6925.

Picksak, G. & Stichtenoth, D.O. (2008) [Prescription of rimonabant in the early stage of pregnancy?]. *Med Monatsschr Pharm*, **31**, 107-108.

Rall, W. (1959) Branching dendritic trees and motoneuron membrane resistivity. *Exp Neurol*, **1**, 491-527.

Rall, W., Burke, R.E., Holmes, W.R., Jack, J.J., Redman, S.J. & Segev, I. (1992) Matching dendritic neuron models to experimental data. *Physiol Rev*, **72**, S159-186.

Rautenberg, P.L., Grothe, B. & Felmy, F. (2009) Quantification of the three-dimensional morphology of coincidence detector neurons in the medial superior olive of gerbils during late postnatal development. *J Comp Neurol*, **517**, 385-396.

Rietzel, H.J. & Friauf, E. (1998) Neuron types in the rat lateral superior olive and developmental changes in the complexity of their dendritic arbors. *J Comp Neurol*, **390**, 20-40.

Rogowski, B.A. & Feng, A.S. (1981) Normal postnatal development of medial superior olivary neurons in the albino rat: a Golgi and Nissl study. *J Comp Neurol*, **196**, 85-97.

Rothman, J.S. & Manis, P.B. (2003) The roles potassium currents play in regulating the electrical activity of ventral cochlear nucleus neurons. *J Neurophysiol*, **89**, 3097-3113.

Schmitt, S., Evers, J.F., Duch, C., Scholz, M. & Obermayer, K. (2004) New methods for the computer-assisted 3-D reconstruction of neurons from confocal image stacks. *Neuroimage*, **23**, 1283-1298.

Scott, L.L., Mathews, P.J. & Golding, N.L. (2005) Posthearing developmental refinement of temporal processing in principal neurons of the medial superior olive. *J Neurosci*, **25**, 7887-7895.

Sholl, D.A. (1953) Dendritic organization in the neurons of the visual and motor cortices of the cat. *J Anat*, **87**, 387-406.

Stotler, W.A. (1953) An experimental study of the cells and connections of the superior olivary complex of the cat. *J Comp Neurol*, **98**, 401-431.

Svirskis, G., Kotak, V., Sanes, D.H. & Rinzel, J. (2004) Sodium along with low-threshold potassium currents enhance coincidence detection of subthreshold noisy signals in MSO neurons. *J Neurophysiol*, **91**, 2465-2473.

Taylor, A.H., Amoako, A.A., Bambang, K., Karasu, T., Gebeh, A., Lam, P.M., Marzcylo, T.H. & Konje, J.C. (2010) Endocannabinoids and pregnancy. *Clin Chim Acta*, **411**, 921-930.

Trattner, B., Berner, S., Grothe, B. & Kunz, L. (2013a) Depolarisation-induced suppression of a glycinergic synapse in the superior olivary complex by endocannabinoids. *J Neurochem.*

Trattner, B., Gravot, C.M., Grothe, B. & Kunz, L. (2013b) Metabolic Maturation of Auditory Neurones in the Superior Olivary Complex. *PLoS One*, **8**, e67351.

Vetter, P., Roth, A. & Hausser, M. (2001) Propagation of action potentials in dendrites depends on dendritic morphology. *J Neurophysiol*, **85**, 926-937.

Wenger, T., Fragkakis, G., Giannikou, P., Probonas, K. & Yiannikakis, N. (1997a) Effects of anandamide on gestation in pregnant rats. *Life Sci*, **60**, 2361-2371.

Wenger, T., Fragkakis, G., Giannikou, P. & Yiannikakis, N. (1997b) The effects of prenatally administered endogenous cannabinoid on rat offspring. *Pharmacol Biochem Behav*, **58**, 537-544.

Werthat, F., Alexandrova, O., Grothe, B. & Koch, U. (2008) Experience-dependent refinement of the inhibitory axons projecting to the medial superior olive. *Dev Neurobiol*, **68**, 1454-1462.

Wilson, R.I. & Nicoll, R.A. (2001) Endogenous cannabinoids mediate retrograde signalling at hippocampal synapses. *Nature*, **410**, 588-592.

Womack, M. & Khodakhah, K. (2002) Active contribution of dendrites to the tonic and trimodal patterns of activity in cerebellar Purkinje neurons. *J Neurosci*, **22**, 10603-10612.

Yin, T.C. & Chan, J.C. (1990) Interaural time sensitivity in medial superior olive of cat. *J Neurophysiol*, **64**, 465-488.

Zhao, Y., Rubio, M.E. & Tzounopoulos, T. (2009) Distinct functional and anatomical architecture of the endocannabinoid system in the auditory brainstem. *J Neurophysiol*, **101**, 2434-2446.

Zhao, Y. & Tzounopoulos, T. (2011) Physiological Activation of Cholinergic Inputs Controls Associative Synaptic Plasticity via Modulation of Endocannabinoid Signaling. *J Neurosci*, **31**, 3158-3168.

Zhou, Y., Carney, L.H. & Colburn, H.S. (2005) A model for interaural time difference sensitivity in the medial superior olive: interaction of excitatory and inhibitory synaptic inputs, channel dynamics, and cellular morphology. *J Neurosci*, **25**, 3046-3058.

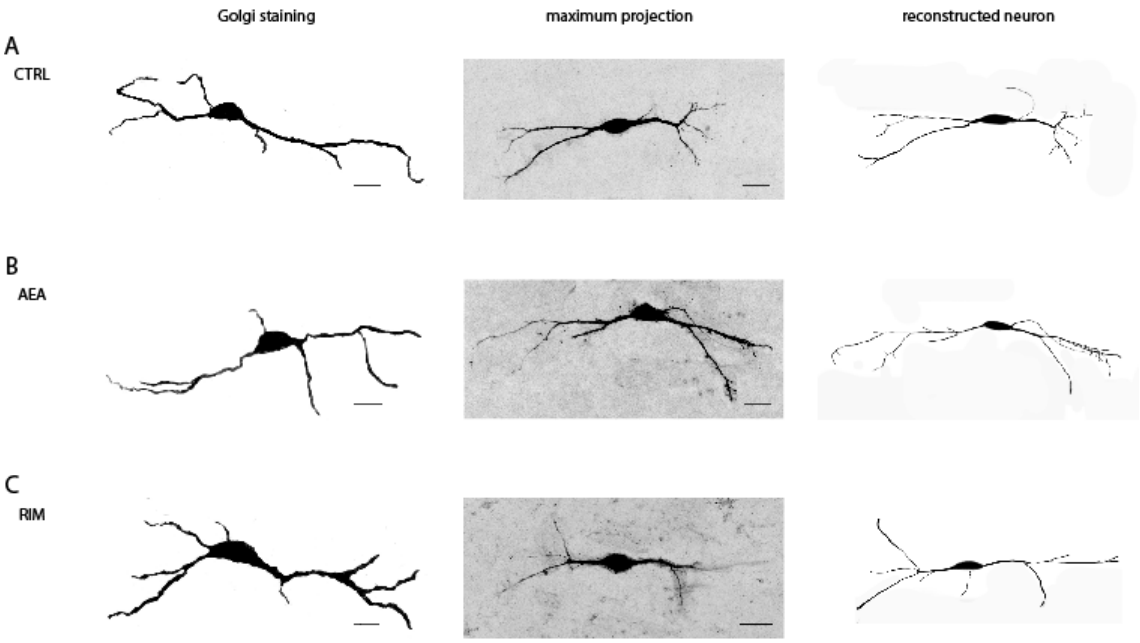

Figure 1. MSO neuron morphology

(A-C) Golgi stainings, maximum projections of confocal images of electroporated neurons and reconstructed skeleton trees corresponding to the maximum projections for the different treatment conditions: CTRL **(A)**, AEA **(B)** and RIM **(C)**. Scale bars = 30µm.

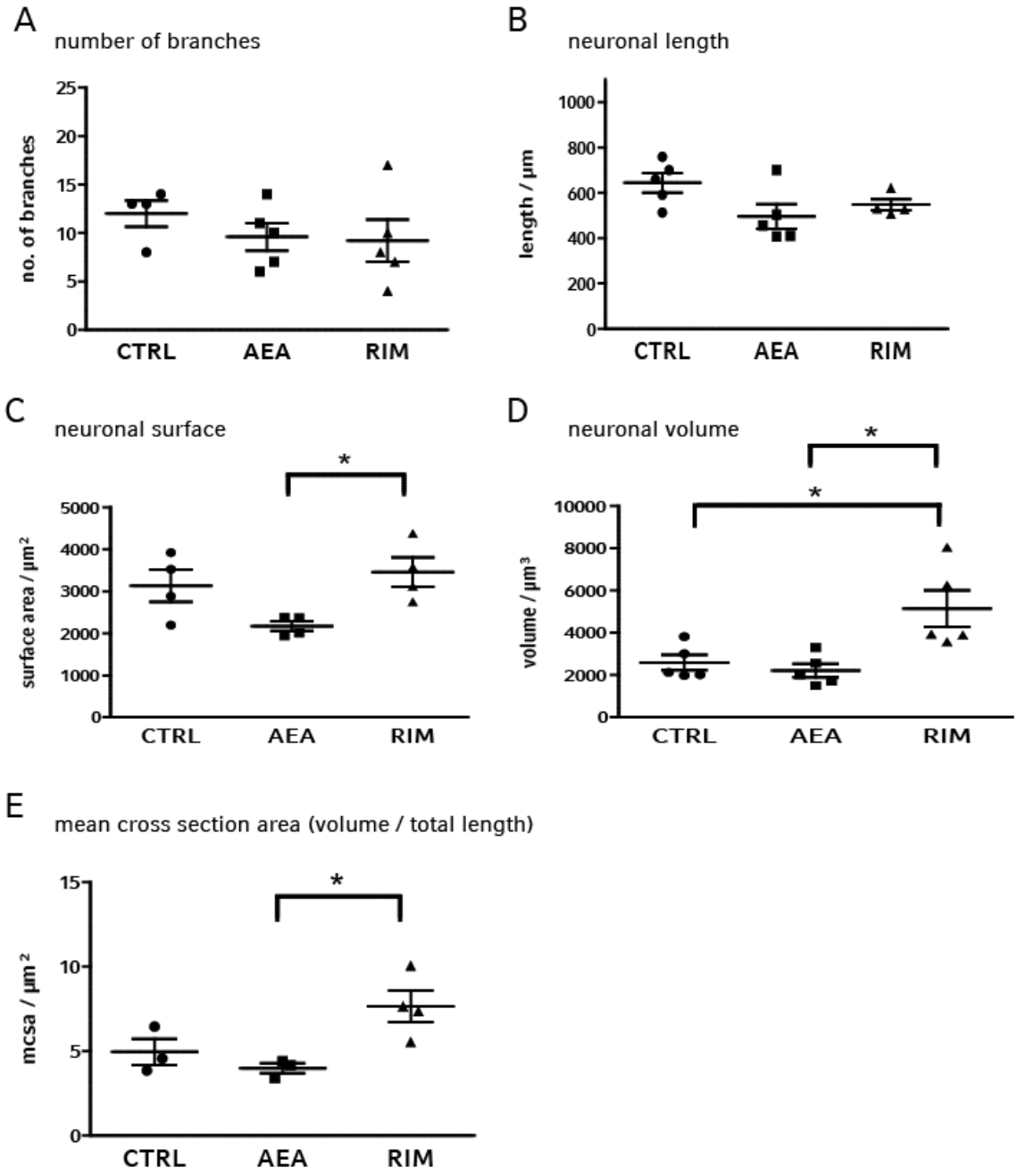

Figure 2. Parameters of the overall cell architecture.

Morphological profile of MSO neurons for CTRL, AEA and RIM conditions. **(A)** Total number of branches (n_{CTRL}=4, n_{AEA}=5, n_{RIM}=5). **(B)** Total neuronal length in µm (n_{CTRL}=5, n_{AEA}=5, n_{RIM}=4). **(C)** Total neuronal surface area in µm², significantly smaller under AEA conditions in comparison to RIM conditions (n_{CTRL} = 4, n_{AEA} = 4, n_{RIM} = 4). **(D)** Total neuronal volume in µm³, significantly increased in RIM neurons compared to CTRL and AEA conditions (n_{CTRL} = 5, n_{AEA} = 5, n_{RIM} = 5). **(E)** Mean cross section area (mcsa) in µm², given by

the quotient of volume and length, is significantly smaller in AEA neurons in comparison to RIM neurons ($n_{CTRL} = 3$, $n_{AEA} = 3$, $n_{RIM} = 4$). (* = $p < 0.05$)

A

soma length

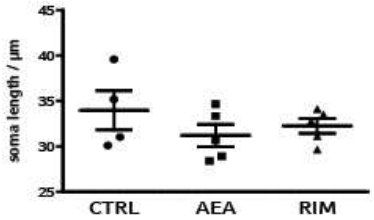

B

soma diameter

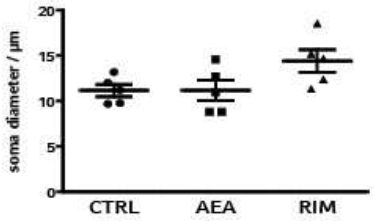

C

soma area / reconstructed neuron

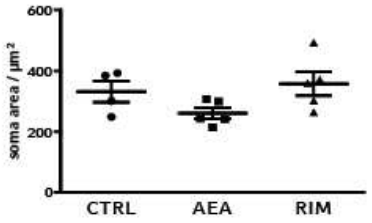

soma area / Golgi staining

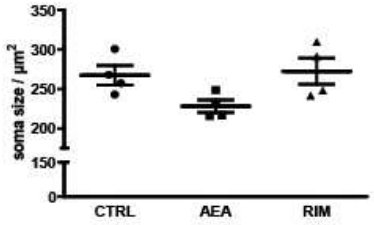

D

soma surface

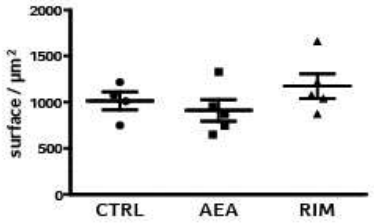

E

soma length / diameter

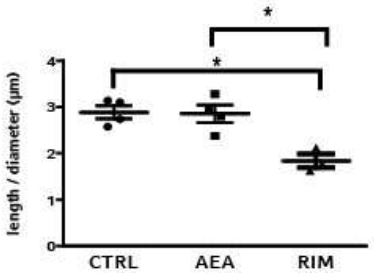

Figure 3. Morphological parameters of the somata

(A) Soma length in µm ($n_{CTRL} = 4$, $n_{AEA} = 5$, $n_{RIM} = 5$), **(B)** soma diameter in µm ($n_{CTRL} = 5$, $n_{AEA} = 5$, $n_{RIM} = 5$), **(D)** soma surface in µm² ($n_{CTRL} = 4$, $n_{AEA} = 5$, $n_{RIM} = 5$) and **(E)** ratio between soma length and diameter ($n_{CTRL} = 4$, $n_{AEA} = 4$, $n_{RIM} = 3$) are depicted for reconstructed neurons of each experimental group. **(C)** displays the soma area in µm² for reconstructed (upper part) and Golgi stained neurons (lower part), respectively. The soma ratio length/diameter was significantly reduced under RIM conditions compared to the CTRL and AEA group. (Scale bars = 30µm, * = $p < 0.05$)

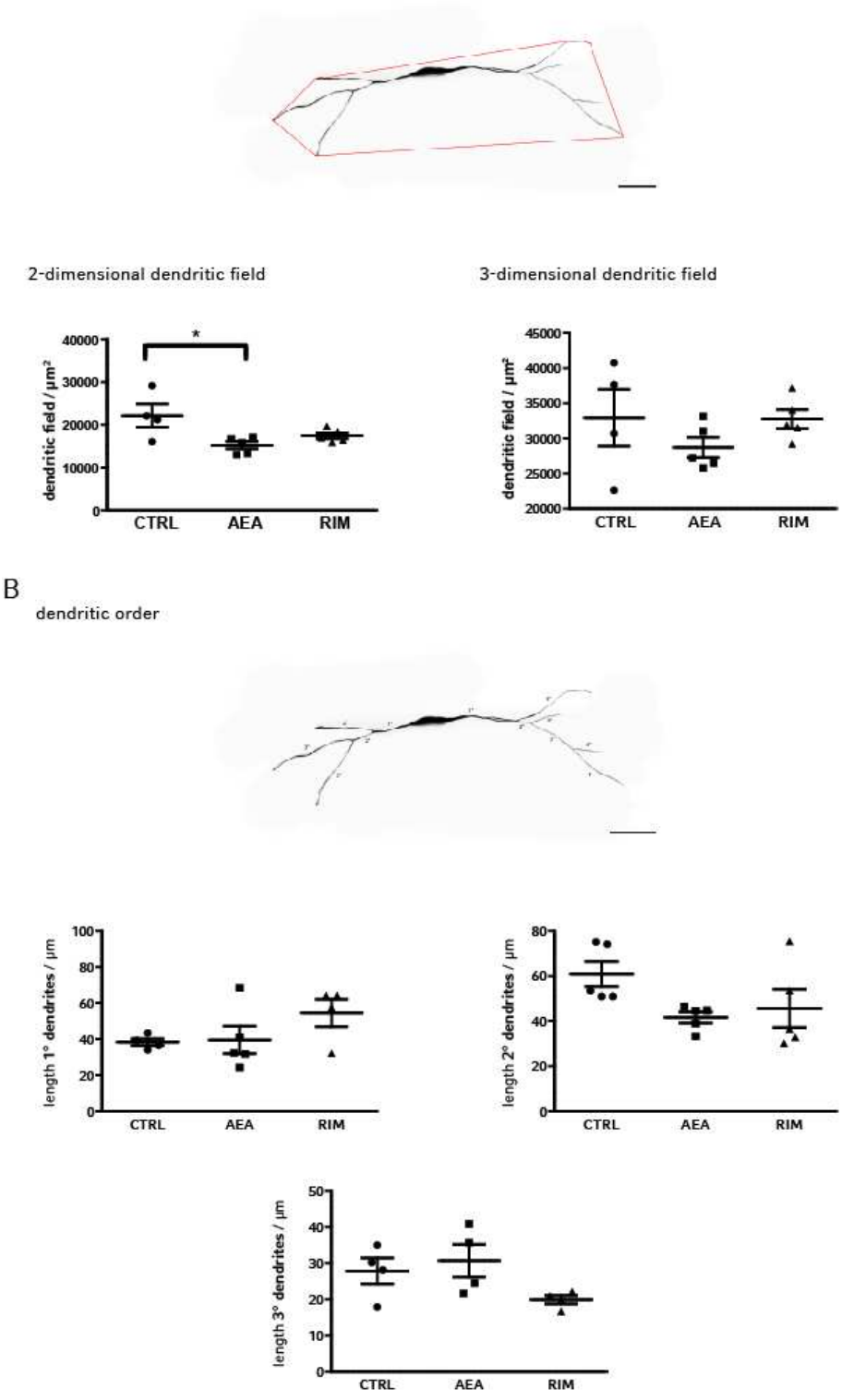

Figure 4. Dendritic morphology.

(A) Dendritic field expansions in µm² were measured by fitting a convex polygon in a two-dimensional space ($n_{CTRL} = 4$, $n_{AEA} = 5$, $n_{RIM} = 5$) or a convex polyhedron in a three-dimensional space ($n_{CTRL} = 4$, $n_{AEA} = 5$, $n_{RIM} = 5$) to each MSO neuron to join the most distal parts of the dendritic arbor. Results for two-dimensional

analysis revealed significantly reduced dendritic field expansions under AEA conditions in comparison to the CTRL group. **(B)** The order of dendritic branches was determined as indicated in example and the length in µm of first ($n_{CTRL} = 4$, $n_{AEA} = 5$, $n_{RIM} = 4$), second ($n_{CTRL} = 5$, $n_{AEA} = 5$, $n_{RIM} = 5$) and third ($n_{CTRL} = 4$, $n_{AEA} = 4$, $n_{RIM} = 4$) order branches was measured. (Scale bar = 30µm, * = $p < 0.05$)

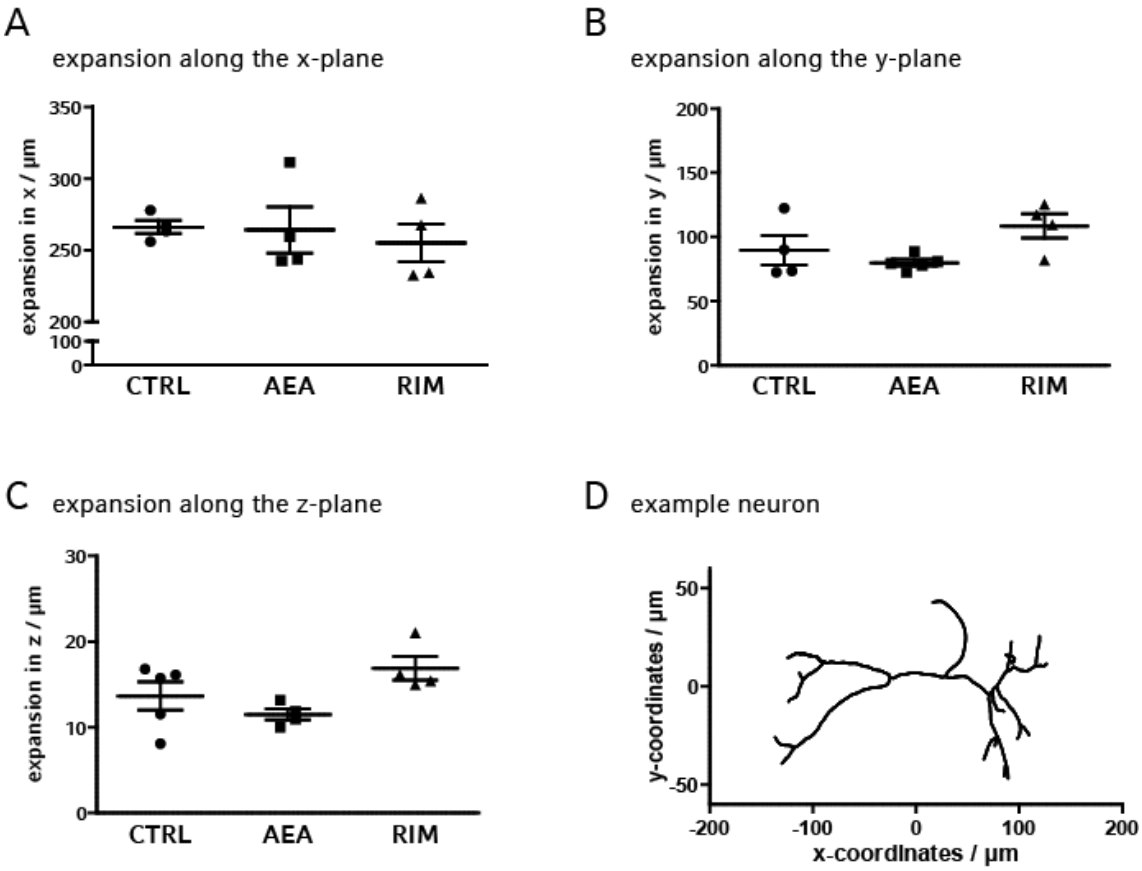

Figure 5. Spatial expansion of the dendritic tree.

(A – C) A Principal Component Analysis was conducted to obtain the principal axis of MSO neurons to transfer them into a three-dimensional coordinate system, resulting in an x- **(A)** ($n_{CTRL} = 4$, $n_{AEA} = 4$, $n_{RIM} = 4$), y- **(B)** ($n_{CTRL} = 4$, $n_{AEA} = 4$, $n_{RIM} = 4$), and z-value **(C)** ($n_{CTRL} = 5$, $n_{AEA} = 4$, $n_{RIM} = 4$) for each cell. **(D)** Sample neuron (CTRL) plotted as skeleton aligned along its principal axis. {0, 0} indicates position of soma center.

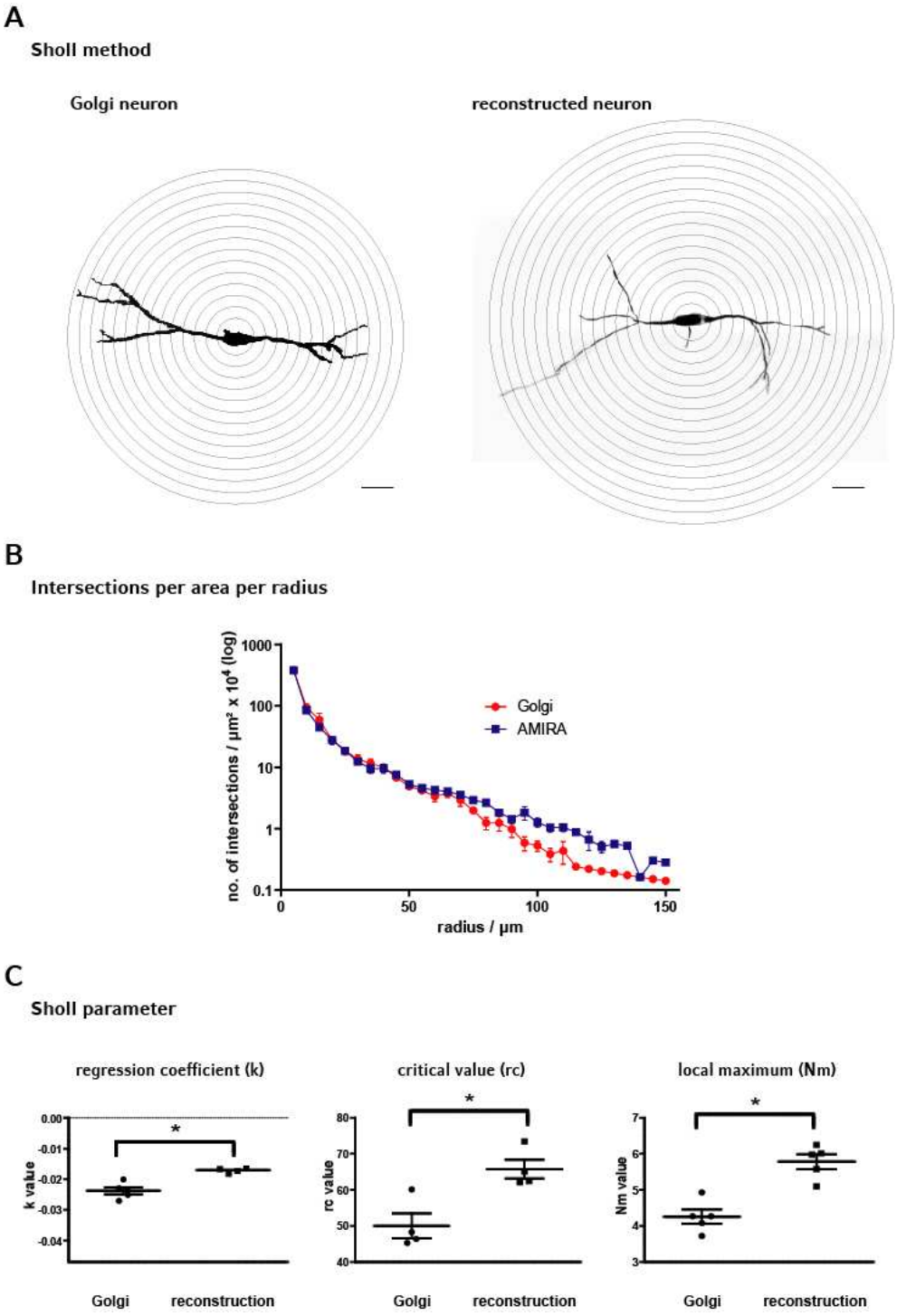

Figure 6. Method comparison: Electroporation vs. Golgi staining

(A) Examples for the procedure of Sholl analysis for either a Golgi stained or an electroporated MSO neuron: Concentric circles with a radius step size of 5 µm around the centre of a neuron intersect the dendritic arbor repeatedly. The first circle intersects every first order dendrite, the last circle comprises the longest dendritic branch. **(B)** Results of Sholl analysis for the CTRL groups of both methods display the intersections per area

*10^4 plotted semi-logarithmically against the distance from centre (n_{Golgi} = 6, $n_{reconstruction}$ = 6). **(C)** Additional Sholl parameters provide further information about the dendritic branching pattern: the regression coefficient k is the slope of the semi-logarithmical function (n_{Golgi} = 5, $n_{reconstruction}$ = 4); low absolute values for k reflect an earlier ramification and a more complex branching pattern and vice versa; the critical value r_c represents the radius at which there is a maximum number of intersections (n_{Golgi} = 4, $n_{reconstruction}$ = 4). r_c is correlated to the local maximum N_m, which provides the number of intersections at r_c (n_{Golgi} = 5, $n_{reconstruction}$ = 5). All Sholl Parameters are significantly increased when analyzing electroporated neurons compared to Golgi stained ones (scale bars = 30µm).

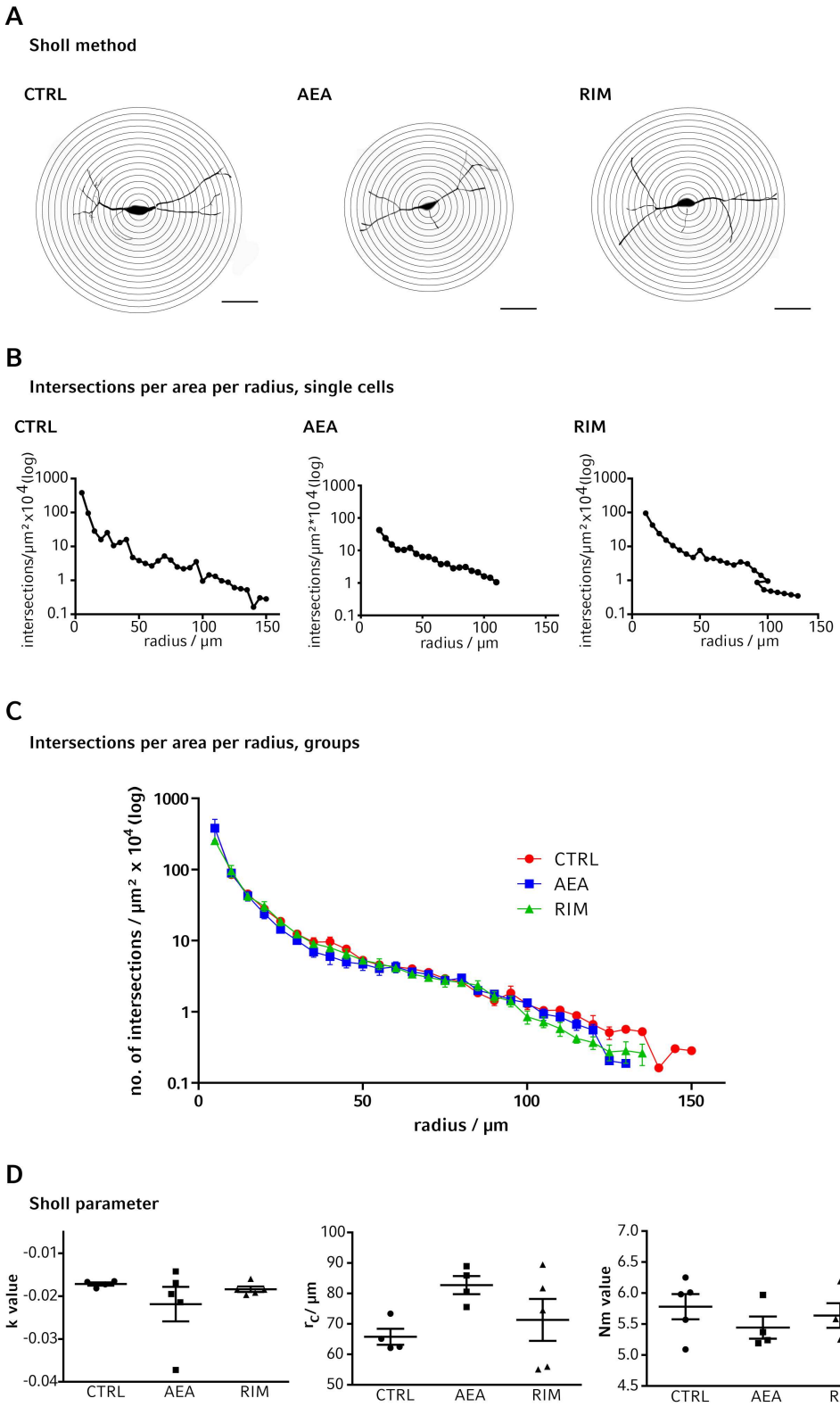

Figure 7. Results of the Sholl analysis.

(A – B) Illustration of the procedure of Sholl analysis for a model MSO neuron of each condition: Concentric circles with a radius step size of 5 µm around the centre of a neuron intersect the dendritic arbor repeatedly.

The first circle intersects every first order dendrite, the last circle comprises the longest dendritic branch **(A)**. The number of intersections per area $*10^4$ for these exemplary neurons are shown in a semi-logarithmical plot against the distance from the centre point (equally to the circle diameter) **(B)**. **(C)** Results of Sholl analysis for the three experimental conditions ($n_{CTRL} = 6$, $n_{AEA} = 6$, $n_{RIM} = 6$) display the intersections per area $*10^4$ plotted semi-logarithmically against the distance from centre. Additionally, a curve was fitted to each data set via a double exponential function and statistical analysis with an extra-sum-of square test revealed a significant difference in these curves ($p < 0.0001$). Note that starting at radius = 90 µm, the amount of data becomes less due to the fact that some neurons were shorter than others. **(D)** Additional parameters obtained by Sholl analysis provide further information about the dendritic branching pattern: the regression coefficient k is the slope of the semi-logarithmical function ($n_{CTRL} = 4$, $n_{AEA} = 5$, $n_{RIM} = 5$); low absolute values for k reflect an earlier ramification and a more complex branching pattern and vice versa; the critical value r_c represents the radius in µm at which the maximum number of intersections occurs ($n_{CTRL} = 4$, $n_{AEA} = 4$, $n_{RIM} = 5$). r_c is correlated to the local maximum N_m, which indicates the number of intersections at r_c ($n_{CTRL} = 5$, $n_{AEA} = 4$, $n_{RIM} = 4$).

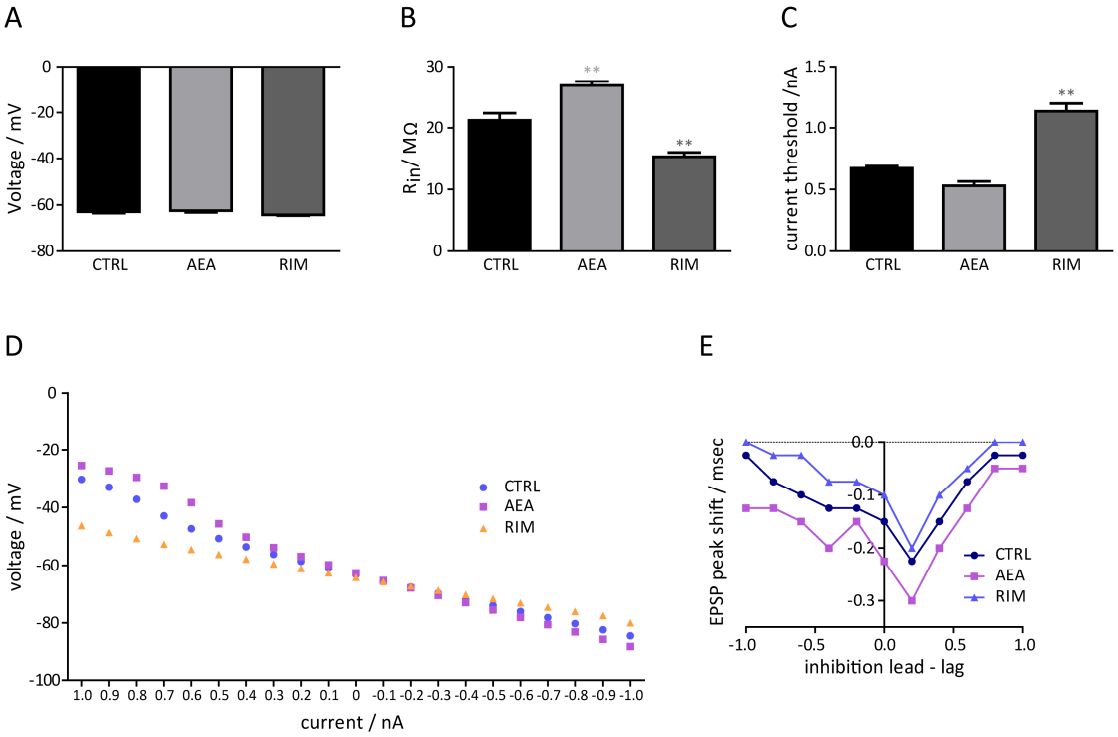

Figure 8. A computational MSO neuron model predicts physiological changes due to morphological alterations

(A) The resting membrane potential of the three groups remains almost unchanged by pharmacological treatment with either AEA or RIM and lies at about -60 mV in all three groups. **(B)** The input resistance (R_{in}) changes from 22 M□ in the CTRL group to 26.6 M□ in AEA-treated animals or 15.3 M□ in animals, which received RIM. **(C)** The current threshold to elicit an action potential is dependent on R_{in} and thus changes from 0.68 nA in the CTRL condition to 0.54 nA in AEA-treated animals or to 1.14 nA in the RIM group. **(D)** An IV curve, showing the membrane potential to different current injections, simulated for the different morphologies underlying the experimental groups, reveals substantial differences in membrane potential responses between CTRL, AEA and RIM group. **(E)** The excitatory inputs were shifted in time relative to the inhibitory input (□t/msec) and the resulting shift in the EPSP in µsec is plotted against this time difference. Negative values on the x-axis correspond to leading inhibition, whereas positive values on the x-axis represent lagging inhibition in msec. The magnitude of the peak shift is altered between the three groups (CTRL max = -225 µsec; AEA max = -300 µsec; RIM max = -200 µsec).

Postsynaptic endocannabinoid signalling modulates responses of adult MSO neurones

Running title: Postsynaptic endocannabinoid signalling in the MSO

Barbara Trattner[1,2], Benedikt Grothe[1] & Lars Kunz[1]

[1]Department of Biology II, Division of Neurobiology, Ludwig Maximilians University Munich, D-82152 Martinsried, Germany

[2]Graduate School of Systemic Neurosciences, Ludwig Maximilians University Munich, D-82152 Martinsried, Germany

Correspondence should be addressed to Barbara Trattner (trattner@bio.lmu.de) or Lars Kunz (lars.kunz@bio.lmu.de); Fax: +49(0)89/2180-74304

CONFLICT OF INTEREST

The authors declare no competing financial interests.

ACKNOWLEDGMENTS

We would like to express our sincere thanks to Ken Mackie, Indiana University, who gave us DAGLα and DAGLβ antibodies as a present. The authors thank the Graduate School of Systemic Neurosciences (GSN-LMU) and the Graduate School 1373 (TU Munich, DFG) for providing a grant to BT. This work was largely funded by the DFG (Collaborative Research Center 870). We thank Felix Felmy for helpful discussions.

ABSTRACT

The neuronal endocannabinoid system (ECS) is generally known for retrograde depression of synaptic inputs via presynaptic cannabinoid receptor 1 (CB1). In this study, however, we report that in the medial superior olive (MSO) of the Mongolian Gerbil (*Meriones unguiculatus*), a brainstem nucleus involved in computing sound localisation, a shift in the expression and functionality of the ECS occurs during auditory development. We previously observed that during the time of hearing onset retrograde endocannabinoid signalling coincides with presynaptic CB1 localisation. After hearing onset the auditory system undergoes a so-called refinement period, during which connections are fine-tuned to the auditory environment. We discovered that after refinement CB1 is localised postsynaptically, whereas endocannabinoid-synthesising enzymes are still expressed in postsynaptic somata and dendrites. Using patch-clamp electrophysiological recordings we found that endocannabinoids on one hand directly act on glycine receptors, depressing their currents, and on the other hand lead to neuronal hyperpolarisation in a CB1-dependent way. Our results suggest that this hyperpolarisation could be mediated by a GIRK conductance, activated by the G-protein coupled to CB1. We could elicit hyperpolarisation by CB1 agonist administration, high neuronal stimulation and/or mGluR1 agonism, which indicates that various mechanisms can trigger endocannabinoid synthesis. Functionally these modulations exerted by the ECS could have a huge impact on the computational properties of MSO neurones, since these neurones rely on precise glycinergic inhibition to allow the integration of physiologically relevant auditory stimuli. In this way the ECS could have a function in adapting the auditory system to changing acoustic environments.

INTRODUCTION

Endocannabinoids are molecules synthesised on demand from membrane fatty acids, which activate the endogenous cannabinoid receptors. Their production is initiated by high cellular activity, which leads to Ca^{2+} influx and thus activation of the enzymes required for their synthesis (Ueda *et al.*, 2011). There are several classes of endocannabinoids, the most prominent ones being anandamide (AEA) and 2-arachidonylglycerol (2-AG), as well as two types of cannabinoid receptors, namely CB1 and CB2, present in mammals. The CB1 receptor is expressed in many different brain areas (Herkenham *et al.*, 1990), whereas CB2 receptors have been described to play an important role in the regulation of the immune system, bone and fat metabolism, to name but a few (Atwood & Mackie, 2010).

The endocannabinoid system (ECS) is best known as a retrograde negative feedback system in many brain areas (Mackie, 2008; Katona & Freund, 2012). In this mode of action high stimulation of a postsynaptic neurone leads to Ca^{2+} influx and thus activation of endocannabinoid-synthesising enzymes (e.g. Diacylglycerollipases α/β, DAGLα/β). Endocannabinoids then bridge the synaptic cleft and target presynaptically located CB1, which leads to the inhibition of voltage-gated Ca^{2+} channels in a G-protein coupled manner. This decrease in intracellular Ca^{2+} rise leads to an attenuation of presynaptic transmitter release and consequently to a decrease in synaptic transmission onto the postsynapse. Thus this mechanism was called depolarisation-induced suppression of inhibition (Pitler & Alger, 1992; 1994; Ohno-Shosaku *et al.*, 2001; Wilson & Nicoll, 2001) or excitation (Kreitzer & Regehr, 2001) (DSI or DSE), depending on whether the transmitter exerted an inhibitory or an excitatory action.

In addition to these well-known retrograde signalling effects, other signalling cascades of endocannabinoid molecules have been described rather recently. In addition to presynaptic CB1-dependent signalling, CB1 receptors located postsynaptically can also directly modulate cellular excitability. Postsynaptic CB1 receptors can interact through their associated G-protein with a variety of ion channels, thus altering the neurone's response properties. An interaction with G-protein coupled inward rectifying K^+ (GIRK) channels (Henry & Chavkin, 1995; Guo & Ikeda, 2004)

for instance can act to decrease the neurone's resting membrane potential (Bacci *et al.*, 2004). Moreover, also a modulation of other types of K^+ channels (Deadwyler *et al.*, 1993; Deadwyler *et al.*, 1995) as well as Ca^{2+} channels has been observed (Mackie & Hille, 1992; Mackie *et al.*, 1995; Twitchell *et al.*, 1997; Lozovaya *et al.*, 2009).

Along with the classical action of endocannabinoids via their specific receptors CB1 and CB2 also a direct binding and modulation of other neurotransmitter receptors has been discovered. Endocannabinoids have for instance been shown to directly interact with glycine receptors, thereby modulating the glycine receptor mediated current. Depending on the brain area and the experimental system, this interaction can lead to attenuation (Lozovaya *et al.*, 2005) or potentiation (Hejazi *et al.*, 2006) of the Cl-current facilitated by the glycine receptor. Moreover, certain endocannabinoids can also directly bind to TRPV1 channels (Ross, 2003) and thereby lead to the induction of synaptic plasticity (Chavez *et al.*, 2010; Puente *et al.*, 2011).

In addition, the ECS has been shown to interact directly and indirectly with a variety of other neurotransmitter systems, mainly by using metabotropic pathways, such as the metabotropic glutamate or acetylcholine receptors to name but a few (Kushmerick *et al.*, 2004; Hashimotodani *et al.*, 2005; Best & Regehr, 2008; Puente *et al.*, 2011; Zhao & Tzounopoulos, 2011; Gyombolai *et al.*, 2012).

In this study we investigated endocannabinoid modulation in the medial superior olive (MSO), which is an auditory nucleus in the brainstem. The MSO computes interaural time differences, i.e. the difference in the arrival time of a sound at the two ears, and thus is critically involved in determining the position of sound sources in our surround and thereby enables orientation in acoustic space (Grothe *et al.*, 2010). To achieve their task, MSO neurones receive inputs from both ears, with glycinergic projections setting the maximum sensitivity within the physiological range (Brand *et al.*, 2002; Grothe, 2003; Pecka *et al.*, 2008). As an experimental animal we chose the Mongolian gerbil (*Meriones unguiculatus*), which is very suited for auditory research as it possesses an audible spectrum

and an organisation of the auditory brainstem similar to that of humans (Heffner & Heffner, 1988; Muller, 1990). We have previously observed retrograde glycinergic DSI as well as glutamatergic DSE in MSO neurones at the time of hearing onset in these animals (Trattner *et al.*, 2013a). Also in other areas of the auditory brainstem, retrograde endocannabinoid signalling has been demonstrated or suggested (Kushmerick *et al.*, 2004; Zhao *et al.*, 2009; Sedlacek *et al.*, 2011; Chi & Kandler, 2012). Since auditory brainstem circuits undergo a period of refinement (Kapfer *et al.*, 2002; Chirila *et al.*, 2007; Rautenberg *et al.*, 2009), during which synaptic connections are adjusted to the auditory environment, we now investigated endocannabinoid signalling in gerbils aged between P22 and P25. At this age the auditory circuitry has matured and reached the full adult-like configuration (Scott *et al.*, 2005; Chirila *et al.*, 2007; Rautenberg *et al.*, 2009; Trattner *et al.*, 2013b). To examine a possible influence of endocannabinoid signalling in the MSO after the refinement period, we studied the distribution of CB1 and the 2-AG synthesising enzymes DAGLα/β immunohistochemically. Additionally, we performed electrophysiological patch-clamp recordings of mature MSO neurones to elucidate the underlying function of the ECS.

MATERIALS & METHODS

Animals

All experiments complied with institutional guidelines as well as national and regional laws. Ethical clearance for animal experiments was granted by the local government of Bavaria (Regierung von Oberbayern). Mongolian gerbils (*Meriones unguiculatus;* both sexes) at postnatal day (P) 22-25 (further referred to P22 since the majority of animals was aged P22) and at P13-15 originating from the animal facility in our department were used.

Immunohistochemistry

The procedure for immunohistochemical stainings was described in detail before (Trattner *et al.*, 2013a; Trattner *et al.*, 2013b). Shortly, animals were anaesthetised using 200 mg/kg body weight pentobarbital (Narcoren®, Merial), i.p, and subsequently transcardially perfused at a flow rate of 4 ml/min with Ringer solution supplemented with 0.1% heparin (Meditech Vertriebs GmbH) for 10 min followed by 4% paraformaldehyde (PFA) for 20 min. The brains were post-fixed overnight in 4% PFA at 4°C. Using a Leica VT1200S Vibratome, 50 µm sections of the auditory brainstem were collected and washed 4 times in 0.1 M phosphate buffered saline (PBS) for 5 min each. Then, unspecific binding sites were saturated using a blocking solution (0.3% Triton X-100, 0.1% saponine and 1% BSA) for 1 hour at room temperature on a shaker. Sections were incubated in the primary antibody mix diluted in blocking solution over night at 4°C on a shaker. Primary antisera used were: chicken anti-MAP2 (1:1000, Neuromics, CH22103), rabbit anti-CB1 (1:300, Alomone, ACR-001), rabbit anti-CB2 (1:300, abcam, ab3561), mouse anti-SV2 (1:500, DSHB, SV2c), rabbit anti-mGluR1 (1:500, abcam, ab82211), rabbit anti-TRPV1 (1:500, Neuromics, RA14113), goat anti-GIRK2 (1:500, abcam, ab65096) as well as rabbit anti-DAGLα (1:500) and rabbit anti-DAGLβ (1:500, both gift from Dr. Ken Mackie, Indiana University). Thereafter, sections were washed 4 times in 0.1 M PBS for 5 min each and incubated with secondary antibodies for 3-4 hours at room temperature on a shaker. Secondary antisera used were: donkey anti-rabbit DyLight 649 (1:300, Dianova, 711-496-152),

donkey anti-rabbit DyLight 488 (1:100, Dianova, 711-486-152), goat anti-rabbit Alexa488 (1:400, Molecular probes, A-11034), donkey anti-mouse Cy5 (1:200, Dianova, 715-176-150), donkey anti-goat Alexa488 (1:400, Molecular probes, A-11055), goat anti-chick Alexa488 (1:400, Molecular probes, A-11039) and donkey anti-chick Cy3 (1:300, Dianova, 703-166-155). Afterwards, the sections were washed 4 times in 0.1 M PBS for 10 min each. Finally, the slices were mounted with Vectashield supplemented with DAPI (H-1200, Vector).

Confocal optical sections were acquired with a Leica 6000CS SP5 confocal laser-scanning microscope (Leica Microsystems, Mannheim) equipped with a Plan 63x/NA1.32 oil immersion objective. Fluorochromes were visualised by using a UV laser with an excitation wavelength of 405 nm (emission 420 – 475 nm for DAPI), an argon laser with an excitation wavelength of 488 nm (emission 494 - 555 nm for Alexa 488/DyLight 488), a DPSS laser with a laser line of 561 nm (emission 565 – 606 nm for Cy3) and a helium-neon laser with an excitation wavelength of 633 nm (emission 640 – 740 nm for DyLight 649). The images were collected sequentially for the different fluorochromes for each optical section. The image size was 512 x 512 pixels. Stacks were obtained with axial distances of 300 nm. Each section image was averaged from four successive line scans to obtain an improved signal-to-noise ratio. The images shown in the figures of this publication are single images from the stacks and thus have an optical axial distance of 300 nm.

Electrophysiological recordings

The procedures carried out to perform electrophysiological recordings have been described previously (Trattner *et al.*, 2013a), but were adapted to the distinct requirements of the respective animal's age and the specific experiment and are thus outlined again here. Animals were anaesthetised with isoflurane and subsequently decapitated. The brains were removed and placed in dissecting solution, which was pre-warmed to room temperature (P22) or cooled on ice (P13-15) and contained (in mM, all from Sigma-Aldrich Chemie GmbH, München, Germany): 50 sucrose, 25 NaCl, 25 $NaHCO_3$, 2.5 KCl, 1.25 NaH_2PO_4, 3 $MgCl_2$, 0.1 $CaCl_2$, 25 glucose, 0.4 ascorbic acid, 3 myo-

inositol and 2 Na-pyruvate. The pH amounted to 7.4 when bubbled with 95% O_2 and 5% CO_2. Horizontal brainstem sections of 200 µm thickness were cut using a VT1000S vibratome (Leica, Wetzlar, Germany). Slices were incubated in extracellular recording solution, which was continuously bubbled with 95% O_2 and 5% CO_2, for 45 min at 36°C and then stored at room temperature until use. The extracellular recording solution contained (in mM, all from Sigma-Aldrich): 125 NaCl, 25 $NaHCO_3$, 2.5 KCl, 1.25 NaH_2PO_4, 2 $CaCl_2$, 1 $MgCl_2$, 25 glucose, 0.4 ascorbic acid, 3 *myo*-inositol and 2 Na-pyruvate.

For recording, slices were transferred into a chamber mounted on a microscope (Olympus BX51WI, Olympus Europa GmbH, Hamburg, Germany) and continuously perfused with fresh extracellular recording solution at room temperature (≈ 22°C).

Voltage-clamp whole-cell recordings were performed with an EPC9 amplifier (HEKA Elektronik Dr. Schulze GmbH, Lambrecht/Pfalz, Germany) on visually identified MSO neurones. Cells were clamped at -60 mV unless stated otherwise. Series resistance was compensated to a residual of 3-4 M□. Glass pipettes used for recording had a resistance between 2.0 and 4.5 M□. The intracellular solution for voltage-clamp recordings contained in mM (all from Sigma-Aldrich): 105 Cs-gluconate, 26.7 CsCl, 10 HEPES, 20 TEA-Cl, 3.3 $MgCl_2$, 2 Na_2ATP, 0.2 NaGTP, 3 Na-phosphocreatine and 1 EGTA. The solution was adjusted to pH 7.2 with CsOH. Glycinergic postsynaptic currents were pharmacologically isolated by adding 50 µM D-APV (BioTrend), 20 µM DNQX (BioTrend), 10 µM gabazine (Sigma Aldrich) and 2 µM rimonabant (Cayman Chemicals) to the extracellular recording solution. Excitatory postsynaptic currents were pharmacologically isolated by supplementing the extracellular solution with 0.5 µM strychnine (Sigma Aldrich) and 10 µM gabazine. To investigate the effects of the ECS on evoked postsynaptic currents the following CB1 antagonists and agonists were used: rimonabant (2 µM, Cayman Chemical), AM251 (2 µM), WIN-55,212-2 mesylate (1 µM, BioTrend) and anandamide (1 µM, Cayman Chemical).

Glycinergic currents were evoked by placing a bipolar tungsten electrode at the fibre bundle originating in the ipsilateral MNTB. Excitatory currents were evoked by placing the stimulation electrode dorso-lateral of the MSO, to stimulate fibres originating in the ipsilateral cochlear nucleus.

Fibres were stimulated with a rate of 0.33 Hz and pulse duration of 0.2 msec. The stimulus strength was adjusted to the precise number and position of fibres that were affected by the stimulus electrode. The recording protocol used to obtain evoked currents, consisted of a pre-depolarisation for 19.80 msec from the resting membrane potential, which was clamped at -60 mV, before the actual stimulus was delivered to the glycinergic fibres for 0.2 msec, to disentangle currents evoked by the change in the membrane potential and currents elicited by the actual fibre stimulation. Starting at -60 mV, the neurone was depolarised in 10 mV steps in 11 sweeps and the currents were recorded depending on the membrane potential. To yield the actual evoked current, the current change caused only by the change in membrane potential (pre-depolarisation) was subtracted from the current obtained after the stimulation. Before starting an experiment, we ensured that the baseline current amplitude was stable for at least 21 stimulations. For quantification all currents were normalised to the average baseline current before the administration of CB1 agonists.

To investigate K^+ and Ca^{2+} currents, we blocked all synaptic currents (i.e. 50 µM D-APV, 20 µM DNQX, 10 µM gabazine and 0.5 µM strychnine) as well as sodium currents (5 mM QX314 (Sigma Aldrich) intracellularly) and I_h currents (50 µM ZD7288 (BioTrend)). We used the same composition of the intracellular solution for voltage-clamp recordings given above, but without TEA-Cl.

For current-clamp recordings the dissection procedure and the extracellular solutions used were identical, however the intracellular solution had a different composition, i.e. (in mM): 72.5 K-gluconate, 2.5 KCl, 1 Mg-ATP, 1 K_2-ATP, 0.15 Na_2-GTP, 3.75 Na_2-phosphocreatine, 7.5 HEPES and 1 EGTA. The solution was adjusted to pH 7.25 with KOH. CB1 agonists and antagonists were administered in the concentrations given above. To block the HCN channels, we used 50 µM ZD7288. To test the effect of mGluR1 receptors on the membrane potential we used 50 µM of the mGluR1 agonist DHPG (BioTrend). To evoke the endocannabinoid action on the membrane potential by activity we used the following sine wave stimulus, which was injected via the recording electrode into the neurone: 800 pA, 150 Hz, 1 sec, with 100 msec breaks repeated for 40 times.

As a general step protocol we initially injected -500 pA for 200 msec and then increased the current in 100 pA steps for 12 sweeps with 500 msec pauses in between. To determine the membrane time constant (τ) we injected -10 pA for 500 msec and obtained τ by a mono-exponential fit. In order to investigate the current threshold required to elicit an action potential, we injected 25 pA for a duration of 2 msec and increased the current by 25 pA increments for 40 sweeps. The action potential halfwidth was calculated as the full width at the half maximum of the action potential. The action potential refractory period was determined by stimulating the neurone twice with 1000 pA for 1 msec each with a 1 msec break in between. In the following 49 sweeps the inter stimulus interval was successively increased by 0.2 msec increments.

Statistical Analysis

All statistical analysis was performed in Prism 5.0 (Graphpad). Average values are given as mean ± s.e.m. Generally, data was normalised for each cell to the baseline condition, where no CB1 agonists/antagonists or stimulation was present to account for differences occurring during the course of the experiment rather than emphasising differences between cells. The data was tested for a deviation from 1.0, representing the normalised baseline condition with a one-sample t-test. Whenever, original data were directly compared, we used a repeated-measures ANOVA followed by a *post hoc* Tukey test. The IV curves of K^+ and Ca^{2+} currents without AEA, with AEA and after wash-out of AEA were fitted with a 6^{th} order polynomial and these best-fits were statistically compared to each other for difference between them. The significance level employed in this study was set at $p < 0.05$.

RESULTS

Immunohistochemical localisation of the ECS indicates a postsynaptic signalling mechanism

CB1 receptors are mainly expressed somatically and along the dendrites in MSO neurones of P22 animals, as indicated by the co-localisation with a positive MAP2 signal (Figure 1A). There is only very little, if any, co-localisation of CB1 with the presynaptic marker SV2. The 2-AG synthesising enzymes DAGL α/β are also expressed somatically in MSO neurones at P22, as indicated by the overlap of the DAGLα/β staining with the MAP2 signal (Figure 1B). Additionally, we checked for the presence of CB2 immunoreactivity, but neither neuronal nor glial CB2 expression was observed (data not shown).

Glycine receptor mediated postsynaptic currents are depressed by endocannabinoids

In spite of the absence of presynaptic CB1 receptor protein at P22 (Figure 1A), we investigated whether a presynaptic CB1 effect is present in adult gerbils. For this purpose, we had to change the stimulus protocol, as we could not hold MSO P22 neurones in voltage-clamp configuration during the 5 sec 0 mV depolarisation stimulus that we used previously to elicit endocannabinoid-dependent retrograde depolarisation-induced suppression of neurotransmitter release in younger animals (Trattner *et al.*, 2013a). Thus, glycinergic currents were evoked by stimulation of glycinergic fibres and pharmacologically isolated by blocking other synaptic inputs with 50 µM D-APV, 20 µM DNQX and 10 µM gabazine, while obtaining whole-cell voltage-clamp recordings from MSO neurones. Since we could not elicit DSI by postsynaptic depolarisation we washed in AEA to investigate endocannabinoid signalling. In the presence of rimonabant, we found that AEA reversibly depressed glycinergic current amplitudes (Figure 2B, 2C). This indicates a postsynaptic mode of action directly via glycine receptors, instead of a presynaptic pathway, as CB1 receptors have been blocked during the experiment. All currents were normalised to the currents before wash-in of AEA that corresponded to the same holding potential (Figure 2A, 2C). Depending on the holding potential, AEA depressed the current amplitude by up to 50% (Figure 2C). Wash-out of AEA again recovered

the initial baseline and values. The decay time constant τ of the evoked current remained mostly unchanged by treatment with AEA, however at holding potentials between -20 and -10 mV, which marks the area around the reversal potential of the glycinergic currents, it showed a prominent decrease by up to 50%, which was unaffected by wash-out (Figure 2D).

Excitatory evoked currents are not modulated by endocannabinoids

We performed recordings to investigate, whether excitatory currents were also subject to postsynaptic modulation by endocannabinoids. We stimulated excitatory fibres originating in the ipsilateral cochlear nucleus and isolated excitatory currents pharmacologically by adding 0.5 μM strychnine and 10 μM gabazine. The stimulation and recording procedure were identical to that of glycinergic currents (Figure 3A). All currents were normalised to the currents before wash-in of AEA that corresponded to the same holding potentials (Figure 3A, 3B). AEA did not lead to a change in excitatory current amplitude at the holding potentials investigated (Figure 3C). Also the normalised τ of the excitatory currents was not subject to a significant change by endocannabinoid signalling (Figure 3D).

The resting membrane potential is hyperpolarised by CB1 agonism

We monitored the resting membrane potential (V_r) in current-clamp mode, which was normalised to its value before AEA wash-in. We observed a significant hyperpolarisation of the cell's membrane potential after wash-in of AEA for 15 min, which was reversible upon wash-out (Figure 4A, 4B). The average V_r values were -49.0 ± 0.8 mV before AEA administration and -53.0 ± 2.0 mV thereafter. This hyperpolarising effect of AEA is independent of the often reported run-down of the I_H current, which occurs during long-term recordings and leads to a hyperpolarisation of the cell. Recordings in the presence of the HCN inhibitor ZD7288 (50 μM) showed a V_r of 57 ± 3 mV. However, upon wash-in of AEA, the neurone further hyperpolarised significantly to an average value of -63 ± 3 mV. This

hyperpolarisation was again fully reversible upon the wash-out of AEA (Figure 4C, 4D). We checked, whether the postsynaptic CB1-dependent effect is also present in animals aged between P13 and P15, which were previously shown not to express any postsynaptic CB1 receptors, but only show retrograde depression of postsynaptic currents via presynaptic CB1 receptors (Trattner *et al.*, 2013a). We found in these younger animals that AEA exerted no effect on V_r (Figure 4E, 4F). Under baseline conditions, V_r amounted to -49.0 ± 0.5 mV and after application of AEA V_r hardly changed to -47.5 ± 0.6 on average.

Hyperpolarisation is triggered by stimulation of intrinsic endocannabinoid release

We tried to elicit the hyperpolarising effect of endocannabinoids on the membrane potential by stimulation of the neurone, rather than by application of CB1 agonists. We used a sine wave stimulus described in the Materials & Methods section, which mimics a high-frequent action potential train of a long duration and thus represents a more physiological condition than high CB1 agonist concentrations applied to the slice. We monitored the change in V_r before and after stimulation and then repeated the same stimulation in the presence of the CB1 antagonist rimonabant. Before stimulation the resting membrane potential amounted to -50.0 ± 1.4 mV. Stimulation induced a prominent and significant hyperpolarisation to a mean value of -58.0 ± 5.6 mV, which was completely blocked by the wash-in of rimonabant (Figure 5B, 5C).

We investigated whether stimulation of mGluR1 receptors could facilitate endocannabinoid synthesis and thus hyperpolarisation. We applied the mGluR1 agonist DHPG during our recording and observed that already without stimulation V_r was significantly decreased (15 min DHPG: -57.0 ± 4.2 mV) when compared to the baseline condition (Figure 5A, 5C). Additional stimulation in the presence of DHPG led to a further significant reduction in the V_r (15 min DHPG + stimulation: -61.0 ± 7.0 mV), indicating that mGluR1 stimulation alone is sufficient to drive endocannabinoid synthesis (Figure 5C). Rimonabant administration blocked the stimulation- and DHPG-evoked hyperpolarisation. In support of our electrophysiological findings, we could also show by

immunohistochemical stainings that mGluR1 receptors are abundantly expressed by MSO neurones at P22 (Figure 5D).

Action potential refractory period and halfwidth are modulated by endocannabinoids

We tested whether the endocannabinoid system affects other parameters of neuronal activity in current-clamp recordings of P22 MSO neurones. The action potential threshold showed no change upon wash-in of AEA (Figure 6A). The refractory period between two action potentials decreased significantly from an original mean value of 3.8 ± 0.3 msec to a mean value of 2.8 ± 0.5 msec, however this decrease was not reversible upon blocking the CB1 receptor with the specific antagonist AM251 (Figure 6B). The membrane time constant τ was not affected by endocannabinoid signalling, however, the variance increased during the course of the recording, which might me due to long recording durations (Figure 6C). The mean action potential halfwidth (i.e. the full width at half maximum) also decreased significantly from a mean value of 0.54 ± 0.08 msec to 0.40 ± 0.04 msec upon administration of AEA but this effect again was not reversible upon CB1 antagonism (Figure 6D).

Inwardly-rectifying K^+ currents might mediate endocannabinoid-induced hyperpolarisation

We asked which currents could mediate the hyperpolarisation evoked by endocannabinoids. From the literature it is well-known that endocannabinoids can modulate Ca^{2+} and K^+ channels (Mackie & Hille, 1992; Mackie *et al.*, 1995). Especially G-protein coupled inward rectifiers were reported to show an increased conductance upon endocannabinoid signalling and thereby they mediate hyperpolarisation (Henry & Chavkin, 1995; Bacci *et al.*, 2004). Thus, we performed voltage-clamp recordings of MSO neurones, in the presence of the synaptic transmission blockers 50 µM D-APV, 20 µM DNQX, 10 µM gabazine and 0.5 µM strychnine as well as 5 mM QX314 to block sodium currents and 50 µM ZD7288 to block the I_h current contribution. In the MSO cells from animals

aged > P22, we found a reversible increase in a small inward current at potentials negative to the resting membrane potentials (Figure 7A, 7B), which could represent an increased GIRK conductance. In addition a non-reversible change in the currents between -40 to -10 mV was observed, which could represent either a change in Ca^{2+} or TRPV1 conductance. A statistical comparison of nonlinear fits of the curves corresponding to the three experimental conditions rendered the conclusion that different curves are required for the different data sets. By immunohistochemical stainings we could demonstrate the presence of GIRK2 in MSO neurones of animals older than P22 (Figure 7E). Moreover, we found by immunohistochemistry that TRPV1 channels are abundantly expressed in MSO neurones of that postnatal age (Trattner, unpublished observation)

We repeated the same experiments in MSO neurones of animals aged between P13-15, which neither showed a postsynaptic expression of CB1 receptors nor a cannabinoid-evoked hyperpolarisation. In these neurones, there was no increase in an inward current at hyperpolarising membrane potentials (Figure 7C, 7D). The only observation is that a decrease in a current occurring in the baseline condition between -20 and 0 mV is non-reversibly inhibited by endocannabinoid signalling. This current could correspond to a Ca^{2+} influx, which has often been shown to be decreased by endocannabinoid signalling. However, since the current is non-reversible, the current decrease could also be owing to a run-down in Ca^{2+} currents, which is often observed in electrophysiological recordings of a long duration.

DISCUSSION

Conclusion

We report that in MSO neurones of Mongolian gerbils, which already possess a matured auditory system, endocannabinoid signalling takes place in a mainly postsynaptic manner. Unlike previously observed in animals during the time of hearing onset, where retrograde inhibition of synaptic transmission is present (Trattner *et al.*, 2013a), we found that after the refinement of auditory circuits the anatomical localisation and physiological function of the system change:

(1) CB1 is now expressed postsynaptically in neurones (Figure 1A). Synapses express only very limited amounts of CB1. The endocannabinoid-synthesising enzymes DAGLα/β are still expressed by the neurones themselves (Figure 1B).

(2) Electrophysiological recordings suggest that endocannabinoid signalling is functional in two ways: First, the membrane potential is hyperpolarised in a CB1-dependent way (Figure 4). We have indications that this might be enabled by an increase in a GIRK conductance activated through CB1 (Figure 7). Second, endocannabinoids directly bind to the glycine receptor and depress its current in a CB1-independent way (Figure 2).

Decreased glycine receptor mediated current could shift the dynamic range of MSO neurones

It has been previously observed that endocannabinoids can directly modulate glycinergic currents, however depending on the subunit composition of the glycine receptor, the concentration of the CB1 agonists, brain regions and experimental models, the outcome of this modulation varies (Lozovaya *et al.*, 2005; Hejazi *et al.*, 2006; Yang *et al.*, 2008; Lozovaya *et al.*, 2011). Using 1 µM AEA, we found up to 50% reduction of glycine receptor-mediated current (Figure 2C) which was reversible upon wash-out. Our results are in line with the depression in glycinergic currents observed by Lozovaya and colleagues in rat hippocampal pyramidal and cerebellar Purkinje cells (Lozovaya *et al.*, 2005), however the effects that we observed are comparatively smaller in amplitude. We could not find a

difference in the decay time constant of the current. Reasons for these ambiguities might be a possible difference in receptor subunit composition or species specific alterations in the subunits themselves. Functionally, however, our data suggests that endocannabinoids decrease the current that is passed by glycine receptors, which would have tremendous effects on the physiological performance of MSO neurones. It has been shown that precise inhibition by glycinergic projections enables the coding of physiologically relevant interaural time differences in the MSO (Brand *et al.*, 2002; Grothe, 2003; Pecka *et al.*, 2008). They reported that if strychnine is applied, the steepest slope of the ITD function of MSO neurones is shifted to ITDs outside the physiological range and thereby the dynamic range within the physiological range is reduced (Brand *et al.*, 2002). Our findings suggest that endocannabinoids partially antagonise the glycine receptors and thus might shift the dynamic range of MSO neurones to changing acoustic environments, when physiologically released during times of high neuronal activity.

Endocannabinoid-evoked membrane hyperpolarisation could allow adaptation to high stimulus strengths

Additionally, we found another effect, which is mediated by endocannabinoids in MSO neurones. The membrane potential was decreased in a CB1-dependent fashion after the application of AEA (Figure 1A). This effect was also elicited by high neuronal stimulation and/or mGluR1 agonism and was sensitive to CB1 antagonists (Figure 5C). It has been previously shown that endocannabinoids can act to decrease the resting membrane potential of neurones (Bacci *et al.*, 2004; 2005) and it was suggested that this effect could be mediated by GIRK channels, which can be activated by CB1-coupled G-proteins (Henry & Chavkin, 1995; Guo & Ikeda, 2004). AEA administration led to a hyperpolarisation of 4 mV and stimulation to one of about 8 mV. These values are comparable to previous results in neocortical interneurones, where also reductions in the membrane potential between 5 and 10 mV have been found (Bacci *et al.*, 2004). Moreover we also found indications that this effect might be mediated by an inwardly rectifying K^+ conductance carried by GIRK 2 channels (Figure 7).

Functionally, this mechanism could lead to a general change in the response properties of MSO neurones at high stimulation rates, which is when endocannabinoids are physiologically thought to be released. It would be plausible that the excitability of MSO neurones is reduced, thus preventing an over-stimulation. However, we did not observe a change in action potential threshold, only action potential halfwidth and refractory period showed a trend to be decreased during AEA administration. This suggests that neurones could fire at higher frequencies and adjust to higher stimulus inputs.

Together the endocannabinoid-induced hyperpolarisation and decrease in glycine receptor mediated current could act to adjust the physiology of MSO neurones to extreme sound environments and high input stimuli, which would initiate endocannabinoid synthesis.

Endocannabinoids could physiologically be released from various sources

Endocannabinoids could be released in an autocrine manner, since MSO neurones were positively stained for DAGLα/β enzymes, or in a paracrine way, by neighbouring neurones. However, endocannabinoid action is mostly limited to the immediate area surrounding their production (Brown *et al.*, 2003). Endocannabinoid synthesis could be initiated by high cellular activity, which would allow Ca^{2+} influx through voltage-gated Ca^{2+} channels. In our study we showed that high stimulation of the neurone itself can give rise to the CB1-dependent effect of hyperpolarisation, indicating that cellular activity alone might be sufficient to trigger endocannabinoid signalling (Figure 5C). Additionally high network activity, would lead to the release of neurotransmitters such as glutamate or possibly also acetylcholine from synaptic terminals, activating metabotropic glutamate (Kushmerick *et al.*, 2004) or acetylcholine receptors (Zhao & Tzounopoulos, 2011), respectively. These metabotropic receptors facilitate Ca^{2+} influx and can thereby initiate endocannabinoid synthesis. We report in our study that administration of the mGluR1 agonist DHPG can elicit endocannabinoid-dependent membrane hyperpolarisation, suggesting that metabotropic glutamate receptors could represent a Ca^{2+} source relevant for triggering

endocannabinoid synthesis in the MSO indeed. Also activation of $G_{q/11}$ proteins coupled to muscarinic or serotonergic metabotropic receptors could provide DAG and high intracellular Ca^{2+} (Best & Regehr, 2008; Gyombolai *et al.*, 2012). In some cases also an interaction, such as a coincidence detection of $G_{q/11}$ activity and increased $[Ca^{2+}]_i$ might be required to elicit endocannabinoid synthesis (Hashimotodani *et al.*, 2005).

It has been shown that endocannabinoids can be supplied by glial cells (Navarrete & Araque, 2008; 2010) or that glial cells can release glutamate (Fellin & Carmignoto, 2004; Fellin *et al.*, 2004) onto neurones to trigger endocannabinoid synthesis indirectly within the neurones. It is worthwhile noting that different sources may exist for different endocannabinoid compounds (Puente *et al.*, 2011).

It remains to be investigated, which possibilities to trigger endocannabinoid synthesis are valid for MSO neurones. In this report we provide evidence that auto-stimulation as well as metabotropic glutamate receptor stimulation are sufficient to elicit endocannabinoid signalling.

REFERENCES

Aguado, T., Monory, K., Palazuelos, J., Stella, N., Cravatt, B., Lutz, B., Marsicano, G., Kokaia, Z., Guzman, M. & Galve-Roperh, I. (2005) The endocannabinoid system drives neural progenitor proliferation. *FASEB J*, **19**, 1704-1706.

Allaman, I., Belanger, M. & Magistretti, P.J. (2011) Astrocyte-neuron metabolic relationships: for better and for worse. *Trends Neurosci*, **34**, 76-87.

Ashton, J.C., Friberg, D., Darlington, C.L. & Smith, P.F. (2006) Expression of the cannabinoid CB2 receptor in the rat cerebellum: an immunohistochemical study. *Neurosci Lett*, **396**, 113-116.

Astley, S.J. & Little, R.E. (1990) Maternal marijuana use during lactation and infant development at one year. *Neurotoxicol Teratol*, **12**, 161-168.

Atwood, B.K. & Mackie, K. (2010) CB2: a cannabinoid receptor with an identity crisis. *Br J Pharmacol*, **160**, 467-479.

Bacci, A., Huguenard, J.R. & Prince, D.A. (2004) Long-lasting self-inhibition of neocortical interneurons mediated by endocannabinoids. *Nature*, **431**, 312-316.

Bacci, A., Huguenard, J.R. & Prince, D.A. (2005) Modulation of neocortical interneurons: extrinsic influences and exercises in self-control. *Trends Neurosci*, **28**, 602-610.

Baek, J.H., Zheng, Y., Darlington, C.L. & Smith, P.F. (2008) Cannabinoid CB2 receptor expression in the rat brainstem cochlear and vestibular nuclei. *Acta Otolaryngol*, **128**, 961-967.

Ballesteros-Yanez, I., Valverde, O., Ledent, C., Maldonado, R. & DeFelipe, J. (2007) Chronic cocaine treatment alters dendritic arborization in the adult motor cortex through a CB1 cannabinoid receptor-dependent mechanism. *Neuroscience*, **146**, 1536-1545.

Belanger, M., Allaman, I. & Magistretti, P.J. (2011) Brain energy metabolism: focus on astrocyte-neuron metabolic cooperation. *Cell Metab*, **14**, 724-738.

Berghuis, P., Rajnicek, A.M., Morozov, Y.M., Ross, R.A., Mulder, J., Urban, G.M., Monory, K., Marsicano, G., Matteoli, M., Canty, A., Irving, A.J., Katona, I., Yanagawa, Y., Rakic, P., Lutz, B., Mackie, K. & Harkany, T. (2007) Hardwiring the brain: endocannabinoids shape neuronal connectivity. *Science*, **316**, 1212-1216.

Best, A.R. & Regehr, W.G. (2008) Serotonin evokes endocannabinoid release and retrogradely suppresses excitatory synapses. *J Neurosci*, **28**, 6508-6515.

Brand, A., Behrend, O., Marquardt, T., McAlpine, D. & Grothe, B. (2002) Precise inhibition is essential for microsecond interaural time difference coding. *Nature*, **417**, 543-547.

Brown, S.P., Brenowitz, S.D. & Regehr, W.G. (2003) Brief presynaptic bursts evoke synapse-specific retrograde inhibition mediated by endogenous cannabinoids. *Nat Neurosci*, **6**, 1048-1057.

Caird, D. & Klinke, R. (1983) Processing of binaural stimuli by cat superior olivary complex neurons. *Exp Brain Res*, **52**, 385-399.

Chavez, A.E., Chiu, C.Q. & Castillo, P.E. (2010) TRPV1 activation by endogenous anandamide triggers postsynaptic long-term depression in dentate gyrus. *Nat Neurosci*, **13**, 1511-1518.

Chevaleyre, V., Takahashi, K.A. & Castillo, P.E. (2006) Endocannabinoid-mediated synaptic plasticity in the CNS. *Annu Rev Neurosci*, **29**, 37-76.

Chi, D.H. & Kandler, K. (2012) Cannabinoid receptor expression at the MNTB-LSO synapse in developing rats. *Neurosci Lett*, **509**, 96-100.

Chirila, F.V., Rowland, K.C., Thompson, J.M. & Spirou, G.A. (2007) Development of gerbil medial superior olive: integration of temporally delayed excitation and inhibition at physiological temperature. *J Physiol*, **584**, 167-190.

Cole, K.S. & Hodgkin, A.L. (1939) Membrane and Protoplasm Resistance in the Squid Giant Axon. *J Gen Physiol*, **22**, 671-687.

Deadwyler, S.A., Hampson, R.E., Bennett, B.A., Edwards, T.A., Mu, J., Pacheco, M.A., Ward, S.J. & Childers, S.R. (1993) Cannabinoids modulate potassium current in cultured hippocampal neurons. *Receptors Channels*, **1**, 121-134.

Deadwyler, S.A., Hampson, R.E., Mu, J., Whyte, A. & Childers, S. (1995) Cannabinoids modulate voltage sensitive potassium A-current in hippocampal neurons via a cAMP-dependent process. *J Pharmacol Exp Ther*, **273**, 734-743.

Despres, G., Hafidi, A. & Romand, R. (1991) Immunohistochemical localization of nerve growth factor receptor in the cochlea and in the brainstem of the perinatal rat. *Hear Res*, **52**, 157-165.

Duch, C. & Levine, R.B. (2000) Remodeling of membrane properties and dendritic architecture accompanies the postembryonic conversion of a slow into a fast motoneuron. *J Neurosci*, **20**, 6950-6961.

Erecinska, M., Cherian, S. & Silver, I.A. (2004) Energy metabolism in mammalian brain during development. *Prog Neurobiol*, **73**, 397-445.

Evers, J.F., Schmitt, S., Sibila, M. & Duch, C. (2005) Progress in functional neuroanatomy: precise automatic geometric reconstruction of neuronal morphology from confocal image stacks. *J Neurophysiol*, **93**, 2331-2342.

Fellin, T. & Carmignoto, G. (2004) Neurone-to-astrocyte signalling in the brain represents a distinct multifunctional unit. *J Physiol*, **559**, 3-15.

Fellin, T., Pascual, O., Gobbo, S., Pozzan, T., Haydon, P.G. & Carmignoto, G. (2004) Neuronal synchrony mediated by astrocytic glutamate through activation of extrasynaptic NMDA receptors. *Neuron*, **43**, 729-743.

Fuxe, K., Dahlstrom, A.B., Jonsson, G., Marcellino, D., Guescini, M., Dam, M., Manger, P. & Agnati, L. (2010) The discovery of central monoamine neurons gave volume transmission to the wired brain. *Prog Neurobiol*, **90**, 82-100.

Goldberg, J.M. & Brown, P.B. (1969) Response of binaural neurons of dog superior olivary complex to dichotic tonal stimuli: some physiological mechanisms of sound localization. *J Neurophysiol*, ***32***, 613-636.

Gonzalez-Lima, F. & Jones, D. (1994) Quantitative mapping of cytochrome oxidase activity in the central auditory system of the gerbil: a study with calibrated activity standards and metal-intensified histochemistry. *Brain Res*, **660**, 34-49.

Grothe, B. (2003) New roles for synaptic inhibition in sound localization. *Nat Rev Neurosci*, **4**, 540-550.

Grothe, B., Pecka, M. & McAlpine, D. (2010) Mechanisms of sound localization in mammals. *Physiol Rev*, **90**, 983-1012.

Guinan, J.J., Norris, B.E. & Guinan, S.S. (1972) Single Auditory Units in the Superior Olivary Complex: II: Locations of Unit Categories and Tonotopic Organization. *International Journal of Neuroscience*, **4**, 147-166.

Guo, J. & Ikeda, S.R. (2004) Endocannabinoids modulate N-type calcium channels and G-protein-coupled inwardly rectifying potassium channels via CB1 cannabinoid receptors heterologously expressed in mammalian neurons. *Mol Pharmacol*, **65**, 665-674.

Gyombolai, P., Pap, D., Turu, G., Catt, K.J., Bagdy, G. & Hunyady, L. (2012) Regulation of endocannabinoid release by G proteins: a paracrine mechanism of G protein-coupled receptor action. *Mol Cell Endocrinol*, ***353***, 29-36.

Hashimotodani, Y., Ohno-Shosaku, T., Tsubokawa, H., Ogata, H., Emoto, K., Maejima, T., Araishi, K., Shin, H.S. & Kano, M. (2005) Phospholipase Cbeta serves as a coincidence detector through its Ca2+ dependency for triggering retrograde endocannabinoid signal. *Neuron*, **45**, 257-268.

Hassfurth, B., Grothe, B. & Koch, U. (2010) The mammalian interaural time difference detection circuit is differentially controlled by GABAB receptors during development. *J Neurosci*, **30**, 9715-9727.

Heffner, R.S. & Heffner, H.E. (1988) Sound localization and use of binaural cues by the gerbil (Meriones unguiculatus). *Behav Neurosci*, **102**, 422-428.

Hejazi, N., Zhou, C., Oz, M., Sun, H., Ye, J.H. & Zhang, L. (2006) Delta9-tetrahydrocannabinol and endogenous cannabinoid anandamide directly potentiate the function of glycine receptors. *Mol Pharmacol*, **69**, 991-997.

Henry, D.J. & Chavkin, C. (1995) Activation of inwardly rectifying potassium channels (GIRK1) by co-expressed rat brain cannabinoid receptors in Xenopus oocytes. *Neurosci Lett*, **186**, 91-94.

Herkenham, M., Lynn, A.B., Little, M.D., Johnson, M.R., Melvin, L.S., de Costa, B.R. & Rice, K.C. (1990) Cannabinoid receptor localization in brain. *Proc Natl Acad Sci U S A*, **87**, 1932-1936.

Hines, M.L. & Carnevale, N.T. (1997) The NEURON simulation environment. *Neural Comput*, **9**, 1179-1209.

Hines, M.L. & Carnevale, N.T. (2000) Expanding NEURON's repertoire of mechanisms with NMODL. *Neural Comput*, **12**, 995-1007.

Hoffpauir, B.K., Grimes, J.L., Mathers, P.H. & Spirou, G.A. (2006) Synaptogenesis of the calyx of Held: rapid onset of function and one-to-one morphological innervation. *J Neurosci*, **26**, 5511-5523.

Kandler, K. (2004) Activity-dependent organization of inhibitory circuits: lessons from the auditory system. *Curr Opin Neurobiol*, **14**, 96-104.

Kandler, K., Clause, A. & Noh, J. (2009) Tonotopic reorganization of developing auditory brainstem circuits. *Nat Neurosci*, **12**, 711-717.

Kapfer, C., Seidl, A.H., Schweizer, H. & Grothe, B. (2002) Experience-dependent refinement of inhibitory inputs to auditory coincidence-detector neurons. *Nat Neurosci*, **5**, 247-253.

Katona, I. & Freund, T.F. (2012) Multiple functions of endocannabinoid signaling in the brain. *Annu Rev Neurosci*, **35**, 529-558.

Kawaguchi, K., Habara, T., Terashima, T. & Kikkawa, S. (2010) GABA modulates development of cerebellar Purkinje cell dendrites under control of endocannabinoid signaling. *J Neurochem*, **114**, 627-638.

Kawamura, Y., Fukaya, M., Maejima, T., Yoshida, T., Miura, E., Watanabe, M., Ohno-Shosaku, T. & Kano, M. (2006) The CB1 cannabinoid receptor is the major cannabinoid receptor at excitatory presynaptic sites in the hippocampus and cerebellum. *J Neurosci*, **26**, 2991-3001.

Keimpema, E., Barabas, K., Morozov, Y.M., Tortoriello, G., Torii, M., Cameron, G., Yanagawa, Y., Watanabe, M., Mackie, K. & Harkany, T. (2010) Differential subcellular recruitment of monoacylglycerol lipase generates spatial specificity of 2-arachidonoyl glycerol signaling during axonal pathfinding. *J Neurosci*, **30**, 13992-14007.

Keimpema, E., Tortoriello, G., Alpar, A., Capsoni, S., Arisi, I., Calvigioni, D., Hu, S.S., Cattaneo, A., Doherty, P., Mackie, K. & Harkany, T. (2013) Nerve growth factor scales endocannabinoid signaling by regulating monoacylglycerol lipase turnover in developing cholinergic neurons. *Proc Natl Acad Sci U S A*, **110**, 1935-1940.

Kernell, D. & Zwaagstra, B. (1989) Dendrites of cat's spinal motoneurones: relationship between stem diameter and predicted input conductance. *J Physiol*, **413**, 255-269.

Kil, J., Kageyama, G.H., Semple, M.N. & Kitzes, L.M. (1995) Development of ventral cochlear nucleus projections to the superior olivary complex in gerbil. *J Comp Neurol*, **353**, 317-340.

Kiss, A. & Majorossy, K. (1983) Neuron morphology and synaptic architecture in the medial superior olivary nucleus. Light- and electron microscope studies in the cat. *Exp Brain Res*, **52**, 315-327.

Kreitzer, A.C. & Regehr, W.G. (2001) Retrograde inhibition of presynaptic calcium influx by endogenous cannabinoids at excitatory synapses onto Purkinje cells. *Neuron*, **29**, 717-727.

Kushmerick, C., Price, G.D., Taschenberger, H., Puente, N., Renden, R., Wadiche, J.I., Duvoisin, R.M., Grandes, P. & von Gersdorff, H. (2004) Retroinhibition of presynaptic Ca2+ currents by endocannabinoids released via postsynaptic mGluR activation at a calyx synapse. *J Neurosci*, **24**, 5955-5965.

Leake, P.A., Hradek, G.T., Chair, L. & Snyder, R.L. (2006) Neonatal deafness results in degraded topographic specificity of auditory nerve projections to the cochlear nucleus in cats. *J Comp Neurol*, **497**, 13-31.

Leao, R.N., Sun, H., Svahn, K., Berntson, A., Youssoufian, M., Paolini, A.G., Fyffe, R.E. & Walmsley, B. (2006) Topographic organization in the auditory brainstem of juvenile mice is disrupted in congenital deafness. *J Physiol*, **571**, 563-578.

Leibold, C. (2010) Influence of inhibitory synaptic kinetics on the interaural time difference sensitivity in a linear model of binaural coincidence detection. *J Acoust Soc Am*, **127**, 931-942.

Liu, W.M., Duan, E.K. & Cao, Y.J. (2002) Effects of anandamide on embryo implantation in the mouse. *Life Sci*, **71**, 1623-1632.

London, M. & Hausser, M. (2005) Dendritic computation. *Annu Rev Neurosci*, **28**, 503-532.

Lozovaya, N., Min, R., Tsintsadze, V. & Burnashev, N. (2009) Dual modulation of CNS voltage-gated calcium channels by cannabinoids: Focus on CB1 receptor-independent effects. *Cell Calcium*, **46**, 154-162.

Lozovaya, N., Mukhtarov, M., Tsintsadze, T., Ledent, C., Burnashev, N. & Bregestovski, P. (2011) Frequency-Dependent Cannabinoid Receptor-Independent Modulation of Glycine Receptors by Endocannabinoid 2-AG. *Front Mol Neurosci*, **4**, 13.

Lozovaya, N., Yatsenko, N., Beketov, A., Tsintsadze, T. & Burnashev, N. (2005) Glycine receptors in CNS neurons as a target for nonretrograde action of cannabinoids. *J Neurosci*, **25**, 7499-7506.

Mackie, K. (2008) Signaling via CNS cannabinoid receptors. *Mol Cell Endocrinol*, **286**, S60-65.

Mackie, K. & Hille, B. (1992) Cannabinoids inhibit N-type calcium channels in neuroblastoma-glioma cells. *Proc Natl Acad Sci U S A*, **89**, 3825-3829.

Mackie, K., Lai, Y., Westenbroek, R. & Mitchell, R. (1995) Cannabinoids activate an inwardly rectifying potassium conductance and inhibit Q-type calcium currents in AtT20 cells transfected with rat brain cannabinoid receptor. *J Neurosci*, **15**, 6552-6561.

Magnusson, A.K., Kapfer, C., Grothe, B. & Koch, U. (2005) Maturation of glycinergic inhibition in the gerbil medial superior olive after hearing onset. *J Physiol*, **568**, 497-512.

Magnusson, A.K., Park, T.J., Pecka, M., Grothe, B. & Koch, U. (2008) Retrograde GABA signaling adjusts sound localization by balancing excitation and inhibition in the brainstem. *Neuron*, **59**, 125-137.

Mainen, Z.F. & Sejnowski, T.J. (1996) Influence of dendritic structure on firing pattern in model neocortical neurons. *Nature*, **382**, 363-366.

Mathews, P.J., Jercog, P.E., Rinzel, J., Scott, L.L. & Golding, N.L. (2010) Control of submillisecond synaptic timing in binaural coincidence detectors by K(v)1 channels. *Nat Neurosci*, **13**, 601-609.

Meseke, M., Evers, J.F. & Duch, C. (2009) Developmental changes in dendritic shape and synapse location tune single-neuron computations to changing behavioral functions. *J Neurophysiol*, **102**, 41-58.

Mukhtarov, M., Ragozzino, D. & Bregestovski, P. (2005) Dual Ca2+ modulation of glycinergic synaptic currents in rodent hypoglossal motoneurones. *J Physiol*, **569**, 817-831.

Mulder, J., Aguado, T., Keimpema, E., Barabas, K., Ballester Rosado, C.J., Nguyen, L., Monory, K., Marsicano, G., Di Marzo, V., Hurd, Y.L., Guillemot, F., Mackie, K., Lutz, B., Guzman, M., Lu, H.C., Galve-Roperh, I. & Harkany, T. (2008) Endocannabinoid signaling controls pyramidal cell specification and long-range axon patterning. *Proc Natl Acad Sci U S A*, **105**, 8760-8765.

Muller, M. (1990) Quantitative comparison of frequency representation in the auditory brainstem nuclei of the gerbil, Pachyuromys duprasi. *Exp Brain Res*, **81**, 140-149.

Nakamura, P.A. & Cramer, K.S. (2011) Formation and maturation of the calyx of Held. *Hear Res*, **276**, 70-78.

Navarrete, M. & Araque, A. (2008) Endocannabinoids mediate neuron-astrocyte communication. *Neuron*, **57**, 883-893.

Navarrete, M. & Araque, A. (2010) Endocannabinoids potentiate synaptic transmission through stimulation of astrocytes. *Neuron*, **68**, 113-126.

Ohno-Shosaku, T., Maejima, T. & Kano, M. (2001) Endogenous cannabinoids mediate retrograde signals from depolarized postsynaptic neurons to presynaptic terminals. *Neuron*, **29**, 729-738.

Pecka, M., Brand, A., Behrend, O. & Grothe, B. (2008) Interaural time difference processing in the mammalian medial superior olive: the role of glycinergic inhibition. *J Neurosci*, **28**, 6914-6925.

Pickel, V.M., Chan, J., Kash, T.L., Rodriguez, J.J. & MacKie, K. (2004) Compartment-specific localization of cannabinoid 1 (CB1) and mu-opioid receptors in rat nucleus accumbens. *Neuroscience*, **127**, 101-112.

Picksak, G. & Stichtenoth, D.O. (2008) [Prescription of rimonabant in the early stage of pregnancy?]. *Med Monatsschr Pharm*, **31**, 107-108.

Pitler, T.A. & Alger, B.E. (1992) Postsynaptic spike firing reduces synaptic GABAA responses in hippocampal pyramidal cells. *J Neurosci*, **12**, 4122-4132.

Pitler, T.A. & Alger, B.E. (1994) Depolarization-induced suppression of GABAergic inhibition in rat hippocampal pyramidal cells: G protein involvement in a presynaptic mechanism. *Neuron*, **13**, 1447-1455.

Puente, N., Cui, Y., Lassalle, O., Lafourcade, M., Georges, F., Venance, L., Grandes, P. & Manzoni, O.J. (2011) Polymodal activation of the endocannabinoid system in the extended amygdala. *Nat Neurosci*, **14**, 1542-1547.

Pysh, J.J. (1970) Mitochondrial changes in rat inferior colliculus during postnatal development: an electron microscopic study. *Brain Res*, **18**, 325-342.

Rall, W. (1959) Branching dendritic trees and motoneuron membrane resistivity. *Exp Neurol*, **1**, 491-527.

Rall, W., Burke, R.E., Holmes, W.R., Jack, J.J., Redman, S.J. & Segev, I. (1992) Matching dendritic neuron models to experimental data. *Physiol Rev*, **72**, S159-186.

Rautenberg, P.L., Grothe, B. & Felmy, F. (2009) Quantification of the three-dimensional morphology of coincidence detector neurons in the medial superior olive of gerbils during late postnatal development. *J Comp Neurol*, **517**, 385-396.

Rietzel, H.J. & Friauf, E. (1998) Neuron types in the rat lateral superior olive and developmental changes in the complexity of their dendritic arbors. *J Comp Neurol*, **390**, 20-40.

Rogowski, B.A. & Feng, A.S. (1981) Normal postnatal development of medial superior olivary neurons in the albino rat: a Golgi and Nissl study. *J Comp Neurol*, **196**, 85-97.

Ross, R.A. (2003) Anandamide and vanilloid TRPV1 receptors. *Br J Pharmacol*, **140**, 790-801.

Rothman, J.S. & Manis, P.B. (2003) The roles potassium currents play in regulating the electrical activity of ventral cochlear nucleus neurons. *J Neurophysiol*, **89**, 3097-3113.

Rusu, S.I. & Borst, J.G. (2011) Developmental changes in intrinsic excitability of principal neurons in the rat medial nucleus of the trapezoid body. *Dev Neurobiol*, **71**, 284-295.

Ryugo, D.K., Montey, K.L., Wright, A.L., Bennett, M.L. & Pongstaporn, T. (2006) Postnatal development of a large auditory nerve terminal: the endbulb of Held in cats. *Hear Res*, **216-217**, 100-115.

Sanes, D.H., Song, J. & Tyson, J. (1992) Refinement of dendritic arbors along the tonotopic axis of the gerbil lateral superior olive. *Brain Res Dev Brain Res*, **67**, 47-55.

Schmitt, S., Evers, J.F., Duch, C., Scholz, M. & Obermayer, K. (2004) New methods for the computer-assisted 3-D reconstruction of neurons from confocal image stacks. *Neuroimage*, **23**, 1283-1298.

Scott, L.L., Mathews, P.J. & Golding, N.L. (2005) Posthearing developmental refinement of temporal processing in principal neurons of the medial superior olive. *J Neurosci*, **25**, 7887-7895.

Sedlacek, M., Tipton, P.W. & Brenowitz, S.D. (2011) Sustained firing of cartwheel cells in the dorsal cochlear nucleus evokes endocannabinoid release and retrograde suppression of parallel fiber synapses. *J Neurosci*, **31**, 15807-15817.

Sholl, D.A. (1953) Dendritic organization in the neurons of the visual and motor cortices of the cat. *J Anat*, **87**, 387-406.

Smith, P.H., Joris, P.X. & Yin, T.C. (1998) Anatomy and physiology of principal cells of the medial nucleus of the trapezoid body (MNTB) of the cat. *J Neurophysiol*, **79**, 3127-3142.

Sonntag, M., Englitz, B., Kopp-Scheinpflug, C. & Rubsamen, R. (2009) Early postnatal development of spontaneous and acoustically evoked discharge activity of principal cells of the medial nucleus of the trapezoid body: an in vivo study in mice. *J Neurosci*, **29**, 9510-9520.

Stotler, W.A. (1953) An experimental study of the cells and connections of the superior olivary complex of the cat. *J Comp Neurol*, **98**, 401-431.

Svirskis, G., Kotak, V., Sanes, D.H. & Rinzel, J. (2004) Sodium along with low-threshold potassium currents enhance coincidence detection of subthreshold noisy signals in MSO neurons. *J Neurophysiol*, **91**, 2465-2473.

Taschenberger, H., Leao, R.M., Rowland, K.C., Spirou, G.A. & von Gersdorff, H. (2002) Optimizing synaptic architecture and efficiency for high-frequency transmission. *Neuron*, **36**, 1127-1143.

Taschenberger, H. & von Gersdorff, H. (2000) Fine-tuning an auditory synapse for speed and fidelity: developmental changes in presynaptic waveform, EPSC kinetics, and synaptic plasticity. *J Neurosci*, **20**, 9162-9173.

Taylor, A.H., Amoako, A.A., Bambang, K., Karasu, T., Gebeh, A., Lam, P.M., Marzcylo, T.H. & Konje, J.C. (2010) Endocannabinoids and pregnancy. *Clin Chim Acta*, **411**, 921-930.

Trattner, B., Berner, S., Grothe, B. & Kunz, L. (2013a) Depolarisation-induced suppression of a glycinergic synapse in the superior olivary complex by endocannabinoids. *J Neurochem*.

Trattner, B., Gravot, C.M., Grothe, B. & Kunz, L. (2013b) Metabolic Maturation of Auditory Neurones in the Superior Olivary Complex. *PLoS One*, **8**, e67351.

Trattner, B., Grothe, B. & Kunz, L. (in preparation-a) Postsynaptic endocannabinoid signalling modulates responses of adult MSO neurones.

Trattner, B., Klein, A., Jansen, L., Stransky, M., Rautenberg, P.L., Grothe, B. & Kunz, L. (in preparation-b) The role of the endocannabinoid system in morphological development of neurons in the medial superior olive.

Tritsch, N.X., Rodriguez-Contreras, A., Crins, T.T., Wang, H.C., Borst, J.G. & Bergles, D.E. (2010) Calcium action potentials in hair cells pattern auditory neuron activity before hearing onset. *Nat Neurosci*, **13**, 1050-1052.

Tritsch, N.X., Yi, E., Gale, J.E., Glowatzki, E. & Bergles, D.E. (2007) The origin of spontaneous activity in the developing auditory system. *Nature*, **450**, 50-55.

Twitchell, W., Brown, S. & Mackie, K. (1997) Cannabinoids inhibit N- and P/Q-type calcium channels in cultured rat hippocampal neurons. *J Neurophysiol*, **78**, 43-50.

Ueda, N., Tsuboi, K., Uyama, T. & Ohnishi, T. (2011) Biosynthesis and degradation of the endocannabinoid 2-arachidonoylglycerol. *Biofactors*, **37**, 1-7.

Vannucci, R.C., Nardis, E.E., Vannucci, S.J. & Campbell, P.A. (1981) Cerebral carbohydrate and energy metabolism during hypoglycemia in newborn dogs. *Am J Physiol*, **240**, R192-199.

Vetter, P., Roth, A. & Hausser, M. (2001) Propagation of action potentials in dendrites depends on dendritic morphology. *J Neurophysiol*, **85**, 926-937.

Walcher, J., Hassfurth, B., Grothe, B. & Koch, U. (2011) Comparative post-hearing development of inhibitory inputs to the lateral superior olive in gerbils and mice. *J Neurophysiol*.

Wenger, T., Fragkakis, G., Giannikou, P., Probonas, K. & Yiannikakis, N. (1997a) Effects of anandamide on gestation in pregnant rats. *Life Sci*, **60**, 2361-2371.

Wenger, T., Fragkakis, G., Giannikou, P. & Yiannikakis, N. (1997b) The effects of prenatally administered endogenous cannabinoid on rat offspring. *Pharmacol Biochem Behav*, **58**, 537-544.

Werthat, F., Alexandrova, O., Grothe, B. & Koch, U. (2008) Experience-dependent refinement of the inhibitory axons projecting to the medial superior olive. *Dev Neurobiol*, **68**, 1454-1462.

Wilson, R.I. & Nicoll, R.A. (2001) Endogenous cannabinoids mediate retrograde signalling at hippocampal synapses. *Nature*, **410**, 588-592.

Womack, M. & Khodakhah, K. (2002) Active contribution of dendrites to the tonic and trimodal patterns of activity in cerebellar Purkinje neurons. *J Neurosci*, **22**, 10603-10612.

Wong-Riley, M. & Carroll, E.W. (1984) Effect of impulse blockage on cytochrome oxidase activity in monkey visual system. *Nature*, **307**, 262-264.

Wong-Riley, M.T., Merzenich, M.M. & Leake, P.A. (1978) Changes in endogenous enzymatic reactivity to DAB induced by neuronal inactivity. *Brain Res*, **141**, 185-192.

Wong-Riley, M.T., Tripathi, S.C., Trusk, T.C. & Hoppe, D.A. (1989a) Effect of retinal impulse blockage on cytochrome oxidase-rich zones in the macaque striate cortex: I. Quantitative electron-microscopic (EM) analysis of neurons. *Vis Neurosci*, **2**, 483-497.

Wong-Riley, M.T., Trusk, T.C., Tripathi, S.C. & Hoppe, D.A. (1989b) Effect of retinal impulse blockage on cytochrome oxidase-rich zones in the macaque striate cortex: II. Quantitative electron-microscopic (EM) analysis of neuropil. *Vis Neurosci*, **2**, 499-514.

Woolf, N.K. & Ryan, A.F. (1984) The development of auditory function in the cochlea of the mongolian gerbil. *Hear Res*, **13**, 277-283.

Yang, Z., Aubrey, K.R., Alroy, I., Harvey, R.J., Vandenberg, R.J. & Lynch, J.W. (2008) Subunit-specific modulation of glycine receptors by cannabinoids and N-arachidonyl-glycine. *Biochem Pharmacol*, **76**, 1014-1023.

Yin, T.C. & Chan, J.C. (1990) Interaural time sensitivity in medial superior olive of cat. *J Neurophysiol*, **64**, 465-488.

Zhao, Y., Rubio, M.E. & Tzounopoulos, T. (2009) Distinct functional and anatomical architecture of the endocannabinoid system in the auditory brainstem. *J Neurophysiol*, **101**, 2434-2446.

Zhao, Y. & Tzounopoulos, T. (2011) Physiological Activation of Cholinergic Inputs Controls Associative Synaptic Plasticity via Modulation of Endocannabinoid Signaling. *J Neurosci*, **31**, 3158-3168.

Zhou, Y., Carney, L.H. & Colburn, H.S. (2005) A model for interaural time difference sensitivity in the medial superior olive: interaction of excitatory and inhibitory synaptic inputs, channel dynamics, and cellular morphology. *J Neurosci*, **25**, 3046-3058.

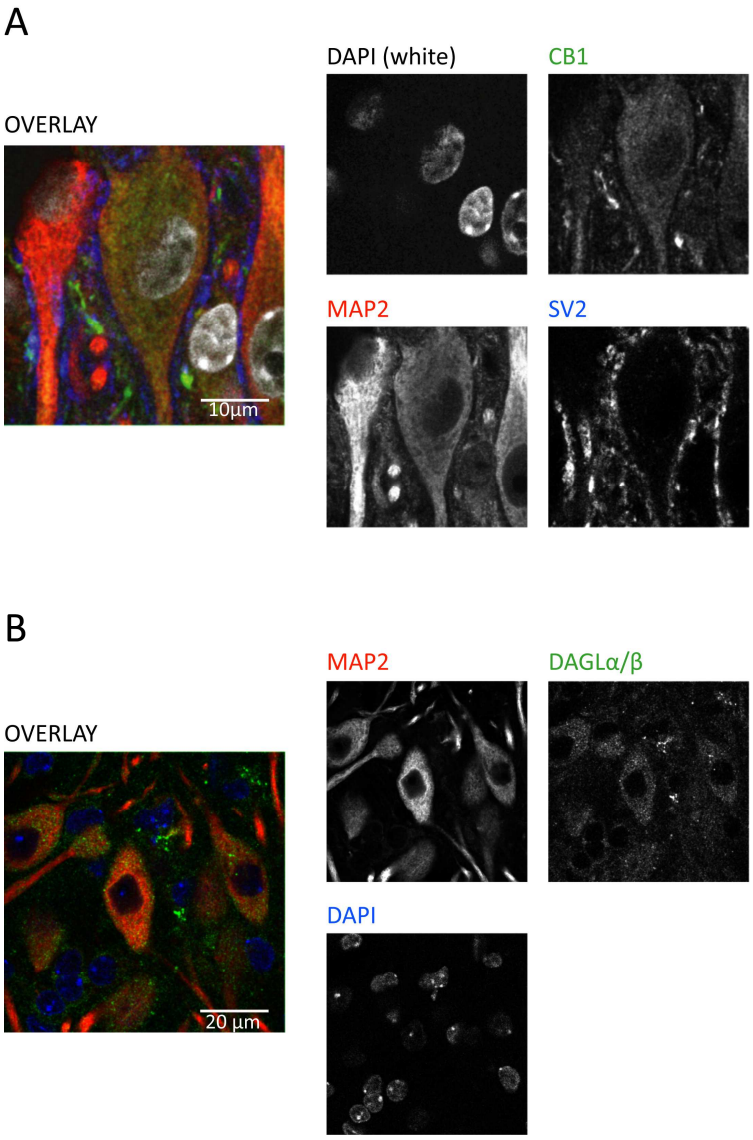

Figure 1. Immunohistochemical stainings for CB1 and DAGLα/β

A Representative immunohistochemical stainings of MSO neurones at P25 for CB1 (green), MAP2 (red), SV2 (blue) and DAPI (white). **B** Representative immunohistochemical stainings of MSO neurones at P25 for MAP2 (red), DAGLα/β (green) and DAPI (blue).

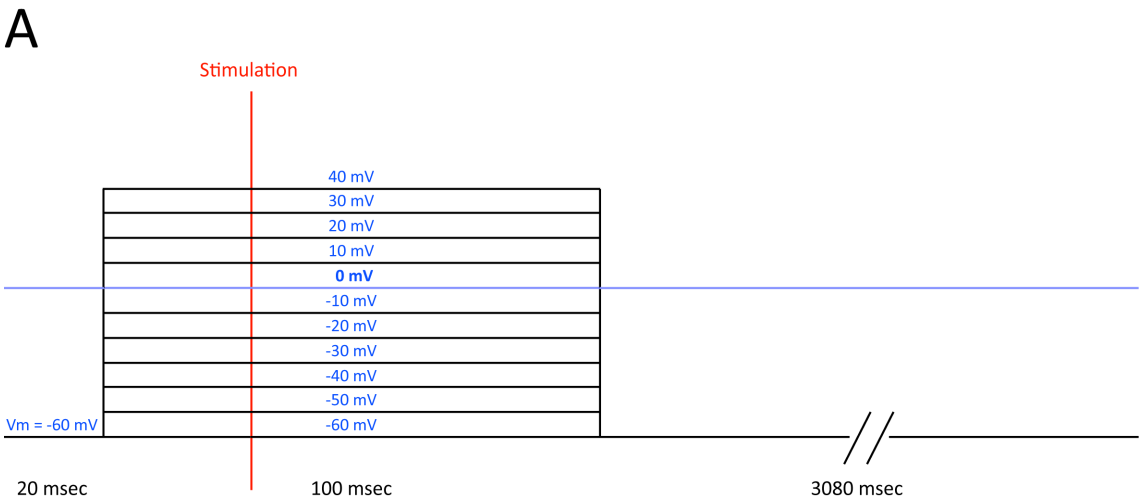
A
Stimulation
40 mV
30 mV
20 mV
10 mV
0 mV
-10 mV
-20 mV
-30 mV
-40 mV
-50 mV
-60 mV
Vm = -60 mV
20 msec
100 msec
3080 msec

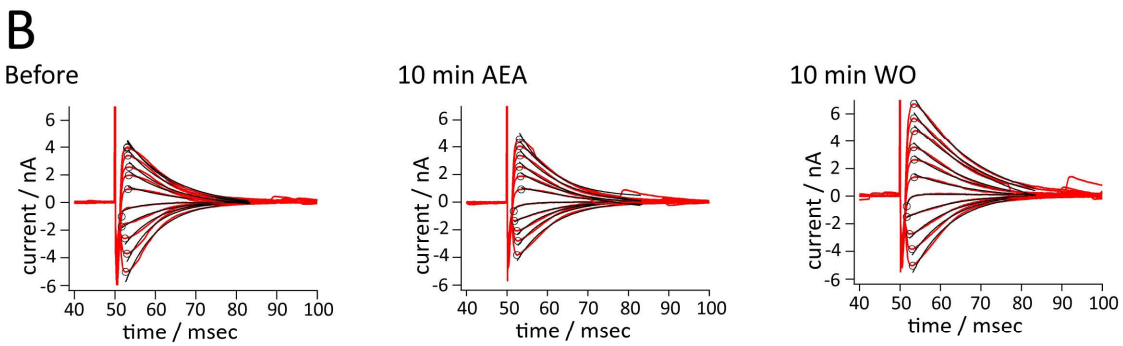
B
Before
10 min AEA
10 min WO
current / nA
time / msec

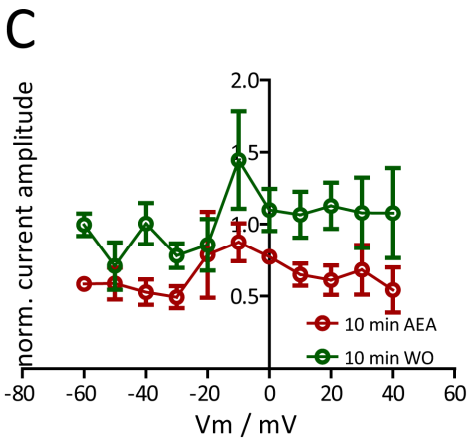
C
norm. current amplitude
10 min AEA
10 min WO
Vm / mV

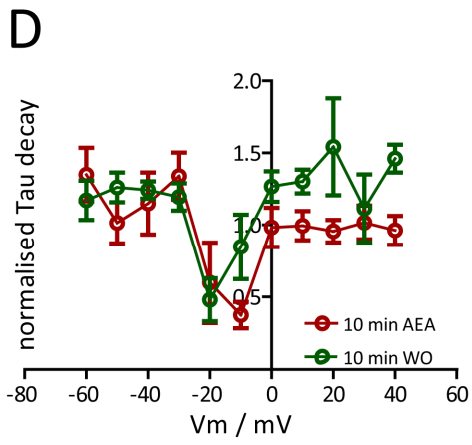
D
normalised Tau decay
10 min AEA
10 min WO
Vm / mV

Figure 2. Modulation of glycinergic evoked currents in MSO P22 neurones by endocannabinoids

A The stimulation protocol used to record pharmacologically isolated glycinergic evoked currents contained a pre-depolarisation before the actual stimulus was delivered to the glycinergic fibres, to disentangle currents evoked by the change in the membrane potential and currents elicited by the actual fibre stimulation. **B** Sample traces are given for the baseline condition (Before), for 10 min of bath-applied anandamide (10 min AEA) and for 10 min of wash-out (10 min WO) of AEA of the same cell (MSO P22). **C** The evoked currents of the 10 min AEA condition and of the 10 min WO condition were normalised to the baseline condition ($n = 6$). The reduction in glycine receptor mediated current by AEA administration is significant ($p < 0.05$) in a one sample t-test for a difference from 1, which represents the baseline value before drug application. **D** The decay time constants (τ) of the 10 min AEA condition and the 10 min WO condition were normalised to the baseline condition ($n = 6$). Both the normalised τ curve obtained by AEA administration as well as that obtained by wash-out was found not to significantly differ from 1.0.

A

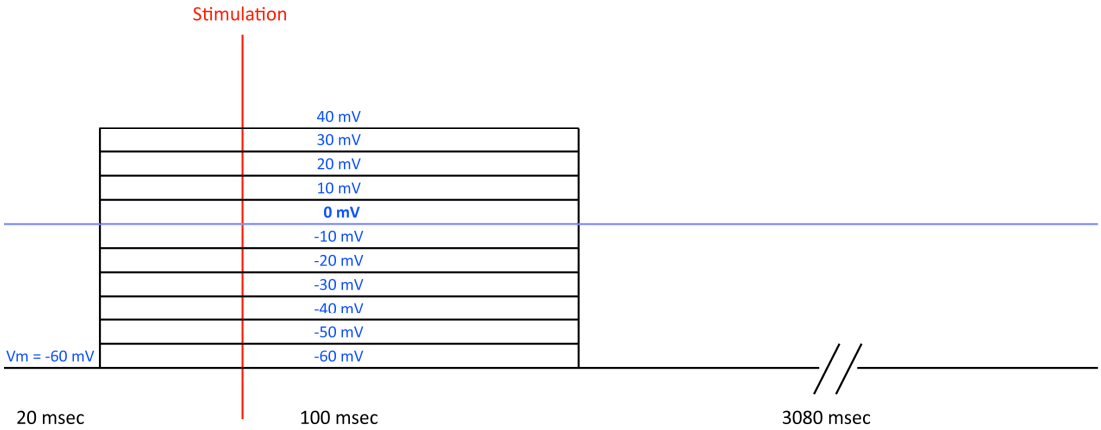
Stimulation
40 mV
30 mV
20 mV
10 mV
0 mV
-10 mV
-20 mV
-30 mV
-40 mV
-50 mV
-60 mV
Vm = -60 mV
20 msec
100 msec
3080 msec

B

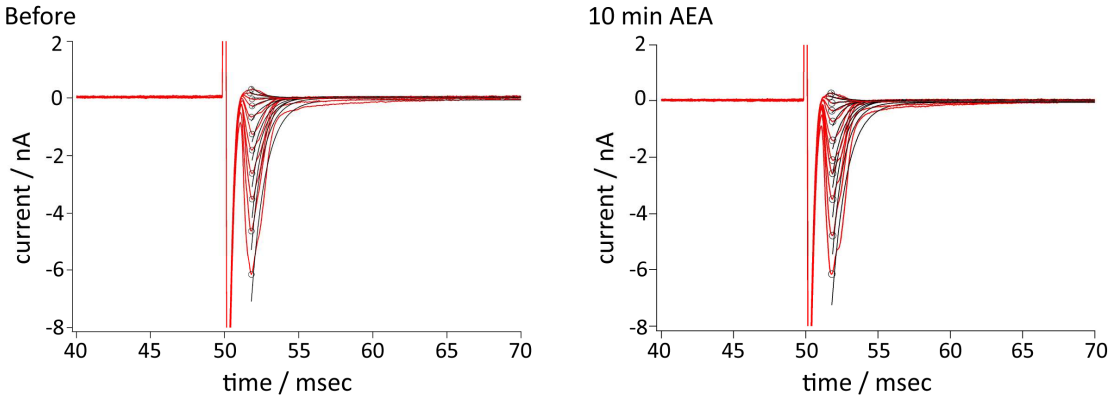
Before
10 min AEA
current / nA
time / msec
2
0
-2
-4
-6
-8
40
45
50
55
60
65
70

C

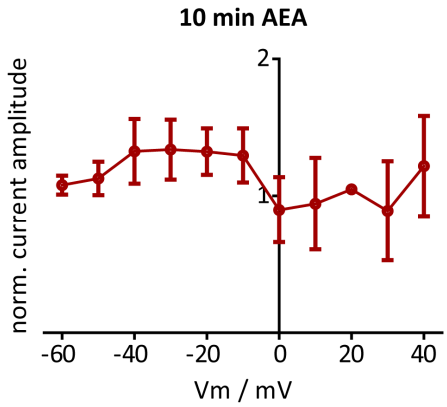
10 min AEA
norm. current amplitude
Vm / mV
2
1
-60
-40
-20
0
20
40

D

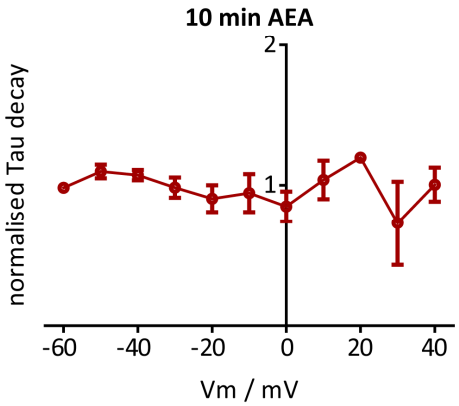
10 min AEA
normalised Tau decay
Vm / mV
2
1
-60
-40
-20
0
20
40

Figure 3. Excitatory evoked currents in MSO P22 neurones are not influenced by endocannabinoid signalling

A The stimulation protocol used to record pharmacologically isolated excitatory evoked currents contained a pre-depolarisation before the actual stimulus was delivered to the excitatory fibres to disentangle currents evoked by the change in the membrane potential and currents elicited by the actual fibre stimulation. **B** Sample traces are given for the baseline condition (Before) and for 10 min of bath-applied anandamide (10 min AEA) of the same cell (MSO P22). **C** The evoked currents of the 10 min AEA condition were normalised to the baseline condition (n = 5). AEA did not lead to a significant change in excitatory current amplitude. **D** The decay time constants (τ) of the 10 min AEA condition were normalised to the baseline condition (n = 5). The normalised τ of the excitatory currents was not subject to a significant change by endocannabinoid signalling.

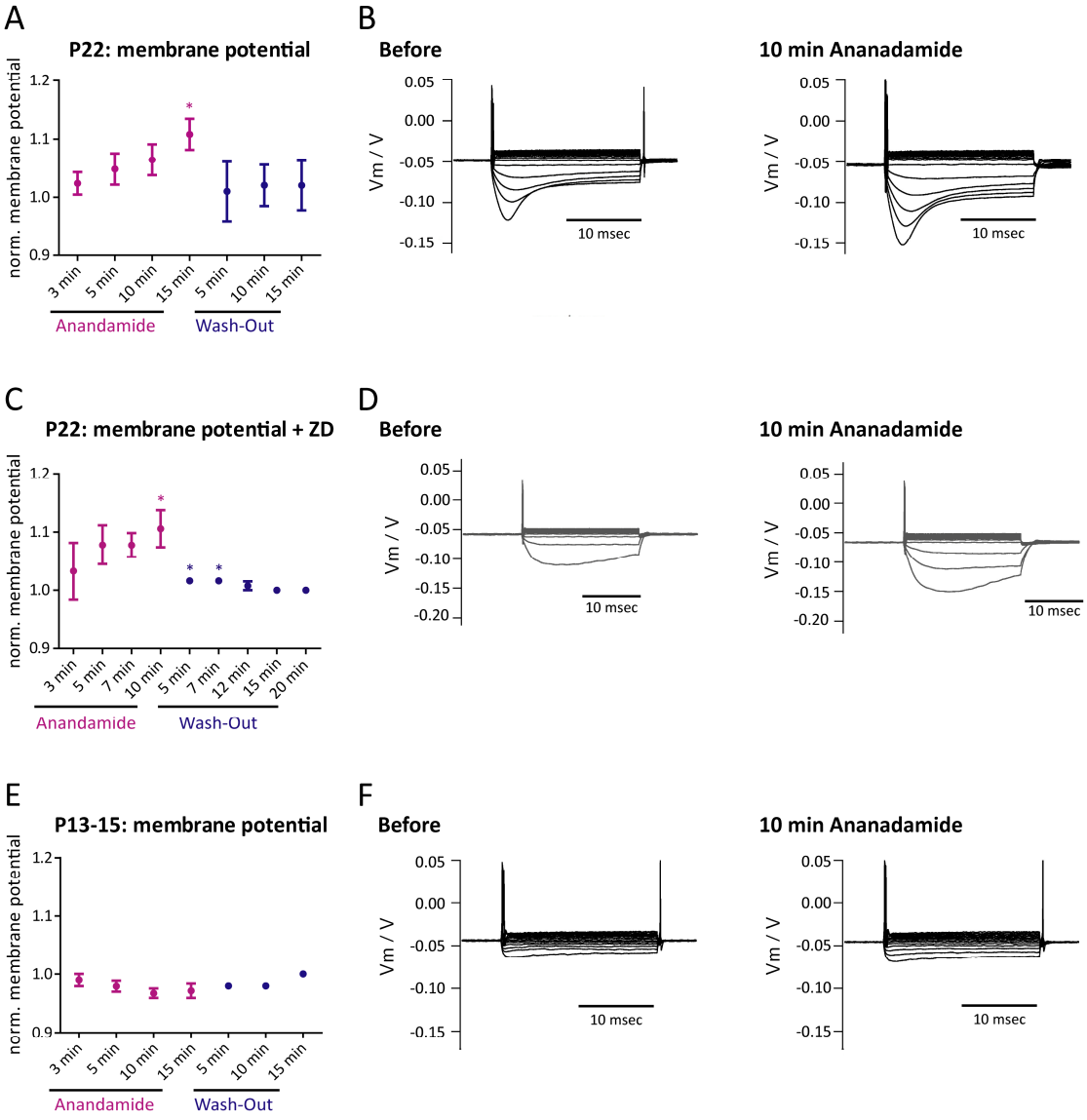

Figure 4. Endocannabinoid-dependent modulation of the resting membrane potential

A, E V_r normalised to the condition before the bath-application of AEA in MSO P22 (A) (n = 5) or MSO P13-15 (E) (n = 5) neurones. **B, F** Representative sample traces of current-clamp recordings of MSO P22 (B) or MSO P13-15 (F) neurones. **C** V_r during the presence of HCN inhibitor ZD7288 normalised to the condition before the bath-application of AEA (MSO P22, n = 5). **D** Representative sample traces of current-clamp recordings of MSO P22 in the presence of ZD7288. * : $p < 0.05$

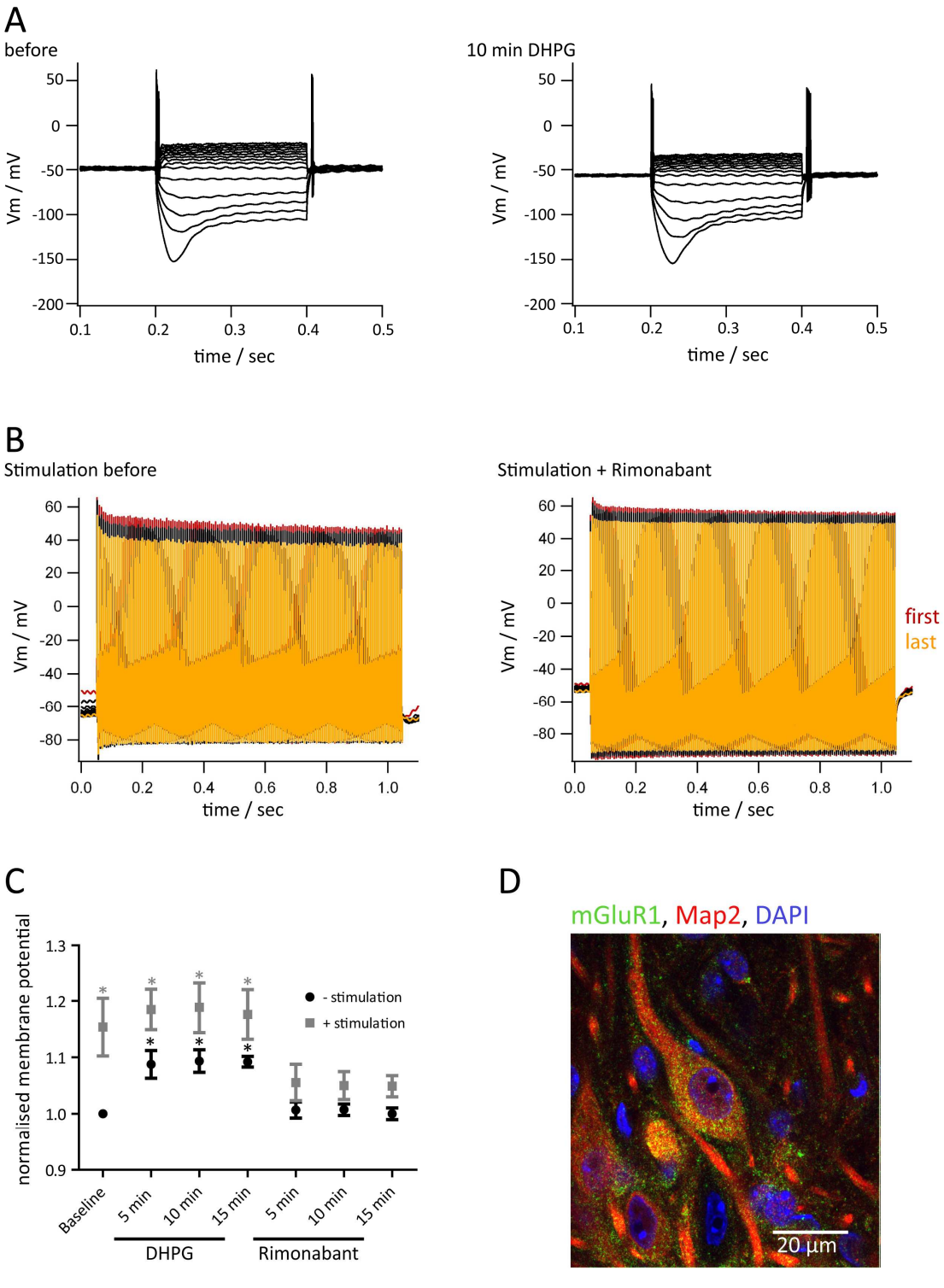
A
before
10 min DHPG
Vm / mV
time / sec
B
Stimulation before
Stimulation + Rimonabant
first
last
C
normalised membrane potential
- stimulation
+ stimulation
Baseline
5 min
10 min
15 min
DHPG
Rimonabant
D
mGluR1, Map2, DAPI
20 µm

Figure 5. Endocannabinoid-dependent hyperpolarisation can be elicited by mGluR1 agonism and/or high neuronal stimulation

A Sample traces of an MSO P22 cell before (left) and 10 min after DHPG application (right). **B** Sample traces of an MSO P22 cell during high frequency stimulation before (left) and 10 min after rimonabant application (right). The trace corresponding to the first stimulation is depicted in red and the trace corresponding to the 40^{th} stimulation (last) is depicted in yellow. **C** V_r during DHPG bath application and subsequent wash out of the drug with high frequency stimulation (+ stimulation, grey square) and without stimulation (- stimulation, black circle) in MSO P22 (n = 6). **D** Representative immunohistochemical staining for mGluR1 (green), MAP2 (red) and DAPI (blue) of MSO P22 cells. * : $p < 0.05$

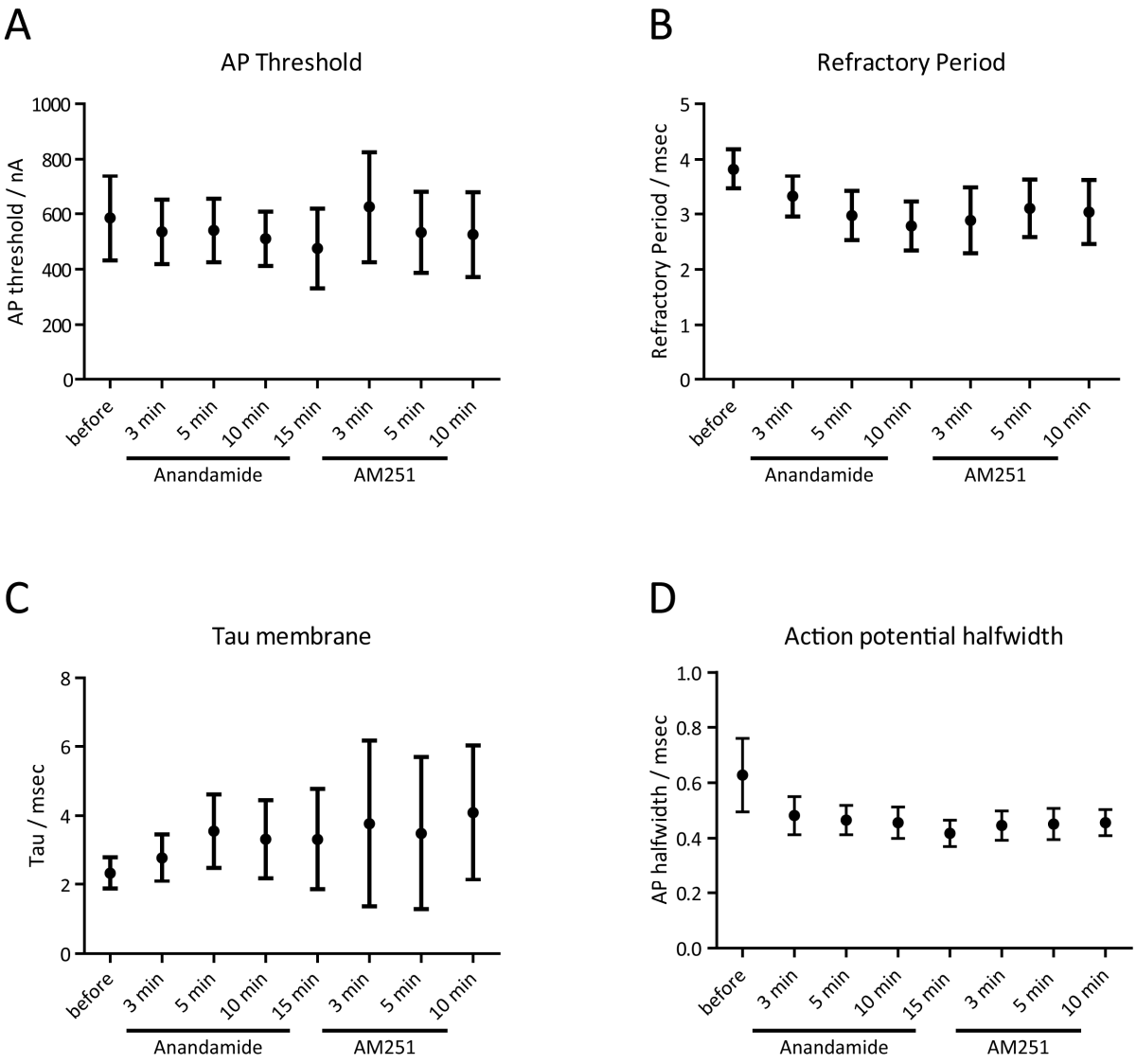

Figure 6. Membrane properties and action potential parameters under the influence of endocannabinoid signalling in MSO P22 neurones

A, C Current threshold for eliciting an AP (A) as well as membrane time constant τ (C) were unaffected by AEA (1 µM) and AM251 (2 µM) (n = 5). **B, D** In contrast, refractory period between two action potentials (B) as well as action potential halfwidth (D) showed a trend to AEA (1 µM) – induced reduction ($p < 0.05$, repeated ANOVA with *post hoc* Tukey test). However, AM251 (2 µM) could not antagonise this action (n = 5).

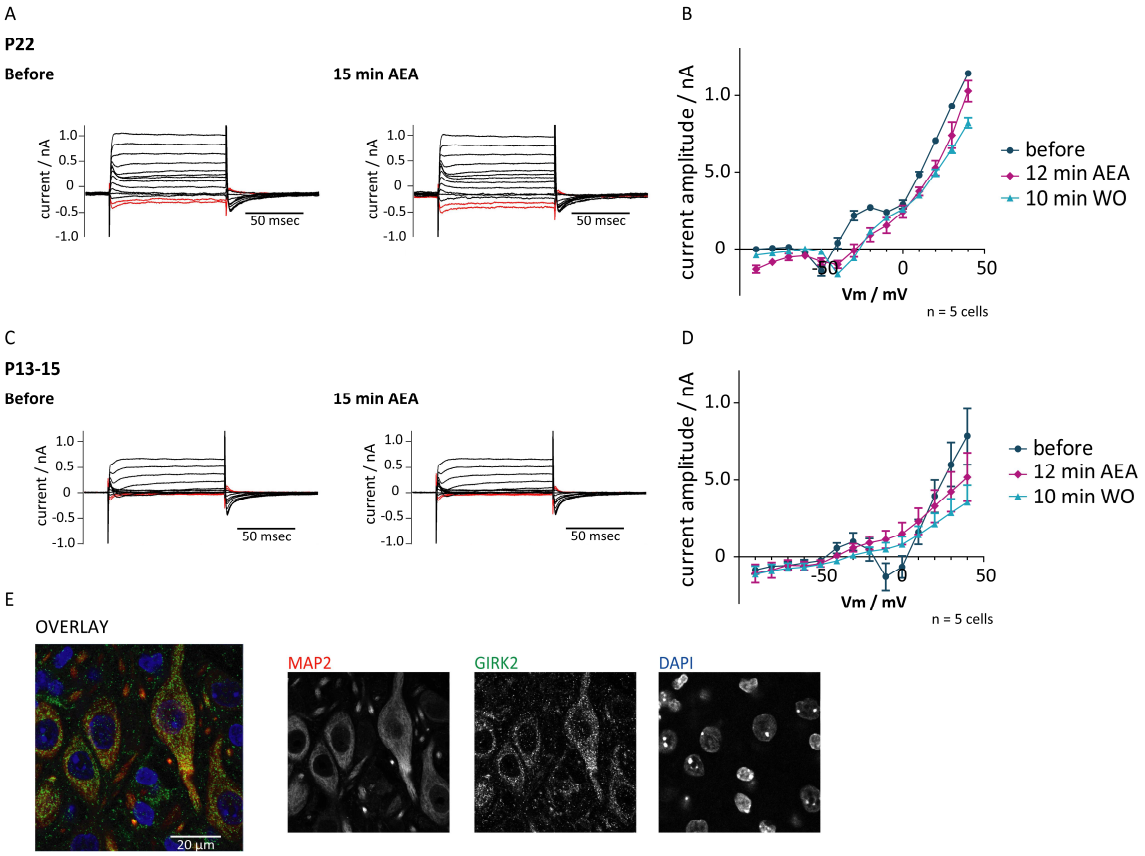

Figure 7. Possible currents underlying the endocannabinoid-dependent hyperpolarisation in MSO neurones at P22

A, C Representative sample traces of voltage-clamp recordings in MSO P22 (A) or MSO P13-15 (C) neurones in the presence of DNQX (20 µM), D-APV (50 µM), strychnine (0.5 µM), ZD7288 (50 µM), gabazine (10 µM) and QX314 (5 mM). The currents evoked by the potentials -90 mV and -80 mV are depicted in red, as GIRK conductance would occur in this range. **B, D** Current-voltage relations for MSO P22 (B) (n = 5) or MSO P13-15 (D) (n = 5) during control condition (before), 12 min AEA bath application and 10 min wash-out (10 min WO) (n = 5). **E** Representative immunohistochemical staining of MAP2 (red), GIRK2 (green) and DAPI (blue) of MSO P22 neurones.

Discussion

The role of the endocannabinoid system in morphological development of MSO neurones

When discussing neuronal signal processing, one generally considers electrophysiological parameters as well as receptor and ion channel expression to be the important and relevant factors for the physiological output of a neurone. However, the morphology of the neurone, such as its dendritic arborisations, the localisation of the axon as well as the soma shape and size, already have a great impact on the biophysical properties, i.e. how currents and potentials are processed. The architecture of a neurone determines to a great extent the computation of neuronal output and the behavioural function of a signalling cascade (Rall *et al.*, 1992; Mainen & Sejnowski, 1996; Duch & Levine, 2000; Womack & Khodakhah, 2002; London & Hausser, 2005; Meseke *et al.*, 2009). Thus alterations in neuronal morphology can significantly affect the functional result of neuronal firing. Especially in MSO neurones, where precise signal processing is of great behavioural importance for ITD computation (Goldberg & Brown, 1969; Grothe *et al.*, 2010) and thus for orientation and navigation within an auditory environment, slight changes in neuronal morphology could have tremendous effects on an individual's ability to localise sound sources effectively. In MSO neurones particularly their well-defined cell-structure greatly contributes to setting the highest sensitivity of ITD detection in the physiological range (Zhou *et al.*, 2005). Additionally, the precise arrangements of synaptic inputs – specifically inhibitory terminals – and receptors are of great importance for establishing neuronal physiology that enables ITD detection (Brand *et al.*, 2002; Kapfer *et al.*, 2002; Magnusson *et al.*, 2008; Pecka *et al.*, 2008; Leibold, 2010).

When I administered a CB1 agonist or antagonist to developing Mongolian gerbils several changes in MSO morphology became apparent, the most prominent ones being an increase in the number and thickness of primary dendrites induced by the CB1 antagonist rimonabant (Trattner *et al.*, in preparation-b). By programming an MSO model in the NEURON environment, it became obvious that slight changes in the amount and thickness of primary dendrites already influence passive

parameters of the neurones to a great extent (Trattner *et al.*, in preparation-b). The input resistance for instance is drastically decreased if dendrites increase in number or in diameter. The internal resistance, which is inversely proportional to the length constant λ (Cole & Hodgkin, 1939), determines the electrotonic conduction of potentials along the dendrites. If the dendrite diameter is increased, potentials can travel further via passive electrotonic conduction because the internal resistance is decreased (Rall, 1959; Kernell & Zwaagstra, 1989; Vetter *et al.*, 2001). The length constant λ thereby directly affects the generation of action potentials via the summation of inputs at the axon hillock. In MSO neurones this could have important consequences for the integration of inputs from both dendrites, which are summed up and processed by the neurone. This could lead to changes in ITD detection and thus cause behavioural consequences for the organism.

The changes that I observed in the dimensions of the dendritic field, which was decreased upon the administration of AEA and increased in the dorso-ventral direction after the treatment with RIM (Trattner *et al.*, in preparation-b), could lead to changes in input specificity of the individual neurones, given that the fibres targeting MSO neurones do not adjust their position according to the changes in MSO neuronal morphology. The MSO possesses a dorso-ventral tonotopic axis (Goldberg & Brown, 1969; Kandler *et al.*, 2009) which is formed through the tonotopic projections of inputs that the MSO receives (Guinan *et al.*, 1972; Caird & Klinke, 1983; Werthat *et al.*, 2008). By spanning a decreased (AEA) or an increased (RIM) area (Trattner *et al.*, in preparation-b) across the tonotopic axis, it is conceivable that the inputs, which an individual neurone receives, might result from altered frequency channels. This could thereby impair the tonotopy of the circuit connectivity. For the LSO it has even been shown that the morphology of individual neurones depends on their specific tonotopic position (Rietzel & Friauf, 1998), which possibly represents an additional adjustment to the input stimulus.

Considering the mechanism through which endocannabinoids can shape neuronal morphology, very few details are known. Since endocannabinoids can physiologically control neurotransmitter release through retrograde DSI (Pitler & Alger, 1992; 1994; Ohno-Shosaku *et al.*, 2001; Wilson & Nicoll, 2001) or DSE (Kreitzer & Regehr, 2001) signalling, it is conceivable that changes in transmitter

levels shape dendritogenesis in developing neurones. This was also postulated by Kawaguchi and colleagues, who found that endocannabinoids modulate dendritic morphological development in cerebellar Purkinje cells by interfering with GABA signalling through $GABA_A$ receptors (Kawaguchi *et al.*, 2010). CB1 receptors have also been shown to be present extrasynaptically, both by myself (Trattner *et al.*, 2013a) and others (Pickel *et al.*, 2004; Kawamura *et al.*, 2006). Thus it would be possible that endocannabinoid volume transmission by lateral diffusion of endocannabinoids in the plasma membrane can lead to activation of these extrasynaptic CB1 receptors (Fuxe *et al.*, 2010), which could activate downstream signalling cascades involved in causing a morphological change. Due to the hydrophobicity of endocannabinoids their action is however generally described as a localised one (Brown *et al.*, 2003) and thus volume transmission is probably rather limited.

In addition to direct endocannabinoid signalling, it was also suggested that the interplay of other neuromodulators - such as cocaine, which slows down dopamine re-uptake in the central nervous system - with the CB1-dependent endocannabinoid system can lead to changes in dendritic field and synapse number (Ballesteros-Yanez *et al.*, 2007) in cortical areas, which are known to be thoroughly modulated by endocannabinoids during their development. Especially during early cortical development and morphogenesis, endocannabinoids are involved in progenitor proliferation (Aguado *et al.*, 2005), axon targeting (Berghuis *et al.*, 2007; Mulder *et al.*, 2008; Keimpema *et al.*, 2010) as well as shaping the connectivity and setting projection patterns of neurones (Keimpema *et al.*, 2013). It has been suggested that nerve growth factor (NGF) is involved in regulating the availability of 2-AG and thereby controls correct morphological development in an endocannabinoid-dependent way (Keimpema *et al.*, 2013). Since NGF expression (Despres *et al.*, 1991) has been documented in the auditory brainstem of perinatal rats and presence of CB1 receptors has been shown in many SOC nuclei (Kushmerick *et al.*, 2004; Zhao *et al.*, 2009; Chi & Kandler, 2012) including the MSO (Trattner *et al.*, 2013a; Trattner *et al.*, in preparation-a; Trattner *et al.*, in preparation-b), it is conceivable that similar mechanisms of axonal sorting and target selection exist in the auditory system.

Thus, it can be summarised that the endocannabinoid system can act at many stages of morphological development. Endocannabinoid-dependent adjustment of dendritic morphology as we observed it in developing MSO neurones (Trattner *et al.*, in preparation-b) has been observed in other brain areas too (Ballesteros-Yanez *et al.*, 2007; Kawaguchi *et al.*, 2010) but seems to represent only one possibility by which the endocannabinoid system can interfere with morphological development. Additionally endocannabinoids have been shown to regulate neuronal progenitor proliferation (Aguado *et al.*, 2005) as well as axonal outgrowth and projection patterns (Mulder *et al.*, 2008; Keimpema *et al.*, 2013).

Endocannabinoid-signalling in the developing and maturating MSO

We found that in Mongolian gerbils aged between P10 and P15, retrograde endocannabinoid modulation of excitatory glutamatergic and inhibitory glycinergic currents in the form of DSE and DSI respectively, is present to a similar extent in both MSO and LSO (Trattner *et al.*, 2013a).

Generally, DSI has been mainly described for GABAergic synapses (Pitler & Alger, 1992; 1994; Ohno-Shosaku *et al.*, 2001; Wilson & Nicoll, 2001). So far glycinergic DSI has only been reported once in hypoglossal motor neurones (Mukhtarov *et al.*, 2005) and suggested for the LSO (Chi & Kandler, 2012). DSE has been described for glutamatergic synapses (Kreitzer & Regehr, 2001). Not surprisingly, the duration and the kinetics of DSI and DSE are generally in the same range, since the mechanism behind depolarisation-induced suppression of transmitter release targets only the fusion of transmitter vesicles with the presynaptic membrane, but is independent of the transmitter contained within these vesicles (Katona & Freund, 2012). The glycinergic DSI that we report at developing MSO and LSO synapses (Trattner *et al.*, 2013a) showed the same decay kinetics as GABAergic DSI previously reported (Ohno-Shosaku *et al.*, 2001; Wilson & Nicoll, 2001), which is plausible for the reasons outlined above. However the glycinergic DSI reported by Mukhtarov and colleagues showed a significantly slower recovery and time course (Mukhtarov *et al.*, 2005). We can only speculate that species-specific differences, alterations in the stimulus protocol or recording procedure could account for these differences.

Before hearing onset, which occurs in gerbils between P12 and P13 (Woolf & Ryan, 1984), neurones in the auditory brainstem are stimulated by spontaneous activity, which is generated in cochlear hair cells (Tritsch *et al.*, 2007; Tritsch *et al.*, 2010). This spontaneous activity is required for the precise development of auditory circuits and for the fine-tuning of tonotopic maps in the auditory brainstem (Kandler, 2004; Leake *et al.*, 2006; Leao *et al.*, 2006). Since retrograde endocannabinoid signalling in the form of DSI and DSE suppresses excitatory and inhibitory inputs to a given neurone, when that neurone is highly active, this negative feedback could be important to balance the strength of spontaneous activity and protect neurones from high-frequent or persistent synaptic stimulus inputs.

Thereby the endocannabinoid system could contribute to the functional development of auditory circuits in the LSO and MSO before hearing onset (Chi & Kandler, 2012).

After hearing onset, the endocannabinoid system could provide a means to adjust and adapt to the strength of auditory inputs. Due to the hydrophobicity of endocannabinoids, their action in the brain is usually limited to the immediate area of their release and remains thus local (Brown *et al.*, 2003). In that respect it is conceivable that the endocannabinoid system could act to specifically decrease certain inputs relative to others and thereby for instance enable signal detection and sound localisation in ambient noise.

Interestingly, we found by means of electrophysiological recordings that both DSI and DSE are present in principal neurones of the MSO and LSO (Trattner *et al.*, 2013a). Immunohistochemical co-localisation of CB1 with presynaptic markers for both excitatory glutamatergic (VGlut1) and inhibitory glycinergic (GlyT2) synapses was observed (Trattner *et al.*, 2013a). Our physiological recordings indicate that both excitatory and inhibitory inputs are regulated to a similar extent (Trattner *et al.*, 2013a). Since a balance between excitation and inhibition is essential so that MSO and LSO neurones can precisely compute the localisation of sound sources in the environment (Brand *et al.*, 2002; Grothe, 2003; Pecka *et al.*, 2008; Grothe *et al.*, 2010) the endocannabinoid system might regulate the input strength without affecting this balance.

An overview of the different endocannabinoid modulation mechanisms between P10 – P15 in the MSO is provided by Figure 1.

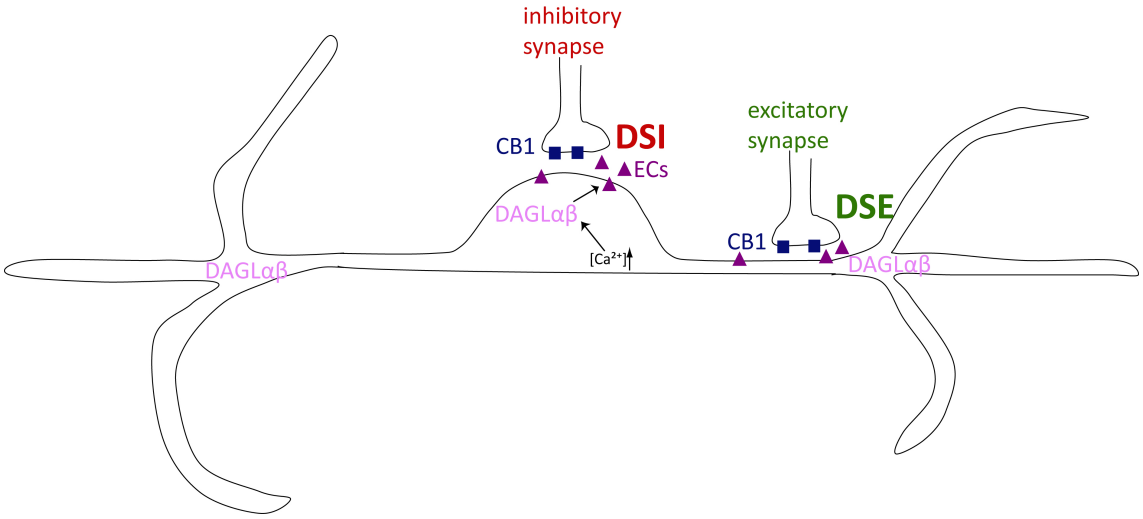

Figure 1. Overview of the endocannabinoid modulation present between P10 and P15 in the MSO

During the time of hearing onset endocannabinoids, produced by the DAGLα/β enzymes upon high stimulation of MSO neurones, signal retrogradely via CB1 receptors located at inhibitory and excitatory presynaptic terminals. Via a process called depolarisation-induced suppression of inhibition (DSI) and excitation (DSE) they decrease the input stimuli that MSO neurones receive. Thereby they could adjust the input strength of either spontaneous activity before hearing onset or sound-evoked stimulation after hearing onset.

After hearing onset the SOC of Mongolian gerbils undergoes a period of refinement, during which auditory synapses are adjusted and fine-tuned to the auditory environment until they reach their adult-like configuration, which is mostly achieved by about P21 (Chirila *et al.*, 2007; Kandler *et al.*, 2009; Rautenberg *et al.*, 2009).

After the refinement period, i.e. in animals P > 22, we found that CB1 expression shifts from a presynaptic localisation to postsynaptic and extrasynaptic expression in MSO neurones, however DAGLα/β enzymes still continue to be expressed somatically (Trattner *et al.*, in preparation-a). We could not find presynaptic DSI/DSE in animals P > 22, however glycinergic currents are depressed by AEA, through a pathway which is unaffected by CB1 antagonists such as RIM (Trattner *et al.*, in preparation-a). These results suggest that after the completion of refinement, endocannabinoids can

directly modulate glycine receptors as has been previously shown in rat hippocampal and cerebellar neurones (Lozovaya *et al.*, 2005). By these means, the endocannabinoid system specifically targets only glycinergic inputs, since excitatory glutamateric projections to the MSO cease to be modulated by endocannabinoids through DSE (Trattner *et al.*, in preparation-a). As precise glycinergic inhibition is vital for the correct coding of physiologically relevant ITDs (Brand *et al.*, 2002; Grothe, 2003; Pecka *et al.*, 2008), changes in the strength of glycinergic inputs could affect the physiological function of MSO cells. If the glycine receptor antagonist strychnine is applied *in vivo*, the firing peak of MSO neurones is shifted to ITDs within the physiological range and thereby the dynamic range within the physiological range is reduced (Brand *et al.*, 2002). Glycinergic inhibition thus adjusts the ITD function such that maximal sensitivity occurs within the physiological range (Brand *et al.*, 2002). Since the endocannabinoid modulation present in MSO neurones P > 22 reduces the glycine receptor current up to 50% (Trattner *et al.*, in preparation-a) – depending on the holding potential – it is conceivable that endocannabinoids could act to shift the dynamic range of MSO neurones to changing acoustic environments. This also seems plausible with respect to the fact that endocannabinoids are generally thought to be released upon high input stimuli, which would in the case of the MSO possibly represent extreme auditory environments.

Moreover, postsynaptically located CB1 receptors are physiologically functional in MSO P > 22 neurones in a way that they lead to a hyperpolarisation of the membrane (Trattner *et al.*, in preparation-a), in a possibly similar mechanism as has been previously described by others (Bacci *et al.*, 2004; 2005). The G-protein associated with CB1 has been shown to interact with GIRK channels (Henry & Chavkin, 1995; Guo & Ikeda, 2004) and lead to an increase in the K^+ current that they pass. This results in hyperpolarisation, as the membrane potential is shifted closer towards the K^+ equilibrium potential. Consistently we also found an increase in inward K^+ current at holding potentials negative to the resting membrane potential (Trattner *et al.*, in preparation-a), which could correspond to a GIRK conductance. Additionally we could show the presence of GIRK2 channels in MSO neurones P > 22 immunohistochemically (Trattner *et al.*, in preparation-a). However a physiological characterisation of the channel mediating the increase in inward current at

hyperpolarising potentials has not been carried out owing to a lack of specific pharmacological blockers for GIRK channels. It is plausible that this mechanism allows adaptation to high-frequent or persistent synaptic stimuli, as we also observed a decrease in action potential halfwidth and refractory period (Trattner *et al.*, in preparation-a). These findings suggest that this endocannabinoid-dependent modulation enables the neurones to fire at higher frequencies and thereby adjust to higher stimulus frequencies.

For an overview of the possible mechanism by which the endocannabinoid system operates after refinement of auditory circuits, please refer to Figure 2.

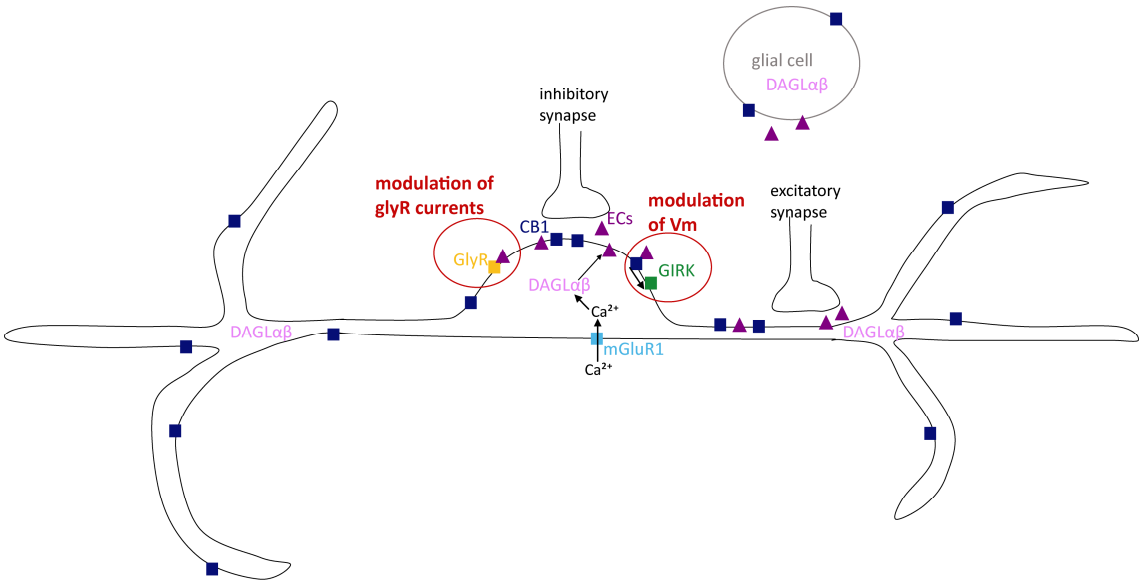

Figure 2. Endocannabinoid modulation after auditory refinement in the MSO

In MSO neurones P > 22, endocannabinoids produced within the MSO neurone by the enzymes DAGLα/β can modulate glycinergic currents in a CB1-independent way – possibly by direct interaction with glycine receptors. In addition endocannabinoids modulate the resting membrane potential in a CB1-dependent pathway, which involves an increase in the conductance of G-protein coupled inward rectifying K^+ channels (GIRK). Endocannabinoid release can be triggered by high cellular activity – possibly through activation of voltage-gated Ca^{2+} channels – or mGluR1 agonism. In contrast to young animals (P10-P15), excitatory and inhibitory synaptic inputs of adult MSO neurones (P > 22) are no longer modulated by retrograde

endocannabinoid signalling in the form of DSI or DSE. Glial cells, which also express low amounts of the enzymes DAGLα/β could represent an additional source of endocannabinoids in the superior olivary complex.

Endocannabinoids have been shown to signal additionally via transient receptor potential vanilloid receptor 1 (TRPV1) (Chavez *et al.*, 2010; Puente *et al.*, 2011). We found high TRPV1 expression in adult MSO P > 22 neurones by immunohistochemical stainings (Trattner, unpublished results, Figure 3), which could represent another modulation mechanism of endogenous endocannabinoids. Physiological data on endocannabinoid signalling via TRPV1 in the MSO has however not been obtained owing to a lack of specific pharmacological blockers.

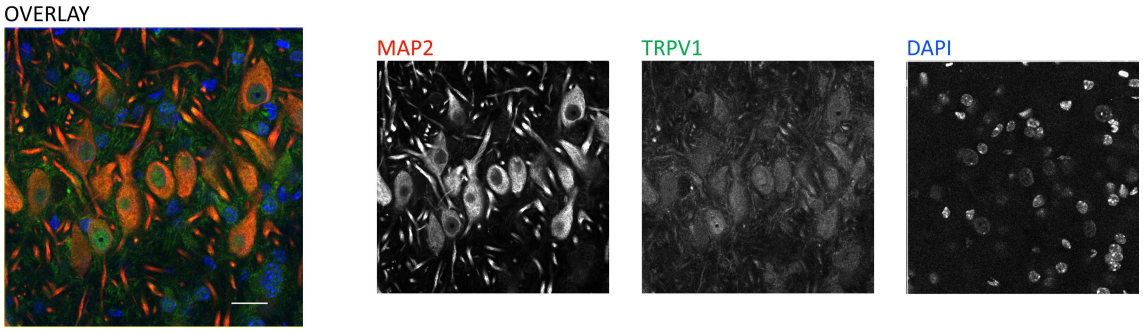

Figure 3. Expression of TRPV1 in adult MSO neurones

TRPV1 is abundantly expressed in MSO neurones at P > 22. MAP2 was used to stain MSO somata and dendrites and DAPI to visualise the nuclei. The scale bar represents 20 µm.

Considering the physiological sites and conditions of endocannabinoid release throughout development, various sources are conceivable. In animals P10-15, we were able to elicit endocannabinoid release from postsynaptic neurones by constant depolarisation to 0 mV for 5 sec or by using a 200 Hz square wave stimulus with a maximum of 40 mV, which mimics the potential changes during an action potential train. These effects were dependent on an intracellular rise in Ca^{2+} concentration (Trattner *et al.*, 2013a). Our results further indicate that activity of DAGLα/β is

necessary to drive endocannabinoid, i.e. 2-AG, synthesis (Trattner *et al.*, 2013a). In animals P > 22 we could elicit endocannabinoid release with a 150 Hz sine wave stimulus or pharmacological activation of metabotropic glutamate receptors (Trattner *et al.*, in preparation-a).

In many brain areas the interplay between the endocannabinoid system and metabotropic receptor systems has been described. Generally, metabotropic receptors can facilitate Ca^{2+} influx into the postsynapse, which is required for endocannabinoid synthesis. Additionally metabotropic receptors can activate downstream signalling pathways that facilitate endocannabinoid synthesis by activating enzymes or giving rise to precursors. In the auditory brainstem two types of metabotropic transmitter systems have been shown to be involved in endocannabinoid signalling. In the MNTB activation of metabotropic glutamate receptors triggers the Ca^{2+}-dependent release of endocannabinoids that activates presynaptic CB1 receptors (Kushmerick *et al.*, 2004). In the cochlear nucleus (CN) activation of muscarinic acetylcholine receptors leads to endocannabinoid signalling, which can convert long-term potentiation (LTP) to long-term depression (LTD) (Zhao & Tzounopoulos, 2011). In other brain areas it has been observed that activation of $G_{q/11}$ proteins coupled to metabotropic receptors could provide DAG and high intracellular Ca^{2+} concentrations required for endocannabinoid synthesis (Best & Regehr, 2008; Gyombolai *et al.*, 2012). In some cases also an interaction in the way of a coincidence detection of $G_{q/11}$ activity and elevated intracellular Ca^{2+} concentration might be required to trigger endocannabinoid synthesis (Hashimotodani *et al.*, 2005).

An additional source for endocannabinoids could be either via direct release of endocannabinoids by glial cells (Navarrete & Araque, 2008; 2010), which we have also observed to express DAGLα/β enzymes in our immunohistochemical stainings (Trattner, unpublished observation), or via glutamateric release from glial cells onto neurones (Fellin & Carmignoto, 2004; Fellin *et al.*, 2004), which could stimulate endocannabinoid synthesis within the neurones. It is also worthwhile noting, that different sources may exist for different endocannabinoid compounds (Puente *et al.*, 2011).

Metabolic maturation in the SOC – relation to auditory function?

Metabolic markers we used are enzymes, proteins or cellular structures, whose abundance can indicate the metabolic state the neurone is in. Glucose transporters, mitochondria, mitochondrial enzymes or the Na^+/K^+ ATPase, which is important for establishing the cellular membrane potential, are such metabolic markers. We observed that the expression of those markers starts to increase before hearing onset in the principal nuclei of the SOC and reaches saturation only after the refinement period following hearing onset (Trattner *et al.*, 2013b). However, depending on the specific nucleus, different markers show different onsets and slopes of expression. The MNTB for instance, which was shown to mature very early in physiological terms (Kil *et al.*, 1995; Hoffpauir *et al.*, 2006), up-regulates GLUT3 well-before hearing onset. However, in the MSO and LSO (Trattner *et al.*, 2013b), which undergo a high degree of activity-dependent refinement after hearing onset (Sanes *et al.*, 1992; Rietzel & Friauf, 1998; Chirila *et al.*, 2007; Rautenberg *et al.*, 2009; Walcher *et al.*, 2011), GLUT3 only starts to be expressed at hearing onset. One could argue that MSO and LSO use fuel other than glucose before hearing onset such as ketone bodies or lactate (Vannucci *et al.*, 1981), however it is known that these substrates become more important during hyperglycaemia (Erecinska *et al.*, 2004) or metabolic cooperation between neurones and astrocytes (Allaman *et al.*, 2011; Belanger *et al.*, 2011). I also performed immunohistochemical stainings of lactate dehydrogenase (LDH) and monocarboxylate transporter 1 (MCT1), which are two proteins involved in lactate or ketone body metabolism. Their expression level was very low in MSO and LSO and moderate in the MNTB. However, their expression was not developmentally regulated between P9 and P30 (Trattner, unpublished observation; refer to Figure 4). These findings support the hypothesis that lactate and ketone metabolism are of lesser importance for energy production in the SOC.

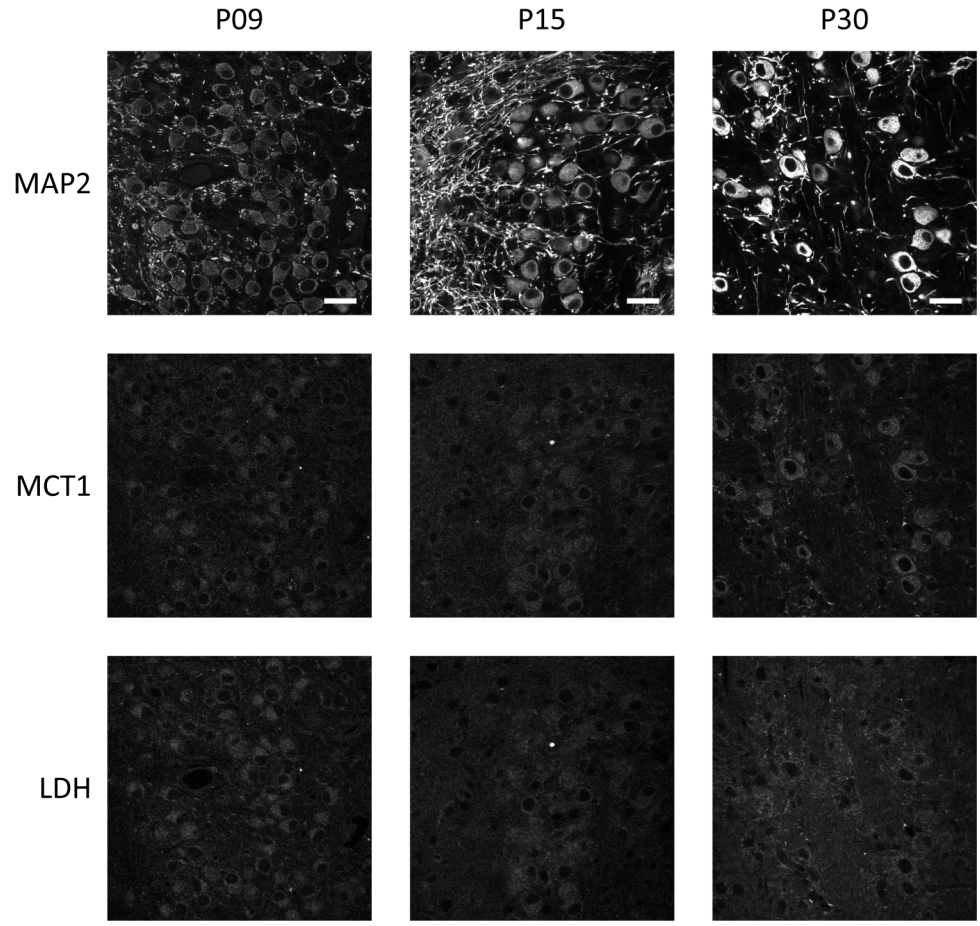

Figure 4. Expression levels of MCT1 and LDH in the developing MNTB

This figure shows the expression and distribution of monocarboxylate transporter 1 (MCT1) and lactate dehydrogenase (LDH) at different developmental time points (P09, P15, and P30), spanning the time before hearing onset until the full maturation and refinement of auditory circuits. Microtubule-associated protein 2 (MAP2) was used to visualise the somata and dendrites of the cells.

Scale bars represent 30 µm.

With this respect it is also interesting to discuss that the levels of all metabolic markers investigated were highest and showed the fastest onset in the MNTB when compared to the MSO and LSO (Trattner *et al.*, 2013b). The early onset of metabolic maturation in the MNTB could depend on its comparatively early physiological maturation, as mentioned before (Kil *et al.*, 1995; Hoffpauir *et al.*, 2006; Nakamura & Cramer, 2011; Rusu & Borst, 2011). The requirement for high energy production

could relate to the specific synaptic transmission requirement in MNTB neurones, such as increased neurotransmitter re-uptake or high ion channel maintenance, as well as the high firing frequencies exhibited by the MNTB (Taschenberger & von Gersdorff, 2000; Sonntag *et al.*, 2009). The high expression of GLUT3, the high mitochondrial density and COX activity have been described for the developing MNTB before (Gonzalez-Lima & Jones, 1994; Smith *et al.*, 1998).

The increase in the expression of metabolic markers during the time of hearing onset is related to the functional development in the SOC nuclei and not a general developmental effect, which merely coincides with hearing onset. In other parts of the brain such as the cerebellum no up-regulation of these markers is observed during the time period of hearing onset (Trattner *et al.*, 2013b). It has been previously shown in different auditory regions of the brain that the up-regulation of metabolic markers such as mitochondria coincides with the functional onset of hearing (Pysh, 1970; Ryugo *et al.*, 2006). When animals for instance were deafened unilaterally, those areas which are mainly innervated by the non-functional ear have significantly lower expression and activity of mitochondria (Wong-Riley *et al.*, 1978). In the visual system it was shown that if one eye was temporarily inactivated by TTX administration, the cortical columns receiving inputs from this eye showed a lower COX reactivity compared to the intact eye. This phenomenon was reversible, once the eye regained function (Wong-Riley & Carroll, 1984; Wong-Riley *et al.*, 1989a; Wong-Riley *et al.*, 1989b). These results strongly suggest that neurones up-regulate their energy production on demand in order not to produce more ATP than required. This tight homeostasis ensures that ATP is not generated unless it is also spent, which is a very efficient mechanism to keep the metabolic cost low. Since we also found a strong correlation between the up-regulation of metabolic markers and the time period of hearing onset, which was specific for auditory nuclei (Trattner *et al.*, 2013b), it is conceivable that the beginning of functionally relevant activity marked by hearing onset is necessary for the increase in metabolic maturation. However further experiments are required to address whether the ability to process auditory information is actually required for the rise in metabolic marker expression. By blocking auditory perception through cochlear ablation or mechanical obstruction of the ear canal and subsequent assessment of metabolic marker levels one could

determine whether the ability to hear is necessary for the observed increase in metabolic marker expression.

Mathematically calculated ATP consumption for MSO, LSO and MNTB during several developmental time points ranging from before hearing onset until the SOC has reached its refined "adult-like" configuration correlates well with the time course of increase in metabolic markers as found by immunohistochemistry (Trattner *et al.*, 2013b). Especially the fast metabolic maturation in the MNTB, which is almost completed by the time of hearing onset, is very consistent with the rise in calculated ATP consumption. With mathematical modelling however, the total ATP consumption was highest for the MSO and not for the MNTB as suggested by immunohistochemistry (Trattner *et al.*, 2013b). Possible explanations for these discrepancies are that MSO neurones exhibit an extremely low input resistance, which is due to their high membrane conductivity necessary for precise coincidence detection. As the total energy calculated is highly influenced by the input resistance, high values of total energy requirements could result from the low input resistance in MSO neurones. In the MNTB, its extremely high firing frequencies up to 800 Hz (Taschenberger & von Gersdorff, 2000; Taschenberger *et al.*, 2002; Sonntag *et al.*, 2009), which have to be maintained over a short period of time, could drastically raise the energy demand to actual values higher than calculated. Additionally, the synaptic specialisations of the large Calyx of Held synapse might have higher maintenance and housekeeping costs than normal synaptic structures, which might again lead to a higher real energy demand than actually calculated.

Taken together, immunohistochemical stainings and mathematical modelling of energy consumption both support the idea that the functional onset of hearing represents a driving force for metabolic maturation. Metabolic maturation coincides with physiological maturation, which is best supported by the observations in the MNTB, where both metabolic maturation as well as physiological maturation occur very early in development.

References

Aguado, T., K. Monory, et al. (2005). "The endocannabinoid system drives neural progenitor proliferation." FASEB J **19**(12): 1704-1706.

Allaman, I., M. Belanger, et al. (2011). "Astrocyte-neuron metabolic relationships: for better and for worse." Trends Neurosci **34**(2): 76-87.

Bacci, A., J. R. Huguenard, et al. (2004). "Long-lasting self-inhibition of neocortical interneurons mediated by endocannabinoids." Nature **431**(7006): 312-316.

Bacci, A., J. R. Huguenard, et al. (2005). "Modulation of neocortical interneurons: extrinsic influences and exercises in self-control." Trends Neurosci **28**(11): 602-610.

Ballesteros-Yanez, I., O. Valverde, et al. (2007). "Chronic cocaine treatment alters dendritic arborization in the adult motor cortex through a CB1 cannabinoid receptor-dependent mechanism." Neuroscience **146**(4): 1536-1545.

Belanger, M., I. Allaman, et al. (2011). "Brain energy metabolism: focus on astrocyte-neuron metabolic cooperation." Cell Metab **14**(6): 724-738.

Berghuis, P., A. M. Rajnicek, et al. (2007). "Hardwiring the brain: endocannabinoids shape neuronal connectivity." Science **316**(5828): 1212-1216.

Best, A. R. and W. G. Regehr (2008). "Serotonin evokes endocannabinoid release and retrogradely suppresses excitatory synapses." J Neurosci **28**(25): 6508-6515.

Brand, A., O. Behrend, et al. (2002). "Precise inhibition is essential for microsecond interaural time difference coding." Nature **417**(6888): 543-547.

Brown, S. P., S. D. Brenowitz, et al. (2003). "Brief presynaptic bursts evoke synapse-specific retrograde inhibition mediated by endogenous cannabinoids." Nat Neurosci **6**(10): 1048-1057.

Caird, D. and R. Klinke (1983). "Processing of binaural stimuli by cat superior olivary complex neurons." Exp Brain Res **52**(3): 385-399.

Chavez, A. E., C. Q. Chiu, et al. (2010). "TRPV1 activation by endogenous anandamide triggers postsynaptic long-term depression in dentate gyrus." Nat Neurosci **13**(12): 1511-1518.

Chi, D. H. and K. Kandler (2012). "Cannabinoid receptor expression at the MNTB-LSO synapse in developing rats." Neurosci Lett **509**(2): 96-100.

Chirila, F. V., K. C. Rowland, et al. (2007). "Development of gerbil medial superior olive: integration of temporally delayed excitation and inhibition at physiological temperature." J Physiol **584**(Pt 1): 167-190.

Cole, K. S. and A. L. Hodgkin (1939). "Membrane and Protoplasm Resistance in the Squid Giant Axon." J Gen Physiol **22**(5): 671-687.

Despres, G., A. Hafidi, et al. (1991). "Immunohistochemical localization of nerve growth factor receptor in the cochlea and in the brainstem of the perinatal rat." Hear Res **52**(1): 157-165.

Duch, C. and R. B. Levine (2000). "Remodeling of membrane properties and dendritic architecture accompanies the postembryonic conversion of a slow into a fast motoneuron." J Neurosci **20**(18): 6950-6961.

Erecinska, M., S. Cherian, et al. (2004). "Energy metabolism in mammalian brain during development." Prog Neurobiol **73**(6): 397-445.

Fellin, T. and G. Carmignoto (2004). "Neurone-to-astrocyte signalling in the brain represents a distinct multifunctional unit." J Physiol **559**(Pt 1): 3-15.

Fellin, T., O. Pascual, et al. (2004). "Neuronal synchrony mediated by astrocytic glutamate through activation of extrasynaptic NMDA receptors." Neuron **43**(5): 729-743.

Fuxe, K., A. B. Dahlstrom, et al. (2010). "The discovery of central monoamine neurons gave volume transmission to the wired brain." Prog Neurobiol **90**(2): 82-100.

Goldberg, J. M. and P. B. Brown (1969). "Response of binaural neurons of dog superior olivary complex to dichotic tonal stimuli: some physiological mechanisms of sound localization." J Neurophysiol **32**(4): 613-636.

Gonzalez-Lima, F. and D. Jones (1994). "Quantitative mapping of cytochrome oxidase activity in the central auditory system of the gerbil: a study with calibrated activity standards and metal-intensified histochemistry." Brain Res **660**(1): 34-49.

Grothe, B. (2003). "New roles for synaptic inhibition in sound localization." Nat Rev Neurosci **4**(7): 540-550.

Grothe, B., M. Pecka, et al. (2010). "Mechanisms of sound localization in mammals." Physiol Rev **90**(3): 983-1012.

Guinan, J. J., B. E. Norris, et al. (1972). "Single Auditory Units in the Superior Olivary Complex: II: Locations of Unit Categories and Tonotopic Organization." International Journal of Neuroscience **4**(4): 147-166.

Guo, J. and S. R. Ikeda (2004). "Endocannabinoids modulate N-type calcium channels and G-protein-coupled inwardly rectifying potassium channels via CB1 cannabinoid receptors heterologously expressed in mammalian neurons." Mol Pharmacol **65**(3): 665-674.

Gyombolai, P., D. Pap, et al. (2012). "Regulation of endocannabinoid release by G proteins: a paracrine mechanism of G protein-coupled receptor action." Mol Cell Endocrinol **353**(1-2): 29-36.

Hashimotodani, Y., T. Ohno-Shosaku, et al. (2005). "Phospholipase Cbeta serves as a coincidence detector through its Ca2+ dependency for triggering retrograde endocannabinoid signal." Neuron **45**(2): 257-268.

Henry, D. J. and C. Chavkin (1995). "Activation of inwardly rectifying potassium channels (GIRK1) by co-expressed rat brain cannabinoid receptors in Xenopus oocytes." Neurosci Lett **186**(2-3): 91-94.

Hoffpauir, B. K., J. L. Grimes, et al. (2006). "Synaptogenesis of the calyx of Held: rapid onset of function and one-to-one morphological innervation." J Neurosci **26**(20): 5511-5523.

Kandler, K. (2004). "Activity-dependent organization of inhibitory circuits: lessons from the auditory system." Curr Opin Neurobiol **14**(1): 96-104.

Kandler, K., A. Clause, et al. (2009). "Tonotopic reorganization of developing auditory brainstem circuits." Nat Neurosci **12**(6): 711-717.

Kapfer, C., A. H. Seidl, et al. (2002). "Experience-dependent refinement of inhibitory inputs to auditory coincidence-detector neurons." Nat Neurosci **5**(3): 247-253.

Katona, I. and T. F. Freund (2012). "Multiple functions of endocannabinoid signaling in the brain." Annu Rev Neurosci **35**: 529-558.

Kawaguchi, K., T. Habara, et al. (2010). "GABA modulates development of cerebellar Purkinje cell dendrites under control of endocannabinoid signaling." J Neurochem **114**(2): 627-638.

Kawamura, Y., M. Fukaya, et al. (2006). "The CB1 cannabinoid receptor is the major cannabinoid receptor at excitatory presynaptic sites in the hippocampus and cerebellum." J Neurosci **26**(11): 2991-3001.

Keimpema, E., K. Barabas, et al. (2010). "Differential subcellular recruitment of monoacylglycerol lipase generates spatial specificity of 2-arachidonoyl glycerol signaling during axonal pathfinding." J Neurosci **30**(42): 13992-14007.

Keimpema, E., G. Tortoriello, et al. (2013). "Nerve growth factor scales endocannabinoid signaling by regulating monoacylglycerol lipase turnover in developing cholinergic neurons." Proc Natl Acad Sci U S A **110**(5): 1935-1940.

Kernell, D. and B. Zwaagstra (1989). "Dendrites of cat's spinal motoneurones: relationship between stem diameter and predicted input conductance." J Physiol **413**: 255-269.

Kil, J., G. H. Kageyama, et al. (1995). "Development of ventral cochlear nucleus projections to the superior olivary complex in gerbil." J Comp Neurol **353**(3): 317-340.

Kreitzer, A. C. and W. G. Regehr (2001). "Retrograde inhibition of presynaptic calcium influx by endogenous cannabinoids at excitatory synapses onto Purkinje cells." Neuron **29**(3): 717-727.

Kushmerick, C., G. D. Price, et al. (2004). "Retroinhibition of presynaptic Ca2+ currents by endocannabinoids released via postsynaptic mGluR activation at a calyx synapse." J Neurosci **24**(26): 5955-5965.

Leake, P. A., G. T. Hradek, et al. (2006). "Neonatal deafness results in degraded topographic specificity of auditory nerve projections to the cochlear nucleus in cats." J Comp Neurol **497**(1): 13-31.

Leao, R. N., H. Sun, et al. (2006). "Topographic organization in the auditory brainstem of juvenile mice is disrupted in congenital deafness." J Physiol **571**(Pt 3): 563-578.

Leibold, C. (2010). "Influence of inhibitory synaptic kinetics on the interaural time difference sensitivity in a linear model of binaural coincidence detection." J Acoust Soc Am **127**(2): 931-942.

London, M. and M. Hausser (2005). "Dendritic computation." Annu Rev Neurosci **28**: 503-532.

Lozovaya, N., N. Yatsenko, et al. (2005). "Glycine receptors in CNS neurons as a target for nonretrograde action of cannabinoids." J Neurosci **25**(33): 7499-7506.

Magnusson, A. K., T. J. Park, et al. (2008). "Retrograde GABA signaling adjusts sound localization by balancing excitation and inhibition in the brainstem." Neuron **59**(1): 125-137.

Mainen, Z. F. and T. J. Sejnowski (1996). "Influence of dendritic structure on firing pattern in model neocortical neurons." Nature **382**(6589): 363-366.

Meseke, M., J. F. Evers, et al. (2009). "Developmental changes in dendritic shape and synapse location tune single-neuron computations to changing behavioral functions." J Neurophysiol **102**(1): 41-58.

Mukhtarov, M., D. Ragozzino, et al. (2005). "Dual Ca2+ modulation of glycinergic synaptic currents in rodent hypoglossal motoneurones." J Physiol **569**(Pt 3): 817-831.

Mulder, J., T. Aguado, et al. (2008). "Endocannabinoid signaling controls pyramidal cell specification and long-range axon patterning." Proc Natl Acad Sci U S A **105**(25): 8760-8765.

Nakamura, P. A. and K. S. Cramer (2011). "Formation and maturation of the calyx of Held." Hear Res **276**(1-2): 70-78.

Navarrete, M. and A. Araque (2008). "Endocannabinoids mediate neuron-astrocyte communication." Neuron **57**(6): 883-893.

Navarrete, M. and A. Araque (2010). "Endocannabinoids potentiate synaptic transmission through stimulation of astrocytes." Neuron **68**(1): 113-126.

Ohno-Shosaku, T., T. Maejima, et al. (2001). "Endogenous cannabinoids mediate retrograde signals from depolarized postsynaptic neurons to presynaptic terminals." Neuron **29**(3): 729-738.

Pecka, M., A. Brand, et al. (2008). "Interaural time difference processing in the mammalian medial superior olive: the role of glycinergic inhibition." J Neurosci **28**(27): 6914-6925.

Pickel, V. M., J. Chan, et al. (2004). "Compartment-specific localization of cannabinoid 1 (CB1) and mu-opioid receptors in rat nucleus accumbens." Neuroscience **127**(1): 101-112.

Pitler, T. A. and B. E. Alger (1992). "Postsynaptic spike firing reduces synaptic GABAA responses in hippocampal pyramidal cells." J Neurosci **12**(10): 4122-4132.

Pitler, T. A. and B. E. Alger (1994). "Depolarization-induced suppression of GABAergic inhibition in rat hippocampal pyramidal cells: G protein involvement in a presynaptic mechanism." Neuron **13**(6): 1447-1455.

Puente, N., Y. Cui, et al. (2011). "Polymodal activation of the endocannabinoid system in the extended amygdala." Nat Neurosci **14**(12): 1542-1547.

Pysh, J. J. (1970). "Mitochondrial changes in rat inferior colliculus during postnatal development: an electron microscopic study." Brain Res **18**(2): 325-342.

Rall, W. (1959). "Branching dendritic trees and motoneuron membrane resistivity." Exp Neurol **1**: 491-527.

Rall, W., R. E. Burke, et al. (1992). "Matching dendritic neuron models to experimental data." Physiol Rev **72**(4 Suppl): S159-186.

Rautenberg, P. L., B. Grothe, et al. (2009). "Quantification of the three-dimensional morphology of coincidence detector neurons in the medial superior olive of gerbils during late postnatal development." J Comp Neurol **517**(3): 385-396.

Rietzel, H. J. and E. Friauf (1998). "Neuron types in the rat lateral superior olive and developmental changes in the complexity of their dendritic arbors." J Comp Neurol **390**(1): 20-40.

Rusu, S. I. and J. G. Borst (2011). "Developmental changes in intrinsic excitability of principal neurons in the rat medial nucleus of the trapezoid body." Dev Neurobiol **71**(4): 284-295.

Ryugo, D. K., K. L. Montey, et al. (2006). "Postnatal development of a large auditory nerve terminal: the endbulb of Held in cats." Hear Res **216-217**: 100-115.

Sanes, D. H., J. Song, et al. (1992). "Refinement of dendritic arbors along the tonotopic axis of the gerbil lateral superior olive." Brain Res Dev Brain Res **67**(1): 47-55.

Smith, P. H., P. X. Joris, et al. (1998). "Anatomy and physiology of principal cells of the medial nucleus of the trapezoid body (MNTB) of the cat." J Neurophysiol **79**(6): 3127-3142.

Sonntag, M., B. Englitz, et al. (2009). "Early postnatal development of spontaneous and acoustically evoked discharge activity of principal cells of the medial nucleus of the trapezoid body: an in vivo study in mice." J Neurosci **29**(30): 9510-9520.

Taschenberger, H., R. M. Leao, et al. (2002). "Optimizing synaptic architecture and efficiency for high-frequency transmission." Neuron **36**(6): 1127-1143.

Taschenberger, H. and H. von Gersdorff (2000). "Fine-tuning an auditory synapse for speed and fidelity: developmental changes in presynaptic waveform, EPSC kinetics, and synaptic plasticity." J Neurosci **20**(24): 9162-9173.

Trattner, B., S. Berner, et al. (2013). "Depolarisation-induced suppression of a glycinergic synapse in the superior olivary complex by endocannabinoids." J Neurochem.

Trattner, B., C. M. Gravot, et al. (2013). "Metabolic Maturation of Auditory Neurones in the Superior Olivary Complex." PLoS One **8**(6): e67351.

Trattner, B., B. Grothe, et al. (in preparation). "Postsynaptic endocannabinoid signalling modulates responses of adult MSO neurones."

Trattner, B., A. Klein, et al. (in preparation). "The role of the endocannabinoid system in morphological development of neurons in the medial superior olive."

Tritsch, N. X., A. Rodriguez-Contreras, et al. (2010). "Calcium action potentials in hair cells pattern auditory neuron activity before hearing onset." Nat Neurosci **13**(9): 1050-1052.

Tritsch, N. X., E. Yi, et al. (2007). "The origin of spontaneous activity in the developing auditory system." Nature **450**(7166): 50-55.

Vannucci, R. C., E. E. Nardis, et al. (1981). "Cerebral carbohydrate and energy metabolism during hypoglycemia in newborn dogs." Am J Physiol **240**(3): R192-199.

Vetter, P., A. Roth, et al. (2001). "Propagation of action potentials in dendrites depends on dendritic morphology." J Neurophysiol **85**(2): 926-937.

Walcher, J., B. Hassfurth, et al. (2011). "Comparative post-hearing development of inhibitory inputs to the lateral superior olive in gerbils and mice." J Neurophysiol.

Werthat, F., O. Alexandrova, et al. (2008). "Experience-dependent refinement of the inhibitory axons projecting to the medial superior olive." Dev Neurobiol **68**(13): 1454-1462.

Wilson, R. I. and R. A. Nicoll (2001). "Endogenous cannabinoids mediate retrograde signalling at hippocampal synapses." Nature **410**(6828): 588-592.

Womack, M. and K. Khodakhah (2002). "Active contribution of dendrites to the tonic and trimodal patterns of activity in cerebellar Purkinje neurons." J Neurosci **22**(24): 10603-10612.

Wong-Riley, M. and E. W. Carroll (1984). "Effect of impulse blockage on cytochrome oxidase activity in monkey visual system." Nature **307**(5948): 262-264.

Wong-Riley, M. T., M. M. Merzenich, et al. (1978). "Changes in endogenous enzymatic reactivity to DAB induced by neuronal inactivity." Brain Res **141**(1): 185-192.

Wong-Riley, M. T., S. C. Tripathi, et al. (1989). "Effect of retinal impulse blockage on cytochrome oxidase-rich zones in the macaque striate cortex: I. Quantitative electron-microscopic (EM) analysis of neurons." Vis Neurosci **2**(5): 483-497.

Wong-Riley, M. T., T. C. Trusk, et al. (1989). "Effect of retinal impulse blockage on cytochrome oxidase-rich zones in the macaque striate cortex: II. Quantitative electron-microscopic (EM) analysis of neuropil." Vis Neurosci **2**(5): 499-514.

Woolf, N. K. and A. F. Ryan (1984). "The development of auditory function in the cochlea of the mongolian gerbil." Hear Res **13**(3): 277-283.

Zhao, Y., M. E. Rubio, et al. (2009). "Distinct functional and anatomical architecture of the endocannabinoid system in the auditory brainstem." J Neurophysiol **101**(5): 2434-2446.

Zhao, Y. and T. Tzounopoulos (2011). "Physiological Activation of Cholinergic Inputs Controls Associative Synaptic Plasticity via Modulation of Endocannabinoid Signaling." J Neurosci **31**(9): 3158-3168.

Zhou, Y., L. H. Carney, et al. (2005). "A model for interaural time difference sensitivity in the medial superior olive: interaction of excitatory and inhibitory synaptic inputs, channel dynamics, and cellular morphology." J Neurosci **25**(12): 3046-3058.

Abbreviations

2-AG	2-Arachidonylglycerol
AEA	Anandamide
ATP	Adenosine-5'-Triphosphate
CB1	Cannabinoid receptor 1
CB2	Cannabinoid receptor 2
CN	Cochlear Nucleus
COX	Cytochrome *c* oxidase
GABA	γ – Aminobutyric Acid
GBC	Globular Bushy Cell
GLUT	Glucose transporter
DAG	Diacylglycerol
DAGL	Diacylglycerollipase
DAPI	4',6-Diamidino-2-Phenylindole
DSE	Depolarisation-induced Suppression of Excitation
DSI	Depolarisation-induced Suppression of Inhibition
GlyT2	Glycine Transporter 2
GIRK	G-Protein-coupled Inward Rectifying K^+ channel
IC	Inferior Colliculus

ILD	Interaural Level Difference
ITD	Interaural Time Difference
LDH	Lactate Dehydrogenase
LNTB	Lateral Nucleus of the Trapezoid Body
LSO	Lateral Superior Olive
LTD	Long-Term Depression
LTP	Long-Term Potentiation
MAP2	Microtubule-associated protein 2
MCT1	Monocarboxylate Transporter 1
MNTB	Medial Nucleus of the Trapezoid Body
MSO	Medial Superior Olive
NGF	Nerve Growth Factor
P	Postnatal day
RIM	Rimonabant
SBC	Spherical Bushy Cell
SOC	Superior Olivary Complex
SPN	Superior Periolivary Nucleus
TRPV1	Transient Receptor Potential Vanilloid 1 receptor
VGlut1	Vesicular Glutamate transporter 1
VNTB	Ventral Nucleus of the Trapezoid Body

Acknowledgements

First of all, I would like to thank my supervisor Lars Kunz for supporting my thesis and providing guidance and support along the way. I profited greatly from our insightful debates and discussions on science as well as your encouragement and deliberate approach for new or difficult experiments. Secondly, I am very grateful to the other constant members of my thesis advisory committee, Benedikt Grothe and Felix Felmy as well as the guest members for offering important advices and critically discussing my work. I am also very much obliged to the whole GSN team, who managed and organised my transcripts and were helpful at all times. Additionally, I am very thankful to my colleagues in the lab, who offered valuable advices and help during my thesis and who made my time at this institute very enjoyable. Specifically I would like to thank Céline Gravot, Alexandra Klein, Lara Jansen and Sarah Berner, whose B.Sc. theses or research project I supervised, and who in addition to being hard-working and motivated, were also very pleasant companions in the lab. Sincere thanks are also given to Susanne Radtke-Schuller, Stefan Keplinger, Olga Alexandrova, Hilde Wohlfrom, Melanie Sotgia, Simone, Fischer, Julian Ammer, Philipp Rautenberg, Michael Stransky, Simon Lehnert and Mike Myoga for discussions about my data, help with new methods or general support and friendship.

Last but not least, I would like to express my sincere gratitude to my family and friends, who always emotionally encouraged me to pursue a PhD. I am especially grateful to my parents and my grandmother for their continuous and unconditional support and to my husband for his unfailing resourcefulness. Special thanks go to my grandfather, who had been my ally since childhood and who would have loved to see me graduate. I am, as ever, deeply beholden to all of you.

Eidesstattliche Versicherung / Affidavit

Hiermit versichere ich an Eides statt, dass ich die vorliegende Disseration „Endocannabinoid modulation and metabolic maturation in the superior olivary complex“ selbstständig angefertigt habe, mich außer der angegebenen keiner weiteren Hilfsmittel bedient habe und alle Erkenntnisse, die aus dem Schrifttum ganz oder annähernd übernommen sind, als solche kenntlich gemacht und nach ihrer Herkunft unter Bezeichnung der Fundstelle einzeln nachgewiesen habe.

I hereby confirm that the dissertation “Endocannabinoid modulation and metabolic maturation in the superior olivary complex” is the result of my own work and that I have only used sources or materials listed and specified in the dissertation.

München,

Barbara Trattner

Contribution for all papers

- Barbara Trattner, Céline Marie Gravot, Benedikt Grothe and Lars Kunz; Metabolic Maturation of Auditory Neurones in the Superior Olivary Complex; in: PLOS ONE 2013 8(6); e67351

For this paper, I conceived the entire immunohistochemical and histological experiments as well as the analysis. I conducted half of all stainings and analysed half of the cells alone. The other half was processed by Céline Gravot, whom I supervised during her B.Sc. thesis. In addition I designed the figures and wrote the initial version of the manuscript.

- Barbara Trattner, Sarah Berner, Benedikt Grothe and Lars Kunz; Depolarisation-induced suppression of a glycinergic synapse in the superior olivary complex by endocannabinoids; in: Journal of Neurochemistry 2013

For this paper, I partly conceived the experiments. I conducted all the electrophysiological recordings as well as their analysis alone. I planned all the immunohistochemical stainings and conducted the stainings for DAGLα/β alone and supervised Sarah Berner, who was a practical student in the lab, during CB1 stainings. I designed all the figures for the paper and wrote the initial version of the manuscript.

- Barbara Trattner, Alexandra Klein, Lara Jansen, Michael Stransky, Philipp Rautenberg, Benedikt Grothe and Lars Kunz; The role of the endocannabinoid system in morphological development of neurones in the medial superior olive (unpublished manuscript)

For this paper, I wrote the animal license for ethical clearance, planned all the experiments and conducted all drug administrations and neurone electroporation. I established the AMIRA reconstruction procedure and reconstructed several neurones. In addition I supervised all Golgi

stains and conducted several stainings on my own. I supervised all analysis and designed all figures. I computed the computational NEURON model on my own. I wrote the initial version of the manuscript of the study.

- Barbara Trattner, Benedikt Grothe and Lars Kunz; Postsynaptic endocannabinoid signalling modulates responses of adult MSO neurones (unpublished manuscript):

For this paper, I partly conceived the experiments. I conducted all the electrophysiological recordings as well as their analysis alone. I conducted all immunohistochemical stainings. I designed all the figures for the paper and wrote the initial version of the manuscript.